Advanced control with semi-empirical and data based modelling for falling film evaporators

by
Adriaan Lodewicus Haasbroek

Thesis presented in partial fulfilment of the requirements for the degree Master of Science in Engineering at Stellenbosch University

Supervisor: Prof. W.H. Steyn
Department of Electrical & Electronic Engineering

Co-supervisor: Dr. L. Auret
Department of Process Engineering

March 2013

Declaration

By submitting this thesis electronically, I declare that the entirety of the work contained therein is my own, original work, that I am the sole author thereof (save to the extent explicitly otherwise stated), that reproduction and publication thereof by Stellenbosch University will not infringe any third party rights and that I have not previously in its entirety or in part submitted it for obtaining any qualification.

March 2013

Abstract

This work focussed on a local multiple chamber falling film evaporator (FFE). The FFE is currently under operator control and experiencing large amounts of lost production time due to excessive fouling. Furthermore, the product milk dry mass fraction (W_P) is constantly off specification, negatively influencing product quality, while the first effect temperature (T_{E1}) runs higher than the recommended 70°C (this is a main cause of fouling).

A two month period of historical data were received with the aim to develop a controller that could outperform the operators by keeping both control variables, W_P and T_{E1}, at desired set points while also increasing throughput and maintaining product quality.

Access to the local plant was not possible and as such available process data were cleaned and used to identify two data based models, transfer function and autoregressive with exogenous inputs (ARX) models, as well as a semi-empirical-model. The ARX model proved inadequate to predict T_{E1} trends, with an average T_{E1} correlation to historical data of 0.36, compared to 0.59 and 0.74 for the transfer function and semi-empirical-models respectively. Product dry mass correlations were similar between the models with the average correlations of 0.47, 0.53 and 0.51 for the semi-empirical, transfer function and ARX models respectively. Although the semi-empirical showed the lowest W_P correlation, it was offset by the T_{E1} prediction advantage. Therefore, the semi-empirical model was selected for controller development and comparisons. The success of the semi-empirical model was in accordance with previous research [**1**] [**2**] [**3**], yet other studies have concluded that ARX modelling was more suited to FFE modelling [**4**].

Three controllers were developed, namely: a proportional and integral (PI) controller as base case, a linear quadratic regulator (LQR) as an optimal state space alternative and finally, to make full use of process knowledge, a predictive fuzzy logic controller (PFC). The PI controller was able to offer zero offset set point tracking, but could not adequately reject a feed dry mass (W_F) disturbance (as proposed and reported by Winchester [**5**]). The LQR was combined with a Kalman estimator and used pre-delay states. In order to offer increased disturbance rejection, the feedback gains of the disturbance states were tuned individually. The altered LQR and PFC solutions proved to adequately reject all modelled disturbances and outperform a cascade controller designed by Bakker [**6**]. The maximum deviation in W_P was a fractional increase of 0.007 for LQR and 0.005 for FPC, compared to 0.012 for PI and 0.0075 for the cascade controller [**6**] (W_F disturbance fractional increase of 0.01). All the designed controllers managed to reduce the standard deviation of operator controlled W_P and T_{E1} by at least 700% and 450%, respectively. The same level of reduction was seen for maximum control variable deviations (370%), the integral of the absolute error (300%) and the mean squared error (900%). All these performance metrics point to the controllers performing better than the operator based control.

In order to prevent manipulated variable saturation and optimise the feed flow rate (F_1), a fuzzy feed optimiser (FFO) was developed. The FFO focussed on maximising the available evaporative capacity of the FFE by optimising the motive steam pressure (P_S), which supplied heat to the effects. By using the FFO for each controller the average feed flow rate was increased by 4.8% (±500kg/h) compared to the operator control. In addition to flow rate gain, the controllers kept T_{E1} below 70°C and W_P on specification. As such, the overall product quality also increased as well as decreasing the down time due to less fouling.

Opsomming

Hierdie projek het op ‘n vallende film verdamper (VFV) gefokus. Die VFV word tans beheer deur operateurs en ondervind groot hoeveelhede verlore produksie tyd a.g.v oormatige aangroeisels. Die vorming van aangroeisels is grootliks te danke aan die eerste effek temperatuur (T_{E1}) wat gereeld 70°C oorskrei. Die produk droë massa fraksie (W_P) is ook telkens nie op die gewenste vlak nie, wat produk kwaliteit negatief beinvloed.

Data, wat oor ‘n twee maand periode strek, was verkry met die doelstelling om ‘n beheerder te ontwerp wat beter sou vaar as die operateurs, deur beide W_P en T_{E2} om ‘n nou stelpunt te beheer. Ter selfde tyd moet die ontwerpte beheerder die produksie tempo en produk kwaliteit verhoog.

Geen toegang tot die plaaslikke VFV was moontlik nie, dus was die data skoongemaak en gebruik om twee data gebasseerde modelle te identifiseer, nl. oordragsfunksie en outoregressiwe met eksogene insette (ORX) modelle, asook ‘n semi-empiriese model. Die ORX model kon nie T_{E1} goed voorspel nie, met ‘n korrelasie faktor (tot die historiese data) van 0.36, vergeleke met die 0.59 en 0.74 van die oordragsfunksie en semi-empiriese modelle onderskeidelik. W_P korrelasie faktore was meer konstant tussen die modelle, met waardes van 0.47, 0.53 en 0.51 vir die semi-empiriese, oordragsfunskie en ORX modelle onderskeidelik. Alhoewel die semi-empiriese model die laagste W_P korrelasie vertoon het, was die tekortkoming vergoed deur die beter T_{E1} voorspelling. Gevolglik was die semi-empiriese model gebruik vir beheerder ontwerp en vergelyking. Die sukses van die semi-empiriese model stem ooreen met vorige studies [**1**] [**2**] [**3**], tog het ander studies al bevind dat die ORX model beter gepas is vir die VFV proses [**4**].

Drie beheerders was ontwikkel, nl. ‘n proporsionele en integreerder (PI) beheerder as basis geval, ‘n liniêre kwadratiese reguleerder (LKR) as optimale toestands beheer alternatief en laastens ‘n voorspellende wasige logika beheerder (VWB) om volle gebruik van proseskennis te maak. Die PI beheerder kon foutlose volging van die stelpunte lewer, maar kon nie ‘n inset voer droë massa fraksie (W_F) versteuring (soos voorgestel en weergegee deur Winchester [**5**]) na wense verwerp nie. Die LKR was saamgevoeg met ‘n Kalman afskatter en het gebruik gemaak van onvertraagde toestande. Die versteuringstoestande was individueel verstel om beter versteurings verweping te weeg te bring. Die aangepaste LKR en VWB kon beide die W_F versteuring verwerp en het beter gevaar as ‘n kaskade beheer oplossing wat deur Bakker [**6**] ontwerp was. Die W_P afwyking is beperk tot ‘n fraksie droë masse verandering van 0.007 vir LKR en 0.005 vir VWB, vergeleke met die afwykings van 0.012 vir die PI beheerder asook die 0.0075 van die kaskade beheerder [**6**]. Die ontwerpte beheerder kon ook die standaard afwyking van beide W_P en T_{E1} met ten minste 700% en 450% onderskeidelik verminder. Soortgelyke verbeterings was gesien vir die maksimum beheer veranderlikke afwyking (370%), die integraal van die absolute fout (300%) en die gemiddelde fout (900%). Dus het die ontwerpte beheerders wesenlik verbeter op die operateur beheer.

Ten einde om gemanipuleerde veranderlikke versadiging te voorkom, asook die voer vloei (V_1) te optimiseer, was ‘n wasige logika optimiseerder (WVO) ontwerp. Die WVO het die beskikbare verdampingskapasiteit ten volle benut deur te sorg dat die stoom druk (P_S), wat energie verskaf vir verdamping, ge-optimiseerd bly. ‘n Gemiddelde V_1 stygging van 4.8% (±500kg/uur), vergeleke met operateur beheer, is waargeneem. Al die beheerders kon steeds die W_P en T_{E1} stelpunte volg en dus T_{E1} onder 70°C hou (wat verminderde vormasie van aangroeisels tot gevolg gehad het). Daarom het die produk kwailiteit verhoog en die verlore produksie tyd verminder.

Acknowledgements

I wish to express my sincere gratitude to the following people who made my project possible:

- Prof. W.H. Steyn for his leadership, immense patience and advice.
- Dr. L. Auret for her voice of reason and guidance.
- Everyone at General Electric who made working fun and always helped wherever possible.
- My parents, brother and Marlis for their love, support and patience whenever I wanted to discuss something for the twentieth time.
- Everyone in the ESL, in specific the satellite students, who made Stellenbosch a fantastic place to be.
- Special thanks to Guy and Phillip, who have walked this engineering road with me.
- God, the Holy Trinity, for His love and ever present guidance.

Contents

Nomenclature

ARX	=	Auto regressive with exogenous inputs
BN	=	Big negative
BP	=	Big positive
CV	=	Control variables
D	=	Disturbance
FFE	=	Falling film evaporator
FFO	=	Fuzzy feed optimiser
IAE	=	Integral of the absolute error
LQR	=	Linear quadratic regulator
MIMO	=	Multiple input multiple output
MSE	=	Mean squared error
MV	=	Manipulated variables
MVR	=	Mechanical vapour recompressor
PFC	=	Predictive fuzzy controller
PID	=	Proportional and integral and derivative
R	=	Correlation
SISO	=	Single input single output
SN	=	Small negative
SP	=	Set point
SP	=	Small positive
TF	=	Transfer function
TVR	=	Thermal vapour recompressor
Z	=	Zero

A_h	=	Area of the distribution plate holes	(m^2)
A_C	=	Condenser tube surface area	(m^2)
A_d	=	Area of distribution plate	(m^2)
A_E	=	Surface area, losses from effect	(m^2)
A_{holes}	=	Total area of holes	(m^2)
A_{plate}	=	Plate cross section area	(m^2)
A_S	=	Surface area, losses from shell and tubing	(m^2)
A_{tank}	=	Tank cross section area	(m^2)
A_{TVR}	=	TVR compressor parameter	(m.s)
B_{TVR}	=	TVR compressor parameter	($m^{0.03}.s^{0.06}/kg^{0.03}$)
c_d	=	Distribution plate discharge coefficient	(-)
$c_{p,met}$	=	Heat capacity of metal	(J/kg.°C)
$c_{p,milk}$	=	Milk heat capacity	(J/kg.°C)
$c_{p,TS}$	=	Adjusted heat capacity of milk	(J/kg.°C)
$c_{p,water}$	=	Heat capacity of water	(J/kg°C)
C_{TVR}	=	TVR compressor parameter	-
E	=	Error	(-)
F_1	=	Flow rate to first evaporator effect	(kg/hr)
F_P	=	Flow rate of product (concentrated milk)	(kg/hr)
$G_c(s)$	=	Controller transfer function	(-)
$G_d(s)$	=	Disturbance transfer function	(-)
$G_D(z)$	=	Effect of pre-pasteurisation temperature on pasteuriser temperature	(-)
$G_p(s)$	=	Plant transfer function	(-)
$G_P(z)$	=	Effect of steam valve position on pasteuriser	(-)

		temperature	
$G_S(z)$	=	Effect of steam valve position on evaporation temperature	(-)
$G_v(s)$	=	Valve transfer function	(-)
$G_W(z)$	=	Effect of condenser cooling water valve position on evaporation temperature	(-)
H	=	Enthalpy contained within the system envelope	(J/kg)
h_d	=	Height of liquid above distribution plate	(m)
Hk	=	Enthalpy of the mass flow crossing envelope boundaries	(J/kg)
Hr	=	Tube riser height	(m)
H_{steam}	=	Steam enthalpy	(J/kg)
$I_{effect,i}$	=	Thermal inertia of metal/liquid/vapour in effect	(J/°C)
$I_{shell,i}$	=	Thermal inertia of metal/liquid/vapour in effect	(J/°C)
K_C	=	Controller gain	(-)
K_{pr}	=	Process gain	(-)
L_1	=	Level inside first effect	(%)
L_2	=	Level inside second effect	(%)
L_C	=	Length of condenser tubes	(m)
L_H	=	Level of evaporator holding tank	(%)
M	=	Mass contained within the system envelope	(kg)
m_{comp}	=	Mass flow of milk vapour pulled from effect	(kg/s)
$m_{cond,i+1}$	=	Mass flow of condensed vapour on shell side of the next effect	(kg/s)
m_d	=	Mass flow rate from distribution plate	(kg/s)
$m_{dist,i}$	=	Mass flow from distribution plate	(kg/s)
m_e	=	Mass flow rate at the bottom of the tubes	(kg/s)
m_{feed}	=	Feed mass flow rate	(kg/s)
m_{flash}	=	Mass flow of milk flashed	(kg/s)
M_k	=	Mass flowing into or out of envelope	(kg/s)
m_{met}	=	Mass of metal in effect	(kg)
M_P	=	Overshoot	(-)
$M_{product,i}$	=	Mass flow of concentrated milk exiting effect	(kg/s)
m_{steam}	=	Mass of driving steam flowing to TVR	(kg/s)
m_{tubes}	=	Mass evaporation rate inside the tubes	(kg/s)
N_C	=	Number of condenser tubes	
$N_{TE1/TE2}$	=	Number of tubes effect 1/2	-
P_C	=	Condenser pressure	(bar)
P_{E1}	=	Pressure inside first effect	(s)
P_H	=	Pressure in holding tubes	(bar)
P_{Hom}	=	Homogeniser pressure	(bar)
P_S	=	Steam pressure	(bar)
Q	=	Weighting matrices (LQR)	(-)
q_{comp}	=	Latent enthalpy of vapour removed to TVR	(W)
q_{cond}	=	Heat flow to the condenser	(W)
$q_{eloss,i}$	=	Heat loss to surroundings from effect	(W)
q_{feed}	=	Net enthalpy from the feed milk to the effect	(W)
$q_{shell,i}$	=	Heat loss to surroundings from shell	(W)
$q_{shell,i+1}$	=	Heat transfer to shell of next effect	(W)
T_C	=	Waste water temperature	(°C)
$T_{CW,i}$	=	Cooling water inlet temperature	(°C)
T_d	=	Derivative time	(s)

T_E	=	Effect temperature	(°C)
T_{E1}	=	Temperature of first effect	(°C)
T_{E2}	=	Temperature of second effect	(°C)
$T_{feed,i}$	=	Temperature of feed to ith effect	(°C)
T_H	=	Temperature in holding tubes	(°C)
Thermal inertia	=	Energy required to change an effect temperature	(J/°C)
T_{Hom}	=	Homogeniser temperature	(°C)
T_I	=	Integral time	(s)
T_P	=	Temperature of product	(°C)
$t_{s,2\%}$	=	Settling time	(s)
$T_{s,i}$	=	Temperature ith effect shell	(°C)
u_c	=	Condenser heat transfer coefficient	(W/m2°C)
U_C	=	Condenser heat transfer coefficient	(W/ m².°C)
U_e	=	Shell to tube heat transfer coefficient	(W/ m².°C)
v_{ff}	=	Velocity of falling film	(m/s)
W_{comp}	=	Net enthalpy of steam entering the TVR	(W)
W_D	=	Dry mass fraction, liquid leaving distribution plate.	(-)
W_E	=	Total solids fraction at the bottom of the tubes	-
W_F	=	Feed dry mass fraction	(-)
Ws	=	Net work done on the envelope	(W)
α_{F1}	=	Feed flow rate to product dry mass disturbance factor	(-)
α_{TH}	=	Feed temperature to product dry mass disturbance factor	(-)
α_{TS}	=	Density relational coefficient	-
α_{WF}	=	Feed dry mass to product dry mass disturbance factor	(-)
ρ_d	=	Density of milk leaving the distribution plate	kg/m3
ρ_{milk}	=	Milk density	(kg/m^3)
ρ_{water}	=	Water density	(kg/m^3)
τ_C	=	Residence time of cooling water in condenser tubes	(s)
τ_e	=	Falling film residence time	(s)
τ_{pr}	=	Process time constant	(s)
τ_{TC}	=	Time constant within the condenser tubes	(s)
ω_n	=	Natural frequency	(rad/s)
ω_{TS}	=	Milk dry mass fraction (total solids)	-
L	=	Length of tubes	(m)
$U(s)$	=	Laplace domain inputs	(-)
$Y(s)$	=	Laplace domain outputs	(-)
g	=	Gravity coefficient	(kg/m.s²)
q	=	Net heat flow into the envelope	(W)
ζ	=	Damping factor	(-)
λ	=	Latent heat of vapourisation	(J/kg)
λ	=	Latent heat of vapourisation	(J/kg)

List of figures

List of Tables

Chapter 1 - Introduction

1.1 Milk concentration background

Evaporative and drying processes form an integral part of modern day food processing where they are mainly employed to reduce the moisture content of the product, either for storage as a powder or for longer shelf live. There are many different evaporator designs, each geared to a specific concentration scenario. These designs influence the operational costs, production volume and final product quality.

This work's main focus is a falling film evaporator (FFE) used as a pre-concentrator to a downstream spray dryer that produces milk powder. FFEs are mainly employed for this pre-concentration as they use about ten times less energy per unit mass of water removed than spray dryers. Looking only at concentration, the €67 billion European dairy sector has adopted FFEs as the industry standard [**7**].

FFEs can have multiple evaporation chambers and different ways of recycling vapour heat to further increase energy efficiency. A schematic representation of the two effect FFE investigated is shown below in Figure 1-1:

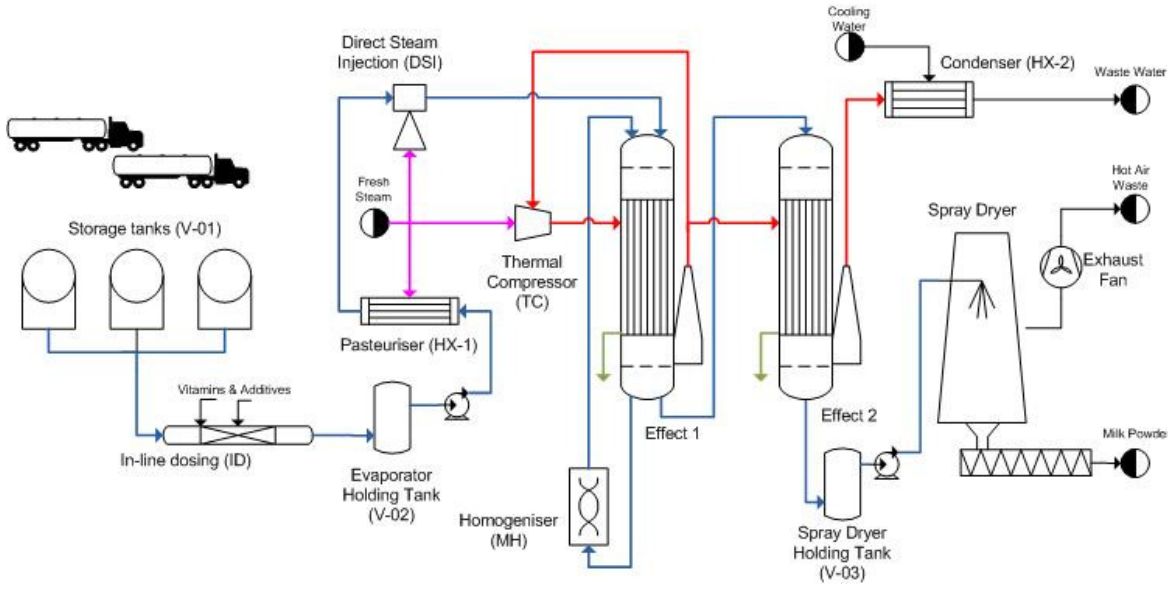

Figure 1-1: Falling film process flow diagram

1.2 Brief process description

FFEs normally consist of multiple effects to increase evaporation efficiency. Milk enters an effect at higher temperature and pressure than the effect to ensure constant evaporation and proper use of the motive steam. Once in the effect, a distribution plate evenly directs flow to the tubes, with steam on the shell side supplying heat for evaporation. The flows inside the tubes are driven by gravity and form a thin film on the walls which enhances heat transfer and lends the name to FFEs. The milk vapours are pulled from each effect by condensation, either on the shell side of the following effect or a condenser, creating a vacuum that lowers the boiling point of milk.

A compact description of a particular two effect milk concentration process is given here to explain the most important control requirements:

Raw milk is treated by in-line vitamin enrichment before it is sent to a feed tank. From the feed tank, the milk passes through a moderate temperature pasteuriser (70°C – 80°C) to deactivate most pathogens. A direct steam injector follows the pasteuriser to eradicate the final pathogens and pre-heat the milk to a temperature above that of the evaporator chambers (± 104°C). This is done under raised pressures (2 – 3 bar) to ensure that the milk does not vapourise inside the tubing.

Once inside the evaporator effect, some milk immediately forms vapour due to the rapid exposure to a low pressure system (flash evaporation). The remaining liquid milk flows down the inside of long vertical tubes heated by fresh steam and/or recycled vapour. These tubes facilitate most of the evaporation. The concentrated milk is directed to a second evaporator (which functions similarly to the first evaporator) to increase heat recovery and drive the final pre-concentration.

The milk then exits the FFE section into a holding tank from where it is fed to a spray dryer which produces the final milk powder product.

1.3 Current control and control requirements

For the particular process considered, control of the FFE is currently performed manually by operators. They rely on process knowledge as well as operational experience to ensure that the evaporators perform well, i.e. keeping the milk dry mass at a steady preset level as well as regulating internal temperatures and flow rates. Additionally, the control objectives can be expanded into seven broad categories [**8**]:

I. Safe operation:
   - At all times the process should be controlled to minimise risk to personnel.
   - Pressure inside holding tubes to not fall below 2bar to ensure no boiling
   - Pasteuriser temperature kept above 70°C to ensure no build up of pathogens inside the effects
   - Emergency control action needs to be specified for dangerous disturbances such as the rapid increase of steam supply pressure or drastic decline in feed flow

II. Environmental protection:
   - Of paramount importance during plant design and operation.
   - FFEs process large amounts of milk that could contain harmful pathogens; as such the control during start-up, shut-down, and cleaning operation has to ensure correct disposal of process liquids.

III. Equipment protection:
   - Required for safe operation and environmental protection
   - Control of pumps and feed flow rate to ensure pumps do not run dry
   - Prevent excessive fouling by maintaining effect temperatures below 70°C
   - Controller action needs to be limited and smooth acting to prevent equipment from being damaged by frequent large set point changes

IV. Smooth operation and production rate
   - Again smooth controller action is required to limit stress on units such as pumps
   - Feed flow needs to be sufficient to keep all tubes wet without inducing flooding or overflow in the distribution plate
   - Production rate needs to be sufficient to keep downstream dryer in constant operation

V. Product quality
   - Product viscosity needs to be kept under 100cP [**5**], implying that a maximum W_P

VI. Profit
   - Evaporate as much water as possible in the FFE
   - Keep the dry mass and production rates as close to the upper limit as possible

VII. Monitoring and diagnostics

From the above list it is clear that operators need to attempt to maintain high production rates, which require high heat transfer, implying high temperatures. However, milk proteins tend to become unstable at high temperatures and starts to denaturise rapidly above 70°C, causing product quality loss and excessive fouling inside an evaporator. Fouling increases both downtime and maintenance costs. Temperature control can be seen as a balance between competing objectives: maintaining sufficiently high temperatures to maintain high production rates while ensuring sufficiently low temperatures to prevent fouling.

These competing objectives, combined with process lags and disturbances, result in operators either acting too conservatively to ensure smooth operation, or too aggressively, resulting in milk quality degradation and process downtime. Furthermore, each operator has characteristic control and operational styles, which leads to the spray dryer constantly receiving milk of varying quality and concentration. This in turn compromises downstream operations and finally the milk powder product quality.

1.4 Potential control strategies

Control techniques allow engineers to create unbiased controllers to keep a process at optimal operating conditions – maximising production while adhering to quality and safety requirements. Possible techniques include proportional, derivative and integral (PID) control which has been extensively implemented in the process industry [**9**]. Another possibility is multi-input multi-output (MIMO) state space control which allows the use of powerful optimisation and estimation algorithms for optimal control, in specific the so-called linear quadratic regulator (LQR). Estimators may be simple in nature, i.e. predictive estimator, or fairly complex with optimal parameter specification, i.e. the Kalman estimator. Finally, fuzzy logic control offers a way to preserve expert process knowledge.

Although expert knowledge and operator experience should never be underestimated, state space and PID control techniques have a lot to offer in terms of stability, continuity and optimisation. These forms of controllers can be seen as algorithmic solutions which may provide smoother control when compared to manual control where variable changes are often made in large discrete steps. Algorithmic control does however require process models to add a predictive element which allows for the quick rejection of disturbances. These models range from simple identified statistical models, i.e. transfer functions, to in depth fundamental models.

1.5 Hypothesis

A controller can be designed that will outperform the current control technique as well as increase production rates while still maintaining the desired product quality and safety standards.

1.6 Objectives

Although the ultimate goal of the study is to create a comprehensive control strategy for the evaporator, the work can be divided into smaller objectives:

- **Construct a semi-empirical model of FFE**
  - The first objective involves modifying and aggregating literature fundamental models by altering adjustable parameters to represent the data of the studied FFE.
- **Data-based modelling of FFE**
  - With enough reliable data, computational models such as transfer functions become viable. Together with transfer function modelling, an autoregressive with exogenous inputs (ARX) model will be investigated.
- **Model performance comparison**
  - Both the semi-empirical and data-based modelling results will be compared with process knowledge to see whether the dynamics are similar to that found in literature and provided by plant operators. Validation date will also be used to determine whether the models accurately describe the local FFE.
- **PI controller design and implementation**
  - As PI control is still prevalent throughout the process industry, it will be used as a baseline to compare controller performance.
- **MIMO state space controller combined with LQR optimisation and Kalman-filter estimator design and implementation**
  - A MIMO controller with LQR optimisation will be designed to show the advantages/disadvantages of a more complex formal solution.
- **Fuzzy predictive control with expert rules design and implementation**
  - A fuzzy controller will be developed to illustrate the importance of expert process knowledge how it can be used to quickly develop a controller.
- **Controller performance comparison on simulated and real data**
  - Various aspects of the controller performance e.g. rise time, settling time and the integral of the absolute error will be compared for both simulated and recorded data.

1.7 Scope

The purpose of the simulation model will be to test various control methods as well as provide insight into the internal dynamics of falling film evaporators. As such the model should correlate well with the historical data and adhere to process logic. Deeper modelling of the falling film boundary layers and precise heat transfer coefficients fall outside of the scope of the current work.

Development of a suitable control strategy requires that the solution be advanced enough to manage the process in various operating regions, yet unnecessary additions to the complexity could introduce instability or simply not be valuable enough to justify the design effort. As the current PID controllers for the holding-tank, pasteuriser, DSI unit and feed rate work well, their tuning and operation falls outside the scope of the current work. The assessment and comparison of more advanced state space and fuzzy control to the operator based control will form the core of this work.

1.8 Outline

Chapter 2 contains an overview of milk as a process fluid, especially the properties of milk relevant to product quality. Chapter 3 briefly describes the local FFE operation and available historical data. Chapter 4 gives the relevant control background required to design the various controllers specified in the objectives. Chapter 5 offers a critical review of dairy FFE modelling as well as all the important fundamental process units, while Chapter 6 implements the fundamental theory to develop a semi-empirical FFE model. Chapter 7 investigated data based modelling as alternative to the semi-empirical model. In Chapter 8 the algorithmic controllers are designed and compared to operator control. Finally Chapter 9 offers a complete summary of the conclusions of the various implementation chapters. Chapter 10 suggests future work and other recommendations.

Chapter 2 - Overview of milk as a process fluid

In order to appreciate some of the specific requirements of milk processing a brief summary is given of the properties of milk and main restrictions on milk processing conditions.

2.1 Properties of milk

The composition of normal cow milk is shown below in Table 2-1 [**10**]:

Table 2-1: Common constituents of milk

Constituent	Whole Milk	Skim Milk
Water	87.50%	91.10%
Fat	4.10%	0.10%
Lactose	4.00%	4.30%
Protein	3.30%	3.30%
Salts	1.10%	1.20%

Both whole (full cream) and skim milk are made up of over 80% water; this implies that most of the milk's mass is water – which holds no nutritional value in itself. The density of milk is related to the dry mass fraction (i.e. mass that is not water) as shown in Eq. 2-1 below [**1**]:

$$\rho_{milk} = \frac{\rho_{water}}{[1 - \alpha_{TS}\omega_{TS}]} \qquad \textbf{Eq. 2-1}$$

Where

ρ_{milk}		Milk density	(kg/m^3)
ρ_{water}	=	Water density	(kg/m^3)
α_{TS}	=	Density relational coefficient	-
ω_{TS}	=	Milk dry mass fraction (total solids)	-

The fat and protein content of milk makes it susceptible to bacterial growth, while bacterial contaminants may be present in milk either from a sick animal or other contamination. Diseases such as bovine tuberculosis and brucellosis forced the introduction of pasteurisation to ensure that milk is safe for human consumption [**11**].

2.2 Milk powder

Both the threat of pathogens in milk and high water content are motivators for producing milk powder. Concentrating milk to milk powder decreases its weight dramatically and removes virtually all water, making it very difficult for bacteria to propagate. In turn this makes milk powder ideal for long term storage and inexpensive transportation.

2.2.1 Potential milk processing complications

Milk concentration advantages come at a significant cost. Water reduction causes the viscosity of milk to increase exponentially in the total solids range of 44% - 50% [**10**]. This increase in viscosity can lead to blockages or increased pump duty. In practice an upper limit is placed on the dry mass percentage of the milk while it is being processed (i.e. before final drying stage) which directly limits the viscosity.

Another major difficulty arises when milk is treated at excessive temperatures; at 65°C the β-lactoglobulin protein becomes thermally unstable [**12**] while a soft white deposit starts forming on equipment at temperatures between 75°C and 110°C [**13**]. Other authors also report significant fouling at temperatures above 70°C [**1**] [**2**].

Chapter 3 - Local falling film evaporator

Considering the advantages that milk powder offers, a multitude of milk powder production processes have been developed, including pre-processing units to increase efficiency. This work focuses on a multi-effect falling film evaporator with a thermal vapour recompression (TVR) compressor used for steam recycling. Other options include membrane concentrators, rising film evaporators and mechanical vapour recompression (MVR) [**7**] [**1**]. A brief description of the process studied is given in Sections 3.1. For an in-depth description of the most important unit operations please refer to the fundamental modelling section (Section 5.2).

3.1 Process flow diagram

An overview of the process studied is shown below in Figure 3-1, followed by a description of the liquid milk and vapour paths through the local FFE.

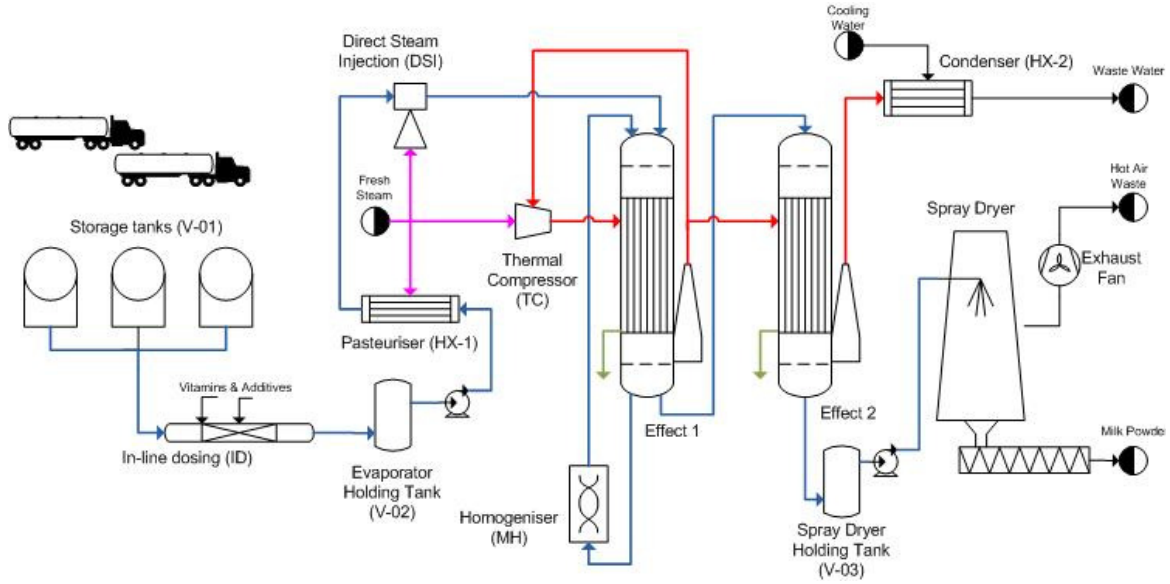

Figure 3-1 : Process flow diagram for the milk powder production facility

3.1.1 Liquid milk path

Fresh milk arrives at the facility and is stored in large tanks (V-01). Samples are taken regularly to determine which vitamins and oils should be added for nutritional purposes. The additions are done with an inline dosing system (ID) before the milk is fed to the evaporator holding tank (V-02). From here the milk is pumped (P-01) to the tube side of the pasteuriser (HX-01) and heated to ±70°C. In some production plants, the heat is supplied by condensed steam from the evaporator shell, but in this case fresh steam is used.

After the pasteuriser, the milk enters the direct steam injection (DSI) chamber where it is directly mixed with fresh steam to increase the temperature rapidly to ±105°C, under at least 3 bar pressure. Before entering the distribution plate at the top of the evaporator effect, the milk is passed through a series of holding tubes to delay flow for a further 15 – 20 seconds to ensure that the high temperature kills all harmful bacteria. Normally milk would easily vapourise at such a high temperature, but the high pressure ensures that no vapour bubbles are formed.

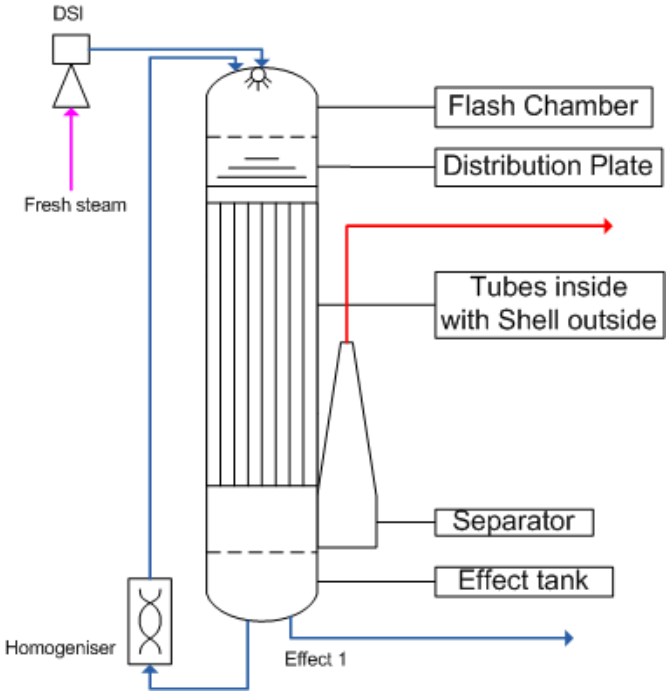

Figure 3-2: Close-up of Effect 1 internals

Liquid milk now enters the first effect as shown in Figure 3-2. Both effects are kept under partial vacuum to lower the boiling point of the milk, usually by vapour suction from downstream units. The decreased boiling point keeps the milk at lower temperatures - limiting heat damage and fouling. When the high pressure milk suddenly encounters a low temperature and low pressure region it undergoes flashing which instantly converts some of the liquid to vapour.

The remaining liquid flows through to the distribution plate and is evenly spread out across all evaporation tubes. The vapour generated in the flash vessel helps ensure that the liquid flows as a thin film inside the tubes – decreasing resistance to heat transfer.

As the liquid is flows due to gravity down the tubes, steam on the shell side provides heat causing evaporation – this is the main method of concentration inside an effect. All the remaining liquid is collected in an effect tank before it is split into two streams: one stream is sent to the homogenizer while the other stream is directed to the next effect. The homogenizer breaks up large fat globules within the milk which would otherwise undergo age thickening. This thickening may cause the liquid to become too viscous for spray drying [**1**]. Product from the homogenizer is fed back to the first effect distribution plate. This recycle stream leads to an increase in the concentration of the whole effect due to longer effective residence time.

Once milk enters the second effect it again flows over a distribution plate. The tubes leading from the second effect distribution plate is heated on the shell side by vapour originating from the first effect. Concentrated milk leaves the second effect and enters a holding tank (V-03) before being pumped to the spray dryer, where the concentrated milk is exposed to hot air which removes the final moisture and produces the milk powder product.

3.1.2 Milk vapour path and steam recycle

Vapour should only be formed once the liquid milk has entered the flash chamber of the first effect as shown in Figure 3-2. The resulting vapour (combined with vapour generated inside the tubes) is pulled by the partial vacuum down through the tubes and into a cyclone separator which removes any entrained liquid. Cyclone separators work by inducing rotational flow which forces the heavier components (liquid droplets) to the side where it can then freely flow downwards while allowing the lighter components (vapour) to be pulled upwards out of the effect.

The vapour leaving the first cyclone separator is split into two streams – one used as heating medium in the second effect with the other fed to the TVR unit. Inside the TVR unit, high pressure steam mixes with the low pressure process vapour creating larger volumes of process steam for the first effect shell side. The volume increases can double the first effect heating efficiency [**2**]. A general rule of thumb is that each kilogram of heating medium evaporates one kilogram of water inside the tubing [**1**].

Vapour used as heating medium for the second effect condenses on the outside of the evaporator tubes and is removed as waste water (this waste water can be used for preheating) – the condensation and subsequent waste water removal maintain the partial vacuum needed inside the first effect [**2**] [**3**].

Finally, the vapour generated in the second effect is again fed to a cyclone separator before being removed towards the condenser (HX-2) where it is cooled to form waste water. The condensation and water removal maintain the second effect partial vacuum.

3.2 Collected data

Roughly two months of historical process data sampled at 120s intervals were received from the case study falling film evaporator. Ten days represented normal, but fragmented operation (i.e. with a lot of shut-down and start-up sequences in between).

Two of the recorded variables provided information on the process condition. The first showed the current milk recipe running, which would affect the in-line dosing and milk properties, with the second variable showing the active control sequence. The control implied the local PID loops and not an overall supervisory control scheme. It was found that this sequence referred to start-up, shut-down and continuous operation states. It was found that only ten days of data represented continuous, but fragmented operation (i.e. with the removed start-up and shut-down sequences in between).

After inspection of the average length of a continuous operation set, the data were split into fifteen data sets of at least 10 hours each. Each data set corresponded to a specific recipe, but the recipes followed randomly on one another. Therefore the continuous sets were named via the chronological order in which they appeared. All the available process tags are shown below:

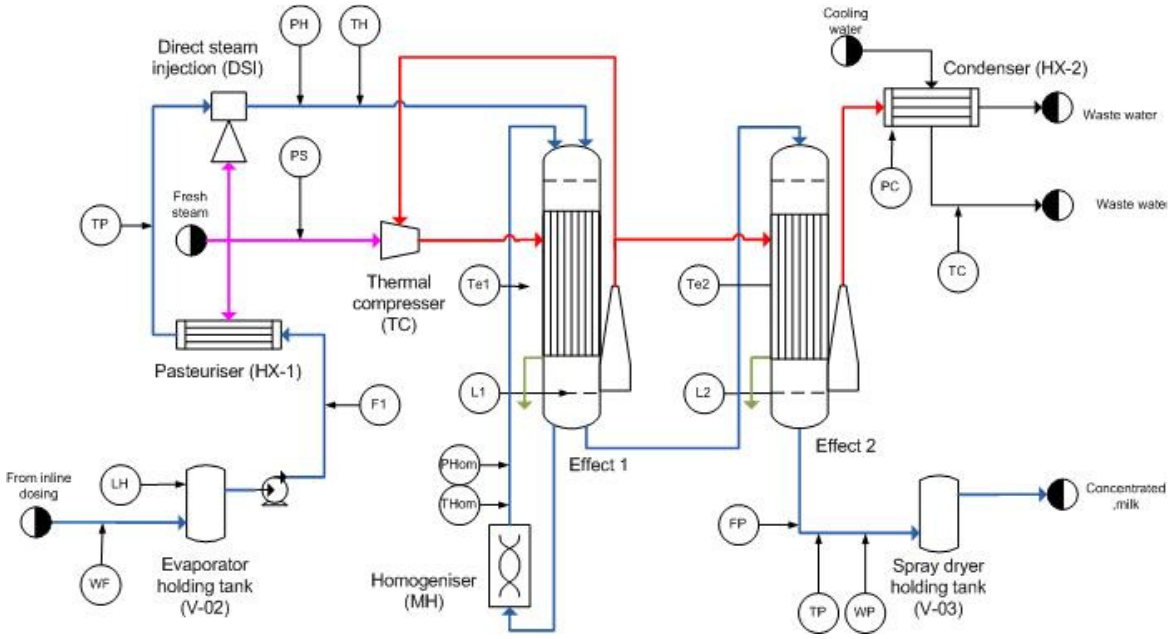

Figure 3-3: Available evaporator data tags

With the tag definitions given in Table 3-1 below:

Table 3-1: Available process tags

Legend	Variable	Units
W_F	Dry mass fraction of feed	(-)
L_H	Level of evaporator holding tank	(%)
F_1	Flow rate to first evaporator effect	(kg/hr)
T_P	Temperature after pasteuriser	(°C)
P_H	Pressure in holding tubes	(bar)
T_H	Temperature in holding tubes	(°C)
P_S	Steam pressure	(bar)
T_{E1}	Temperature of first effect	(°C)
L_1	Level inside first effect	(%)
L_2	Level inside second effect	(%)
P_{Hom}	Homogeniser pressure	(bar)
T_{Hom}	Homogeniser temperature	(°C)
T_{E2}	Temperature of second effect	(°C)
F_P	Flow rate of product (concentrated milk)	(kg/hr)
T_P	Temperature of product	(°C)
W_P	Dry mass fraction of product	(-)
P_C	Condenser pressure	(bar)
T_C	Waste water temperature	(°C)

The data sets, along with the average value of the important variables, are given in Table 3-2 below:

Table 3-2: Historical data sets as well as average variable values

Data set	Number of samples	Recipe	W_F (m/m)	W_P (m/m)	T_{E1} (°C)	T_{E2} (°C)	F_1 (kg/h)	P_S (bar)	T_H (°C)	P_C (bar)
1	357.00	1	35.63	55.68	73.72	72.90	10 586	8.01	104.97	225.81
2	697.00	1	35.89	56.73	74.42	72.95	10 873	6.61	105.01	226.69
3	661.00	2	33.35	201.64	71.61	71.54	10 985	7.04	105.01	249.49
4	430.00	2	34.22	200.91	75.39	72.51	11 307	7.20	104.97	250.04
5	**670.00**	**6**	**33.04**	**51.11**	**71.79**	**71.94**	**10 663**	**8.20**	**105.30**	**254.00**
6	**656.00**	**9**	**34.11**	**62.20**	**76.70**	**76.61**	**11 307**	**8.63**	**104.99**	**228.83**
7	785.00	9	33.91	63.20	71.94	72.11	11 252	8.46	105.02	228.70
8	367.00	9	34.12	62.62	72.10	72.52	11 109	8.39	104.37	233.79
9	1076.00	1	35.51	55.39	70.65	71.21	10 499	7.57	105.01	211.80
10	**653.00**	**1**	**35.24**	**54.50**	**70.61**	**70.62**	**10 263**	**7.88**	**105.00**	**209.26**
11	370.00	1	36.32	55.29	70.67	70.14	10 604	4.96	105.01	211.90
12	**324.00**	**1**	**36.59**	**54.36**	**73.18**	**69.90**	**10 545**	**4.35**	**105.01**	**200.08**
13	579.00	1	36.43	54.55	72.39	67.84	10 802	5.61	104.99	193.46
14	367.00	1	36.28	55.40	70.72	66.56	10 807	4.81	104.98	201.85
15	339.00	2	33.67	199.43	73.06	68.63	11 096.58	5.12	105.00	209.72

Note that the data sets were already split up into training and validation sets (in bold and underlined print), with the exception of historical data set 6, where one half was used for training and the other for validation. The above data sets were again split into smaller 10 hour pieces, with the smaller set number added to the chronological data set number to form new names of the form: historical data set 01_1.

Chapter 4 - Control background

The previous chapter described the local process together with relevant constraints, objectives and current operator based control. As mentioned in the introduction, the operators need to continually weigh the objectives against constraints while relying on experience to predict how the process will react to various disturbances. In addition, the disturbances need to be identified before the process deviates too far from nominal operating conditions. Finally, each operator has a personal bias which influences the particular way in which the process is controlled, e.g. either favouring steam, cooling water or regular feed flow changes to achieve the desired product dry mass.

The control techniques described in this chapter will offer an alternative to operator control and provide ways of prioritising the use of control variables to keep the process at optimal conditions. Firstly, proportional and integral (PI) control will be investigated as a base case controller, thereafter more advanced techniques such as optimal state space design, the linear quadratic regulator (LQR), and fuzzy control will be investigated. Examples from literature will be given when available for dairy falling film evaporators (FFEs).

4.1 PI control

One of the most basic forms of control is to measure the process output (controlled variable), compare it to a given set point and adjust the manipulated variable to drive the process in a direction that will minimise the error. This type of corrective control is called feedback control; a generic block representation is shown below:

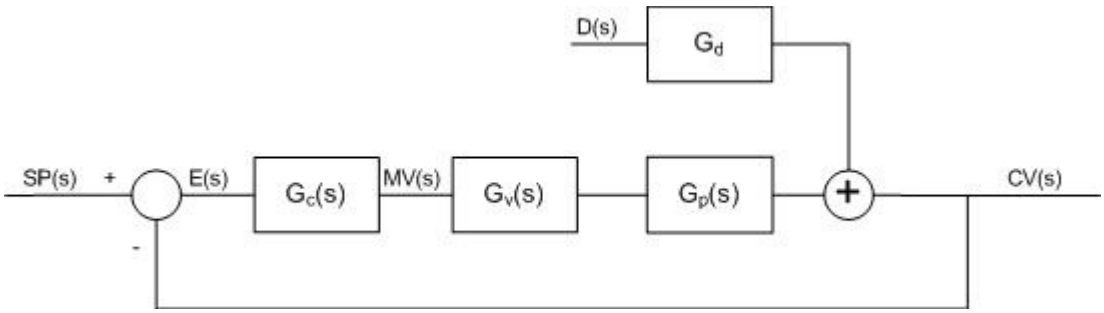

Variables		**Transfer functions**	
SP(s)	Set point	$G_c(s)$	Controller
E(s)	Error	$G_v(s)$	Valve
MV(s)	Manipulated variables	$G_p(s)$	Plant
D(s)	Disturbance	$G_d(s)$	Disturbance
CV(s)	Control variables		

Figure 4-1: Generic feedback control structure, redrawn from [35]

The controller transfer function, $G_c(s)$, may take various forms: one of the most common forms include three methods of using the error to generate the manipulated variables, i.e. using proportional, integral and derivative action, to form the PID controller. The proportional term gives direct quick response to any change in the error (thereby reducing the time constant), the integral action normally provides slow long term action to eliminate any set point offset, while the derivative term takes into account the rate and direction of the error change to increase the controller response for large errors.

4.1.1 Time domain performance specifications

The general form of the continuous PID algorithm including controller gain (K_C), integral (T_I) and derivative time (T_d) is seen below:

$$G_c(s) = \frac{MV(s)}{E(s)} = K_c\left(1 + \frac{1}{T_I s} + T_d s\right) \quad \text{Eq. 4-1}$$

Which, when neglecting the derivative time, can then be written in terms of proportional (K_p) and integral (K_i) gains:

$$G_c(s) = \frac{K_p s + K_i}{s} \quad \text{Eq. 4-2}$$

Assuming $G_p(s)$ is also linear, the following representation can be developed (with K_{pr} and τ the plant gain and time constant):

$$G_p(s) = \frac{K_{pr}}{\tau s + 1} = \frac{K_{pr}/\tau}{\tau s/\tau + 1/\tau} = \frac{b}{s + a} \quad \text{Eq. 4-3}$$

Furthermore, if it is assumed the valve dynamics are a great deal quicker than the process (as claimed by Henningssona et al. [**14**] for dairy processing), the closed loop transfer function ($G_{cl}(s)$) of Figure 4-1 can be expressed as:

$$G_{cl}(s) = \frac{G_p(s)G_c(s)}{1 + G_p(s)G_c(s)} \quad \text{Eq. 4-4}$$

Substituting Eq. 4-2 and Eq. 4-3 into the above equation yields:

$$G_{cl}(s) = \frac{b(K_p s + K_i)}{s(s + a) + b(K_p s + K_i)} \quad \text{Eq. 4-5}$$

With simplification:

$$G_{cl}(s) = \frac{bK_p(s + K_i/K_p)}{s^2 + (a + bK_p)s + bK_p} \quad \text{Eq. 4-6}$$

This can be compared to a second order transfer function of the form (with ω_n the natural frequency and ζ the damping ratio):

$$G(s) = \frac{U(s)}{Y(s)} = \frac{\omega_n^2}{s^2 + 2\zeta\omega_n s + \omega_n^2} \quad \text{Eq. 4-7}$$

The denominator comparison shows that:

$$K_p = \frac{2\zeta\omega_n - a}{b} \quad \text{Eq. 4-8}$$

$$K_i = \frac{\omega_n^2}{b} \quad \text{Eq. 4-9}$$

The controller is parameters are initially selected either by tuning rules [**8**] or by specifying desired maximum overshoot (M_P) and settling time ($t_{s,2\%}$) which can then be used in the following relationships to determine both the natural frequency (ω_n) and damping ratio (ζ) [**15**]:

$$M_p = exp\left(-\pi\zeta/\sqrt{1 - \zeta^2}\right) \quad \text{Eq. 4-10}$$

$$t_{s,2\%} = {}^{4}/_{\zeta\omega_n} \quad \text{Eq. 4-11}$$

The tuning of PID controllers via the specification of desired time domain performance does introduce some complications, most notably that it is difficult to choose the optimal rise (by implication overshoot value) and settling times. Selecting too small times will lead to unstable solutions, while too large times may lead to sub-optimal operation. The correct selection therefore, requires either in depth process knowledge and experience or various trial and error selections. The latter implies extensive testing and is more suitable when a simulation environment is possible, while the first option provides no guarantee that an optimal solution has been found.

4.1.2 Ciancone tuning rules

The time domain performance specification discussed in the above section works well for systems where there is no significant time delay. To overcome process dead time, the time specifications may be relaxed until stable operation is observed. This does, however, require a strong iterative inspection approach where the specifications are consistently detuned until stable operation is observed. There is, however, no guarantee that a stable solution will be found that still offers acceptable control of the process. Another option is to use one of many established tuning rules, including those defined by Ziegler-Nichols or the Ciancone tuning rules [**8**].

Zeigler-Nichols rules determine at which frequency and amplitude ratio a system will become unstable and then adjusts the controller gains to keep the process below these limits. The Ciancone rules use a dimensionless term that incorporates both the process time (τ) constant and dead time (Θ), the fraction dead time ($\Theta/(\Theta + \tau)$), to characterize the process dynamics. The fraction dead time is then used to correlate the controller gain and integral time. This correlation is demonstrated in Figure 4-2 below. Note that, the terms on the y-axes in each of the graphs contain a controller parameter (either K_C or T_i); the value of the whole term is then read off the graph by using the corresponding calculated fraction dead time.

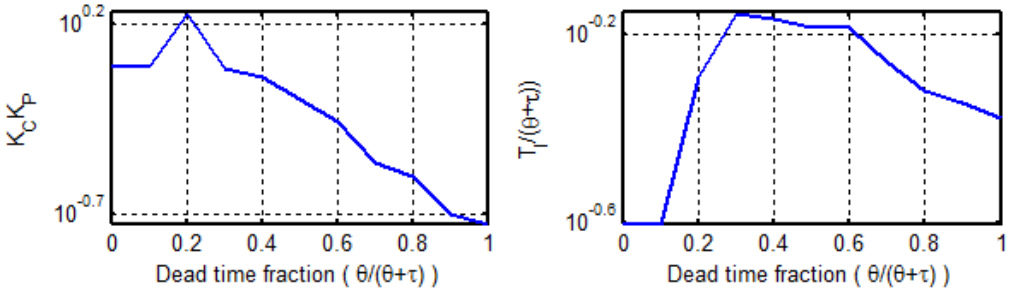

Figure 4-2: Ciancone correlation for disturbance rejection, redrawn from [35**]**

It should also be noted that the Ciancone rules offer a distinction between tuning for set point tracking and disturbance rejection. This allows one the freedom to optimise the PI controller for a certain process.

4.1.3 FFE PI control in literature

Winchester [**5**] and Paramalingam [**2**] tested PI based control for dairy FFEs and found it adequate to reject disturbances when regulating the effect temperature. However, it was found inadequate when rejecting dry mass disturbances inside the product dry mass control loop. Both Winchester [**1**] and Paramalingam [**2**] found that the falling film delays, coupled with the high level of product concentration, prevented adequate disturbance rejection. Winchester [**5**] measured the

performance by introducing a fraction step of 0.01 in feed dry mass fraction (W_F) and assuming control to be adequate if it could successfully maintain any product dry mass fraction ($W_{P)}$ deviation below fractional increase of 0.01 (note that the gain from W_F to W_P is greater than one).

The widespread use of PID control in the dairy industry [**16**] can be attributed to the complexity and high costs associated with advanced control solutions [**6**] as well as the relative ease of tuning and robustness that the PID algorithm provides. In addition to the full PID controller, simplified versions such as only a proportional integral (PI) controller exist.

4.2 State Space control

While PI control may be very effective for simple systems, the solutions can become quite involved for a multi-input multi-output (MIMO) system where multiple control loops need to be designed and tuned. The difficulties become even more pronounced if there exists significant interaction between the loops. In this situation, loop decoupling is required, where the action of a controller is limited to specific control variables. Another solution is to look at the system as a whole instead of breaking it up into smaller parts – the combined controller can then use all of the manipulated variables available to perform control actions. State space representation aims to perform this unification by converting the system to a vector space; this also allows one to take advantage of relatively simple matrix algebra for control design purposes.

4.2.1 Converting a system into state space

There are many ways to produce state space representations [**15**]; one method converts transfer functions into the time domain and then into state space matrices. This solution requires the transfer functions to be additive, i.e. their actions can be summed to produce the process action. The general form for the discrete state space SISO model is shown below [**17**]:

$$\boldsymbol{x}(k+1) = \mathbf{F}\boldsymbol{x}(k) + \mathbf{G}u(k) \qquad \textbf{Eq. 4-12}$$

$$y(k) = \mathbf{H}\boldsymbol{x}(k) + Ju(k) \qquad \textbf{Eq. 4-13}$$

Where **x***(k)* represents the current state of the system with (n x 1) elements for an nth order system, **x(***k+1***)** the state update, **F** the system matrix (n x n), **G** the input matrix (n x 1), **H** the output matrix (1 x n), J a direct transmission scalar, u*(k)* (nx1) the input vector and y*(k)* (nx1) the output vector.

There is also an equivalent continuous form, where **x**(*k*+1) is replaced by $\dot{\mathbf{x}}(t)$ and the matrices **F, G** and **H** replaced by the corresponding **A, B** and **C** matrices. The method of conversion from transfer function to state space is shown below for first order transfer functions; note that higher order functions can also be converted by using intermediate dummy variables. One starts with rewriting the transfer function, Eq. 4-14 with *r*(*t*) (R(s)) and u(*t*) (U(s)) the output and input variables respectively, into the time domain (Eq. 4-16) and then rearranging (Eq. 4-17):

$$G_p(s) = \frac{R(s)}{U(s)} = \frac{K_{pr}}{\tau s + 1} \quad \text{Eq. 4-14}$$

$$\therefore \ \tau \cdot s \cdot R(s) + R(s) = K_{pr} \cdot U(s) \quad \text{Eq. 4-15}$$

$$\tau \frac{dr}{dt} + r = K_{pr} \cdot u(t) \quad \text{Eq. 4-16}$$

$$\frac{dr}{dt} = -{}^{1}/_{\tau} \cdot r + {}^{K_{pr}}/_{\tau} \cdot u(t) \quad \text{Eq. 4-17}$$

The form of Eq. 4-17 is analogous to the continuous state space representation of a single-input single-output (SISO) system, with:

$$\dot{x} = \frac{dr}{dt} \qquad x = r \qquad A = {}^{-1}/_{\tau} \qquad B = {}^{K_{pr}}/_{\tau} \qquad C = 1 \qquad D = 0$$

This continuous form can be converted to discrete form using relationships defined by Franklin et al. [**17**].

4.2.2 Designing an optimal state space controller

With the system represented in discrete state space form, multiple well-established control methods become possible. Generally a state space controller uses both state feedback ($\mathbf{K}_x$) and integral ($\mathbf{K}_i$) terms. A typical Simulink setup for such a controller is shown below:

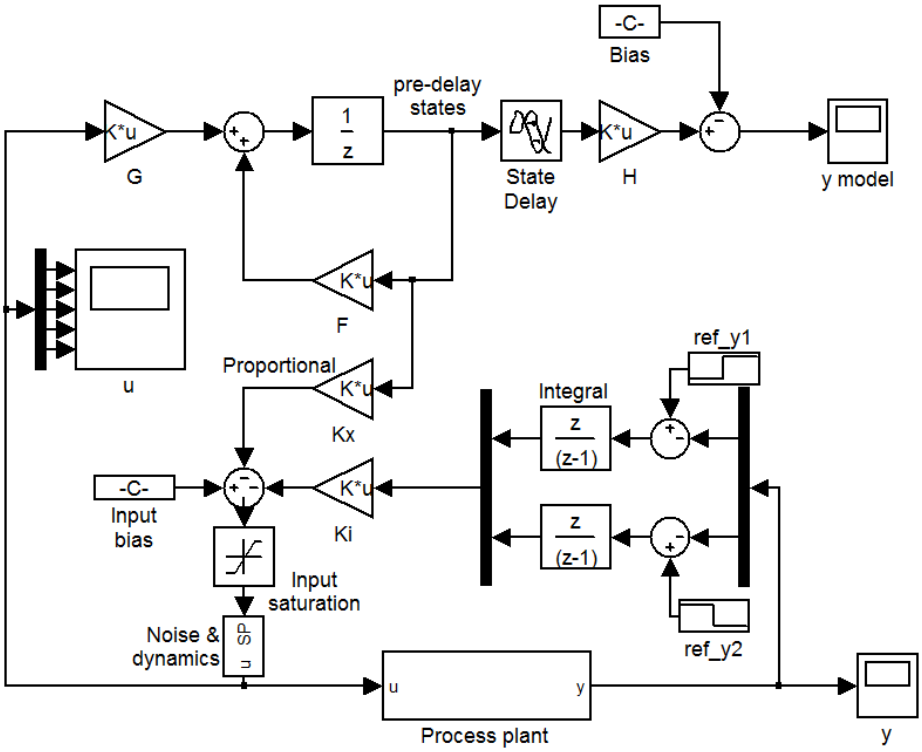

Figure 4-3: General state space controller setup in Simulink

As with SISO transfer functions, it is possible to specify system poles using rise times as well as damping factors to calculate the combined controller gain **K** ($\mathbf{K}_x$ and $\mathbf{K}_i$). For a MIMO system, one can

either specify each pole or place the most important poles at specified locations and the other poles at frequencies that will not affect the final control. It is, however, possible to more generally specify the required dynamics of the system using optimal controls strategies. The focussed optimal strategy for this research will be the linear quadratic regulator (LQR).

The basis of LQR solutions is the defining, and subsequent minimisation, of a cost of control function (J). This cost can be quantified by formulating a function comprised of control effort and state deviations [**17**]:

$$J = \frac{1}{2}\sum_{k=0}^{N}[\mathbf{x}^T\mathbf{Q}_1\mathbf{x} + \mathbf{u}^T\mathbf{Q}_2\mathbf{u}] \qquad \textbf{Eq. 4-18}$$

By adjusting the weighting **Q** matrices one can specify how aggressively each state is altered while also choosing how to use the manipulated variables. Numerical software suites such as Matlab can then solve **K** to minimise J.

4.3 Fuzzy control

Also called fuzzy linguistic control, fuzzy control relies on defining all variables and actions in grey rather than absolute terms. The control rules generally take an IF-THEN form as shown below [**18**] (with *x* and *y* representing the input and output respectively; *A* and *B* a condition of *x* or *y*):

$$\text{IF } (x = \text{A}) \text{ THEN } (\text{y} = \text{B})$$

Fuzzy inference rules allow the condition to be vague, i.e. terms such as large or small are frequently used. This level of vagueness is what makes fuzzy systems unique when compared to the other selected techniques. PI control is based primarily on the error and dynamics of a system, both in absolute terms. LQR control employs complex algorithms to find a mathematical optimal solution, where-in each matrix is calculated to precise values. In contrast, fuzzy inference rules require only that the variables are fuzzy, before general rules may be specified.

4.3.1 Fuzzification and defuzzification

Before fuzzy rules may be used, fuzzification is performed (all the relevant variables are converted into fuzzy variables). The new variables are defined by membership functions such as negative, zero and positive. The membership functions for an arbitrary normalised variable may be defined as:

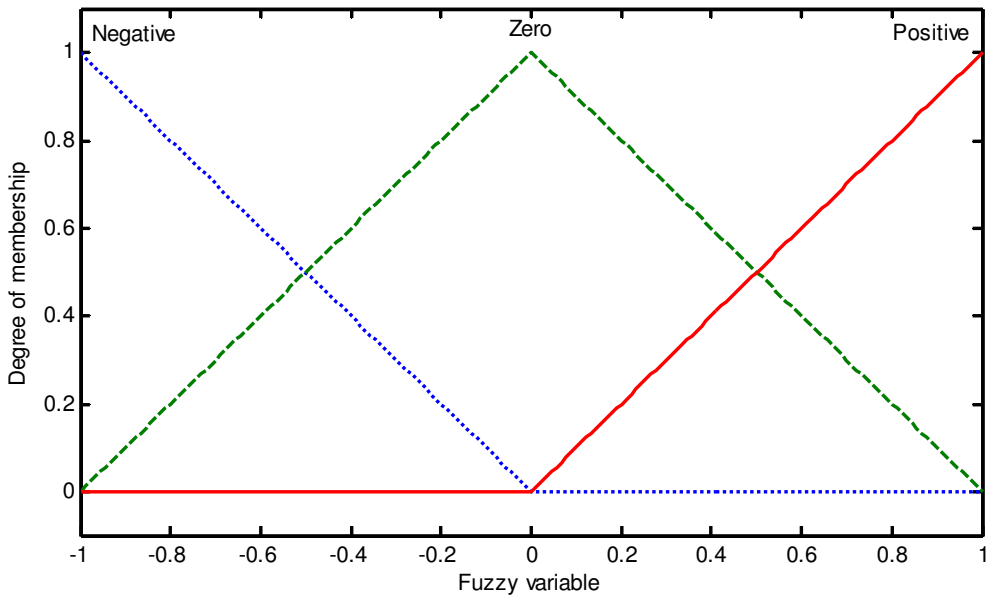

Figure 4-4: General fuzzy variable structure

Note that the functions depicted in Figure 4-4 above overlap, therefore the variable can be both positive and zero at certain values. Although this seems counter intuitive at first, it is a logical realisation of fuzziness, i.e. there is no clear boundary between zero and negative. Therefore a value of 0.1 in the figure above is more negative than a value of 0.3, which is both somewhat negative and somewhat zero.

In practise a rule for each region will be specified, with the result determined from defuzzification - where all the independent membership function IF-THEN rule results are combined to form one action. There are various ways to combine the input membership functions into an output value [**18**].

4.3.2 Fuzzy controller structure

There are various forms of fuzzy controllers; some mimic the PI controller [**19**] to gain the same level of robustness and applicability. Other forms are more static and directly relate the input variables to desired outputs without any error term. These basic forms can also be modified by adding predictive capabilities to increase the effectiveness of fuzzy control on processes with large dead times [**20**] [**21**]. The reader is referred to Kosko [**18**] for a more in-depth fuzzy control discussion and Foley [**22**] for recent application to FFEs.

Chapter 5 - Milk concentration falling film evaporator modelling

The falling film evaporator (FFE) consists of multiple smaller processes, as shown in Figure 3-1, that are dependent both on the overall process condition as well as each part within. Creating advanced control solutions require in depth knowledge of the relevant process and its internal dynamics. Once the controller has been designed, it needs to be validated on the real process. This is problematic on large scale industrial units as production losses, resulting from downtime or ineffective operation, have large financial implications.

Effective modelling may reduce the amount of tests needed on the real process plant by ensuring that the controller design is as close to the final version as possible. Before the controller is implemented, various tuning, stability and optimisation simulations can provide an accurate estimation of real world controller performance.

As stated in the introduction, falling film evaporators (FFE) are the most common form of milk concentration in the multi-billion euro European dairy industry. Literature on the modelling of dairy FFE modelling is, however, fairly sparse (as reported by both Winchester [**1**] and Cunningham [**23**]). Winchester [**1**] suggests that the lack of adequate models might be because of the distributed nature of the falling film process. Parameters change along the length of the tube as well because of varying film thickness. It is also interesting to note that some of these difficulties have been overcome in other industries, for example in paper and pulp black liquor concentrating FFEs [**24**] where the distributed nature of the falling film has been included in the models. These inclusions would need to be re-evaluated while taking into account the nature of milk as a process fluid, before the methods could be included in a dairy simulation model.

There have, however, been successful fundamental models reported in literature [**3**], [**1**]. These models have been used extensively for control [**2**], [**5**]. The fundamental approach given in Section 5.2 is an adaption and accumulation of the tested literature models.

In contrast to the fundamental models there are also applications of data-based modelling for FFEs. Data based modelling identifies the relationship between input and output variables without the need of detailed process knowledge [**25**]. This identification is done by creating generic model structures which can then be fitted to the given process through parameter changes.

The simplest data based method that will be investigated is the use of transfer functions. If a system displays dominant first or second order response to input stimuli (see Section 5.1) and does not show change over time, transfer functions often provide very good representations.

Another option is to use least-square autoregressive with exogenous inputs (ARX) modelling [**25**] [**4**]. For ARX modelling, a general equation is set up where the current output is defined by the previous inputs and outputs, multiplied by a fixed constant vector. ARX modelling lends itself better to computer parameter estimation, compared to transfer function modelling which works best with simple step tests.

Finally advanced data based models, such as artificial neural networks (ANN), have also been applied with success to the FFE modelling problem [**4**] [**26**]. ANNs emulate the structure of a biological brain by defining neurons that accumulate and combine inputs to map a certain input space to an output space. Training occurs by updating both the connections of each neuron as well its output weights,

usually performed by sophisticated training algorithms. Although these networks have been applied to FFEs, the relevant systems were only run on water and as such the full complexity was not observed.

The rest of this section provides a review of two common techniques, i.e. transfer function and fundamental modelling as well as look at previous research relating to the techniques. ANN were left out of the review as both transfer function and ARX modelling showed comparable or adequate results in previous studies [**25**], [**4**].

5.1 Transfer function modelling

A transfer function is defined as the mathematical representation of the input/output relationship of a linear time invariant system in the Laplace domain [**27**]. The output of any process can be described as a function of the inputs acting on the process as shown in Figure 5-1 below:

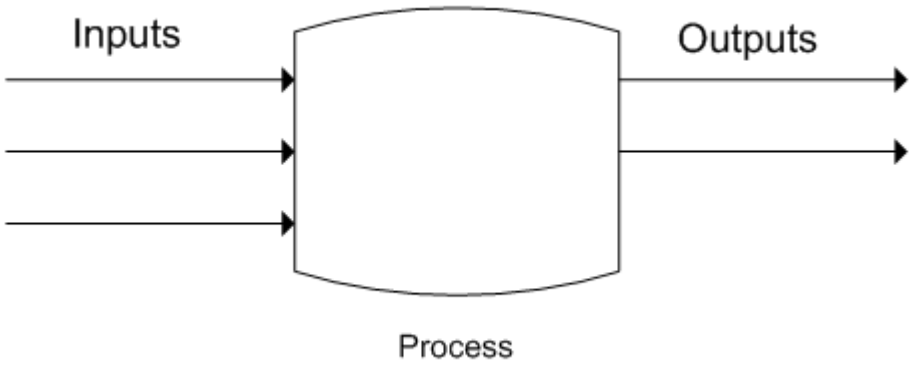

Figure 5-1: Process shown as input/output relationship

General first and second order transfer functions are shown below (Eq. 5-1 and Eq. 5-2):

$$G_1(s) = \frac{Y(s)}{U(s)} = \frac{K_{pr}}{\tau_{pr}s + 1} \quad \textbf{Eq. 5-1}$$

$$G_2(s) = \frac{Y(s)}{U(s)} = \frac{\omega_n^2}{s^2 + 2\zeta\omega_n s + \omega_n^2} \quad \textbf{Eq. 5-2}$$

Where	Variable	Description
	$G_1(s)$	First order transfer function
	$G_2(s)$	Second order transfer function
	$U(s)$	Laplace domain inputs
	$Y(s)$	Laplace domain outputs
	K_{pr}	Process gain
	τ_{pr}	Process time constant (s)
	ω_n	Natural frequency (rad/s)
	ζ	Damping factor

The advantage of these general forms are that the dynamics of most chemical processes may be represented by tuning the parameters of the above equations. Transfer functions can be obtained by

optimal curve fitting of the above equations to experimental data or by performing step tests with input variables and correlating the output to general response curve

5.1.1 System identification using step inputs and transfer functions in literature

As stated previously, Cunningham [**23**] developed transfer functions for an industrial FFE situated in Cork, Ireland with the aim tuning existing PID control or implementing model predictive control. The lack of other comprehensive and validated models available in literature was given as motivation for the study. The Cork facility consisted of two evaporative effects, effluent condenser, pre-heaters, a balance tank and separators.

Note the absence of any vapour compression and recirculation unit. Otherwise the process is similar to the one described in section 3.1. One can therefore assume that the underlying dynamics of the two processes will be similar. As such, if transfer functions could successfully be obtained for the Cork process it may be suitable when modelling any FFE.

The Cork FFE can be represented in terms of the most important discrete transfer functions listed below. Note that the above functions are a discrete equivalent of the Laplace transfer functions of the form seen in Eq. 5-1, found using the z-transform [**8**]. The discrete function are characterised by the use of (z) as opposed to the Laplace domain:

- $G_S(z)$ - Effect of steam valve position on evaporation temperature
- $G_W(z)$ - Effect of condenser cooling water valve position on evaporation temperature
- $G_P(z)$ - Effect of steam valve position on pasteuriser temperature
- $G_D(z)$ - Effect of pre-pasteurisation temperature on pasteuriser temperature

Cunningham [**23**] attempted to identify the four transfer functions shown above. Note that the product dry mass was not included, most likely due to its interdependence on evaporator temperature (refer to Section 3.1). These transfer functions can also be shown in block diagrams:

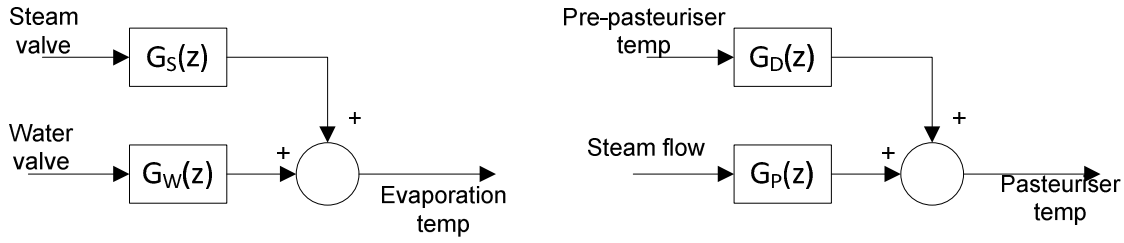

Figure 5-2: Block diagrams for evaporation and pasteuriser temperatures

Cunningham [**23**] initially proposed to use available historical data to regressively fit first order transfer functions to various subsections shown above. The cross correlation of the variables was investigated to determine whether they were sufficiently independent to use for modelling. It was concluded that, because of the control present on the FFE, the input variables changed in a highly correlated manner. Therefore the data collected under normal operation proved insufficient to extract each subsection model. It is not clear, however, which method of curve fitting was used or how far the models would deviate from reality if a large data set were to be used.

To create uncorrelated input variables experiments with manual set point changes were performed to obtain a more representative data set. All process variables were kept as constant as possible while a step was introduced onto a variable. The process output can then be regressively fitted to either Eq. 5-1 or Eq. 5-2. The models gained using the Matlab System Identification toolbox are given below in Table 5-1:

Table 5-1: Transfer functions for selected processes as reported by Cunningham [23] (10s sampling period)

Model	K_{pr} standard deviation($x10^{-3}$)	τ_{pr} standard deviation($x10^{-3}$)
$G_P(z) = \frac{0.078}{z-0.91} z^{-16}$	±10.33	±0.702
$G_D(z) = \frac{0.045}{z-0.93} z^{-1}$	±12.57	±0.105
$G_W(z) = \frac{-0.0089}{z-0.93} z^{-1}$	±0.2916	±0.332
$G_S(z) = \frac{0.0199}{z-0.92} z^{-1}$	±2.73	±0.017

These models have some restricting assumptions inherent when using first order transfer functions, namely that the system is linear time invariant (LTI) and relaxed [**27**] (output of the system constant at initial time). The models in Table 5-1 were all tested on new data sets to assess whether there are any non-linearities which would invalidate the LTI assumptions. The data sets were generated with step changes as shown in Table 5-2:

Table 5-2: Step validation tests performed [23]

Model	Estimation step	Validation step
$G_P(z)$	70°C to 75°C	75°C to 65°C
$G_W(z)$	76.1°C to 60°C	60°C to 75°C

Although Cunningham [**23**] showed that the models yielded good predictions with both additional tests, the data sets themselves raise some doubts not identified by the author:

- The validation sets consisted of step input changes rather than normal operating data with all the variables active. This means that variable interactions and different operating regions were not fully tested.
- The steps used were very similar to the steps from which the models were extracted. Again pointing to the same operating region.
- All the data sets span short operation periods, which is insufficient to rule out time varying dynamics.

The review of Cunningham et al. (2006) shows the worth of transfer functions and the value in not complicating system identification. It should be noted that the validation experiments were far from conclusive. Finally, the effect of recycling steam and vapour in thermo-compressor may introduce further complexities which may affect the LTI assumption. Therefore, although transfer functions may work well, the overall suitability for the local FFE modelling is not assured.

5.2 Fundamental modelling

Transfer function and neural network modelling are experimental data based techniques; fundamental modelling on the other hand requires no experiments and can be developed without any real world process data (although this is not recommended). The trade-off lies in increased developing time as well as the in-depth process knowledge required to apply fundamental laws such as the conservation of both mass and energy correctly. These models are expressed as differential and state equations for each relevant process unit, thereby giving useful insight into the variable relationships which the data driven models investigated in this study do not provide.

The FFE described in Section 3.1 is shown as a flow diagram below in Figure 5-3:

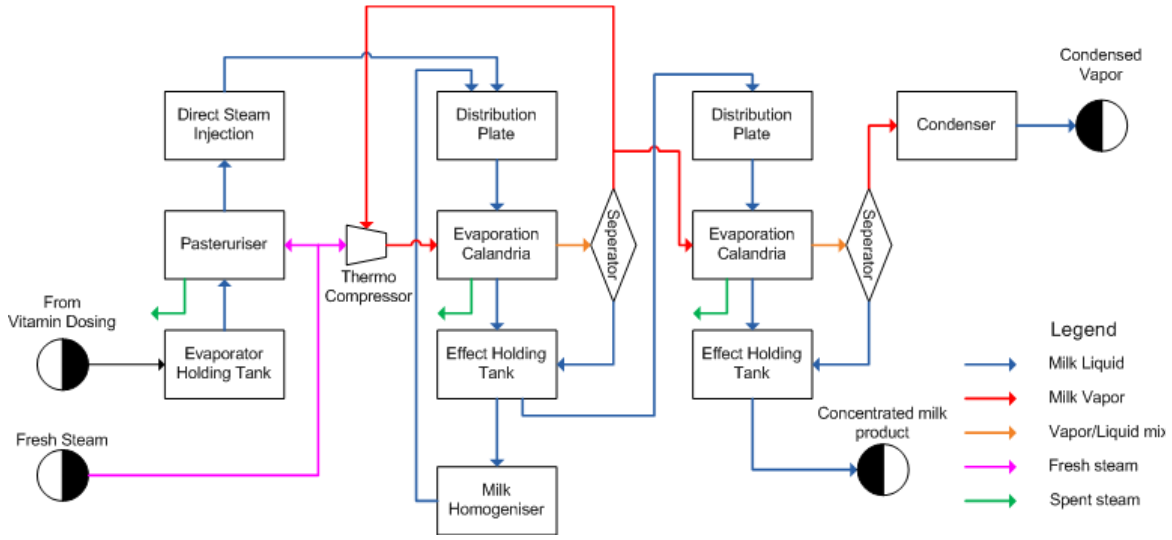

Figure 5-3: Flow diagram of evaporator effects and pasteuriser

Each unit on the flow diagram requires a set of equations describing the dynamic behaviour during operation. As explained in Section 3.1, the pasteuriser, homogeniser and DSI units already have adequate control solutions; the set points of the controllers are also independent of the evaporator effects during normal operation. Therefore they are not included in the overall model to reduce unnecessary complexities. Section 5.2.1 to 5.2.4 review each major unit and describes the differential equations governing their dynamics.

5.2.1 Distribution plate

Before the milk enters the evaporator effect it is kept at high temperature and pressure inside the holding tubes. As the effects are kept under partial vacuum a back pressure valve is required to ensure that the milk is fed at a uniform rate. The back pressure valve consists of a movable membrane that is pressed against a throttling valve (see Figure 5-4) via utility air pressure. The milk can therefore only flow into the FFE at elevated pressure while also ensuring that no back flow is possible.

Also note that the flow rate must be low enough to prevent the fluid from flooding the distribution plate and flowing over the fluid risers seen in Figure 5-5. Lastly as the milk enters the FFE it is suddenly exposed to low temperature and pressure surroundings which causes a portion of the milk to instantly flash.

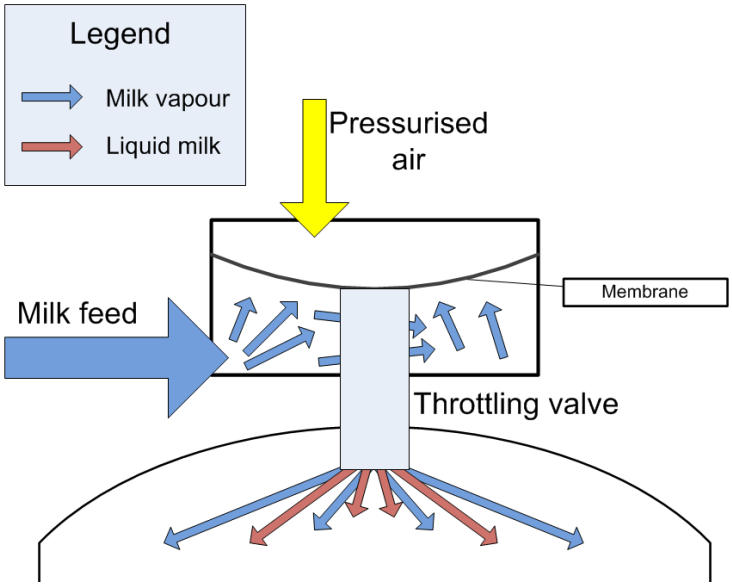

Figure 5-4: Back pressure valve

The remaining liquid flows over a strainer before falling onto the distribution tray from where it enters the falling film tubes as a thin film clinging to the sides as shown in Figure 5-5 below:

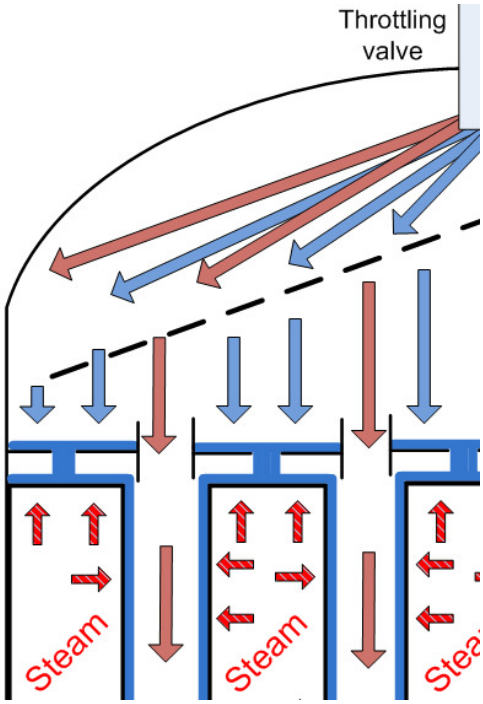

Figure 5-5: Distribution Plate

Liquid flashing above the distribution plate can be assumed to take place until the liquid milk has cooled to the effect temperature [**2**]:

$$m_{flash}(t) = \frac{m_{feed}(t) \cdot c_{p,feed}\left[T_{feed}(t) - T_e(t)\right]}{\lambda} \qquad \textbf{Eq. 5-3}$$

Where	$m_{flash}(t)$	=	Mass flow of milk flashed	kg/s
	$m_{feed}(t)$	=	Feed mass flow rate	kg/s
	$c_{p,feed}$	=	Milk heat capacity	J/(kg.°C)
	$T_{feed}(t)$	=	Temperature of feed	°C
	$T_e(t)$	=	Effect temperature	°C
	λ	=	Latent heat of vapourisation	J/kg

Although the flash term has been omitted by other authors [**3**] [**5**] it will contribute both to the outgoing dry mass fraction and liquid level above the distribution plate (which is in the order of a few millimetres) shown below in Eq. 5-4:

$$\frac{dh_d}{dt} = \frac{m_{feed}(t) - m_{flash}(t) - m_{dist}(t)}{A_d \rho_d} \quad \textbf{Eq. 5-4}$$

Where	h_d	=	Height of liquid above distribution plate	m
	$m_{dist}(t)$	=	Mass flow of liquid leaving the distribution plate	kg/s
	A_d	=	Area of distribution plate	m^2
	ρ_d	=	Density of milk leaving the distribution plate	kg/m^3

Eq. 5-4 assumes perfect mixing and constant density of the liquid holdup which is justified by the small liquid volume and absence of any further evaporation. Next the flow through the distribution plate is defined along with the dry mass fraction [**2**] [**28**]:

$$m_{dist}(t) = \rho_d c_d A_h \sqrt{2 g h_d(t)} \quad \textbf{Eq. 5-5}$$

$$\frac{dw_d}{dt} = \frac{m_{feed}(t) \cdot \left[w_f(t) - w_d(t)\right] + m_{flash}(t) \cdot w_d(t)}{h_d(t) \cdot A_d \cdot \rho_d} \quad \textbf{Eq. 5-6}$$

Where	c_d	=	Distribution plate discharge coefficient	(-)
	A_h	=	Area of the distribution plate holes	m^2
	g	=	Gravity coefficient	$kg/m.s^2$
	$w_f(t)$	=	Feed dry mass fraction	(-)
	$w_d(t)$	=	Dry mass fraction of liquid leaving distribution plate.	(-)

Eq. 5-5 was derived from the Bernoulli equation under the assumptions of small orifice and isobaric conditions [**29**]. Paramalingam [**2**] proposed the addition of the distribution plate height to the liquid height to account for the extra potential energy. As there is uncertainty regarding the exact value of the orifice plate discharge coefficient (c_d) this addition can be lumped with other uncertain parameters.

5.2.2 Energy balance surrounding evaporation effect

Even though some concentration happens with flashing as the milk enters the effect, virtually all the concentration takes place inside the tubes of the evaporation calandria. TVR compressed steam and/or process vapour supply heat through the tube walls.

Energy Balance: Evaporation effect

Starting with the First Law of thermodynamics using enthalpy relationships, neglecting potential and kinetic energy and assuming constant volume for simplification, Eq. 5-7 is found [**1**]:

$$\frac{d[M.H]}{dt} = \sum_{k=1}^{K} M_k H_k + q + W_s \qquad \textbf{Eq. 5-7}$$

Where	M	=	Mass contained within the system envelope	kg
	H	=	Enthalpy contained within the system envelope	J/kg
	M_k	=	Mass flowing into or out of envelope	kg/s
	H_k	=	Enthalpy of the mass flow crossing envelope boundaries	J/kg
	q	=	Net heat flow into the envelope	W
	W_s	=	Net work done on the envelope	W

Eq. 5-7describes the possible reasons for a change in energy of a fluid system, i.e. sum of incoming and outgoing streams ($\sum M_k H_k$), heat transferred over system boundaries (Q) and work done by or to the system.

Taking an energy balance envelope around the evaporation section, i.e. flash chamber, distribution plate, tubes, all the metal/liquid/vapour in the effect and shell of next effect (vacuum condenser shell for the second effect) as shown below in Figure 5-6:

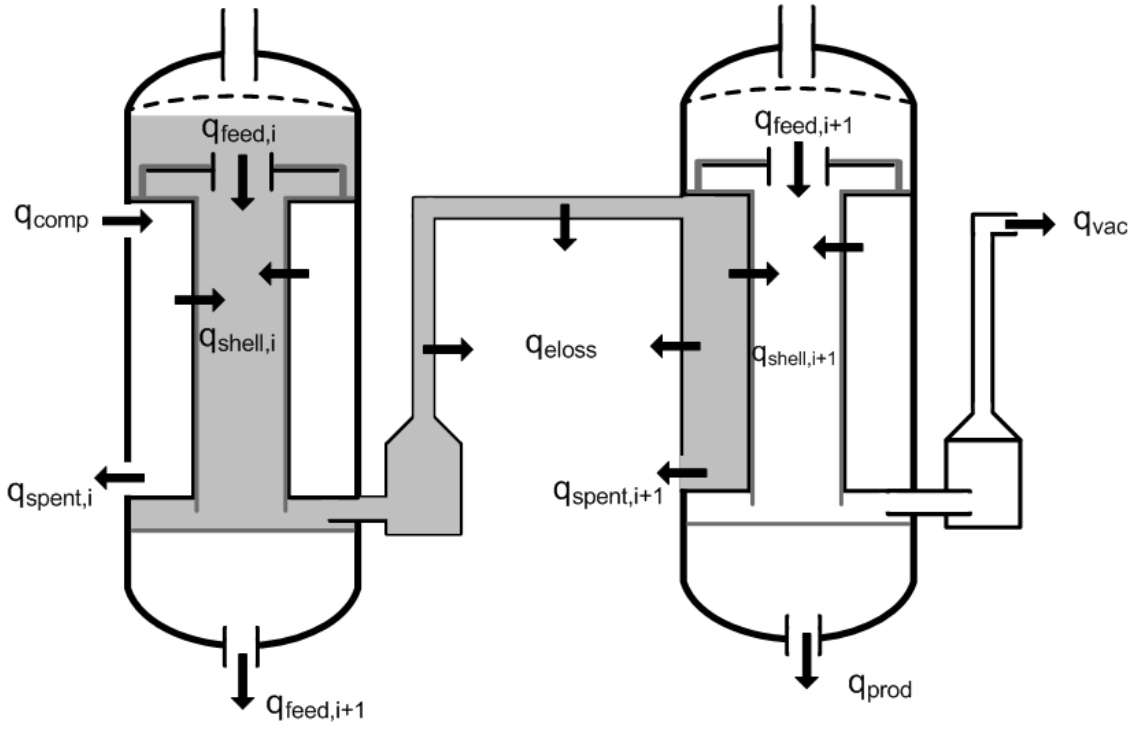

Figure 5-6: Evaporation energy balance envelope

Enthalpy enters the effect through the feed milk and is removed by milk vapour, concentrated liquid milk exiting the effect and condensate leaving the next effect (or condenser). The heating vapour/steam supplies energy from the shell side to the tube side. Heat is removed via the next

effect (or condenser) and some external losses. Eq. 5-8 below describes all the enthalpy and mass flows [**1**] [**2**]:

$$\frac{d[m_{met}c_{p,met}T_{e,i}]}{dt} = m_{dist,i}c_{p,TS}T_{feed,i} + q_{shell,i} - m_{comp}\left(c_{p,water}T_{e,i} + \lambda\right) - m_{cond,i+1}C_{p,water}T_{e,i} - q_{shell,i+1} - q_{eloss,i} - m_{product,i}C_{p,TS}T_{e,i} \quad \textbf{Eq. 5-8}$$

$$\dot{m}_{product,i} = m_{dist,i} - m_{comp} - m_{cond,i} \quad \textbf{Eq. 5-9}$$

$$m_{product,i} \cdot \omega_{e,i} = m_{dist,i} \cdot \omega_{d,i} \quad \textbf{Eq. 5-10}$$

Where	$T_{e,i}$	=	Temperature of ith effect	(°C)
	m_{met}	=	Mass of metal in effect	(kg)
	$c_{p,met}$	=	Heat capacity of metal	(J/kg.°C)
	$m_{dist,i}$	=	Mass flow from distribution plate	(kg/s)
	$c_{p,TS}$	=	Adjusted heat capacity of milk	(J/kg.°C)
	$T_{feed,i}$	=	Temperature of feed to ith effect	(°C)
	$q_{shell,i}$	=	Heat transfer from shell to tube of effect	(W)
	m_{comp}	=	Mass flow diverted to thermo recompressor	(kg/s)
	$c_{p,water}$	=	Heat capacity of water	(J/kg°C)
	λ	=	Latent heat of vapourisation	J/kg
	$m_{cond,i+1}$	=	Mass flow of condensed vapour on shell side of the next effect	(kg/s)
	$q_{shell,i+1}$	=	Heat transfer to shell of next effect	(W)
	$q_{eloss,i}$	=	Heat loss to surroundings from effect	(W)
	$m_{product,i}$	=	Mass flow of concentrated milk exiting effect	(kg/s)

For the second effect $q_{shell,i+1}$ becomes q_{vac} (heat transfer to condenser) and the m_{comp} term falls away as no vapour is directed towards the TVR compressor. Eq. 5-8 is similar to that found in other dynamic FFE models [**3**] [**30**] and can be further simplified to Eq. 5-11 [**1**]:

$$I_{effect,i}\frac{dT_{e,i}}{dt} = q_{feed} + q_{shell,i} - q_{comp} - q_{shell,i+1} - q_{eloss,i} \quad \textbf{Eq. 5-11}$$

Where	$I_{effect,i}$	=	Thermal inertia of metal/liquid/vapour in effect	(J/°C)
	q_{feed}	=	Net enthalpy from the feed milk to the effect	(W)
	q_{comp}	=	Latent enthalpy of vapour removed to TVR	(W)

The use of $q_{shell,i+1}$ (or q_{vac} for the second effect) implies that the balance envelope is taken over a perfectly mixed system as the removal of heat in the next effect can change the upstream effect temperature ($T_{e,i}$) immediately (actual mechanism proposed on following page).

Looking at the second effect, Eq. 5-11 would show that an increase in heat removal inside the condenser would also lower $T_{e,2}$. However taking an energy balance envelope over the condenser, as shown in below in Figure 5-7, an increase in q_{vac} would only further cool the condensed fluid stream and should not affect the hot vapour from the second effect.

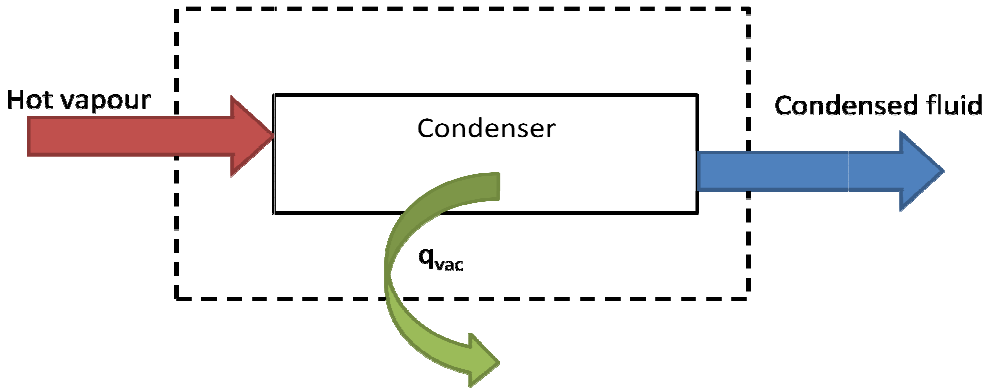

Figure 5-7: Energy balance surrounding the condenser

Yet, Eq. 5-11 (or a similar form thereof) has been used and compared to actual process data by various different authors [**30**] [**2**] [**1**] [**4**] and found to adequately capture the influence of the condenser on the falling film evaporator.

The mechanism by which the downstream condenser (or effect) influences the current effect is more complex than Eq. 5-11 implies. Both effects are operated under a partial vacuum to reduce the boiling point temperature of milk (preventing heat damage). At any given pressure the boiling point remains constant; assuming the heat transfer from the shell side is sufficient the milk will always be at boiling point. If q_{vac} is increased more vapour will condense, lowering the pressure slightly, which in turn will push the boiling point further down. The milk temperature inside the tubes will follow this downward trend and the whole effect temperature will decrease. In conclusion, the end result is the same as shown by Eq. 5-11, therefore, although the mechanism differs, the use of q_{vac} can be seen as an adequate simplification.

Energy Balance: TVR Shell

Once again Eq. 5-7 is used to describe a mass and energy balance around the TVR shell. The TVR provides enthalpy through fresh steam mixed with milk vapour drawn from the first effect while the shell condensate removes enthalpy. Heat is transferred to the tubes for evaporation while some heat is lost to the environment. After simplification the balance is shown as Eq. 5-12 below [**1**]:

$$I_{shell,i}\frac{dT_{s,i}}{dt} = q_{comp} + W_{comp} - q_{shell} - q_{cond} - q_{sloss,i} \qquad \textbf{Eq. 5-12}$$

Where	$I_{shell,i}$	=	Thermal inertia of metal/liquid/vapour in effect	(J/°C)
	$T_{s,i}$	=	Temperature ith effect shell	(°C)
	q_{comp}	=	Latent enthalpy of vapour removed to TVR	(W)
	W_{comp}	=	Net enthalpy of steam entering the TVR	(W)
	q_{cond}	=	Net enthalpy in condensed steam leaving shell side	(W)
	q_{shell}	=	Heat flow from the shell to tube side of effect	(W)
	$q_{sloss,i}$	=	Heat loss to surroundings from shell	(W)

As with Eq. 5-11 the thermal inertia is assumed to be dominated by the metal of each effect.

Mass balance: Falling film

The distributed nature of the falling film gives rise to complex parameters, especially with respect to heat transfer coefficients. As milk flows down the tube the film starts off relatively thick and thins out as more liquid is lost to evaporation. The opposite is true on the shell side where the surface starts off with no condensed steam at the top and thickens towards the bottom as more steam condenses to a liquid. The varying heat transfer distance gives rise to a non-uniform heat transfer coefficient.

Furthermore, uneven bubble formation and/or fouling inside the tubes create both random and systematic deviations in the expected coefficients. Combined with varying falling film velocities and possible hot/cold zones inside the shell, the falling film differential equations [**2**] [**1**] become difficult to integrate. Yet if assumptions are made that these complicating factors are negligible, i.e. constant falling film velocity, uniform heat flow along tube wall and negligible thermal inertia, a relatively simple set of equations is found as shown below:

$$m_e(t) = m_d(t - \tau_e) - m_{tubes}(t) \qquad \textbf{Eq. 5-13}$$

$$\frac{dm_{tubes}}{dt} = \frac{q_{shell}(t) - q_{shell}(t - \tau_e)}{\lambda \cdot \tau_e} \qquad \textbf{Eq. 5-14}$$

$$\tau_e = {}^{L}/_{v_{ff}} \qquad \textbf{Eq. 5-15}$$

$$w_e(t) = \frac{\dot{m}_d(t - \tau_e) \cdot w_d(t - \tau_e)}{m_d(t - \tau_e) - m_{tubes}(t)} \qquad \textbf{Eq. 5-16}$$

Where	m_e	=	Mass flow rate at the bottom of the tubes	(kg/s)
	$\dot{m}_d$		Mass flow rate from distribution plate	(kg/s)
	m_{tubes}	=	Mass evaporation rate inside the tubes	(kg/s)
	q_{shell}	=	Heat transfer from shell side	(W)
	τ_e	=	Falling film residence time	(s)
	L	=	Length of tubes	(m)
	v_{ff}	=	Velocity of falling film	(m/s)
	w_e	=	Total solids fraction at the bottom of the tubes	-
	w_d	=	Total solids fraction from the distribution plate	-
	λ	=	Latent heat of vapourisation	(J/kg)

Eq. 5-13 to Eq. 5-16 are the same as reported by Quaak et al. [**3**]. There are typically more than a hundred tubes in each calandria, under tightly controlled operation. With regular cleaning, the effect of fouling on the film velocity may be eliminated. The assumption of constant heat transfer also does not require a constant heat transfer coefficient [**1**] as the thinner falling film towards the bottom of the tubes will to some extent negate the thickening of the condensate film on the shell side. Furthermore, the heat transfer coefficients are all approximate and small changes may not influence the dynamics of the model greatly.

5.2.3 Thermal vapour recompression

TVR compressors provide a simple robust solution to increase the volume of the heating medium available. There are no moving parts and a small unit can process large volumes as shown below in Figure 5-8:

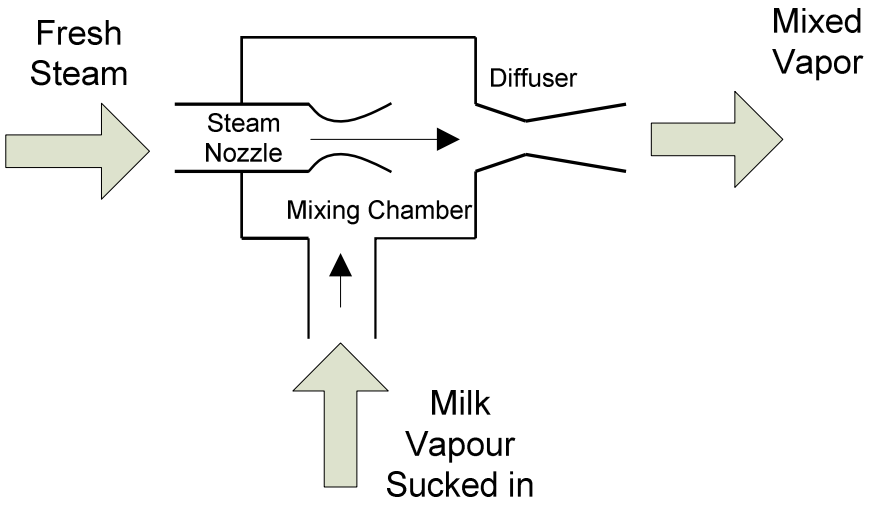

Figure 5-8: Thermal vapour compressor

Referring to Figure 5-8, high pressure steam enters at the steam nozzle where it accelerates before reaching the mixing chamber. The high velocity steam entrains milk vapour, losing some momentum. The internal structure directs the entrained flow towards the diffuser. As the mixed steam exits through the diffuser, the high velocity is converted to back into pressure. The amount of low pressure milk vapour entrained depends on the steam pressure and nozzle structure. The following section aims to quantify the flows and energy of the mixed steam.

Both Quaak [**3**] and Rusell [**4**] did not include TVR compressors in their modelling and as such Winchester [**1**] developed an empirical TVR model which was found to be superior to other fundamental models studied. Paramalingam [**2**] tested this model, but found it overestimated the amount of process vapour recycled. Another fundamental model [**31**] was also compared to that of Winchester [**1**] and found to accurately predict steam usage and process vapour flow rate as this model has a more general form as shown in Eq. 5-17 to Eq. 5-20 below [**2**]:

$$m_{comp} = \frac{A_{TVR} \cdot B_{TVR} \cdot P_{e1} \cdot P_s}{P_s^{C_{TVR}}} \quad \textbf{Eq. 5-17}$$

$$m_{steam} = A_{TVR} \cdot P_s \quad \textbf{Eq. 5-18}$$

$$W_{comp} = \left(H_{steam} - c_{p,water} \cdot T_s\right) m_{steam} \quad \textbf{Eq. 5-19}$$

$$q_{comp} = W_{comp} \cdot m_{comp} \quad \textbf{Eq. 5-20}$$

Where	m_{comp}	=	Mass flow of milk vapour pulled from effect	(kg/s)
	A_{TVR}	=	TVR compressor parameter	(m.s)
	B_{TVR}	=	TVR compressor parameter	($m^{0.03}.s^{0.06}/kg^{0.03}$)

C_{TVR}	=	TVR compressor parameter	-
P_{e1}	=	Pressure inside first effect	(s)
P_s	=	Steam pressure	(Pa)
m_{steam}	=	Mass of driving steam flowing to TVR	(kg/s)
W_{comp}	=	Work done by compressor	(W)
H_{steam}	=	Steam enthalpy	(J/kg)
$c_{p,water}$	=	Heat capacity of water	(J/kg°C)
T_s	=	Temperature of effect shell	(°C)
q_{comp}	=	Latent enthalpy of vapour removed to TVR	(W)

5.2.4 Condenser

The condenser action is considerably more complex than that of TVR and for simplicity a brief description is given. Refer to Winchester [**5**] and Paramalingam [**2**] for the full derivation:

$$\frac{dq_{cond}}{dt} = u_c A_c \frac{dT_{E2}}{dt} - \frac{1}{\tau_{TC}} q_{cond(t)} + \frac{u_c A_c}{\tau_c(t)} \left(T_{E2}(t) - T_{CW,i}\right) \quad \textbf{Eq. 5-21}$$

Where

q_{cond}	=	Heat flow to the condenser	(W)
u_c	=	Condenser heat transfer coefficient	(W/m$_2$°C)
A_c	=	Condenser tube surface area	(m^2)
T_{E2}	=	Second effect temperature	(°C)
τ_{TC}	=	Time constant within the condenser tubes	(s)
τ_c	=	Residence time of cooling water in condenser tubes	(s)
$T_{CW,i}$	=	Cooling water inlet temperature	(°C)

In the condenser the effluent vapour from the second effect is condensed using cooling water. Pressure waves move at the speed of sound and as such it is possible to control the second effect pressure (P_{E2}) by controlling P_C via changes in the cooling water flow rate (F_{CW}) and rate at which the condensed vapour is removed from the condenser. For the milk to evaporate in the effects the vapour pressure that can be exerted by milk must be greater than P_{E2}. Since vapour pressure is only influenced by temperature, T_{E2} can be controlled directly by controlling P_C.

The relationship between F_{CW}, condensate removal and P_C was determined empirically by Russel [**4**], yet not included in the report. As such a simplifying assumption is made that the heat removal inside the condenser (Q_{vac}) can be directly removed from the second effect – which is not the case, but has exactly the same mathematical results; this approach was employed by Winchester [**5**] and Paramalingam [**2**].

Chapter 6 - Semi-Empirical Model Development

Chapter 5 offered a critical literature review of FFE background, modelling and control. This information is used in Chapter 6 to develop and test various models against real world data. Then the most accurate model will be used as a simulation model to compare different control solutions. The methodology for each development and testing phase is described, and consists of an iterative approach to model parameter selection. The final results and comparisons are presented at the end of this chapter.

6.1 Model development methodology

Modelling is an inherently iterative procedure where the purpose of the model drives the development complexity. Although this procedure also has a creative exploratory element when looking for enhancements in accuracy, defining a certain list of stages or steps helps to explain the manner in which the model evolves. These steps and iteration decisions are shown below in Figure 6-1:

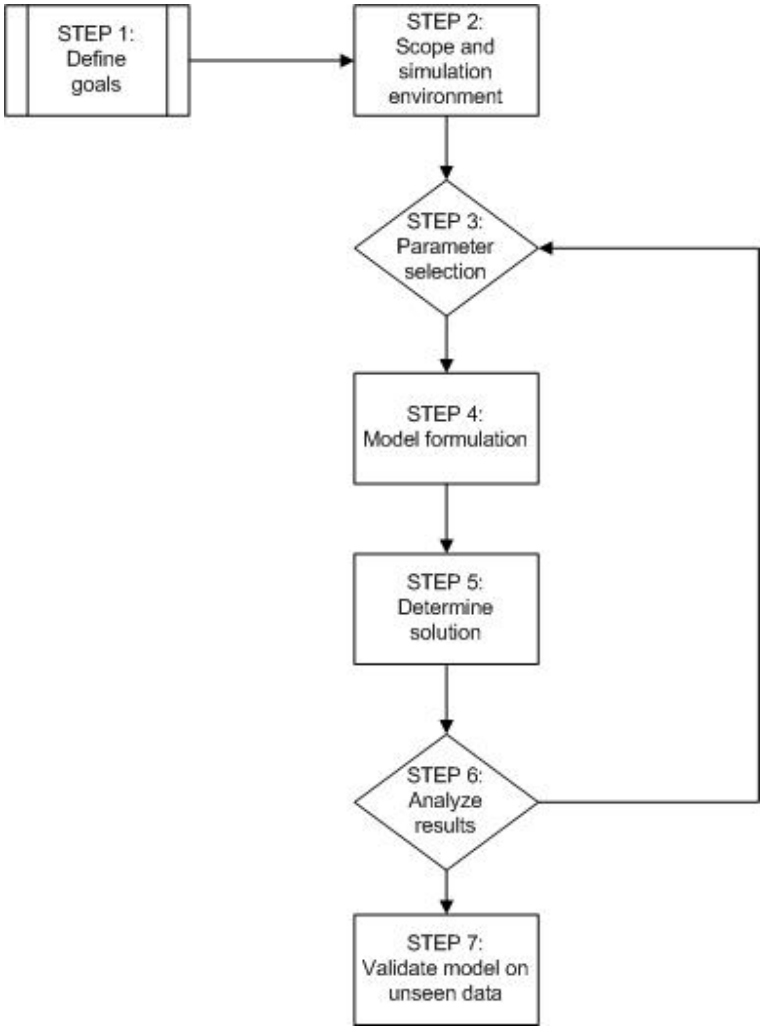

Figure 6-1: Model development steps, with parameter selection iteration

If the process is deterministic, with all the necessary equations available and fully specified, it would theoretically be possible to create a model with one pass of Figure 6-1. However, in real world applications there is always some unspecified and/or unaccounted for process dynamics and as such steps 4-5 become more difficult, i.e. perfect matching to the data sets is virtually impossible. At this point the question of necessary complexity arises – how much of the process needs to be modelled and to what extent. It would make little sense to model the effect of steel expansion at different temperatures on the heat transfer coefficient as the contribution to overall heat exchange is insignificant compared to the effect of steam and fluid temperatures. From this line of thought the importance of a clear definition of a model goal (step 1) becomes apparent. If one knows exactly what is required from a model it becomes easier to know what elements to include.

One method would be to start at a relatively simple model and add complexity as required when analyzing the model. To do this one needs an understanding of exactly where the process boundaries are and in which environment the model will be simulated (step 2). After the process has been defined, all the available parameters need to be estimated or included (step 3). Hereafter the equations can be implemented into the simulation environment (step 4). Then a solution to the set of equations needs to be found, either analytically or by numerical methods (step 5). Once the solution is found it needs to be measured against expected behaviour in a sanity test to make sure the results are not spurious (step 6). The analysis should ideally also include a comparison to real data which can then be used to empirically change parameters defined in step 3. Finally, once several iterations have been done and the model behaves appropriately for whichever goal it is needed, the model has to be compared to unseen data sets to validate its representation of reality (step 7). Validation is done to ensure that the model accurately describes the internal workings and relationships of the variables instead of only reproducing data on which it was fitted.

All steps and accompanying choices are explained in the following subsections.

6.1.1 Step 1: Model goal

As stated previously, the goal drives all decisions surrounding model development, Therefore a clear model goal is stated for this study:

> **The ultimate goal of the model is to provide an accurate simulation on which control solutions can be tested and compared. As such the model specifically needs to simulate the dynamics of both evaporation effects during continuous operation including main disturbances and manipulated variables. Furthermore the model needs to allow for the use of historical data for process evaluation and validation.**

This goal implies that if the model can pass all sanity tests, compare well with historical data and allow for control to be tested it will be considered adequate. The condition of comparing well with historical data will be discussed further in the analysis and validation steps. In addition the statement also allows

for simplifying assumptions and empirical parameter estimations to be made as long as these conditions are still met.

6.1.2 Step 2: Scope and simulation environment

Figure 2-2 shows a PFD for the local process evaporation section including upstream and downstream units. As mentioned in the introduction, FFEs are around ten times as efficient at removing water compared to spray dryers [**7**]. To fully exploit this larger efficiency, most milk concentration processes are designed to remove as much water as possible during the evaporation effects; additionally optimisation can further improve overall cost effectiveness by ensuring the evaporator is used at maximum capacity. Figure 6-2 zooms in on the local FFE while also showing the important variables available in historical data. All the units included in the modelling scope are defined by the envelope surrounding Figure 6-2:

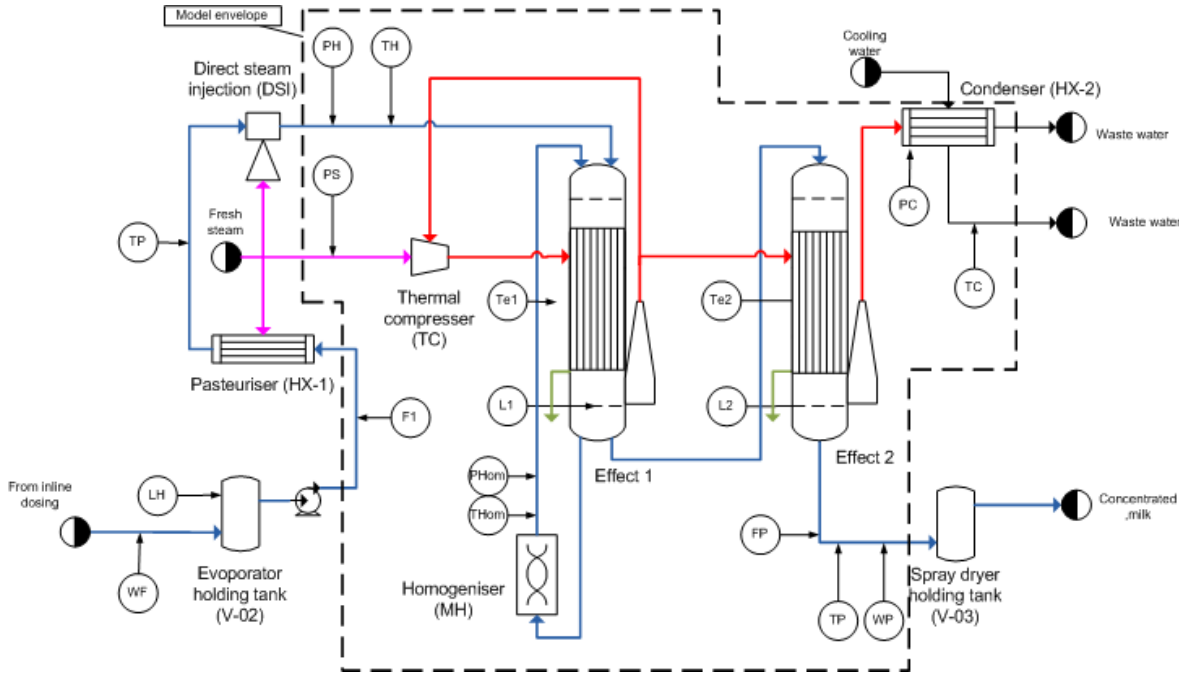

Figure 6-2: Process variables available for modelling purposes

Pasteurisation and DSI units are not included in the model as their operation is assumed to be independent of the evaporation effects and it is also assumed that current PID control is sufficient for set point tracking. Consequently, the temperature after DSI will be seen as a fixed input (with possible noise and disturbances) to the model envelope. The more complex effect relationships (including recycle, film heat transfer, thermal vapour recompression, and condenser operation) will be considered through formulation of dynamic models. All variables tags in Figure 6-2are presented in Table 6-1:

Table 6-1: Measured variable tags

Legend	Variable	Units
W_F	Dry mass fraction of feed	(-)
L_H	Level of evaporator holding tank	(%)
F_1	Flow rate to first evaporator effect	(kg/hr)
T_P	Temperature after pasteuriser	(°C)
P_H	Pressure in holding tubes	(bar)
T_H	Temperature in holding tubes	(°C)
P_S	Steam pressure	(bar)
T_{E1}	Temperature of first effect	(°C)
L_1	Level inside first effect	(%)
L_2	Level inside second effect	(%)
P_{Hom}	Homogeniser pressure	(bar)
T_{Hom}	Homogeniser temperature	(°C)
T_{E2}	Temperature of second effect	(°C)
F_P	Flow rate of product (concentrated milk)	(kg/hr)
T_P	Temperature of product	(°C)
W_P	Dry mass fraction of product	(-)
P_C	Condenser pressure	(bar)
T_C	Waste water temperature	(°C)

In addition to which process units will be modelled, the scope is further defined by the level of accuracy required in each section. It will again be assumed that if the model is fit for the intended goal, the complexity will be sufficient and all other additions are outside the scope.

Before implementing the model differential equations, to simulate and solve the model dynamically, a choice has to be made between using Matlab ODE solvers in the command line or Simulink. After creating test scripts for simple differential systems it was found that using m-files and command line ODE solvers in Matlab offers greater transparency than Simulink, but increases the complexity of including time delays. Simulink additionally provides graphical representation of the connections between units, which is helpful when creating a multi-layered model. These observations are consistent with a previous study comparing computing platforms as shown in Table 6-2 [**32**] below:

Table 6-2: Simulation platform comparison [32]

Feature	Matlab	Simulink	C++
Simulation	Slowest	Fastest	Fast
Programming	Easy, but not transparent	Easy, least transparent	Tedious, but transparent
Debugging	Easy	Easiest	Difficult

The speed and ease of programming in Simulink made it the best choice for FFE simulation. Simulink also allows the use of user defined blocks, essentially m-files, which is useful for quickly inserting complex equations.

6.1.3 Step 3: Structure and parameter selection

With the scope and modelling envelope fixed, the goal allows for simplifying assumptions to be made regarding the structure of the local process during development of the model (the final structure should, however, closely resemble the local process to ensure validity). For example, the recycle can initially be seen as an extra pass within the first effect to minimize the computational complexity. Once the structure and connections are chosen, the necessary unit parameters need to be chosen.

The parameters should ideally be selected based on process knowledge and design specifications, yet no information was available regarding the internal design of the local process. As a result, estimations from literature were used by comparing production capacity and plant design. The FFEs studied by Paramalingam (2004) and Winchester (2000), i.e. Fonterra and Kiwi-Corp respectively, both include process sections with two effects and TVR including well documented plant parameters.

After the first iteration the structure and/or parameters can be altered to better fit real world data. Caution should be taken since, when manipulating many parameters, it would be possible to fit virtually any model to any data set. As a further precaution, all alterations are subject to a sanity check before implementation. The addition of testing data (unseen until model validation) will also ensure that the final model is general and not specific to any one data set.

6.1.4 Step 4: Model formulation

With the unit structure selected (and parameters specified) equations to predict dynamic behaviour can be formulated from fundamental principles. Great care needs to be taken when combining equations from different literature sources to ensure the use of consistent units and correct connections between the equations. Furthermore, the assumptions made with each equation have to be understood before implementation to check for possible clashes.

6.1.5 Step 5: Determine solution

Solving a set of differential equations can be done either analytically or numerically. Analytical solutions offer many advantages to numerical solutions, especially with regard to insight and accuracy, yet for more complex and larger systems a lot of assumptions are required for analytical solutions, which can dramatically decrease their usefulness and applicability. Numerical solutions are an approximation of reality, but provide quicker and more accurate solutions than approximate analytical solutions under the

correct circumstances. Simulink was already chosen as the simulation environment and consequently a numerical solution technique was selected.

6.1.6 Step 6: Analyse results

After each model update and formulation it is necessary to analyse the results to decide whether the model is sufficient with respect to the goal or whether it needs further adaptation. During development the analysis will focus on qualitative properties of the model, i.e. whether the model represents most trends and responds in the correct manner to step tests (by using sanity tests as baseline). After development a quantitative measure of model performance will be calculated via mean squared error (MSE), integral of the absolute error (IAE) and linear correlation values. Each of these performance criteria is briefly explained below:

Sanity check

A set of typical process responses, to both controlled inputs and major disturbances, were included in the historical data, described in Section 3.2. These were defined by the operators to better control the FFE and are shown in Table 6-3 below:

Table 6-3: General step tests and expected process response

Step	Size	Expected Response		Actual Response	
		W_P	T_{E1}	W_P	T_{E1}
W_F	+0.01	↑	–		
T_H	+2°C	↑	↑		
F_1	+10%	↓	–		
P_S	+10%	↑	↑		
F_{CW}	+10%	↓	↓		

The sizes of the steps were determined by inspecting the historical data and using steps no smaller than half the observed maximum deviations. Comparing each model to the expected response of a step in any of the variables shown above will allow one to check whether the underlying dynamics of the model are correct.

Goodness of fit

Using historical data to drive the model one can compare the predicted outputs (y_P) to measured outputs (y_m) both by inspection and numerical analysis. The proposed measures include the MSE, IAE and linear correlation (R) as defined by:

$$MSE = \left(\sum_{i=1}^{n}(y_m - y_p)^2\right)/n \quad \text{Eq. 6-1}$$

$$IAE = \sum_{i=1}^{n}|y_m - y_p| \quad \text{Eq. 6-2}$$

$$R = \frac{\sum_{i=1}^{n}(y_{m,i} - \overline{y_m})(y_{p,i} - \overline{y_p})}{(n-1)\cdot\sigma_{y_m}\sigma_{y_p}} \quad \text{Eq. 6-3}$$

With σ_{y_m} and σ_{y_p} the standard deviations of the measured and predicted outputs respectively, n the number of samples and $\overline{y_m}$ and $\overline{y_p}$ the means.

6.1.7 Step 7: Validate model

The semi-empirical model will be validated by comparing its predictions to data sets which it was not trained on. This will ensure that the model truly represents the local FFE and not just a small subset of the data.

Additionally the model will be compared to data based models in subsequent chapters. These comparisons will provide a more relative validation, where it will be seen whether semi-empirical modelling holds any advantages over other less intensive form of modelling.

6.2 Modelling implementation

Using the steps defined above in conjunction with fundamental equations described in Chapter 5, a FFE model was developed in Simulink. All comparisons to historical data was made on recipe 1 data, the influence of different recipes was included after the final model was developed.

6.2.1 Initial parameter selection

From the PFD shown in Figure 6-2, the process units to be modelled, as well as the corresponding physical parameters, can be summarised as:

Table 6-4: Physical parameters required for modelling

Unit	Variable	Description	Unit
Feed holding tank	A_{tank}	Tank cross section area	m^2
Thermal vapour compressor	A_{TVR}	Compressor parameter	m.s
	B_{TVR}	Compressor parameter	$m^{0.03}s^{0.06}/kg^{0.03}$
	C_{TVR}	Compressor parameter	-
Distribution plate	A_{plate}	Plate cross section area	m^2
	A_{holes}	Total area of holes	m^2
	H_r	Tube riser height	m
	C_D	Orifice discharge coefficient	-
$Effect_{1/2}$	$N_{TE1/TE2}$	Number of tubes effect 1/2	-
	-	Length per tube	m
	A_E	Effect cross section area	m^2
	A_S	Surface area, losses from shell and tubing	m^2
	A_E	Surface area, losses from effect	m^2
	U_e	Shell to tube heat transfer coefficient	$W/m^2.°C$
	Thermal inertia	Energy required to change an effect temperature	J/°C
Condenser	L_C	Length of condenser tubes	m
	N_C	Number of condenser tubes	
	U_C	Condenser heat transfer coefficient	$W/m^2.°C$

Using the continuous operation data sets for recipe 1 found in Section 3.2, the average feed flow for the local plant was found to be 20% larger than Fonterra and 35% smaller than Kiwi-Corp as shown in Table 6-5 below:

Table 6-5: Comparison of feed rates and water removal between local plant, Fonterra and Kiwi-Corp

Plant	Feed (kg/h)	W_F	W_P	Mass Evaporated (kg/h)
Local	10900	0.35	0.55	3963
Fonterra	9000	0.24	0.4	3600
Kiwi-Corp	17000	0.41	0.47	2170

One thing to note about the literature FFE plants is that Fonterra utilises a TVR evaporator (two effects) while Kiwi-Corp also uses MVR evaporation (one effect) in series with a TVR evaporator section (two effects).The MVR effect greatly reduces the concentration burden on the TVR and subsequent effects. Although the local plant processes less milk than Kiwi-Corp, it removes a larger percentage of the water. Therefore the similar operating region and design of Fonterra makes it the obvious choice for parameter estimation. A ratio of 1.2 (feed comparison) was chosen to adjust all necessary variables from Fonterra. If a parameter was not found for Fonterra, one from Kiwi-Corp was adjusted by inspecting the relative size and function of the unit. The values of both literature FFEs are shown in Table 6-6, as well as the initial adjusted/selected parameters.

Table 6-6: Updated parameters

Unit	Variable	Selected			Fonterra			Kiwi-Corp			Units
		Effect 1		Effect 2	Effect 1		Effect 2	Effect 2		Effect 3	
		Pass 1	Pass 2	Pass 3	Pass 1	Pass 2	Pass 3	Pass 6	Pass 7	Pass 8	
Distribution plate	A_{plate}	0.402	0.361	0.462	0.335	0.301	0.385	0.574	0.229	0.147	m^2
	A_{holes}	0.0047	0.0042	0.0049	0.0039	0.0035	0.0041	0.0093	0.0060	0.0051	m^2
	H_R	0.075	0.075	0.075	N/A	N/A	N/A	0.075	0.075	0.075	m
	C_D	0.8			0.8			0.7			-
Effect	N_{TE1}	89	78	101	74	65	84	144	66	43	-
	L_{tubes}	12	12	12	12	12	12	10	10	10	m
	A_{tubes}	167.4	147	189.96	139	122.5	158.3				m^2
	U_e	2000	800	500	2000	800	500	N/A	N/A	N/A	W / m^2.°C
	Thermal Inertia	$4x10^6$		$4x10^6$	N/A		N/A	$1.2x10^6$		$1.2x10^6$	J/°C
	$A_{ext,effect}$	21.5			17.9			N/A			m^2
	$A_{ext,shell}$	47.5			39.6			N/A			
Feed holding tank	A_{tank}	Not available									m^2
Thermal vapour compressor	A_{TVR}	2.13E-07									m.s
	B_{TVR}	58.434									$m^{0.03}s^{0.06}/kg^{0.03}$
	C_{TVR}	0.971									-
Condenser	L_C	-	-	12	-	-	24	-	-	12	m
	N_C	-	-	26	-	-	18	-	-	26	m
	U_C	-	-	1000	-	-	1000	-	-	1000	W / m^2.°C

Both Fonterra and Kiwi-Corp used the same thermal vapour compressor parameters pointing to a possible approximation of TVR design. Paramalingam (2004) tested the model against experimental data and found good agreement. As we have no further information for the local process this modelling assumption (MA) was made as well, namely:

MA 1: TVR design is assumed to be the same as used for Fonterra and Kiwi-Corp.

This approximation neglects the fact that the local plant removes more water than either of the other plants which could potentially mean that the local plant would require more energy from the TVR section.

It should also be noted that the orifice discharge coefficient was not adjusted from Fonterra or Kiwi-Corp. If one assumes that the hole sizes and construction do not change (i.e. only the number of holes and plate surface area changes) it implies that the discharging from the plate will still be governed by the same orifice dynamics.

There are additional variables required for a complete model, including piping lengths, pipe thickness, distribution plate internal design, etc. This led to the second and third major model assumptions:

MA 2: All piping and design variables not estimated are assumed to be such that no restriction is placed on the process during continuous operation.

MA 3: Pump and piping delays are constant.

The above assumptions will be valid as long the process does not deviate far from normal production capacity as the piping will have a constant effect on the system if the flow rates remain nominal.

6.2.2 Initial model structure selection

A viable internal structure had to be selected before the model was formulated. At first a simple setup with various assumptions was preferred in order to quickly assess whether fundamental modelling would sufficient for accurate simulation.

Homogeniser

The first of these assumptions are related to the homogeniser, namely:

MA 4: Homogeniser action is assumed to be negligible in terms of the effect on milk pressure and temperature.

MA 5: The homogeniser is assumed to feed a second pass through effect 1 instead of a recycle.

As explained in Section 5.2, the homogeniser breaks large compounds within the milk to prevent excessive fouling by keeping the liquid less viscous. Although some heat will escape from the milk via piping and the homogeniser itself, the related energy flows can be assumed to form part of the normal surface losses.

TVR and condenser

Steam driving evaporation in effect 1 and cooling water controlling the temperature of effect 2 are the two main manipulated variables for the local process. These two units are however also the most complex mathematically and to decrease development time both units were assumed to produce constant steady state heat flows:

MA 6: TVR function is replaced by a constant heat flow term (Q_{TVR}) entering effect 1

MA 7: Condenser function is replaced by a constant heat term (Q_{vac}) leaving effect 2

To estimate steady state values, the approximation that one kilogram steam produces one kilogram vapour [**2**] was used to predict that 66% of evaporation should take place in the first effect. By including the average feed flow rate, feed- and product dry mass fractions the mass balance shown in Figure 6-3 was constructed:

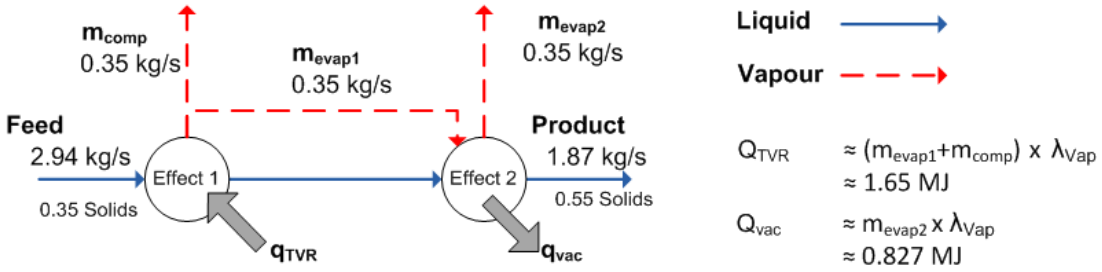

Figure 6-3: Mass balance around both effects

As mentioned, the evaporation taking place in effect 1 is driven by heat from TVR while the entire vapour generated in effect 2 needs to be condensed, implying the relationships seen at the right of Figure 6-3. Assuming that both flows are constant, greatly reduces the dynamic operation of the model, but allows for a proof of theory first approximation model to test both the sanity responses and Simulink environment.

Additional general FFE assumptions

In order to apply the simplifications made to the falling film evaporation rate calculations (Eq. 5-13 and Eq. 5-14) as well as to the distribution plate dynamics (Eq. 5-3 to Eq. 5-6) the following additional assumptions were required:

MA 7: Constant falling film velocity.

MA 8: Perfect mixing in distribution plates, tubes, and holding tanks.

MA 9: Thermodynamic equilibrium between distribution plate and effect as well as between vapour/liquid and metal phases in the effects.

MA 10: Both effects have no internal tanks, with flow out equalling flow in

MA 11: No flashing inside distribution plate.

MA 12: No noise is present in data.

MA 13: Constant milk density over all mass fractions.

MA 14: Constant heat transfer coefficients.

Constant falling film velocity is closely related to the assumption of constant piping delays, i.e. if the system remains close to nominal operation all flows should have constant effects on the system. The delays chosen for the local process were estimated, by comparing flow rates, from Paramalingam [**2**]:

Piping delay between effects	**35s**
First effect falling film time constant	35s
First effect falling film time constant	30s

Assuming perfect mixing requires high throughput and small liquid hold-up, which is not necessarily the case for FFEs. Yet the added complexity of modelling variable distributions within the holding tanks and/or distribution plates cannot be justified by the relatively small errors this assumption should introduce as piping/pump delays will dominate residence times.

By neglecting the inventory tanks, some buffer to flow spikes is removed, yet except for shorter time constants the effect on model predictions will be minimal.

The amount of milk that flashes before entering the evaporation tubes is unknown and by assuming this fraction close to zero we reduce the complexity of the flow equations. The effect of different flashing fractions should be included in later model testing.

In the development stage of the model no noise addition to measured variables is required, as one wishes to compare the model predictions to historical data and noise would only complicate the comparison by introducing random deviations. When different controllers are tested noise will be of paramount importance to test the stability of said controllers.

By assuming no correlation between density and dry mass the development time within Simulink is shortened. This assumption will however need to be revised seeing as reducing the water content of milk will most definitely influence both the density and dry mass.

Heat transfer coefficients will also vary with milk properties, i.e. viscosity or dry mass fraction yet these relationships are unknown. At first a constant value will be assumed. If too many long term deviations between the model and actual data are observed this assumption will have to be reviewed as well.

6.2.3 Approximation model

All of the above assumptions allowed the development of the simplified process shown below in Figure 6-4. Note that only the liquid flows are shown as all vapour flows exit the system as waste products (except for the stream recycled to the TVR). The energy flows with respect to the effects are also shown to better describe individual relationships between the units.

Setup

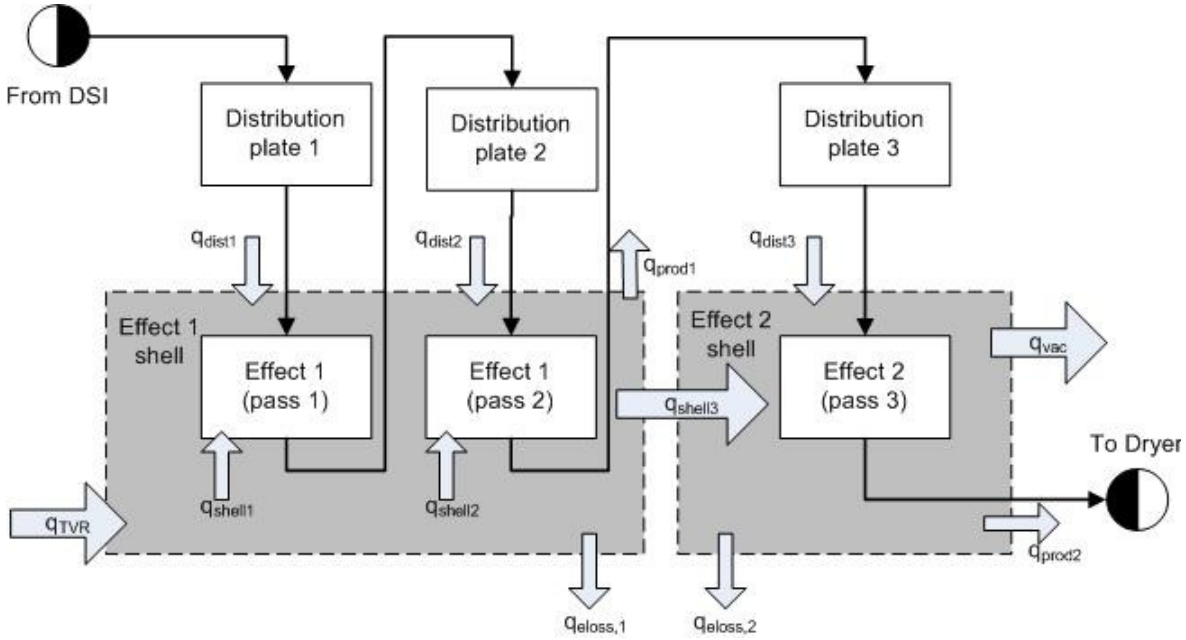

Figure 6-4: First approximation model liquid and heat flows

It is expected that the model will show large deviations when compared to historical data as the dynamic influence of both TVR and condenser actions were assumed to be constant. Again, this first approximation model was simply to perform sanity tests on the core process behaviour (shown in Table 6-3) and test the suitability of the Simulink environment.

Results and discussion

With the Simulink model set up, it was found that complex numbers were generated after about 2000s when calculating flow from the first distribution plate. The only possible point of origin is the square root used in Eq. 5-5, which implies that the fluid height had become negative either because of too little flow or incorrect distribution plate parameters. Closer inspection of the fluid heights above each plate revealed that the heights were still relatively far away from zero, yet at the time when the error was introduced the fluid heights were changing rapidly. Setting the maximum step size for the Simulink environment to 120s forced the solver to not over estimate rapid changes and resulted in correct flow results. Furthermore it was decided to limit fluid heights to being positive as negative values have no physical meaning; this was done by introducing a simulation stopping error if any height became unrealistic.

Sanity tests were run by introducing the steps in Table 6-3; both P_S and F_{CW} steps were replaced with the corresponding steps in constant values of Q_{TVR} and Qvac as shown below:

Table 6-7: General step test and expected process response

Step	Size	At time (s)	Expected Response		Actual Response	
			W_P	T_{E1}	W_P	T_{E1}
W_F	+0.01	1000	↑	–	↑	–
T_H	+2°C	2000	↑	↑	↓	↑
F_1	+10%	3000	↓	–	↓	↑
Q_{TVR}	+10%	4000	↑	↑	↑	↑
Q_{vac}	+10%	7000	↓	↓	↑	↓

There were three unexpected results: firstly when T_{E1} increased for a step in feed flow, secondly the slight decrease in W_P for a step in T_H and lastly that an increase in Q_{vac} saw an increase in W_P.

Although milk enters the distribution plate at higher temperatures than that of the effect, all the excess energy should be expended in the flashing chamber. Yet in assumption MA 11 the flashing was neglected and therefore the excess energy introduced by a feed step was included in the effect energy balance resulting in the increased T_{E1}. The $T_H \rightarrow W_P$ decrease is also a result of neglecting flash. Instead of the extra energy resulting in more milk being flashed, the energy was taken into account in the first effect energy balance. This resulted in a smaller temperature difference between the tube and shell side which in turn caused a slight decrease in W_P.

The $Q_{vac} \rightarrow W_P$ response was a result of the constant Q_{TVR} assumption (MA 6). By using the explanation of the condenser action as seen in section 5.2.4: an increase in cooling water flow rate to the condenser (and consequently an increase in Q_{vac}) will cause the strength of the vacuum to increase which means the milk has to overcome less pressure to evaporate inside effect 2 and as such T_{E2} drops (due to the thermodynamic relationship between vapour pressure and temperature). The T_{E2} decrease temporarily increases the heat flow from the second effect shell as the temperature gradient increases, causing effect 2 to remove more energy from effect 1. As T_{E1} decreases because of the increased heat removal (which also causes a drop in vapour pressure), the TVR section is able to pull less vapour from effect 1 (greater suction is needed to pull the lower pressure vapour from the effect), thus decreasing the overall amount of driving steam to the first effect shell. This will then cause the amount of milk evaporated in effect 1 to decrease (and W_P to decrease as well). In summary, W_P should rise while the T_{E1} drops (effectively an inverse response), but then settles at a lower value owing to less driving steam to both effects. Yet because we assumed Q_{TVR} to be constant, the decrease in pulled vapour from effect 1 was not taken into account and only the increased temperature difference could act on the system, which meant only the upwards W_P trend was observed.

Response curves for T_{E1} and W_P are shown in Figure 6-5 below. Note the constant nature of the process between steps. It clearly shows that the model is stable over a range of constant inputs – which is very important from a control perspective (as the controller will not have to saturate one of the manipulated variables to keep the process constant). Furthermore all the step responses show linear behaviour. Non-linearity might still present in residence and dead times:

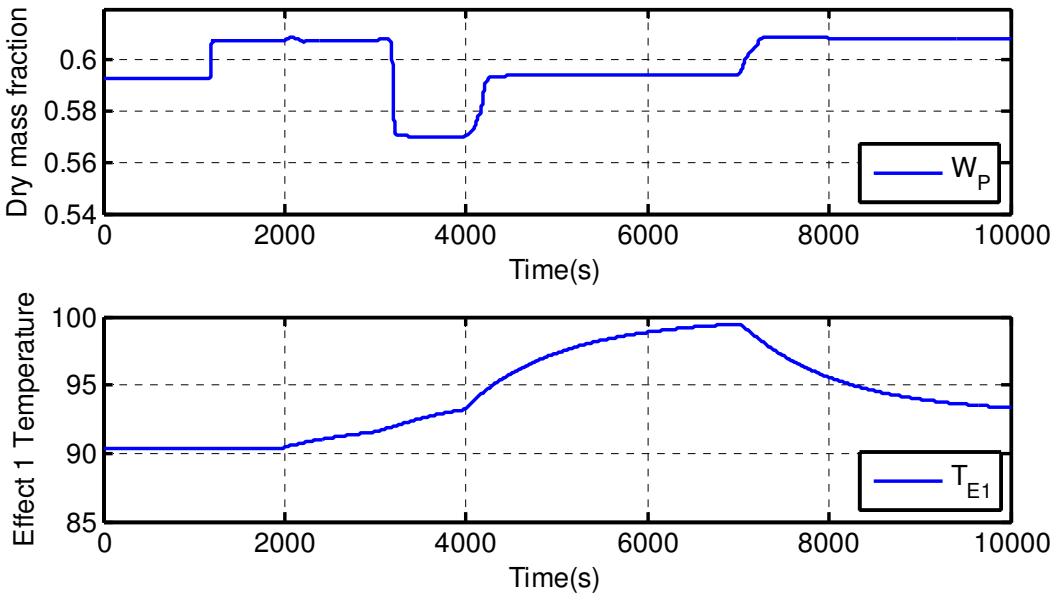

Figure 6-5: Initial approximation model sanity tests, with steps defined in Table 6-7

The last comparison required to evaluate the model is between predicted and historical data (from set 9_2 as described in Section 3.2) to drive the evaporator, shown by Figure 6-6 below:

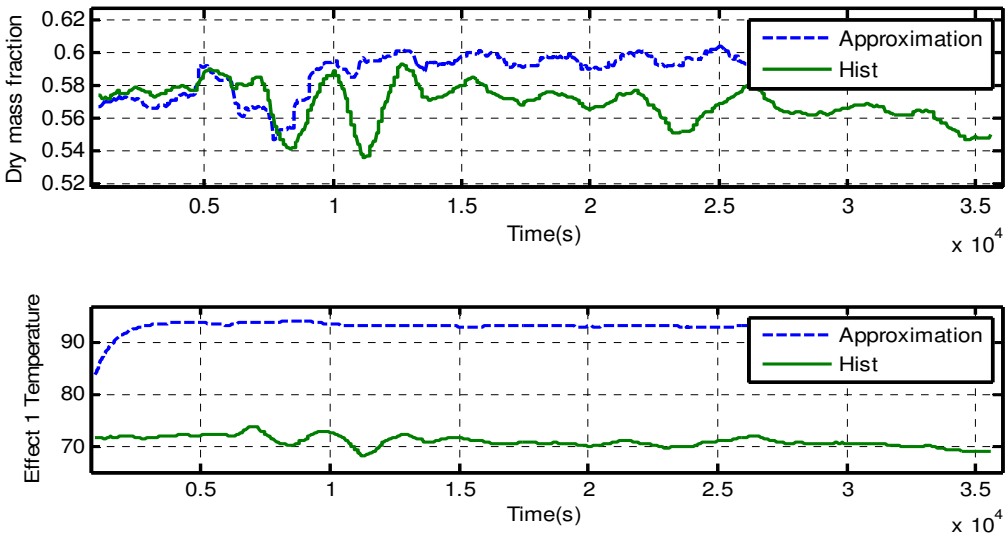

Figure 6-6: Comparison of approximation data results and historical training data set 09_2

Conclusion

The first approximation model clearly shows that semi-empirical modelling should be viable as the process responds correctly to all the steps when the assumptions are reasoned in. When comparing the model to training historical data, great discrepancies were seen with average R values of -0.14 and -0.002 for W_P and T_{E1} respectively.

Even with these low values one cannot rule out the significance of the approximation model; Figure 6-6 on the previous page shows the model trends compared to training data. With the restricting assumptions of constant Q_{TVR} and Q_{vac} taken into account the comparison showed some promise. Especially with W_P predictions which already showed the trends within the historical data to some extent. T_{E1} showed little to no variance – which is expected because of the constant heat flow assumptions.

Yet the assumptions made for the approximation model need to be revised, especially for TVR and condenser function. Note that the predicted T_{E1} values showed a large bias which was again most likely due to the result neglecting TVR and condenser actions.

6.2.4 First revision: Dynamic TVR and condenser action with flashing

The approximation model showed that neglecting flashing introduced a few artefacts while the omission of dynamic TVR and condenser action caused the model to fail one of the sanity tests. Therefore it was decided that the first revision model would add dynamic behaviour for both TVR and condenser action as well as include flashing (80% of the energy that would have been required to raise the feed temperature from that of the effect to the current value).

Setup

The model structure stays exactly the same as seen Figure 6-4 except for the addition of the above mentioned unit dynamics and flash calculations. Variable density was also included as shown by Eq. 2-1, with the constant α_{TS} found by comparing density and total solids concentrations in historical data. A summary of revision 1 model differences is shown below:

Changes in revision 1 model:

- Addition of TVR and condenser dynamic units.
- Addition of flash calculations to take into account the effect of feed temperature.
- Use of variable milk density.
- Sanity step tests revert to changing manipulated variables, P_S and F_{CW}, instead of absolute heat flows Q_{TVR} and Q_{VAC}.

The local FFE estimates product and feed total solids (dry mass fraction) from density measurements. This is done as density measurements are a lot quicker than dry mass fraction analysis. To replicate the estimation, the historical density was used to predict the total solids of the feed. The results were then compared to recorded values in Figure 6-7 below using an initial correlation coefficient (α_{TS}) in Eq. 2-1 from Winchester (2000) of 0.344 as well as adjusted α_{TS} values:

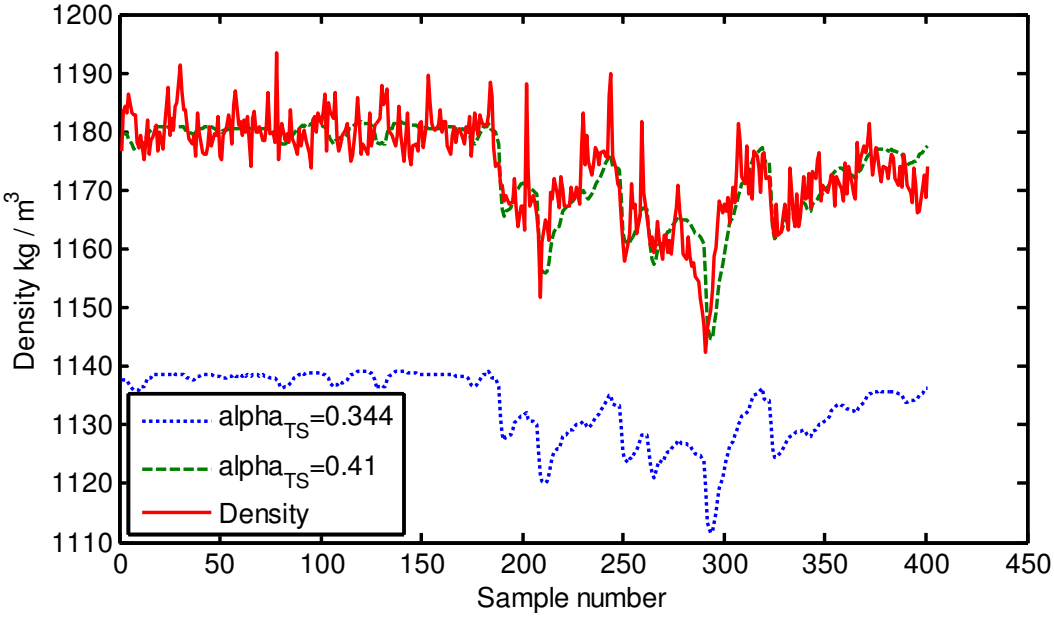

Figure 6-7: Comparison of calculated density and historical density

The final value of α_{TS} is well above those reported by Winchester [**1**] - most likely due to in-line dosing and/or vitamin addition before the milk enters the evaporation effect.

Results and discussion

The sanity step tests were adjusted, reverting to changes in manipulated variables and then run for the new model with the results shown in Table 6-8 below. All responses were in line with expectations, except for an increase in feed rate which still caused an increase in T_{E1}. This implies that the energy contained in the feed was still large enough to influence the effect temperature even with flashing taken into account.

Table 6-8: General step test and expected process response for revision model 1

Step	Size	At time (s)	Expected Response		Actual Response	
			W_P	T_{E1}	W_P	T_{E1}
W_F	+0.01	1000	↑	–	↑	–
T_H	+2°C	2000	↑	↑	↑	↑
F_1	+10%	3000	↓	–	↓	↑
P_S	+10%	4000	↑	↑	↑	↑
F_{CW}	+10%	7000	↓	↓	↓	↓

When the W_P and T_{E1} curves were examined, as shown in Figure 6-8 below, it was revealed that the time constant for each step had increased dramatically. The increase was largely as result of the revised model allowing a more realistic approach to dynamic heat flows, Q_{vac} and Q_{TVR}, by altering physical flow rates which take longer to influence the system instead of directly manipulating the heat flows. The approximation model assumed that the heat flows could be changed instantaneously which, with the large thermal mass of a FFE, is virtually impossible.

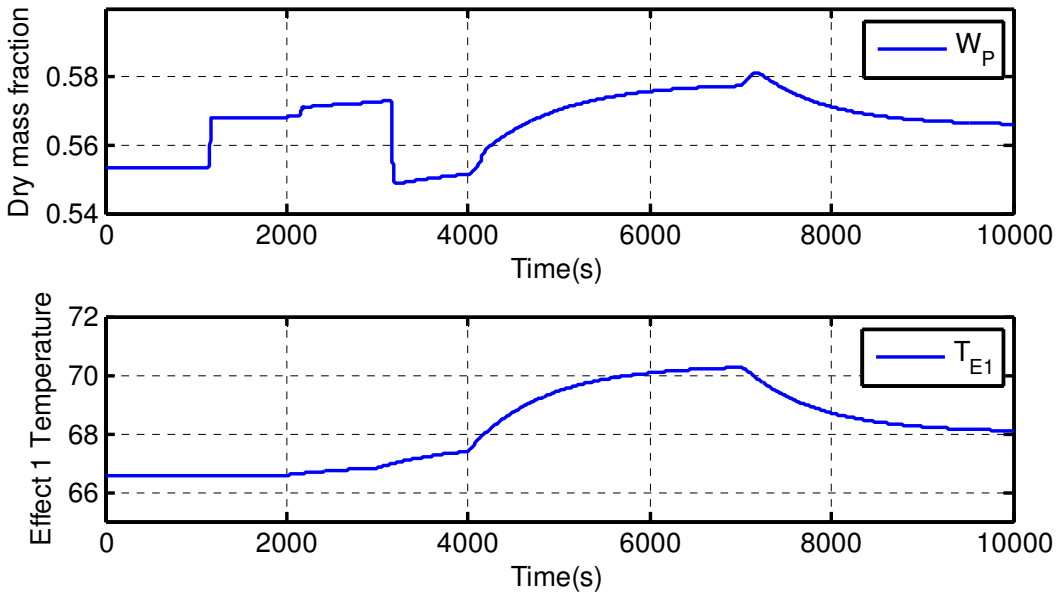

Figure 6-8: First revision model sanity tests

Secondly the $T_H \rightarrow W_P$ action is smoother and in the correct direction as flashing was now taken into account which meant that the vapour flow rose when the high temperature liquid reached the distribution plate.

Also note the clear two step action of $F_{CW} \rightarrow W_P$. The product dry mass was clearly raised temporarily before falling as explained in section 5.2.4, while T_{E1} steadily declines.

The first revision model was compared to the same historical set as before, shown in Figure 6-9 below, the results proved significantly better than that of the approximation model:

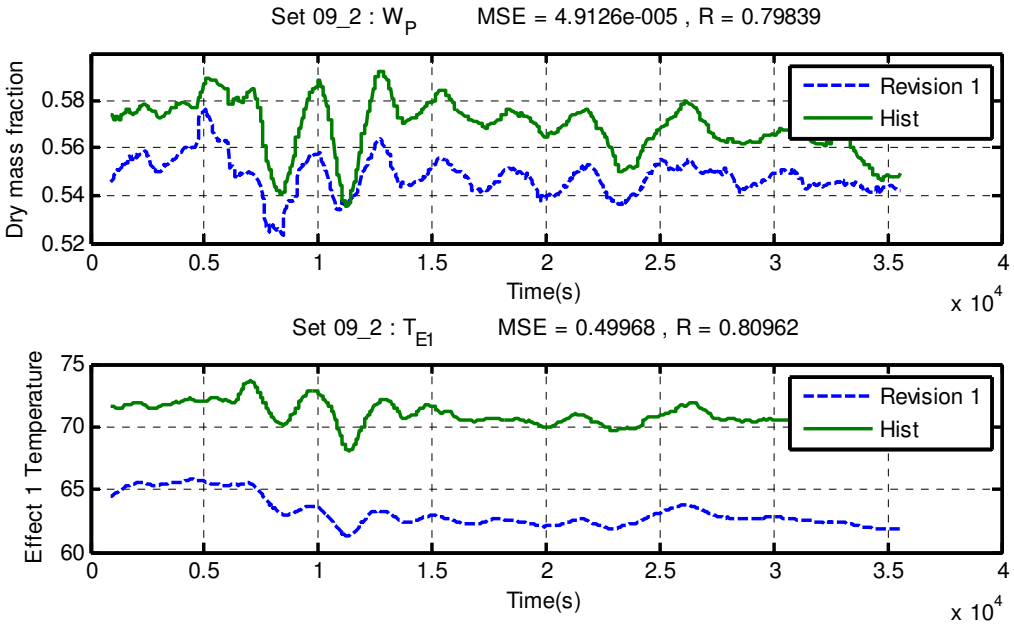

Figure 6-9: First revision model comparison to historical data set 09_2

The major trends in W_P were all represented with the model showing good agreement with a near constant offset. Some improvement was also seen in T_{E1} simulation as major disturbances at 11000s and 26000s were picked up with the bias also greatly reduced.

Conclusions

Even with the higher correlations and improved MSE values the simulation is still not complete as there are unresolved concerns. Firstly the variance of T_{E1} is smaller than observed in historical data, indicating an over estimation of the effect thermal mass and/or general parameter mismatch. Secondly the structure of the model does not yet represent the local FFE, which diminishes the applicability of the model for control simulations.

6.2.5 Second revision: Homogeniser recycle and inventory tanks

The first revision model showed a much greater correlation to historical data compared to that of the approximation model, and continued to hold with sanity tests derived from operator knowledge. Two major structural assumptions were left, namely that no inventory tanks were present inside each effect and that the homogeniser recycle was still considered as an additional pass. The second revision aims to include the inventory tanks within each effect as well as the recycle to remove the structural inconsistencies and provide a platform for sensible parameter tuning.

Setup

Note that Figure 6-10 includes a holding tank below each effect and no longer consists of two passes in the first effect, but a recycle from effect 1 tank to distribution plate 1. Furthermore, both the

recompression and condenser units were included with the dynamic heat flows as implemented in the first revision.

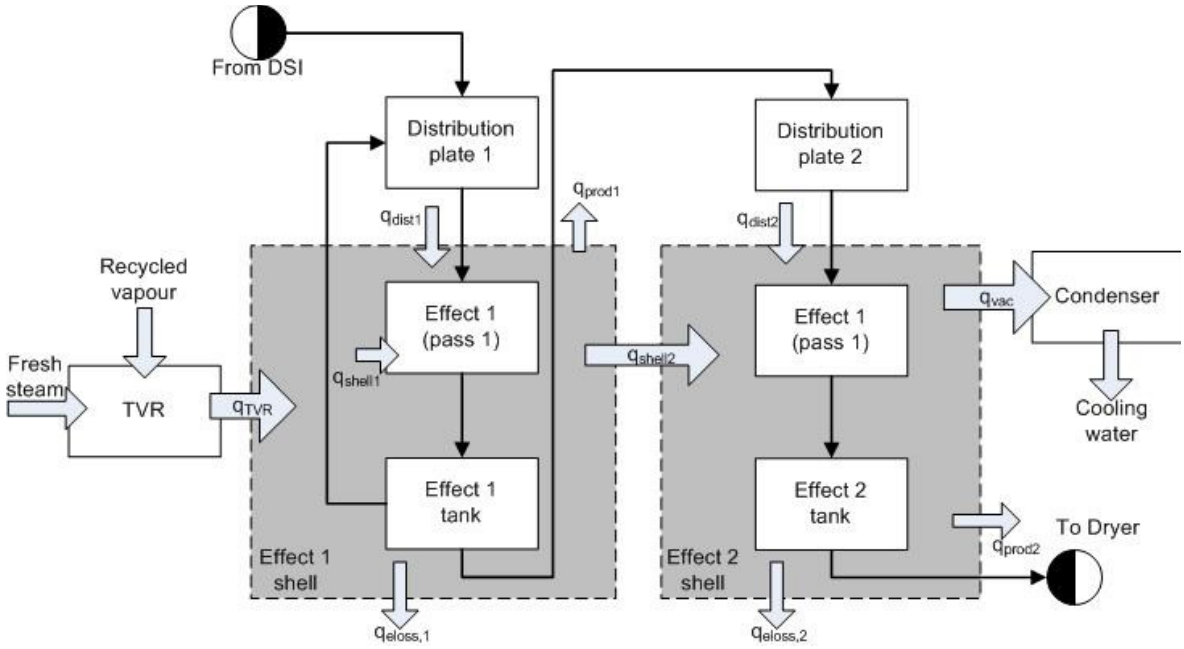

Figure 6-10: Second revision model structure

Figure 6-10 closely resembles the local plant structure shown in Figure 5-3 and the simulation can therefore be deemed satisfactory if the results are consistent with historical data and all the sanity tests are passed. The first effect parameters (plate and hole sizes, heat transfer coefficients, etc.) were at first kept equal to the corresponding pass as chosen in Table 6-6 with possible tuning once the model has been implemented. A summary of the major model changes for revision model 2 is given below;

Changes in revision 2 model:

- Inclusion of inventory tanks within each effect.
- Treating the homogeniser recycle as a recycle instead of an additional pass within effect 1.

Results and discussion

The sanity tests revealed similar results to that of the first revision model, yet all the time constants were again marginally increased as a result of the holding tanks and recycle that provided a buffer against flow and dry mass spikes. Both the sanity test and historical data comparison is shown below in Figure 6-11 and Figure 6-12:

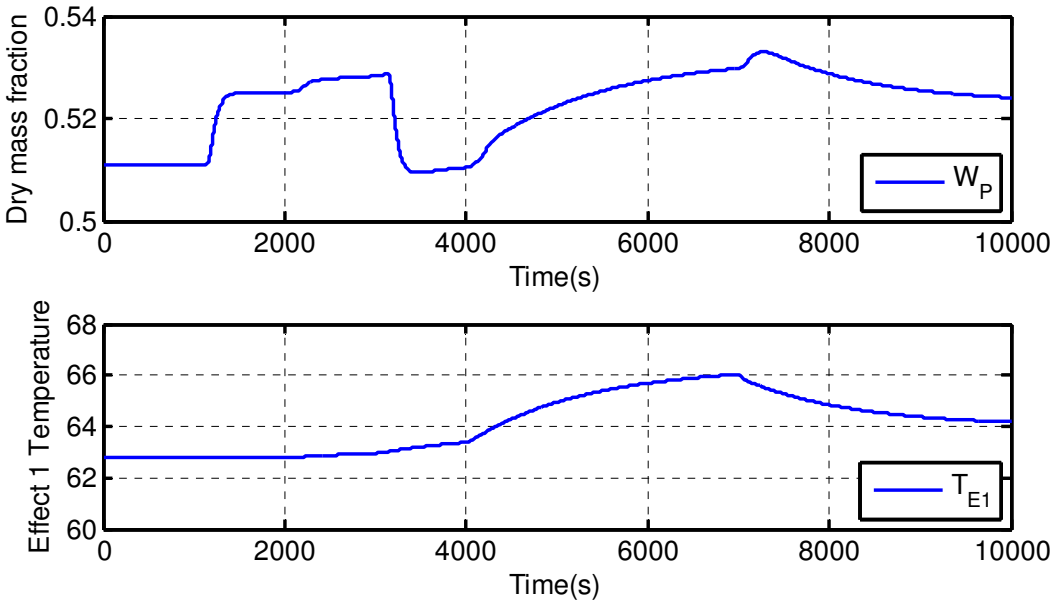

Figure 6-11: Second revision model sanity tests

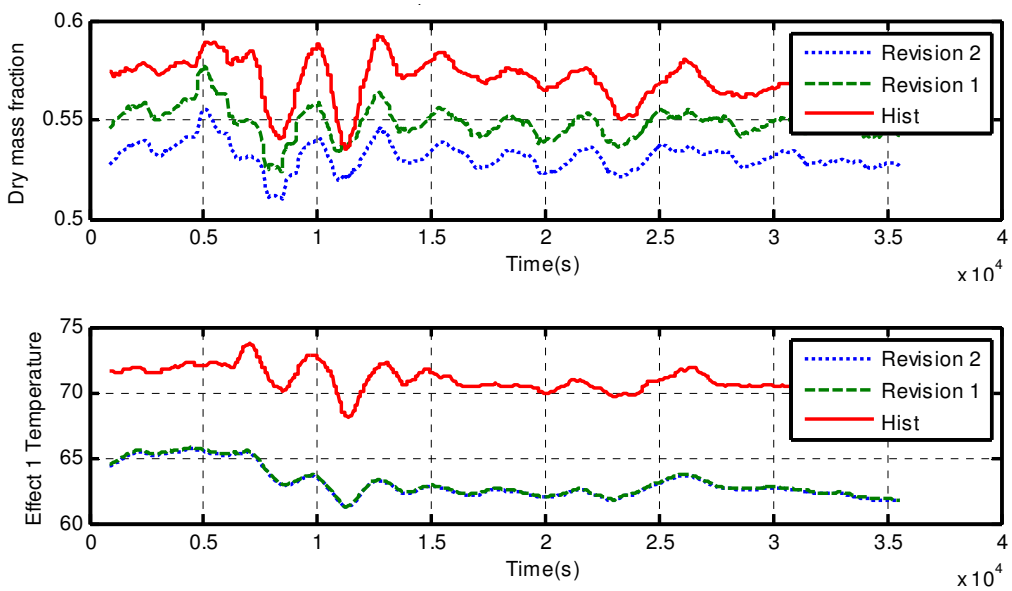

Figure 6-12: Second revision model comparison to historical data set 09_2

The historical comparison revealed that the second revision model reacted similarly to the first revision, yet with an increased W_P bias and smoother response. The increased W_P bias is most likely the result of removing the extra pass and including a homogeniser recycle. Even though the bias is not desirable, the closer resemblance to the local FFE plant structure offer greater value for subsequent control and benefit estimation sections and was therefore preferred. Additionally the bias may be lessened by

tuning in the following sections. The increased smoothing of revision model 2 is shown in Figure 6-13 below:

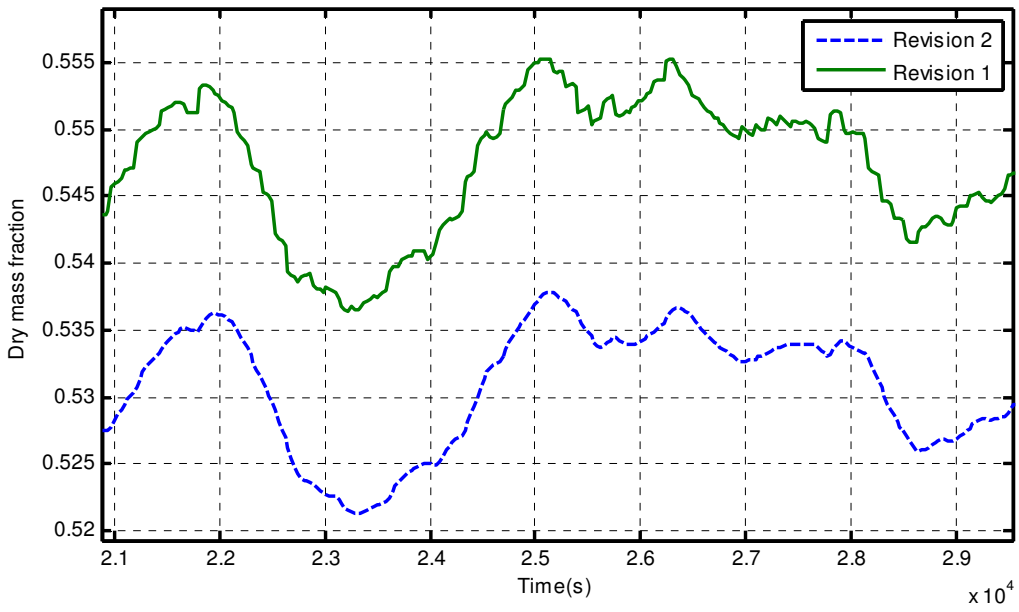

Figure 6-13: Increase smoothness and lag of model revision 2 versus 1 on historical data set 9_2

Finally the sanity step test expected and actual response comparison is shown below in

Table 6-9: General step test and expected process response for revision model 2

Step	Size	At time (s)	Expected Response		Actual Response	
			W_P	T_{E1}	W_P	T_{E1}
W_F	+0.01	1000	↑	–	↑	–
T_H	+2°C	2000	↑	↑	↑	↑
F_1	+10%	3000	↓	–	↓	↑
P_S	+10%	4000	↑	↑	↑	↑
F_{CW}	+10%	7000	↓	↓	↓	↓

Note that the model behaviour in terms of sanity tests were exactly the same as seen for revision model 1. This highlights again that revision model 2 only brought the model structure into alignment with the local process, no drastic change to internal dynamics were sought.

Conclusion

The second revision model brought the model internal structure into agreement with that of the local process, while preserving the desired sanity step responses. Now that the structure is fixed, the physical parameters may be varied to improve the model fit to historical data and compare it to all the data sets to check for additional anomalies. At this stage it should be noted however that the model could already be suitable for control simulations as both the structure and sanity test responses are in-line with expectation and the model is able to successfully capture most deviations in historical data.

6.2.6 Model tuning

The second revision model parameters were tuned (by inspection) to both improve historical fit and investigate the model response to changes in operational parameters, such as heat transfer coefficients. This knowledge could be useful for control.

Thermal inertia

Figure 6-12 clearly shows that the revision models predict T_{E1} well, for the specific training set, but the total variance was less than that seen in the historical data. By reducing the thermal inertia of an effect the resistance to temperature change will be reduced which will allow the model to more quickly pick up changes in T_{E1}. A comparison between both W_P and T_{E1} prediction with varying thermal inertia values is shown in Figure 6-14:

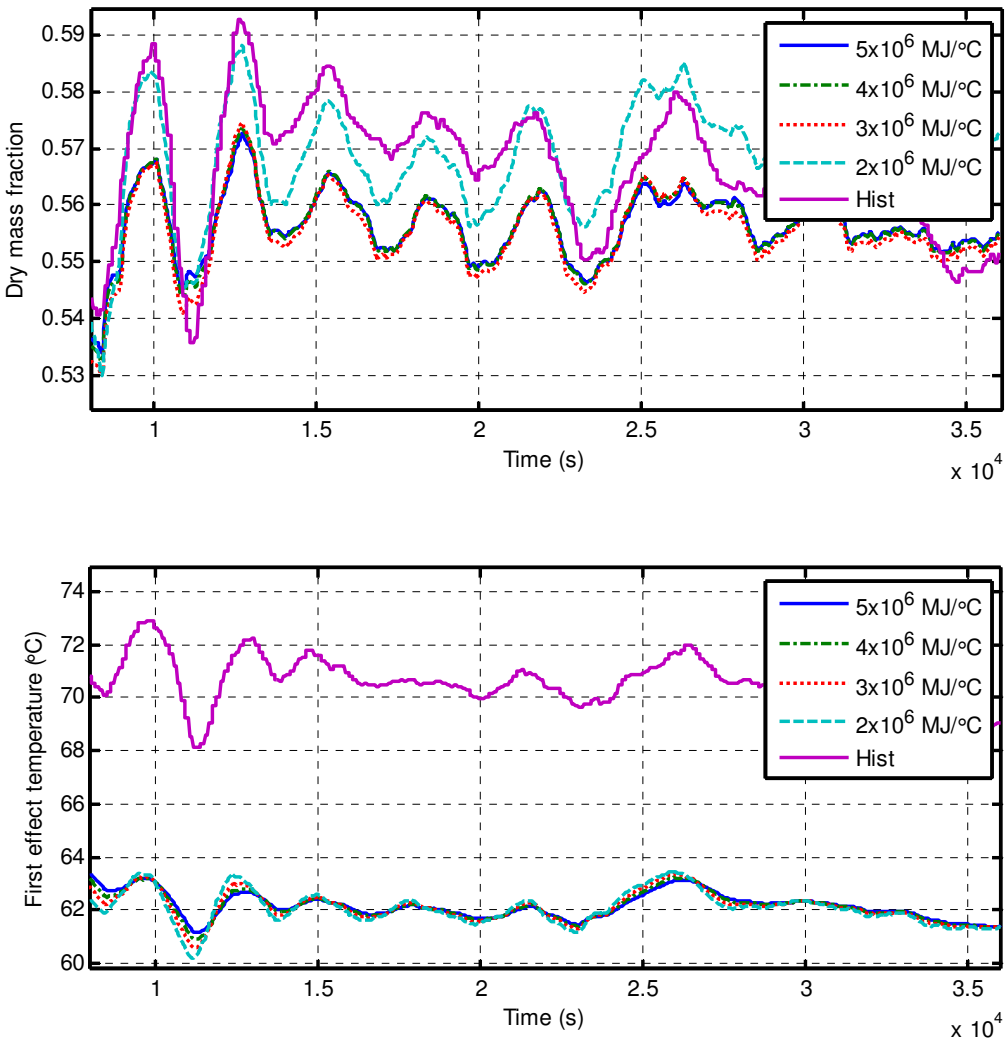

Figure 6-14: Effect of thermal inertia on W_P and T_{E1}

Figure 6-14 clearly shows that at a thermal mass of $2x10^6$ MJ/°C the model shows the most variance and greatest relation to historic data. Below this value the model became unstable because of large

fluctuations in mass evaporated in each effect which caused the distribution plate level to go out of bounds. Thermal mass changes also affect both the bias and variance of W_P, while only the bias of T_{E1} is affected.

Recycle ratio

The recycle ratio (mass to next effect compared to recycled mass to first distribution plate) will affect the amount of milk evaporated as well as the time constants of flow changes.

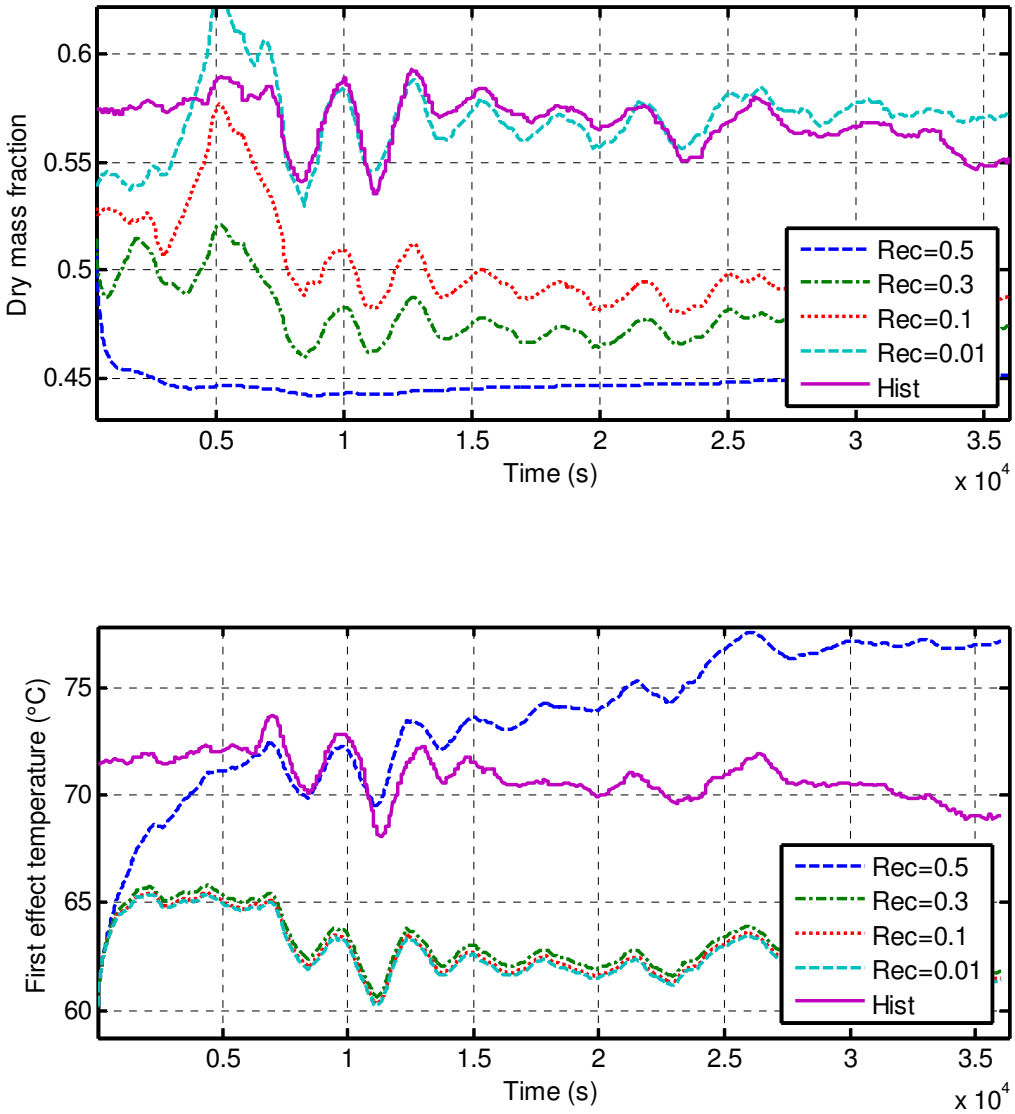

Figure 6-15: Effect of recycle fraction on W_P and T_{E1}

From the above figure it can be seen that decreasing the recycle fraction increases the product dry mass. Only very high recycles influence T_{E1} prediction. The recycle fraction should only be selected in conjunction with other parameters to avoid unaccounted parameter interaction and as such will be left at 0.1 for the remaining parameter selection tests.

Heat transfer coefficients

The shell to tube heat flow is calculated via Eq. 6-4 shown below:

$$q_{shell} = \left(T_{S,i} - T_{E,i}\right) \cdot U_{P,i} \cdot A_{tube,i} \qquad \text{Eq. 6-4}$$

The fundamental model was built on estimated values of the tube area (A_{tube}) and effect pass heat transfer coefficient (U_P). As both U_P and A_{tube} have the same influence on q_{shell}, one cannot unconditionally tune one parameter. Therefore it was decided to fix the tube areas and second effect heat transfer coefficient and then only iterate the first effect coefficient between multiples of the second. This method will ensure that duplicate scenarios are not investigated.

The bases of the heat transfer coefficient values were taken from literature values as shown in Table 6-6 previously. The results are shown below in Figure 6-16 below:

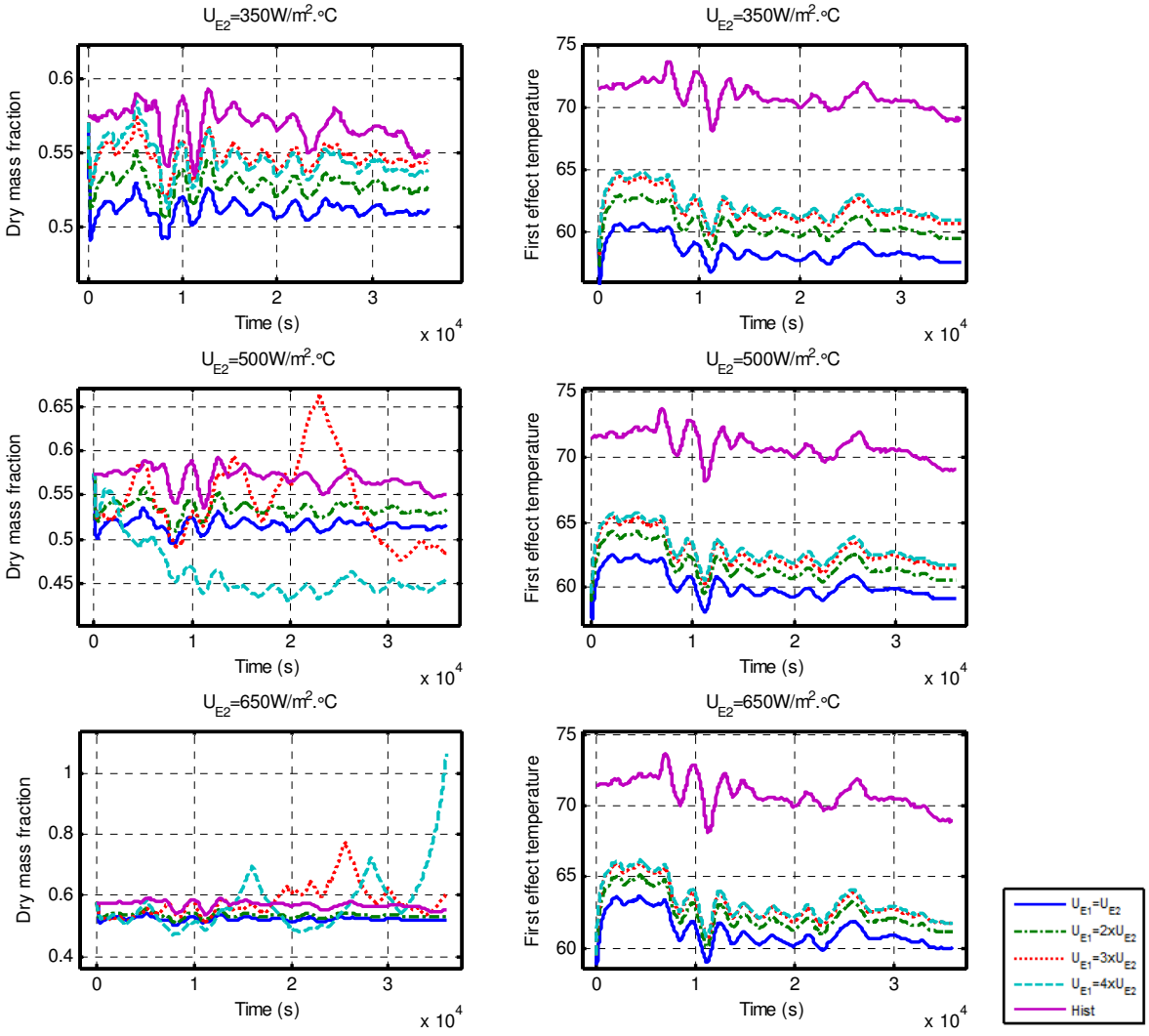

Figure 6-16: Effect of heat transfer coefficients on W_P and T_{E1}

From Figure 6-16 it can be seen that the relative size and absolute values of the heat transfer coefficients play a role in their effect on the model. Values of U_{E2} at or above 800 W/m^2°C caused the model to produce unstable responses. A ratio between U_{E1} to U_{E2} of 1:1 or 2:1 always gave stable operation while both 2:1 and 4:1 ratios provided the best fit on W_P data at a U_{E2} of 350 W/m^2°C. It should be noted that the offset on T_{E1} only depends on the ratio and not the actual size of the two coefficients.

Final model parameters

Combining the trends seen in the above tuning results with trial and error inspection, the following parameters were chosen for the final evaporator model:

Table 6-10: Final model parameters

Unit	Variable	Selected		Units
		Effect 1	Effect 2	
		Pass 1	Pass 3	
Distribution plate	A_{plate}	0.300	0.462	m^2
	A_{holes}	0.0047	0.0049	m^2
	H_R	0.0075	0.0075	m
	C_D	0.8		-
Effect	N_{TE1}	90	100	-
	L_{tubes}	12	12	m
	A_{tubes}	170	190	m^2
	U_e	1800	350	W / m^2.°C
	Thermal Mass	2x10^6	2x10^6	J/°C
	$A_{ext,effect}$	18.0		m^2
	$A_{ext,shell}$	40.0		
Feed holding tank	A_{tank}	N/A		m^2
Thermal vapour compressor	A_{TVR}	2.13E-07		m.s
	B_{TVR}	58.434		m$^{0.03}$s$^{0.06}$ /kg$^{0.03}$
	C_{TVR}	0.971		-
Condenser	L_C	-	12	m
	N_C	-	14	m
	U_C	-	1000	W / m^2.°C

6.2.7 Final model performance

The tuned model was also compared against training data set 09_2, as shown below in Figure 6-17:

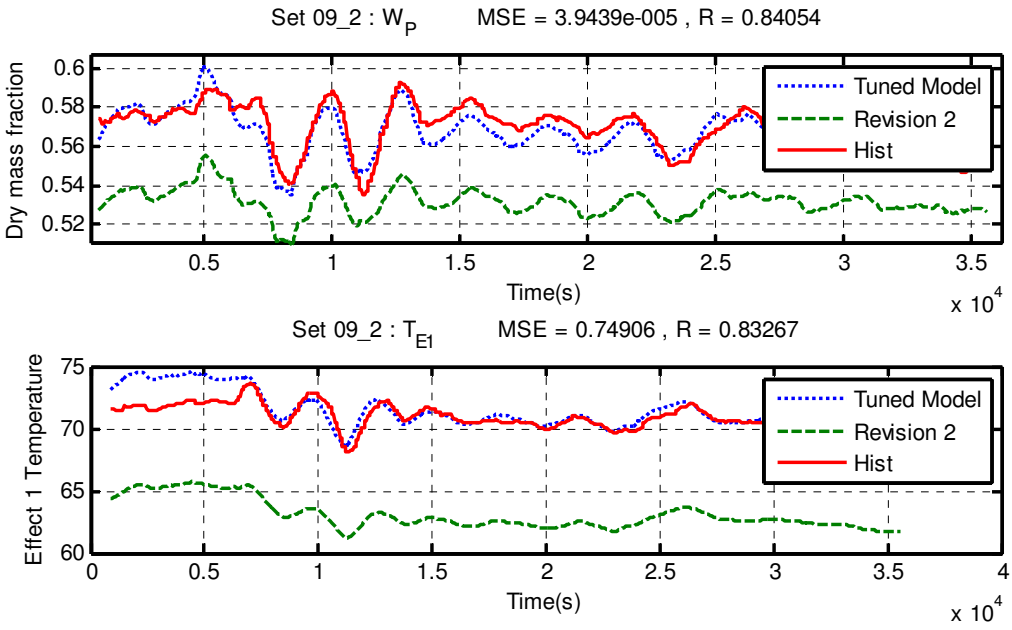

Figure 6-17: Fine tuned model comparison to historical data set 09_2

It can clearly be seen that tuning the heat transfer coefficients and recycle rate for a given data set allows us to achieve very good prediction of both control variables. As the model was specifically trained on this set, only validation on other sets can confirm the prediction capabilities of the model.

As a preface to model validation on validation data sets, a comparison of each revision of the semi-empirical model prediction for training set 09_2 is given below in Table 6-11 :

Table 6-11: Model comparison for training set 09_2

Model	Correlation		MSE	
	W_P	T_{E1}	W_P	T_{E1}
Approximation	-0.146	-0.003	3.58E-04	3.117
First revision	0.798	0.810	4.91E-05	0.500
Second revision	0.803	0.810	5.22E-05	0.490
Tuned final	0.841	0.833	3.94E-05	0.749

Note the pronounced increase in correlation from the approximation model to the final tuned model for both W_P and T_{E1}. Furthermore it is interesting to point out, as mentioned earlier, that the second revision gave almost no improvement over the first, except for correcting model structure. This validates MA 5, i.e. that the homogeniser can be approximated with an extra pass instead of recycle.

The MSE values show the same trends for W_P as observed for correlation, yet it is interesting to see the increase of error for T_{E1} even though the bias decreased significantly. Initially it was decided to compare the models on MSE values while neglecting bias. This ensured that only the dynamic performance was quantified (and not bias, which is easily influenced by tuning). Therefore, even though the tuned model removed virtually all the T_{E1} bias, the MSE increased. The performance decrease is however negligible when compared to the gain in both correlation values as well as W_P MSE decrease.

6.2.8 Model on different training data sets

Training data set 09_2 was extensively used for model tuning and training seeing as it offered a lot of input and output variance which would excite the system over a wide range of states and provide the greatest insight with respect to internal dynamics. To ensure that the model is representative of the FFE in general circumstances, comparisons to different training sets were made with the two worst cases shown below:

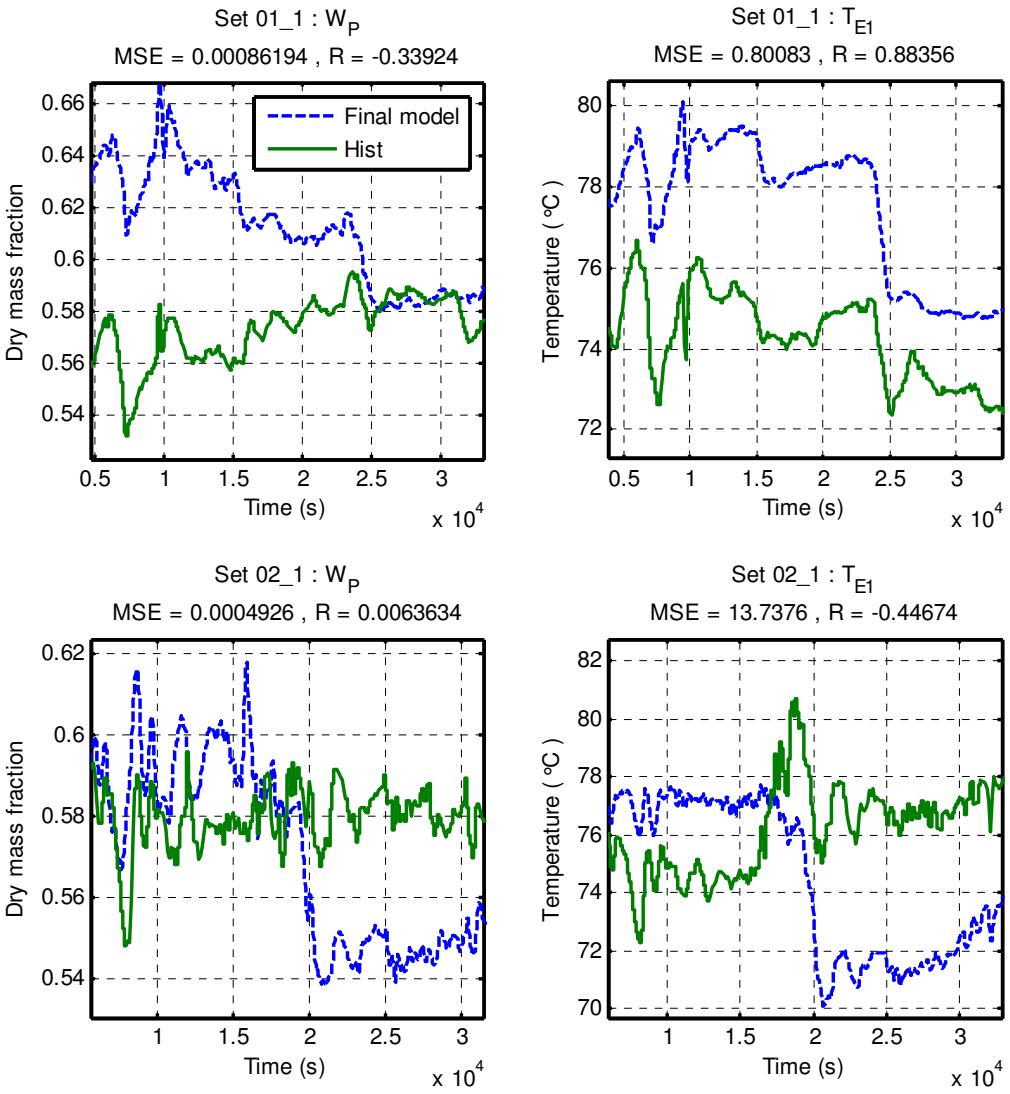

Figure 6-18: Tuned model versus historical data set 01_1 and 02_1

The T_{E1} prediction for set 01_1 captures the dynamic variation very well, yet with a constant bias which points to either different recycle fractions or heat transfer coefficients to those identified. W_P prediction is worse, with a downwards trend observed in the model over the first half of the data set and the opposite, i.e. upwards trend, observed in the historical data. For the second data set the final model shows a sharp downwards trend at ± 18 000s without the accompanying upwards trend seen just before

in the historical data set. In set 02_1, the product dry mass predictions pick up on the small trends seen in the historical data, but also shows a sharp downwards trend at the same time as T_{E1}.

To understand why the model failed to predict the slow trend of set 01_1 W_P and only showed the downward sharp trend for set 02_1, the input trends need to be analysed as well:

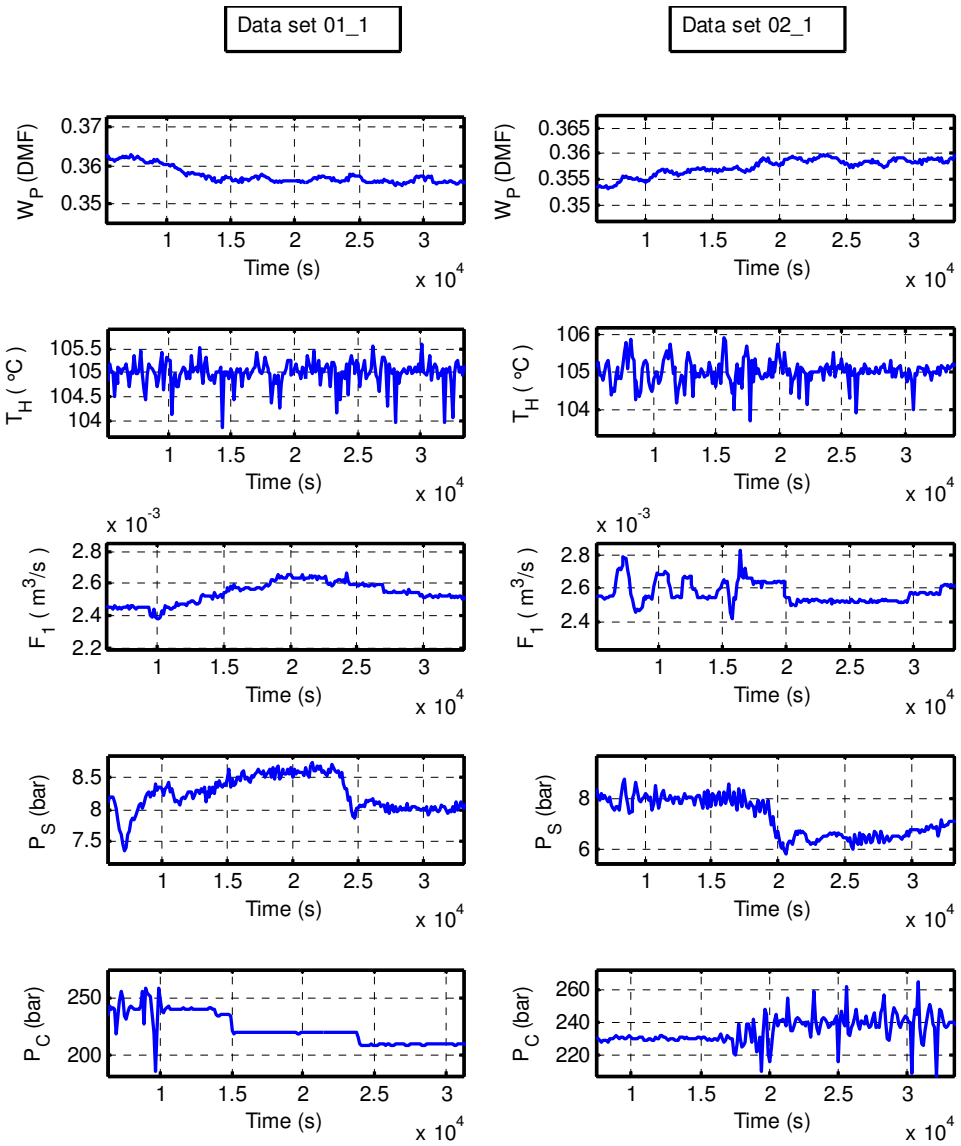

Figure 6-19: Input data from historic set 01_2 (left) and 02_1 (right)

For set 01_1 W_F steadily decreases while P_S increases (until ±23 000s), therefore one possibility is that the model overestimated the effect of W_F while underestimating the effect of the increased steam. Another possibility was that more flashing was observed in the FFE and therefore an increase in F_1 would cause a greater increase in W_P than estimated by the model. Historical set 02_1 conversely implies that less flashing could be occurring inside the FFE than the model predicts: at ±14 500s the feed

rate increased (and then decreased) and stabilised which would cause T_{E1} to increase (and then decrease) while having negligible effect on W_P if flashing was mostly neglected (as seen in Figure 6-18). The decrease in P_S at ± 19 000s would then explain the fall in both the predicted W_P and T_{E1} while it would only counteract the increased feed flow in the actual data. The third possible cause is the condenser pressure which falls sharply at ±15 000s for historical set 01_1 and starts to fluctuate at ± 18 000s for set 01_2. The sharp decrease in set 01_1 would explain the sudden decrease in T_{E1} but not the steady increase of W_P while the fluctuations in P_C for set 02_1 (with the drop in P_S) could account for both W_P and T_{E1} behaviour.

The discrepancies for both set 01_1 and 02_1 are most likely a combination of the possibilities mentioned above. In addition, the long term difference in trends for W_P in set 01_1 will have no effect on control simulations as an integral controller will reject long term offsets. It should be noted again that each data set spans 10 hours worth of operation and the trends observed are relatively slow. The effect of flashing on control can also be easily tested by changing the ratios once the controller has been designed while the effect of P_{CW} (F_{CW} for our model) can be tested by adjusting F_{CW} ranges for the controller.

Two more training sets were investigated, namely set 02_2 and 11_1, with the results of the tuned model shown below:

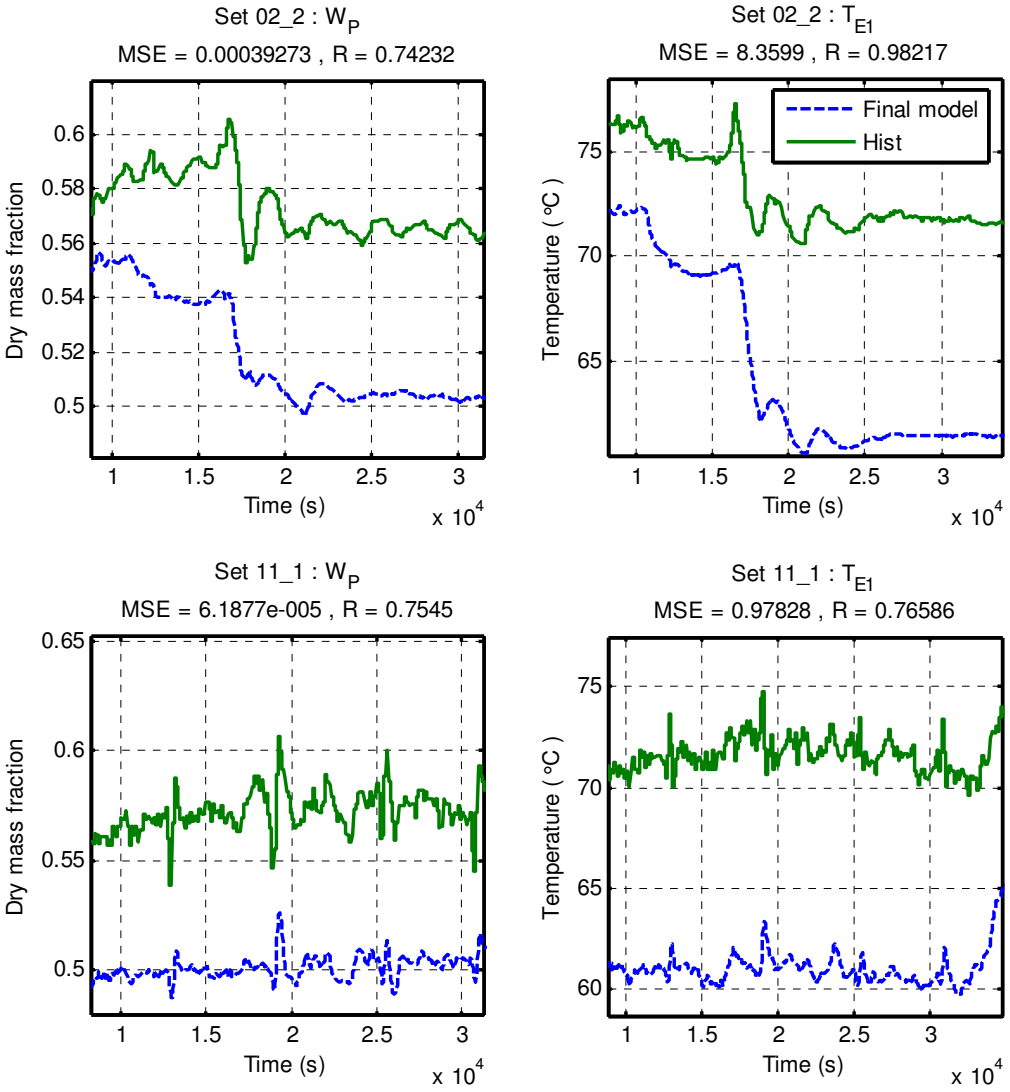

Figure 6-20: Tuned model on historic set 02_2 and 11_1

In both sets the model performed well by predicting most of the deviation seen in historical data as well as the overall trends, except for a region between 10 00s and 17 000s for W_P on set 02_2. The deviations in the model are smaller than those seen in the actual data which could point to either over estimated thermal inertia constant or too conservative condenser pressure action.

As seen with previous comparisons, both set predictions show a significant bias. This bias indicates that either the milk properties, i.e. heat transfer coefficients, or FFE recycle ratio were changed.

6.2.9 Final model performance on different recipes

The model was also tested on each of the available recipe training data sets. As with recipe 1 data it was found that there exists constant bias between prediction and actual values. The dynamic behaviour of the model is more important for control than a constant bias. The bias is most likely because of differences in heat transfer coefficients, recycle rates and in-line dosing between each recipe. The numerical performance result of each recipe (except recipe 6 which only had a validation set) is shown below in Table 6-12.

Note that the correlation value for recipe 1 includes all the data sets, including sets 01_1 and 02_1 which showed low correlation yet still captured most of the system dynamics (as explained in Section 0). These outlier sets reduced the overall correlation drastically for recipe 1, yet the analysis of Section 0 holds and the model is seen as adequate for recipe 1.

Table 6-12: Final model result on training data

		Recipe 1	Recipe 2	Recipe 9
W_P	Correlation	0.32	0.70	0.72
	MSE(x10^3)	0.30	0.33	0.11
T_{E1}	Correlation	0.63	0.60	0.72

The results for both recipe 2 and 9 are comparable or superior to that recipe 1 without any additional training or tuning of the model.

A constant bias was again observed as shown in below:

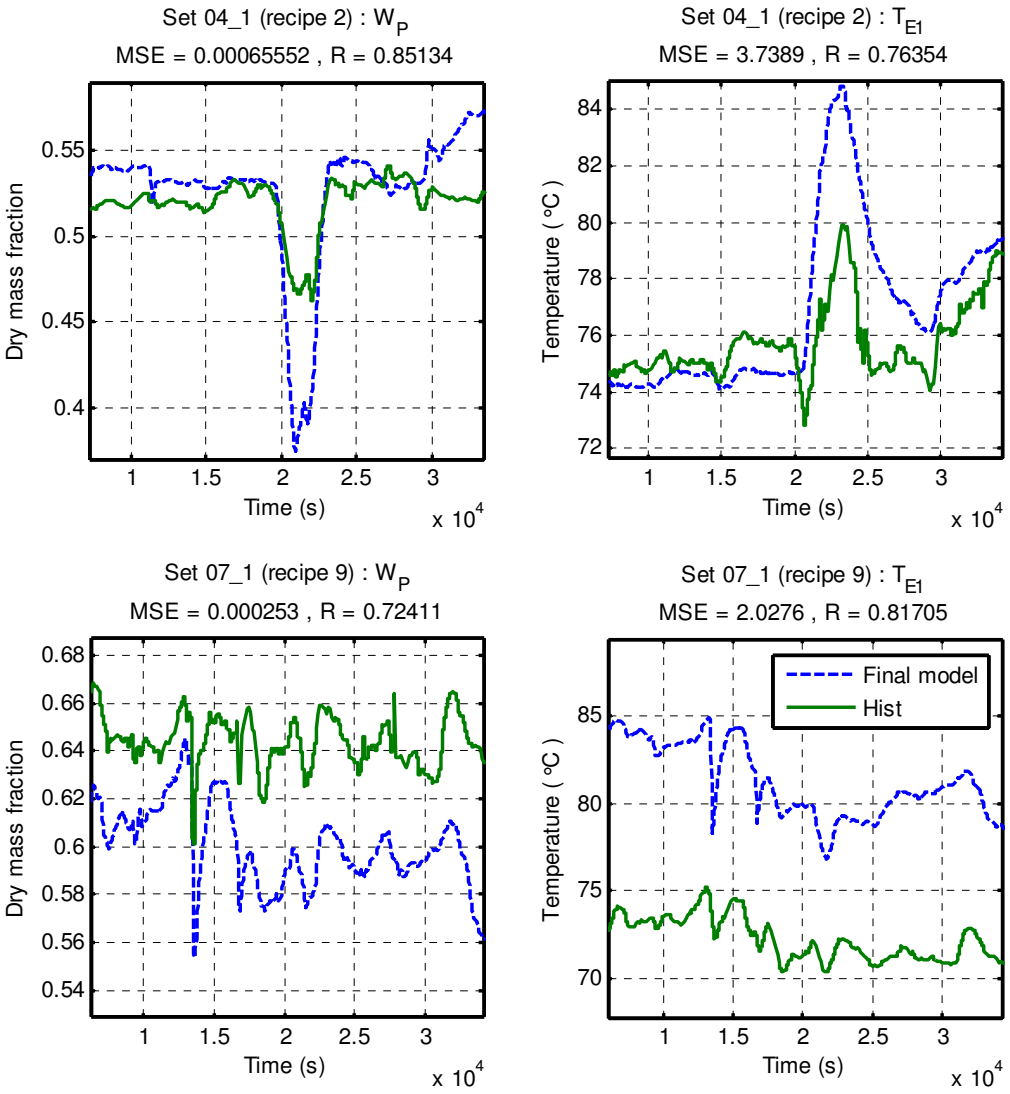

Figure 6-21: Final model prediction compared to historical data – different recipes (2 and 9)

Figure 6-21 shows that the model predicts both W_P and T_{E1} well, except once again for a constant bias. It should be noted that for recipe 2 all historical dry mass fractions were found to be above 2, further inspection points to a faulty dry mass calculation in the historical data with an apparent bias of 1.5.

6.2.10 Model validation against unseen data

With the model parameters fixed, and the training data sets evaluated, unseen historical data was used to further test the generalisation of the model predictions. The first validation set of recipe 1 and 2 is shown below and compared to the predicted values:

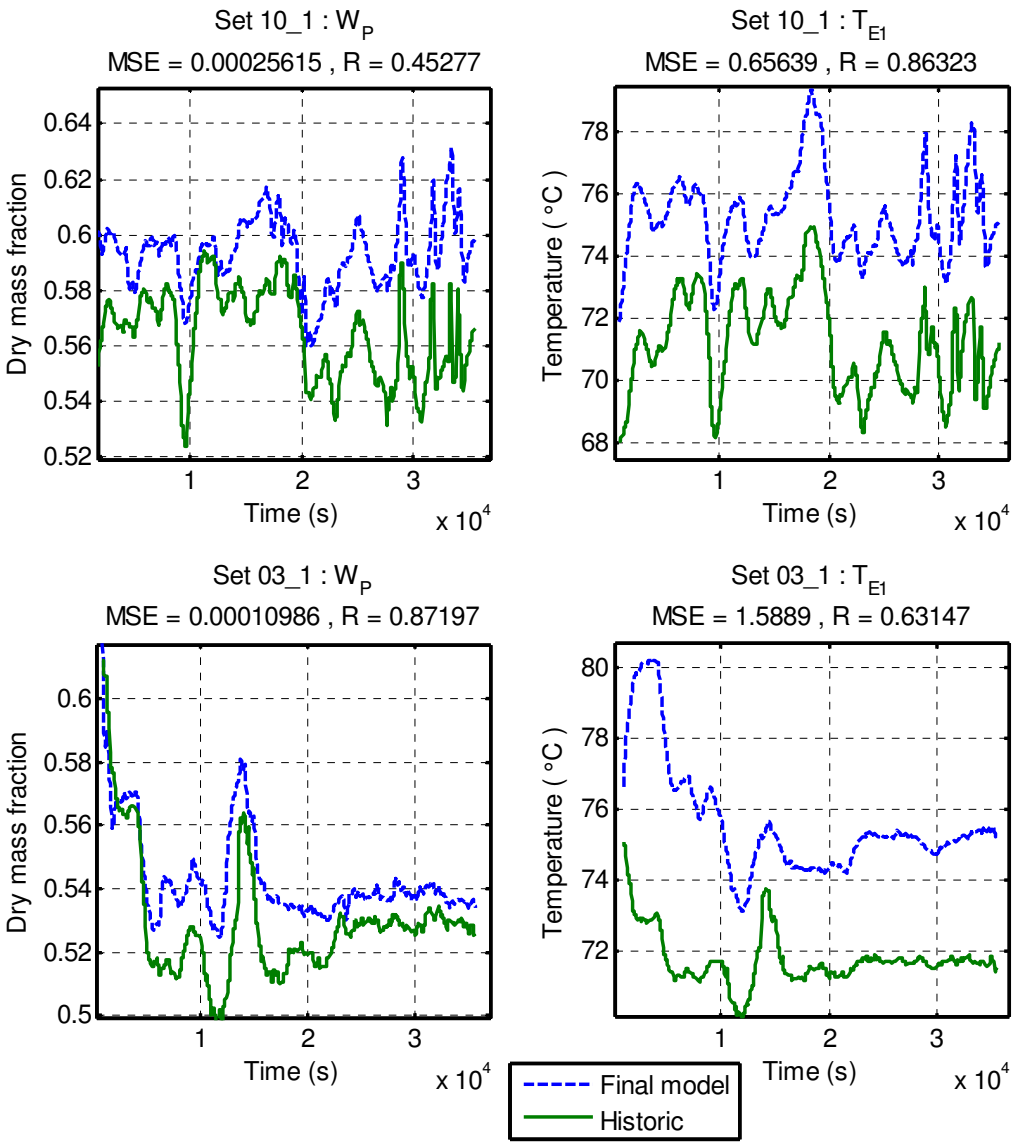

Figure 6-22: Model validation for recipe 1 (set 10_1) and recipe 2 (03_1)

Set 10_1 shows that the model performs well on the first recipe validation data, which was expected as most of the tuning was done on training data for this recipe. For W_P at 15 000s there is a discrepancy, which could be the cause of an unknown disturbance. Set 3_1 shows a lot of variation at the start of the historical data, which points to unsteady process condition, possibly just after start-up. T_{E1} prediction

shows a rapid fall at the start of the set, while the historical data value climbs quickly. After ± 4 000s the prediction follows the actual trends closely which strengthens the argument for initial unsteady process conditions.

The first validation set of recipe 6 and 9 is shown below compared to the predicted values:

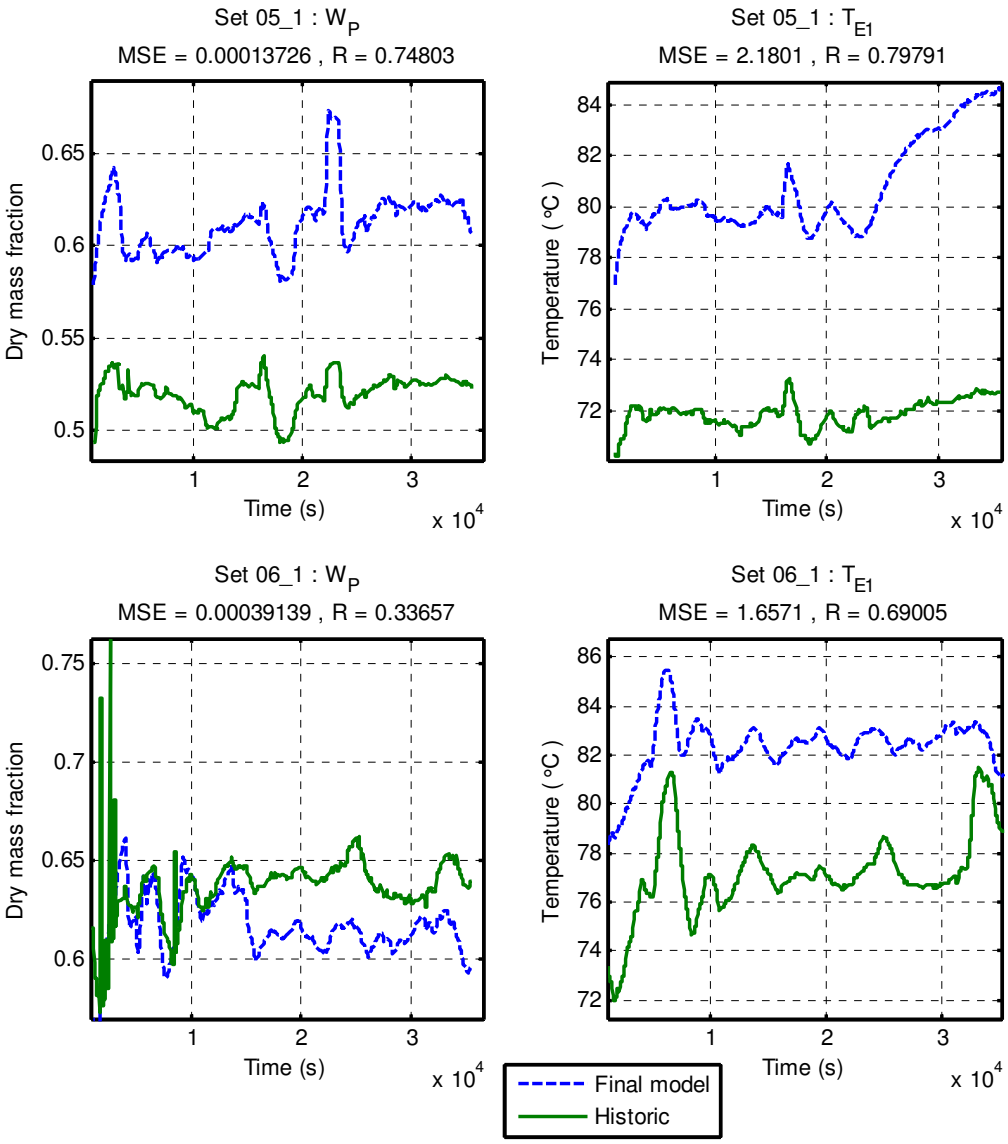

Figure 6-23: Model validation for recipe 6 and 9

Set 5_1 shows that the model predicts both W_P and T_{E1} trends very well even though no training data was available for recipe 6, with only a difference in gain for W_P seen at 22 000s and a T_{E1} slow rise seen at the end of the data set. The overall good correlation and trend predictions confirm that the model may be applied to various recipes without major tuning.

The first historical data set for recipe 9 shows a lot of oscillations initially which also point to some form of unstable process conditions. W_P predictions are however close to the historical data except for a sudden drop in model predictions at ±14 000s that was not seen in the actual values. T_{E1} predictions hold with every major peak in historical data except for a quick rise in historical values at the end of set 6_1. As inspection of the input variables shows no reason for either deviation it can be assumed that there were either unmeasured disturbances or an internal fault inside the FFE such as a blockage or incorrect flow path.

Final model mass balance in validation data

The initial mass balance performed in Section 6.2.2 was redone taking values from one of the validation data sets. The mass flows are shown below in Figure 6-24:

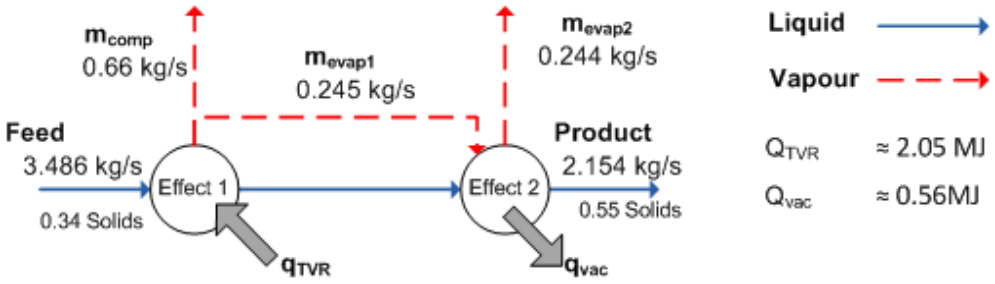

Figure 6-24: Mass balance validation

Note that the flows are very similar than those shown in Figure 6-3, with the one kilogram steam to one kilogram vapour relationship being observed ($m_{evap1} \approx m_{evap2}$). The total amount evaporated from effect 1 is equal to the mass pulled to the compressor (m_{comp}) added to the amount pulled to the second effect (m_{evap1}).

To check the mass balance the mass flowing out was subtracted from the mass entering the system, which yielded an error of 0.46×10^{-3} kg/s or 0.013% of the incoming stream. This error is far within acceptable bounds and can be attributed to minute hold-up inside the effects or purely numerical error. This calculation proves that FFE model handles mass flow rates correctly.

6.2.11 Semi-empirical modelling conclusion

As stated at the start of this chapter, the final model needed to provide an accurate simulation of the local FFE process. This included modelling the system dynamics during continuous operation as well as incorporating the effect of both major disturbances and inputs. Furthermore, various parameters of the process units needed to be estimated by comparison to literature values. The model development methodology followed was an inherently iterative one which started off with the simplest approximation possible and worked towards a final tuned model. Each of these iterations will be concluded.

Before each iteration of the model is evaluated it is important to check the most basic principle of a continuous system, i.e. that all the mass that is entering the system also exits. The mass balance shown

in Figure 6-24 confirms that the final semi-empirical model adheres to this principle with an in minus out error of 0.013%, which might be due to liquid hold-up inside the FFE or Simulink error. In either case this error is negligible.

Approximation model

The approximation model neglected various process aspects, with the most important omissions being both TVR and condenser action. These simplifications greatly decreased the model correlation to historical data, with R values of -0.14 and -0.002 found for W_P and T_{E1} respectively. Even so the approximation model showed that semi-empirical modelling is viable when compared to the sanity checks of Section 6.1.6. Once the simplifying TVR and condenser assumptions were included into the reasoning, it was found that the approximation model did represent the internal dynamics of the local FFE.

It was also concluded that both TVR and condenser action is pivotal to FFE modelling, as these units describe the two main manipulated variables, through which control will be performed. Therefore the approximation model could only be seen as a proof of concept and not a suitable simulation model.

First revision model

The major enhancements made for the first revision model were the addition of the TVR and condenser action. Together with the process units added, it was decided to also include milk flashing and variable milk densities. Flashing increased evaporative capacity slightly by assuming that excess feed energy was used to convert liquid milk into vapour.

Sanity checks proved that the model now responded almost exactly as operator logic dictates, with the only exception that remained being an increase in T_{E1} when an increase in T_H was simulated. It should be noted that the response was not defined by operators but rather conforms to thermodynamic laws, which would imply that some energy also be transferred from the hot feed to the cooler steel in the effect.

The first revision model showed a significant increase in correlation to historical data with correlations of 0.798 and 0.809 seen for W_P and T_{E1} respectively. The addition of the TVR and condenser action clearly enhanced the model viability and confirmed the proof of concept seen in the approximation model.

In contrast to the increased correlation, the first effect temperature reacted far too slowly to input variables, pointing to a possible over estimation of effect thermal mass. This low variation, coupled with some modelling bias observed, highlighted the fact that further parameter tuning was necessary.

Second revision model

Before the required tuning could be performed the model structure had to be brought into line with the local FFE structure to ensure sensible tuning. For example, if the model was tuned while still assuming the homogeniser acted as an extra pass it would cast doubt when extrapolating the model to different process operating conditions.

The model changes included adding inventory tanks to each effect as well as treating the homogeniser as a recycle stream to the first effect. With these changes taken into account the model correlation stayed remarkably similar to that of the first revision model at 0.8 and 0.81 for W_P and T_{E1} respectively. The slight increase showed that the simplifying homogeniser assumption was accurate.

The semi-empirical model could be said to satisfy the model requirements at this stage with suitable historical data representation (from the high correlation values) and structural agreement to the local FFE. However the bias and low variation from the first revision model remained. Furthermore, the effect of model internal parameters such as heat transfer coefficients and recycle ratios were not clear.

Tuned semi-empirical model

The final tuning of the semi-empirical model evaluated the effect of changes in heat transfer coefficients, thermal inertia of the FFE, recycle ratio and structural parameters in order to select the appropriate values.

The heat transfer coefficients were found to interact with one another to influence the FFE model bias both by the relative and absolute size of the coefficients. Higher values tended to produce instability, especially when the second effect coefficient was more than 3 times greater than that of the first effect. Increasing the absolute values also led to the model predicting larger W_P and T_{E1} values, which is theoretically sound. Larger heat transfer coefficients would lead to greater effect temperatures and therefore higher evaporation rates. After inspection it was decided to select 325 W/m2.°C and 1800 W m2.°C.

It was found that lower thermal inertia (or thermal mass) resulted in the greater variation of evaporator effect temperatures. This increase in activity was due to the FFE offering less resistance to temperature changes. At a total FFE thermal inertia of $2x10^6$ J/°C, T_{E1} showed the same magnitude of deviations as seen in historical data.

Recycle ratios (fraction of concentrated milk fed back to the first effect) had a greater influence on W_P bias, with T_{E1} bias only changing at relatively high ratios (>0.5). This is reasonable as W_P is closely related to the amount of feed processed, as well as the feed dry mass concentration with a recycle ratio influencing both, while the effect temperatures are more dependent on TVR and condenser action - which are not influenced by recycle ratio. The recycle ratio selected was 0.1 (product fraction fed back), even though a 0.01 fraction showed better bias reduction. The larger ratio was decided upon as it is more reasonable and other factors such as heat transfer coefficients will also influenced the bias.

The final tuning of the model increased the W_P correlation of the semi-empirical model to 0.84 and 0.83 for W_P and T_{E1} respectively. Note that this was only for training set 09_2 which was extensively used throughout the model development.

Comparison on other training data sets

Training focussed on historical set 09_2, although other training sets were also investigated, when needed, to confirm certain process reactions. One example was where the flashing fraction was changed, where different training sets were also evaluated. Similar situations arose when doubt was

cast upon a certain section in historical data set 09_2 and a different set was used to validate the model action.

After the final model was tuned on recipe 1 data, all the other training data sets were also simulated. The resulting correlations were somewhat surprising; with recipe 1 showing the poorest overall W_P correlation (0.32), while the model performed significantly better on all the other recipes. Recipe 6 showed the highest W_P correlation (0.78), yet only one data set was available. Recipe 2 showed a W_P correlation of 0.70 while recipe 9 yielded a W_P correlation of 0.72.

The low correlation seen for recipe 1 was most likely due to some data sets skewing the results with anomalies. The two worst performing historical training sets (01_1 and 02_1) were investigated. For data set 01_1 the model showed a long term downwards W_P trend while data set 02_1 showed a sudden drop in predicted W_P values which was not seen in the historical trends. It was found that the semi-empirical model still replicated most of the process dynamics well. Additionally a controller would easily be able to negate the long term trend using integral action.

The first effect temperature prediction showed high correlation with historical trends, with the model achieving values over 0.60 for all the recipes.

Furthermore, the fact that the model correlations went up when tested on other recipe training data sets, prove that the model is applicable to a wide range of circumstances as long as the data is reliable.

Comparison on validation data sets

As the tuning parameters were now fixed and the semi-empirical model fully developed, the model was now subjected to unseen data sets to validate its structure and dynamics.

The model performed better than during training for recipe 1 product dry mass and first effect temperature, with correlation values of 0.39 and 0.75 for W_P and T_{E1} respectively. Recipe 2 showed a drastic decrease in correlation, with a W_P correlation that fell to 0.27, while T_{E1} rose to 0.63. Note however that recipe 2 had one data set with correlation values far higher (0.79 and 0.67 for W_P and T_{E1}) and one set with very low values. Therefore it is likely that the second set again contained anomalies. Recipe 6 showed high correlation values (0.74 for W_P and 0.79 for T_{E1}), while recipe 9 showed a decrease in W_P correlation, but an increase in T_{E1} (0.45 for W_P and 0.79 for T_{E1}).

Although the numerical performance metrics did provide a method for comparing the model predictions directly, some doubt was created on how well it performs. Both Figure 6-18 and Figure 6-20 proved that the model could predict the historical trends fairly well and still deliver very poor correlation values. Furthermore, Figure 6-23 shows how well the model performed on validation data, yet only delivered a W_P correlation of 0.38.

In conclusion, the model performed very well on validation sets and it can be said to achieve the goal set out at the start of the chapter to adequately represent the local FFE. The model adheres to all the sanity tests, describes the local FFE dynamics well and includes the functionality of using historical values for simulation.

Chapter 7 - Data based modelling and comparison

In contrast to the knowledge based semi-empirical model developed in Chapter 6 this chapter will focus on developing data based models, specifically transfer function and autoregressive with exogenous inputs (ARX) models. The methodology followed for the semi-empirical modelling was slightly adjusted for the data based models:

- Step 1 : Model goal
- Step 2 : Simulation environment
- Step 3 : Structure selection
- Step 4 : Model identification
- Step 5 : Determine solution
- Step 6 : Analyse and compare model

Note that the model goal stays exactly the same as in Section 6.1.1 while Matlab was also chosen for the simulation environment. The Matlab system identification toolbox will be used to select the model structure, perform subsequent identification and determine the solution. Finally the models will be compared directly to the semi-empirical model of Chapter 6.

7.1 Structure selection

Both the ARX and transfer function models may take on various forms. This section describes the chosen structure as well as selection reasoning.

7.1.1 Transfer function structure

As explained in Section 5.1 transfer function models may take on various forms. In accordance with previous research [**23**] a combination of first order models, each describing an input to output relationship, was chosen. The inputs considered were:

- Feed dry mass (W_F)
- Feed temperature (T_H)
- Feed flow rate (F_1)
- Steam pressure (P_S)
- Condenser pressure (P_C)

With the corresponding model outputs, product dry mass (W_P) and first effect temperature (T_{E1}). For this study all the variable interactions will be assumed to be linear and time invariant. This assumption was made as the FFE generally shows slow response to input variables and it greatly simplifies identification. If a second order structure was assumed it would increase the amount of parameters that need to be identified per transfer function and therefore possibly over train the models. The parameters for a first order transfer function, *G(s)*, are defined in Section 5.1 and again shown in Eq 7-1 below:

$$G(s) = \frac{Y(s)}{U(s)} = \frac{K_{pr}e^{-\theta s}}{\tau_{pr}s + 1} \qquad \textbf{Eq. 7-1}$$

Where *G(s)* Transfer function

$U(s)$	Model input
$Y(s)$	Model output
K_{pr}	Process gain
τ_{pr}	Process time constant
$e^{-\theta s}$	Process time delay

A graphical representation of both groups of transfer function models are shown below in Figure 7-1 with $G_{W,i}$ and $G_{T,i}$ referring to product dry mass and first effect temperature functions respectively.:

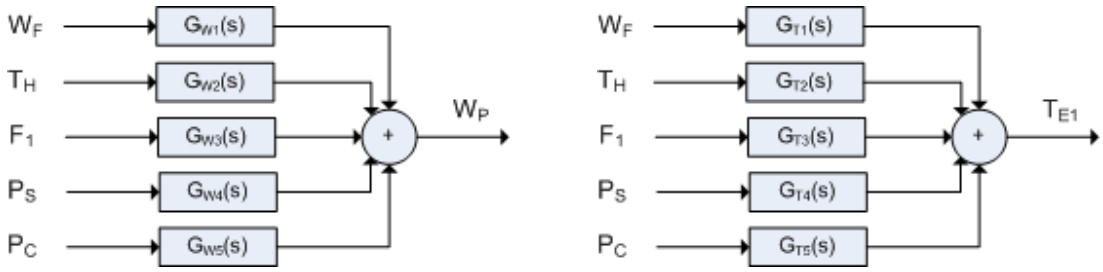

Figure 7-1: Transfer function model for inputs to product dry mass and first effect temperature

From Figure 7-1 another aspect of transfer function modelling is observed, i.e. that the output of each individual function can be added to form the output variable. This can be done as transfer functions model variable deviations, i.e. given a change in input it will predict the change in output. This does however also mean that transfer functions work around a certain variable level.

7.1.2 ARX model structure

The general form of a discrete ARX model is given by the system identification toolbox as:

$$A(q)y(t) = \sum_{i=1}^{nu} \frac{B_i(q)}{F_i(q)} u_i(t - nk_i) + \frac{C(q)}{D(q)} e(t) \qquad \textbf{Eq. 7-2}$$

Where

$A(q)$	Time shift vector with *na* coefficients
$y(t)$	Model output
nu	Number of inputs
$B_i(q)$	Time shift vector with *nb* coefficients
$F_i(q)$	Time shift vector with *nf* coefficients
u_i	Model inputs
nk_i	Number of samples corresponding to input delay
$C(q)$	Time shift vector with *nc* coefficients
$D(q)$	Time shift vector with *nd* coefficients
$e(t)$	Noise estimation

The system identification toolbox also gives an option to estimate the number of model coefficients. This was used as the data based models were created by assuming that the minimum amount of process knowledge was available. For the same reason the structure and inner workings of the ARX model were not investigated to the level seen for the semi-empirical model units.

7.2 Model identification

The larger collection of training data sets from Section 3.2 were reduced to one training set per recipe for both ARX and transfer function modelling. A list of the training sets is given below:

Recipe 1	Historical set 09_2
Recipe 2	Historical set 03_1
Recipe 6	Historical set 05_2
Recipe 9	Historical set 07_1

The data was imported into Matlab's system identification toolbox. Hereafter the set means were removed to ensure only the process dynamics were modelled.

7.2.1 Transfer function identification

The identification of the parameters takes place once the user has specified the structure of each function as well as the estimation method, initial system state and parameter range.

Transfer function identification without limits

Initially identification of the transfer functions was performed without setting any limits on the ranges for each parameter in Eq. 7-1. The results are given in Table 7-1 below:

Table 7-1: Identified first order models for the FFE from historical data

Output \ Input	W_F	T_H	F_1	P_S	P_C
W_P	$\frac{3e^{-494s}}{551s+1}$	$\frac{31e^{-0s}}{1075400s+1}$	$\frac{-90e^{-0s}}{1301s+1}$	$\frac{0.043e^{-18s}}{322s+1}$	$\frac{-0.082e^{-170s}}{6625s+1}$
T_{E1}	$\frac{-785e^{-3600s}}{4086s+1}$	$\frac{40610e^{-166s}}{2.6e^{7}s+1}$	$\frac{-4127.4e^{-47s}}{47s+1}$	$\frac{2.531e^{-0s}}{837s+1}$	$\frac{0.053e^{-3s}}{34s+1}$

A quick inspection of Table 7-1 raises some major concerns. Firstly there is a strong relationship between W_F and T_{E1}, which is highly unlikely seeing as W_F has no effect on FFE temperature. Secondly both TH transfer functions have time constants in excess of 11 days. This is clearly unreasonable if not impossible. Finally the dead time for the $P_S \rightarrow W_P$ transfer function is 19s, again this is highly unlikely as any change in P_S first needs to affect the first effect temperature, then the second and only then will a W_P change be observed. Both effects have a high thermal mass resisting the temperature change as well as holding tanks which will further delay any W_P change.

These inconsistencies can easily be picked up by anyone who has some knowledge of the local FFE. It is however problematic if the identification was attempted purely from an a data point of view as the comparison of the transfer function models to historical data for set 05_2 shows below:

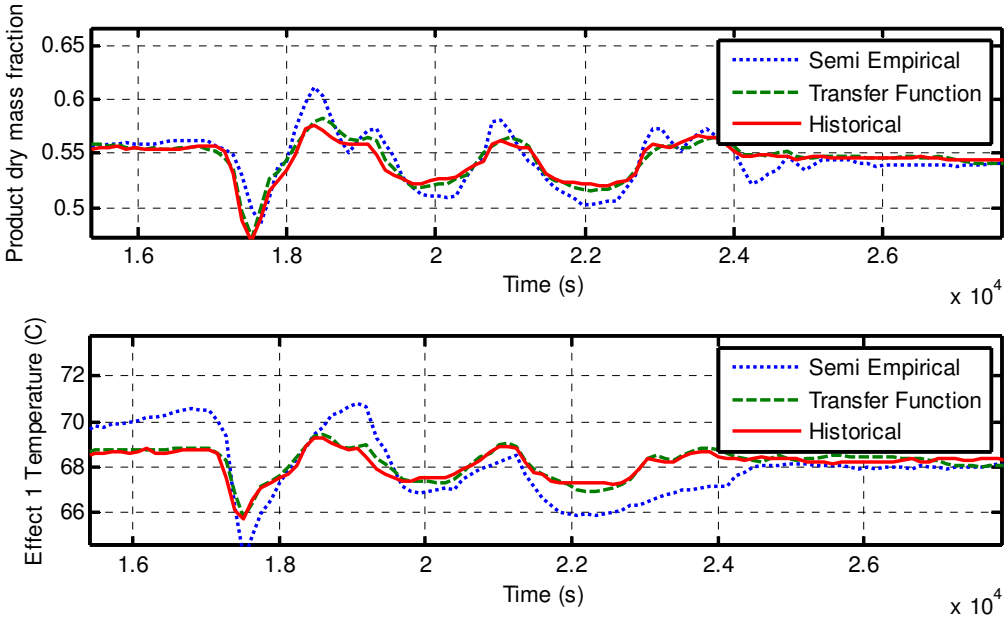

Figure 7-2: Comparison of initial transfer function model and semi-empirical model for data set 05_2 (recipe 6)

Here the transfer function model performs better than the semi-empirical model, which would lead one to think that, however unlikely, the transfer functions shown in Table 7-1 must be correct. This is a prime example of over fitting, where a model with given parameters is only exposed to one data set. If one now uses a different training set the model inaccuracies become apparent:

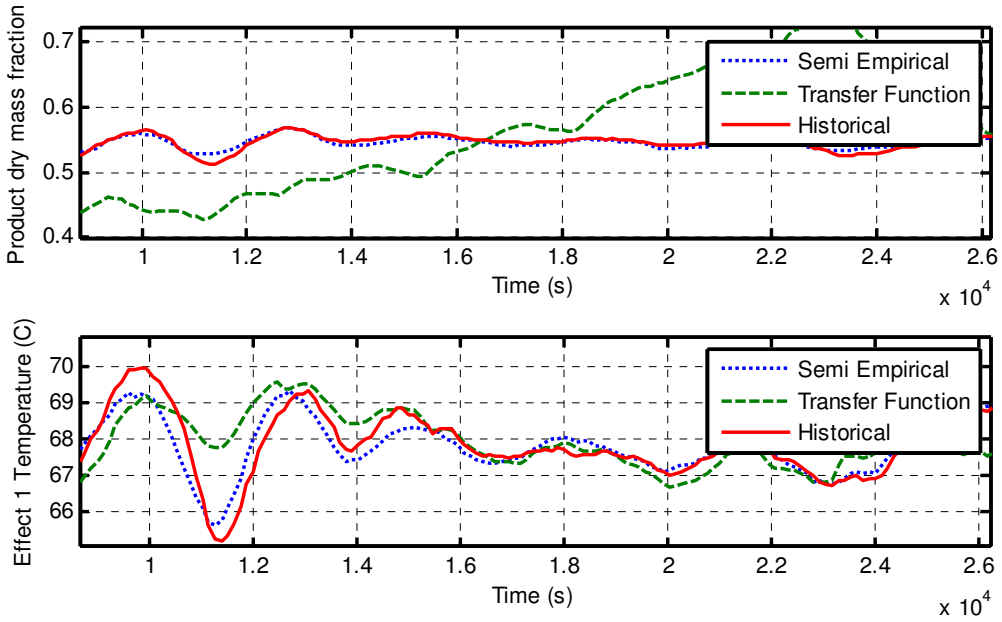

Figure 7-3: Comparison of initial transfer function model and semi-empirical model for data set 09_2 (recipe 1)

Note from Figure 7-3 that the semi-empirical model still performs well, but the transfer function model is completely incorrect. Interestingly enough the T_{E1} prediction of the transfer function has not completely deteriorated, which implies the identification was more successful.

Transfer function identification with limits

To prevent the overtraining of the transfer function models, a training set was selected whereafter the new model was tested on the other training sets. Once the model showed good representation of all the sets it was selected. Additionally certain limits and restrictions were placed on the parameters after thorough inspection of the historical data:

- The $W_F \rightarrow T_{E1}$ transfer function gain was set to 0 to remove it from the overall model.
- All process time constants were limited to below 6 000s.
- All process gains were limited to the correct sign (by comparing to the sanity step test response of Section 6.1.6). Order of magnitude ranges were also implemented.
- The process dead times were limited to values below 1 000s.

The above limits were all estimated from expected process response and relied on process knowledge gained when designing the semi-empirical model. The resulting transfer functions are shown below in Table 7-2:

Table 7-2: Identified first order models for the FFE from historical data

Output \ Input	W_F	T_H	F_1	P_S	P_C
W_P	$\frac{0.85e^{-171s}}{171s+1}$	$\frac{0.0074e^{-132s}}{1000s+1}$	$\frac{-48.37e^{-0.1s}}{0.15s+1}$	$\frac{0.07e^{-25s}}{654s+1}$	$\frac{7e^{-4}e^{-892s}}{3691s+1}$
T_{E1}	0	$\frac{3.3e^{-299s}}{1000s+1}$	$\frac{2953e^{-10s}}{999s+1}$	$\frac{2.5e^{-50s}}{425s+1}$	$\frac{0.04e^{-58s}}{248s+1}$

Although the transfer functions shown in Table 7-2 above do remove a lot of the concerns from Table 7-1, there are still a few suspicious terms. Firstly, the $F_1 \rightarrow W_P$ system has a very short process time constant. Secondly, a few of the dead times are below the historical data sampling rate, of 120s, which causes some concern as these values will be unreliable.

Even with these concerns it was decided to keep the identified transfer function as any further use of process knowledge would remove the design time advantage of transfer function modelling. The newly identified model will be compared to the semi-empirical model together with the subsequent ARX model to offer a more concise assessment.

7.2.2 ARX model identification

The ARX model was identified with the same training sets used for transfer function identification. Furthermore, the system identification tool was used to estimate the order parameters, i.e. *na*, *nb*, *nf*, *nc*, *nd* and *nk*. The resulting model and full time shift vector values are shown in Appendix A.

7.3 Data based models compared to semi-empirical model

As the transfer function and ARX models are very dependent on the initial state for model bias the system identification toolbox was used to estimate the initial state. This put the semi-empirical model at a disadvantage though, seeing as no such initial search is performed on its parameters. In Chapter 6 it was seen that the model bias does not adversely affect the model dynamics. As such, all three types of model were compared after removing the respective mean values and adjusting the outputs variables to fluctuate around a nominal value.

7.3.1 Training data comparison

Firstly two of the training sets were simulated to ensure that the transfer data based models are more robust than the first iteration of the transfer function:

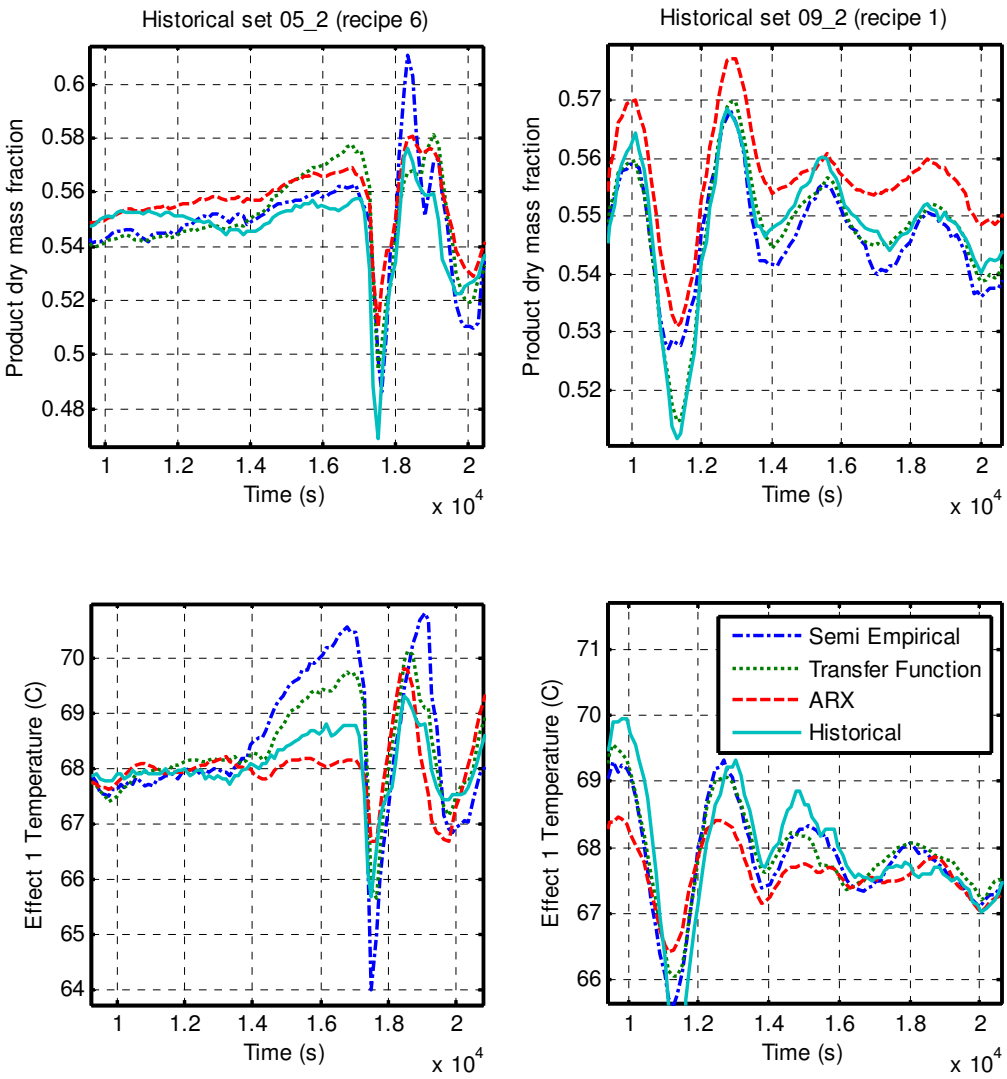

Figure 7-4: Comparison between data based and semi-empirical models for recipe 1 and 6 training data

From Figure 7-4 it can be seen that both the ARX and transfer function models perform well on both training data sets. The ARX model shows less pronounced dynamics than either of the other models. To better quantify the relative model performance simulations were run through all of the training set with the results for correlation (R) and mean squared error (MSE) shown below in Figure 7-5:

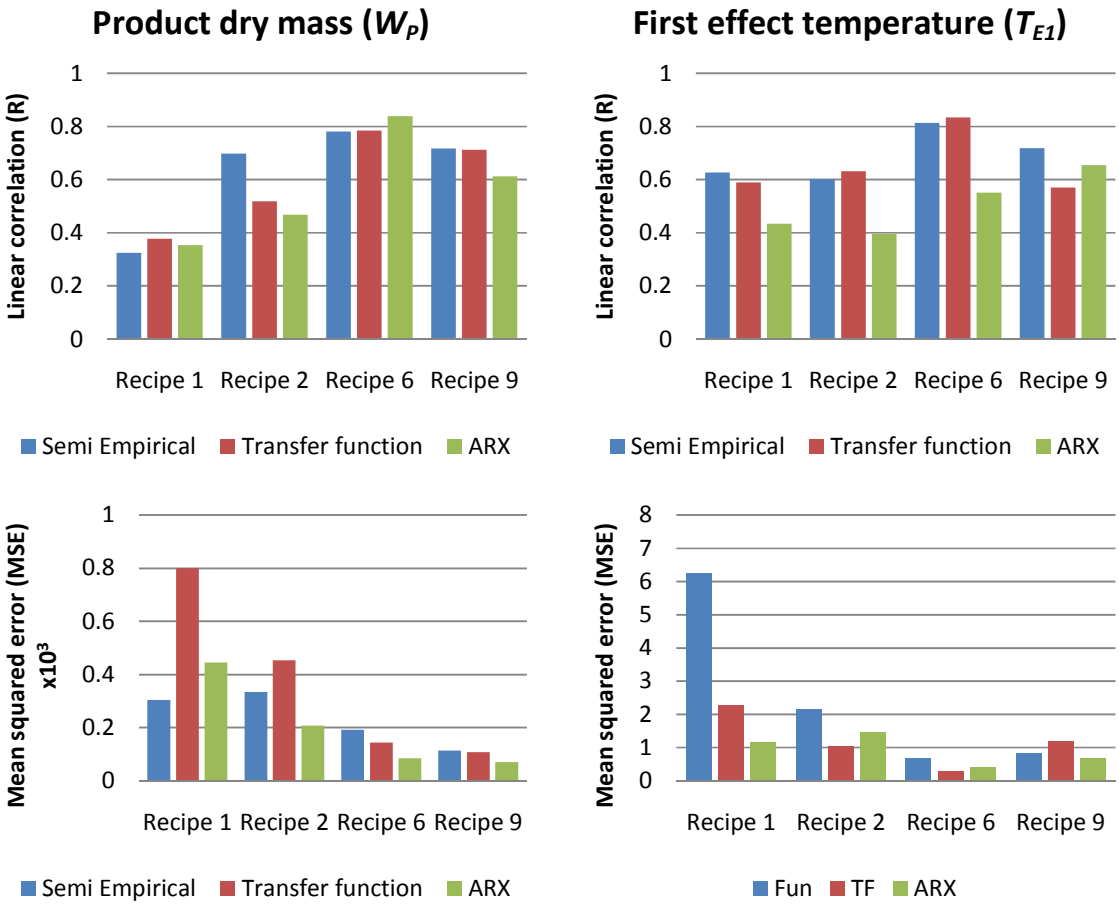

Figure 7-5: Bar charts of model comparisons on training data sets

From the bar charts above a mixed set of results is observed. The T_{E1} correlation of the semi-empirical model predictions to the historical data constantly remained high. The semi-empirical model outperforms each of the other models for recipe 1 and recipe 9, while for recipe 2 and recipe 6 the transfer function model narrowly performs the best. The MSE values give another side of the comparison, with the semi-empirical model showing the worst values for two out of the four recipes. In all but recipe 1 the MSE values are however fairly close.

In product dry mass correlations the results are a lot closer, with the semi-empirical model performing the best for recipe 2, while showing almost exactly the same performance as the other models for recipe 6, recipe 1 and recipe 9. In terms of MSE values the semi-empirical model showed the lowest error for

recipe 1 while the ARX model showed the lowest MSE for the other recipes. The transfer function model showed the worst performance for both recipe 1 and recipe 2.

From the comparisons above, it is clear however that the semi-empirical and transfer function models showed the best extrapolation to the other recipes for both output variables. The ARX model did not perform as well as the other models, specifically with regard to T_{E1} predictions.

7.3.2 Validation data comparison

The models were also compared on the validation data sets. These comparisons will give a better representation of the capacity of each model to be used under different circumstances:

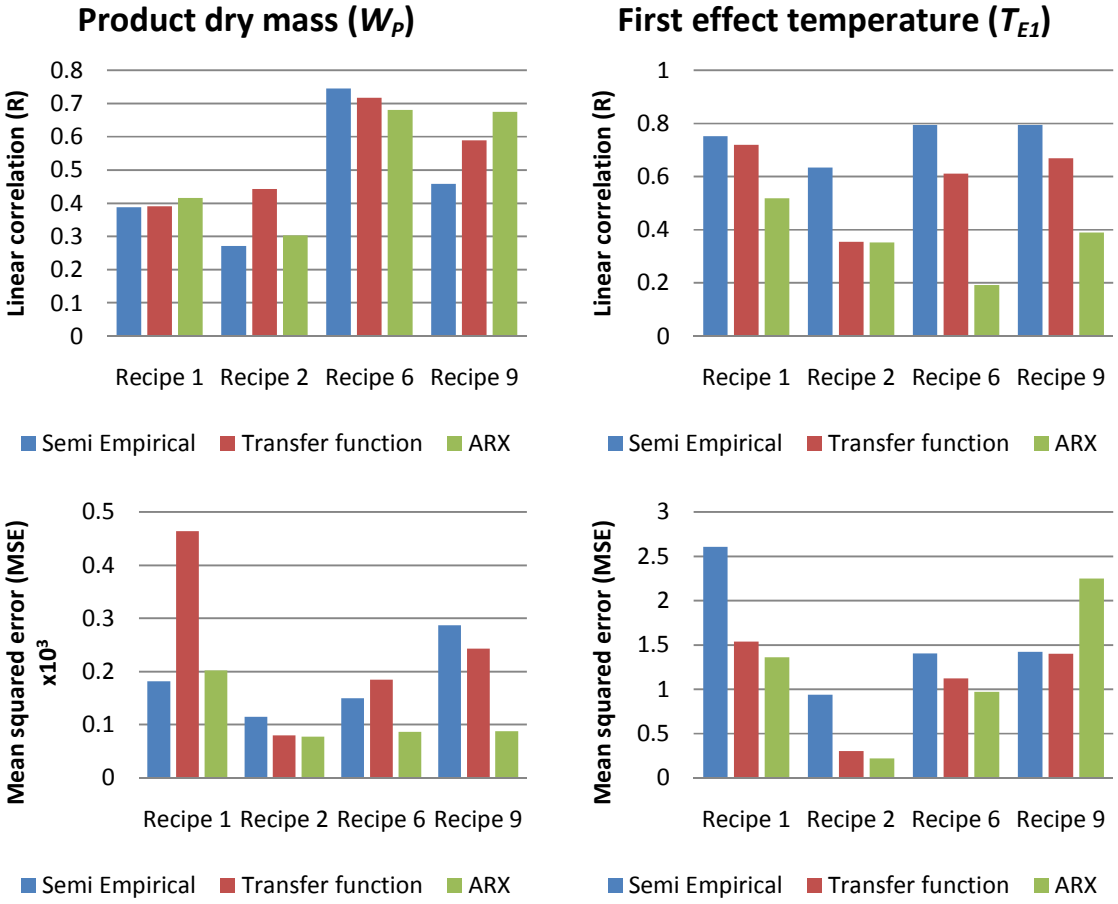

Figure 7-6: Bar charts of model comparisons on validation data sets

In Figure 7-6 above it can be seen that W_P correlations were very similar between the different models, with no model showing a clear advantage over the others. The transfer function model did however not perform the worst for any of the recipes and can be taken as performing the best on the validation W_P data. When comparing MSE values, the transfer function model showed the worst values for recipe 1 and recipe6 while showing high values for the remaining recipes. The ARX model showed the lowest overall errors while the semi-empirical model gave middling results.

When looking at T_{E1} prediction the semi-empirical model showed significantly better correlation to historical data than any of the other models. Furthermore the ARX model again showed poor performance, while the transfer function model showed results in between the other models. Comparing MSE values show that the semi-empirical model showed the worst values for recipe 1, recipe 2 and recipe 6, while the ARX model showed the worst values for recipe 9. It should be noted however that all the MSE values were comparable to the training data and of the same magnitude between the models.

7.4 Data based modelling conclusion

The data based models served a dual purpose. Firstly, to establish a meaningful standard to measure the semi-empirical model against and secondly, offering a simulation alternative to semi-empirical modelling. Therefore the conclusion will be two-fold; firstly comparing the data based models against each other and thereafter against the semi-empirical model.

7.4.1 Transfer function modelling compared to ARX modelling

The main advantage of data based modelling is the development speed and relatively little process knowledge required to formulate and identify the model parameters. In terms of development speed the ARX model required far less work than the transfer function models, which required both structure selection and parameter limits to offer a meaningful result.

The ARX modelling development speed did however come at a price to its prediction accuracy. The transfer function model showed better results for T_{E1} correlation to historical data for both W_P and T_{E1} prediction. Both the transfer function and ARX model showed similar results for W_P with the ARX producing the higher correlation for recipe 2 and recipe 9.

In order for the ARX model to perform better than the transfer function model greater care would need to be taken when estimating the order parameters. Both data based models did however perform remarkably well, yet the transfer function models were superior, even including the fact that more process knowledge and time was required to perform the identification.

7.4.2 Data based modelling compared to semi-empirical modelling

The ARX model T_{E1} predictions were significantly worse than those obtained from both of the other models and prohibit the ARX model from being a viable alternative to semi-empirical modelling.

The transfer function model does however match up a lot better with the semi-empirical model, especially when looking at W_P predictions. The poor T_{E1} predictions may be a result of the two stage condenser action described in Section 5.2.2. Furthermore if a knowledgeable operator was consulted during the identification process the results may improve greatly. Another possible improvement of the transfer function models would be the use of step test data, which has been shown to give better results [**23**].

The main disadvantage of the transfer function model, aside from the poor T_{E1} correlation, is the confidence one has when extrapolating it to different process conditions. This problem was clearly observed comparing Figure 7-2 and Figure 7-3, where the transfer function model showed exceptional

prediction of historical set 05_2, but very poor prediction of historical set 09_2. In short, better data collection and more accurate limit definitions would most likely greatly increase the transfer model accuracy.

The semi-empirical model showed the best T_{E1} prediction correlation values of all the models and showed comparable W_P historical correlation to that of the data based models. In this way the semi-empirical model was further validated in a manner which could not have been done without the data based models.

For the increased development effort the semi-empirical model yields very good extrapolation and if process knowledge is used to tune the model for each recipe, it is possible that the correlation values will improve further. Yet the semi-empirical model performs very well within the poor data environment by compensating the lack of certainty in the data with fundamental knowledge.

Lastly the added advantage of using the fundamental model in future work, possibly the development of certain fault conditions could add a lot of value to the model. For example various valve faults, i.e. hysteresis or fouling, could be included. This would allow for thorough controller validation by inspecting controller response during abnormal system operation. Another possible use would be the training of fault detection algorithms which could then be used on the local FFE. These advantages make the semi-empirical model more suited as simulation environment for controller comparison and as such was chosen for all subsequent simulations.

Chapter 8 - Controller development

In the previous chapters, various simulation models were designed with the aim of providing a platform for controller development and comparison. After various considerations (including model extrapolation ability and validation against historical data) the semi-empirical fundamental model was selected for simulation (hereafter referred to as simulation model or just model). The performance of the model allows sensible benefit estimations to be made in the following chapter.

In this chapter the model will be used as simulation environment to test and develop various controllers, from basic PI to linguistic fuzzy control. By combining the model with both noise and various generated fault conditions the controllers can be extensively tested.

8.1 Control methodology

In this chapter the model is treated as one would treat a real plant. The development methodology followed is an adaptation of that described by Franklin et al [**17**], i.e. using process knowledge and simple system identification to firstly design a trial controller after which more advanced control techniques will be investigated, as shown in the flow chart below:

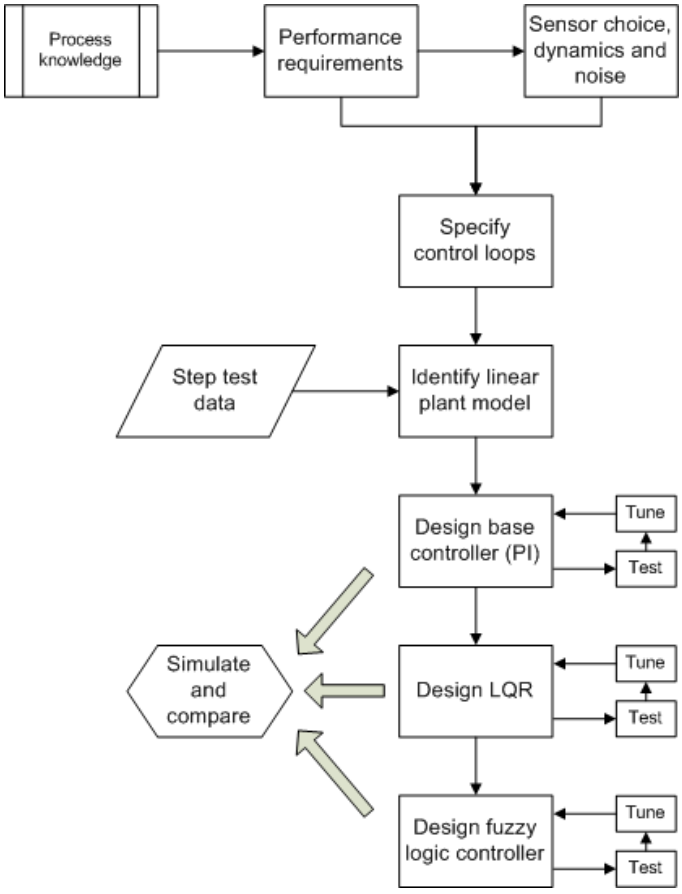

Figure 8-1: Controller development methodology

Controller comparison will be performed by quantifying disturbance rejection and set point following capabilities. These capabilities are expressed in terms of:

- Maximum deviation of controlled variables.
- Absolute measures such the integral of the absolute error (IAE) and the mean squared error (MSE).
- Set point tracking rising and settling times.

The manipulated variable use as well as development effort will also be discussed and compared.

8.2 Performance requirements

The performance requirements are related to the control objectives are summarised below:

- Tightly control the product dry mass (W_P) at pre-defined set points for each recipe as shown below:
- Maintain the first effect temperature close to, but below, 70°C.
- Maximise milk production rate (F_P).

Additionally, it has to be ensured that the controllers are robust, i.e. the controllers should continue to perform well even though some process uncertainties exist. For example, if fouling occurs within the falling film evaporator (leading to decreased heat transfer) the controllers should automatically introduce higher steam pressures to continue delivering the required heat to maintain the system temperature. For this specific case each controller should therefore have integral action, which will compensate for proportional term inaccuracies. Furthermore, the controllers may be detuned slightly to ensure increased delays or other disturbance will not easily produce controller instability.

These objectives need to be met; yet do not fully describe the required performance of the FFE. Winchester (2000), with a similar FFE setup, proposed that the controller should be able to successfully reject the main disturbances: feed dry mass (W_F) and feed temperature (T_H). Adequate rejection is defined as suppressing the output deviation to below the input deviation, i.e. a W_F step disturbance of 0.01 dry mass fraction should not cause a deviation of more than 0.01 fractional increase in the product dry mass (W_P). Additionally, zero offset tracking of set points, stable dynamics and constant production rates are desired.

8.3 Sensor choice, dynamics and noise

For accurate control sensor dynamics, placement and noise are of paramount importance. Firstly the available sensors, Figure 6-2, are again shown below in Table 8-1:

Table 8-1: Available process sensors

Unit	Sensor	Description
Thermal compressor	P_S	Pressure sensor
Effect 1	P_H	Holding tube pressure
	T_H	Holding tube temperature
	T_{E1}	Effect 1 temperature
	L_1	Inventory tank 1 level
Effect 2	T_{E2}	Effect 2 temperature
	L_2	Inventory tank 2 level
	F_P	Product flow rate
	T_P	Product temperature
	W_P	Product dry mass fraction
Condenser	P_C	Condenser pressure
	T_C	Cooling water temperature
Homogeniser	P_{HOM}	Pressure of homogenised flow
	T_{HOM}	Temperature of homogenised flow

8.3.1 Sensor sampling time and control period

As mentioned in the data review, Section 3.2, the recorded data was exported from a SQL database at a sampling interval of 120s. As no additional information was available on sensor update times, values reported in literature for dairy processes were used. Henningssona, et al. [**14**] reported sampling times below 5s in the dairy industry, including density, pressure and flow sensors. A conservative sampling time of 10s was chosen with a corresponding 30s control period.

8.3.2 Additional sensors

The sensors available shown in Table 8-1 proved adequate for simulation purposes when using the semi-empirical fundamental model (except for the lack of a F_{CW} sensor, which was estimated using P_C). A complete control solution does, however, require the addition of a F_{CW} sensor, before the condenser as well as an actuator valve to control the cooling water flow.

8.3.3 Process noise

All processes contain noise which may generally be caused by either sensor measurement or unexplained small variances observed within process trends. Controllers need to be able to filter out process noise and act only on actual process dynamics. If a controller is designed without taking noise into account, it will try and suppress high frequency process noise which may lead to instability. If each control period consists of multiple sample periods one can use smoothing to compensate for excessive noise. Otherwise the controller needs to be slightly detuned to ensure that it does not act on the noise.

Noise was added to the simulation model using the Simulink random number generator with zero mean, different random seeds and sampling times. All sampling times were chosen less than or equal to 10s and in relation to the type of sensor used. The exact same input signals and noise calculations were used for all the controllers. The sensor noisy signals are shown below:

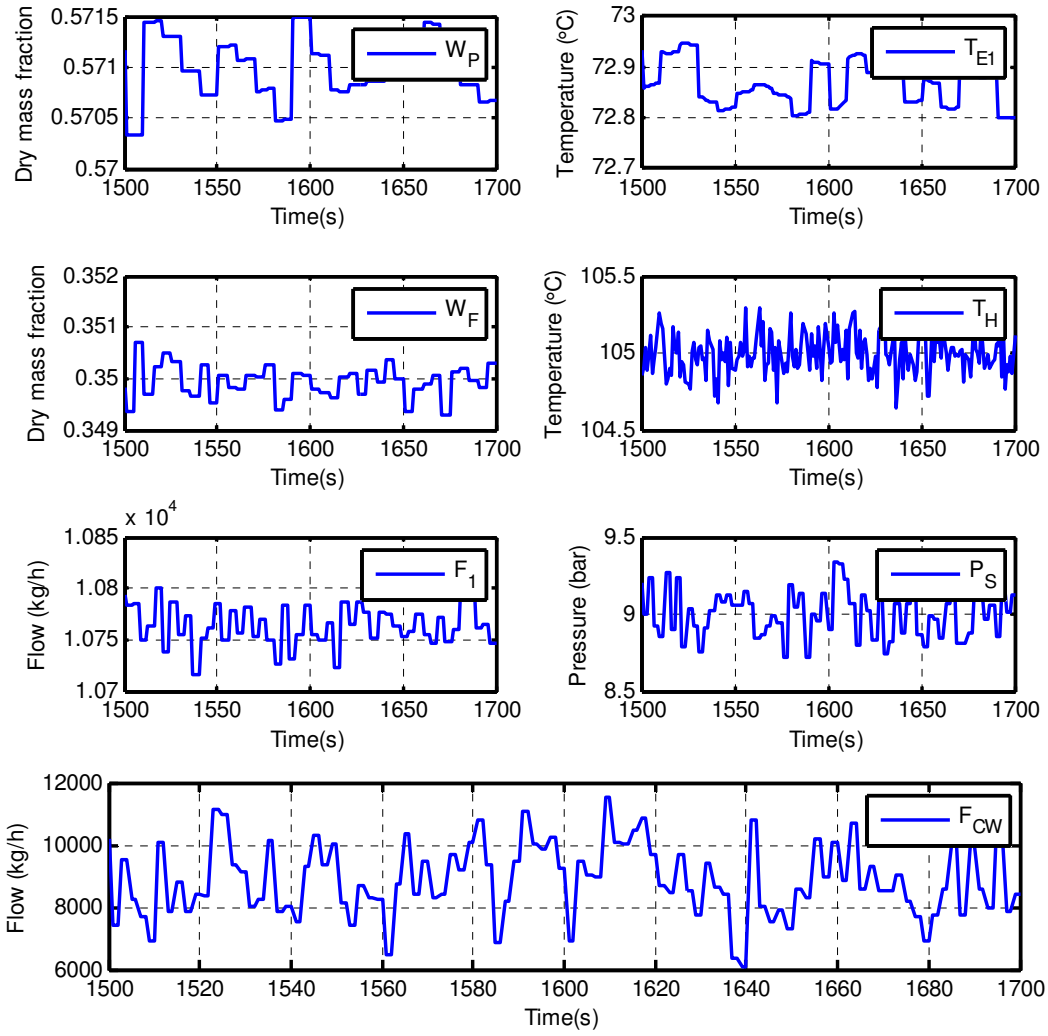

Figure 8-2: Sensor noise (W_P and T_{E1}) as well as process noise addition (W_F, T_H, F_1, P_S and F_{CW})

The addition of noise will ensure that the controller developed will be able to operate under real world conditions. Furthermore, it will give more credence to any benefit estimation done later on.

8.4 Specify control loops, valve dynamics and disturbances

As defined in Section 1.3, the two control variables are the final product dry mass (W_P) and first effect temperature, T_{E1}. The three manipulated variables are: steam pressure (P_S), cooling water flow rate (F_{CW}) and the feed flow rate (F_1). Each output that needs to be controlled requires a corresponding manipulated variable.

8.4.1 Product and temperature control loops

The interaction between cooling water (F_{CW}) and the second effect temperature (T_{E2}) is very quick [**6**], as such it is possible to use T_{E2} as a manipulated variable instead of directly controlling F_{CW}. For the current simulation a $F_{CW} \rightarrow T_{E2}$ PI controller will be designed (an approximation of the real condenser action which includes the complex pressure relationships described in section 5.2.4). The advantage of this approach is that it allows the design of controllers without the need to completely describe the condenser action. Implementing the final control structure on the physical plant would then merely require a new sub level controller for the (F_{CW}, pressure) $\rightarrow T_{E2}$ controller.

The control loops for the SISO controllers can then be selected as:

Loop 1 :	$P_S \rightarrow W_P$
Loop 2 :	$T_{E2} \rightarrow T_{E1}$

8.4.2 Liquid level control loop

In addition to loops 1 and 2, there are further restrictions to FFE operation as explained in Section 1.3, namely the appearance of flooding (distribution plate liquid heights above the vapour risers seen in Figure 5-5) and film breakdown (insufficient liquid loading causing the film not to wet the tubes completely). Flooding will cause excessive liquid inside the tubes which could upset the flow regimes and shorten residence times, thereby reducing the evaporation capacity. Film breakdown will enhance fouling inside the tubes as sections of the milk may lose all water causing deposits to form on the tube walls. The model did not include either of these restraints as the exact dynamics are beyond the scope of this work.

Inspection of the distribution plate fluid levels during simulations revealed that the fluid never reached the risers and as such flooding was unlikely. Therefore the feed flow will be kept constant during initial control simulations. In the latter sections of this work an optimiser will be developed to ensure the FFE operates close to its maximum capacity at all times.

8.4.3 Valve dynamics

Ideally, the valve dynamics could be determined using the recorded data for the local process. The 120s sample period does, however, hamper this identification process as it is expected that the valve dynamics will be very quick. Marlin [**8**] reported on the various typical dynamic responses within chemical processes and estimates the valve action in the region of 1-4s, well below the 120s sampling period. With this in mind, valve dynamics were chosen to show unity gain and a 15s time constant:

$$G_{valve}(s) = \frac{1}{15s + 1} \qquad \textbf{Eq. 8-1}$$

If the dynamic response is found to be slower at the real plant, the local PID loops will need to be re-tuned to resemble Eq. 8-1.

8.4.4 Saturation limits

In practise, all manipulated variables have operating ranges. If a controller is not limited to operate within these ranges, called saturation limits, the manipulated variables will become nonsensical. The

saturation limits were found by inspecting the historical data described in Section 3.2, with the final values selected as:

Table 8-2: Manipulated variable saturation limits

Manipulated variable	Lower	Upper	
P_S	2	10	bar
T_{E2}	57	67	°C

8.4.5 Known disturbances

The main disturbance for dairy FFEs are [**5**] [**1**]:

- Feed dry mass
- Pressure fluctuations
- Fouling
- Dynamic heat transfer coefficients
- Feed temperature
- Ambient temperature
- Cooling water temperature

At, first only feed dry mass and temperature disturbances will be investigated, in line with other controllability studies [**6**] [**5**] while feed flow rate will also be treated as a disturbance until an optimiser is developed.

Dynamic heat transfer coefficients, pressure fluctuations as well as other minor disturbances will be tested at the end of the chapter by using the fault generation capabilities of the semi-empirical model.

8.5 PI controller for T_{E2}

Before the complete linear system identification could be performed for the semi-empirical model, a SISO controller needed to be developed for the $F_{CW} \rightarrow T_{E2}$ condenser action. The methodology followed for this section resembles Figure 8-1, but on a smaller scale.

8.5.1 Identifying linear model

A series of F_{CW} step tests were introduced, while the other variables were kept at nominal values, to investigate the dynamics of the condenser as shown by Table 8-3. The steps, T_{E2} response and fitted first order model predictions are shown in Table 8-3 and Figure 8-3 below:

Table 8-3: Condenser identification steps

Input	Nominal	Step 1 (4 000s)	Step 2 (6 000s)	Step 3 (8 000s)	Units
F_{CW}	9720	+1800	-1080	-720	kg/hr

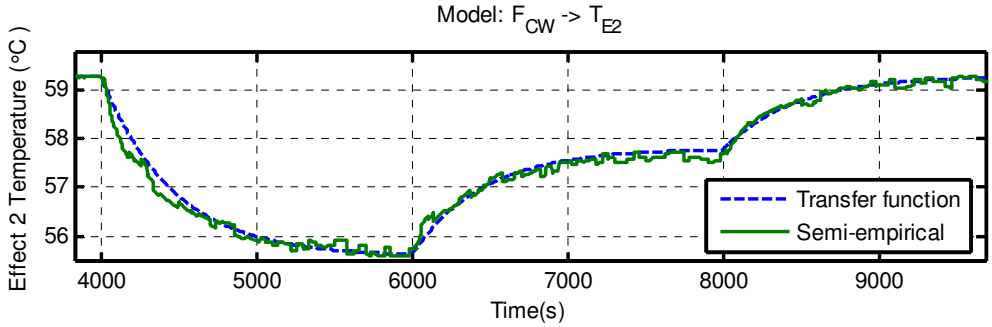

Figure 8-3: Transfer function and semi-empirical model T_{E2} predictions

Step 1 was used for training, while the other two steps were used to validate the identified transfer function. Figure 8-3 clearly shows that the transfer function, shown below, adequately represents the $F_{CW} \rightarrow T_{E2}$ relationship. The second step does show a slight offset, which points to a minor non-linearity in the gains for Eq. 8-2, as no such offset is seen in step 3. It is however very minor and will have virtually no influence on the control.

$$G_{cond}(s) = \frac{T_{E2}(s)}{F_{CW}(s)} = \frac{-0.00204}{460s + 1} \qquad \textbf{Eq. 8-2}$$

8.5.2 Control specifications

During normal FFE operation, the temperature should not vary quickly, due to the high thermal mass filtering out disturbances, therefore the new pseudo manipulated variable T_{E2} should also not be varied very quickly. This allows the choice of a fairly conservative 2% settling time of 700s and damping ratio of 1 which will ensure no overshoot. The settling time specifies the natural frequency, i.e. by re-arranging Eq. 4-3 to Eq. 8-3:

$$\omega_n = \frac{4}{\zeta \cdot t_{s,2\%}} = \frac{4}{1 \cdot 700s} = 0.0057\ rad/s \qquad \textbf{Eq. 8-3}$$

Furthermore, it is assumed that the F_{CW} valve dynamics are similar to the milk feed flow rate (F_1) valve, i.e. unity gain and a time constant less than 30s, and therefore negligible compared to the condenser process. As such, the dynamics can be omitted from the controller structure, Figure 4-1. The PI gains were calculated using Eq. 4-8 and Eq. 4-9 (with $b=K_{cond}/\tau_{cond}=4.43e^{-6}$ and $a=1/\tau_{cond}=0.0022$):

$$K_p = \frac{2\zeta\omega_n - a}{b} = \frac{2(1)(0.0057) - 0.0022}{4.43e^{-6}} = 2086 \qquad \textbf{Eq. 8-4}$$

$$K_i = \frac{\omega_n^2}{b} = \frac{0.0022^2}{4.43e^{-6}} = 7.36 \qquad \text{Eq. 8-5}$$

Finally the controller is converted into discrete form by using the Matlab command ***c2d***, and implemented into Simulink:

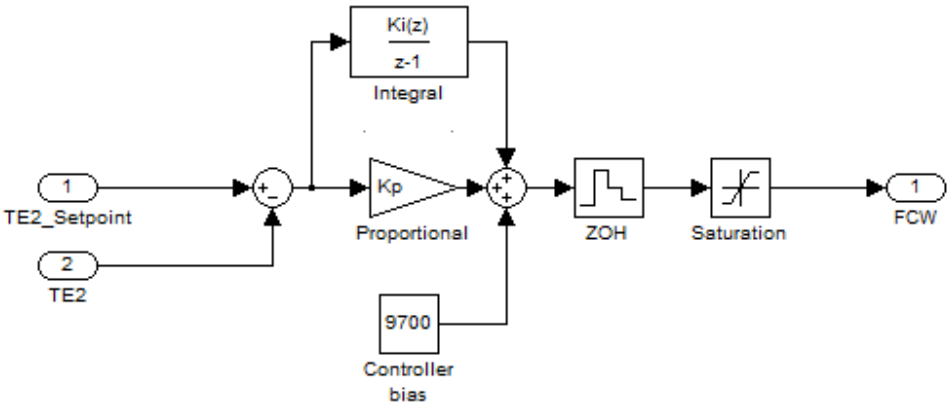

Figure 8-4: Simulink condenser PI controller

8.5.3 Second effect temperature simulations

To test the controller, various T_{E2} set point changes were introduced (without noise addition):

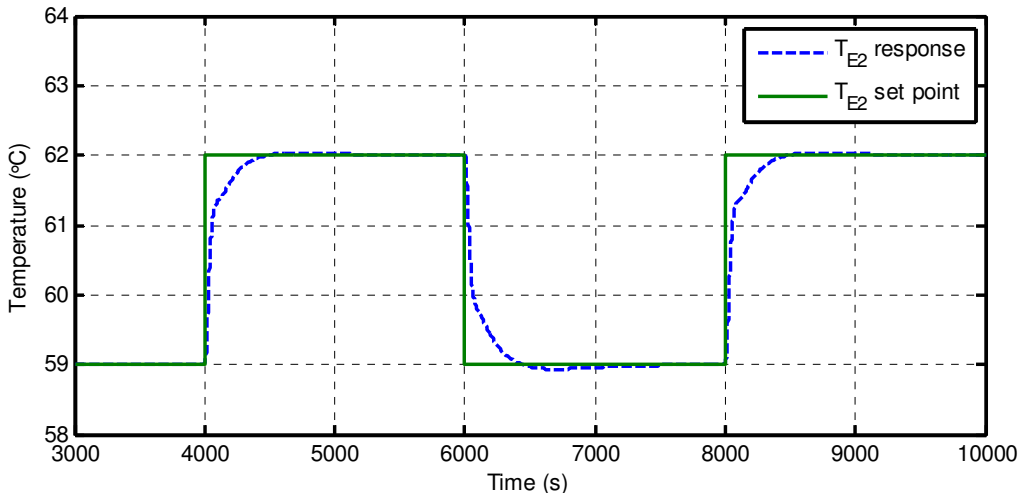

Figure 8-5: Second effect temperature set point tracking without valve dynamics

The design specifications were met with the controller showing a rise time of ±450s and settling time at the specified 700s mark. Virtually no overshoot is seen and zero offset. Set point tracking is also achieved. Note that the controller was tuned very conservatively to ensure stability when the valve dynamics and noise are added.

To test the robustness of the PI controller, the set point changes were again introduced, with the inclusion of both noise and the valve dynamics as determined in sections 8.3.3 and 8.4.3:

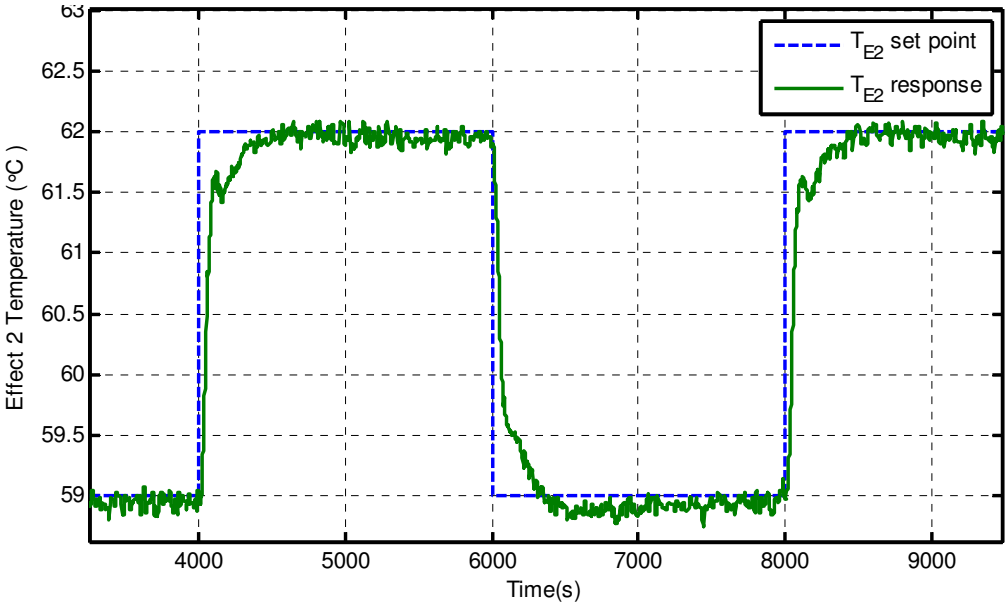

Figure 8-6: Second effect temperature set point tracking including valve dynamics

Comparing Figure 8-5 and Figure 8-6 it is interesting to note that the controller performance did not decrease significantly. Therefore, the conservative settling time and damping ratio chosen were still adequate to insure a quick stable response.

8.6 Linear plant model

In order to properly design the base PI controller, information was needed about the main control loop dynamics. Similarly, the advanced optimal control strategies will also require information about these dynamics. As such, all the major input variables (including disturbances) will be investigated to produce a set of linear transfer functions that can describe the process dynamics around a nominal operating condition.

8.6.1 Producing identification data using step tests

A similar approach to that used by Cunningham [**23**] was taken to generate a representative set of process data for identification by introducing the steps specified in Table 8-4. The nominal values for each variable were taken from training data set 9_2 (recipe 1):

Table 8-4: System identification step tests introduced to fundamental model

	Nominal	Step 1	Step 2	Step 3	Step 4	
W_F	0.35	0.02	-0.01	0.01	-0.02	-
T_H	105	2	-4	1	1	°C
F_1	10000	500	-1000	2000	-500	kg/hr
P_S	7.57	2.2	-3	1	0.5	bar
T_{E2}	59	3	-1	2	-5	°C

It should be noted that a W_F disturbance step would be difficult to achieve in practice on site. One method would be to keep all process variables constant and then introducing a higher weight fraction milk batch into the feed holding tank. However, the tank level would however need to be very low to ensure mixing does not even out the step too much.

8.6.2 Step results and model predictions

The first step for each variable, as defined in the table above, was used in conjunction with the process reaction curves shown by Marlin [**8**] to identify SISO models. Note that increased noise addition was used to simulate a worst case situation, thereby validating the identification procedure followed. The addition will also ensure the method is applicable to the real process even under noisy conditions. All the identified transfer functions are shown below in Table 8-5:

Table 8-5: Identified first order models for the FFE from semi-empirical model data

Input	W_F	T_H	F_1	P_S	T_{E2}
W_P	$\frac{1.47e^{-146}}{97s+1}$	$\frac{0.0022e^{-172s}}{148s+1}$	$\frac{-94.7e^{-110s}}{79s+1}$	$\frac{0.0284e^{-141s}}{186s+1}$	$\frac{-0.0034e^{-46s}}{61s+1}+\frac{0.0097^{-161s}}{215s+1}$
T_{E1}	N/A	$\frac{0.061e^{-48s}}{90s+1}$	$\frac{921e^{-18s}}{201s+1}$	$\frac{1.36e^{-26s}}{108s+1}$	$\frac{0.91e^{-4s6}}{149s+1}$

Note that T_{E2} has a two stage impact on W_P (as explained in section 5.2.4) and that W_F has no effect on T_{E1}. The identification steps for $W_F \rightarrow W_P$ are shown below in Figure 8-7:

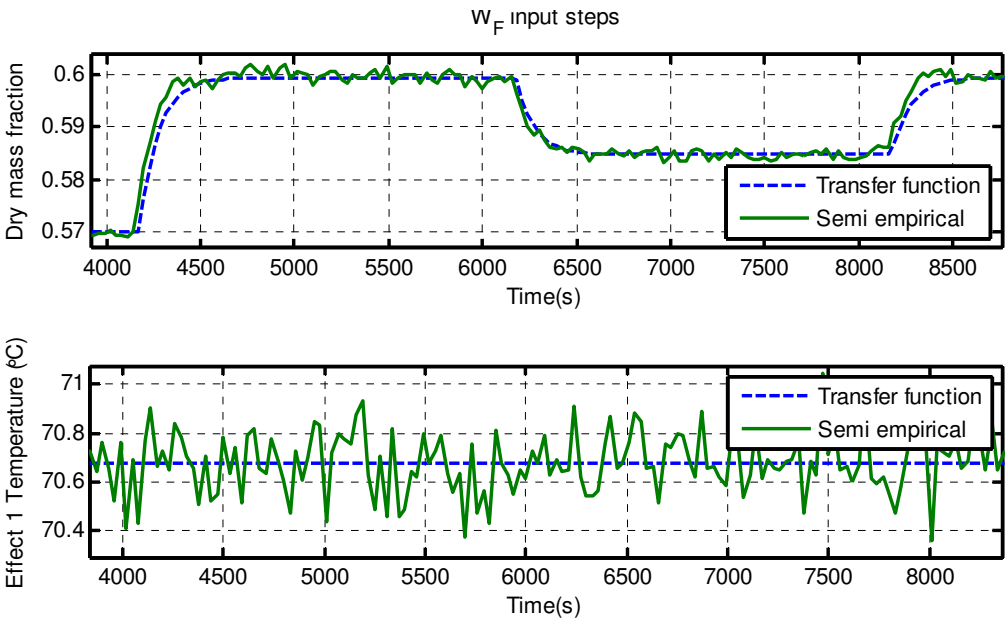

Figure 8-7: First order identification W_F

The identification steps for *PS → (WP, TE1)* and model response is also shown below:

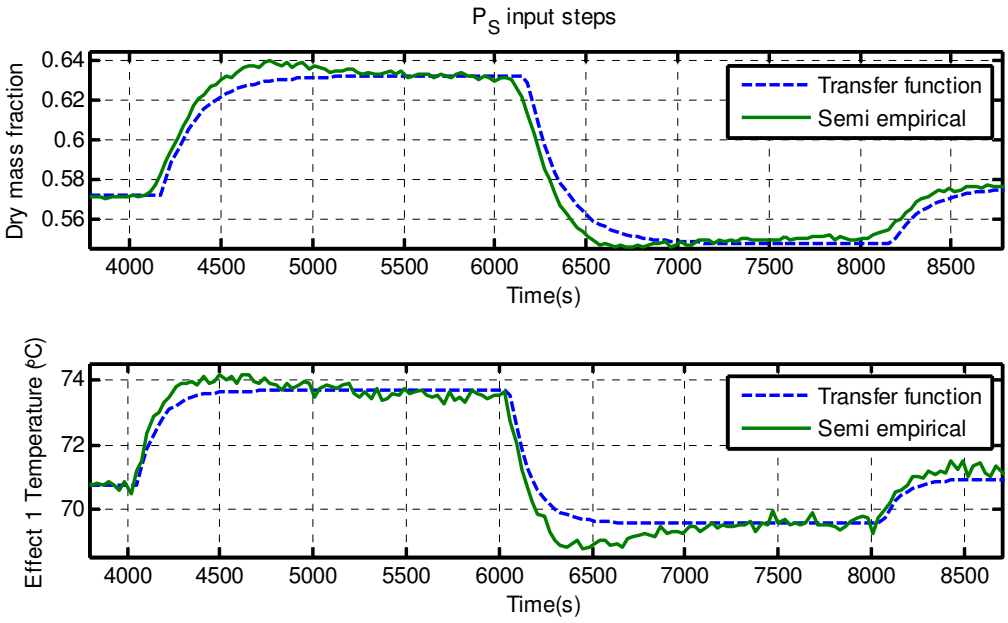

Figure 8-8: First order identification for P_S

Note, the slightly underdamped second order response shown by both W_P and T_{E2}, which is a direct effect of the $F_{CW} \rightarrow T_{E2}$ controller implemented in Section 8.5. The overall controller should not be influenced, as the transient response differs only marginally from the first order model. It would also be possible to de-tune the aforementioned T_{E2} controller, which would remove the overshoot.

8.7 Initial PI controllers

A PI controller will be developed as base case control, against which all other control methods will be evaluated. The valve dynamics will be neglected during the design phase although they will be included during simulation. At first the process dead time will also be ignored.

As discussed at the start of the chapter, the two main control loops are the product dry mass and first effect temperature loops, with the corresponding manipulated variables being steam pressure and second effect temperature. The first order transfer functions for these two loops are shown below:

$P_S \rightarrow W_P$		$T_{E1} \rightarrow T_{E2}$	
$\frac{0.0284e^{-141s}}{186s+1}$	Loop 1	$\frac{0.91e^{-46s}}{149s+1}$	Loop 2

8.7.1 Performance specification design

Loop 1 is more important as tighter control is needed for W_P to prevent product quality losses while loop 2 may be less aggressive if a lower T_{E1} set point is chosen (i.e. below 70°C). For both loops a damping ratio of 0.707 is initially selected, as this should provide quick rise time with little overshoot. The 2% settling time for loop 1 is chosen at 300s while loop 2 is allowed more leeway with a settling time of 500s. These times were selected after rigorous inspection of historical data. Ideally, one would use historical data in conjunction with operator and process knowledge to select optimal time specifications. By again using Eq. 8-3 to calculate ω_n, then Eq. 8-4 as well as Eq. 8-5 to determine both K_p and K_i one can show that:

Table 8-6: PI controller parameters

	K_p	K_i
Loop 1	139.44	2.33
Loop 2	1.52	0.02

Both loop PI controllers were implemented into Simulink as shown by Figure 8-4 previously. The actuator dynamics (steam and cooling water flow) were included as well as noise. Both controllers were also converted to discrete form with a sampling time of 30s.

The initial set of controller constants provided unstable operation with large oscillations and virtually no set point tracking; the results are shown below in Figure 8-9:

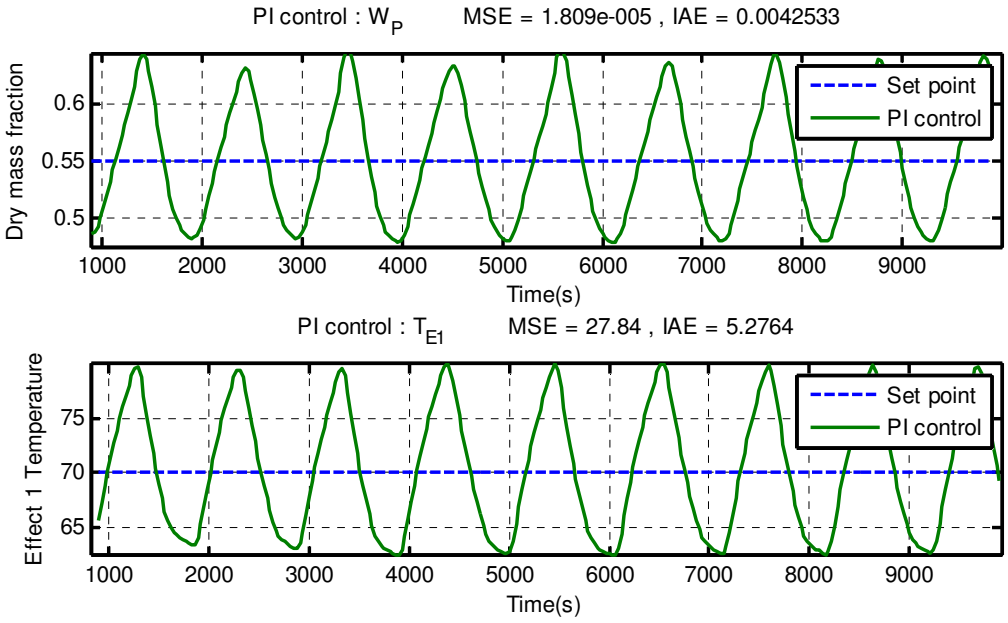

Figure 8-9: First performance parameters, PI control

The oscillation seen in the above figure was most likely due the significant process dead time (141s) seen for the $P_S \rightarrow W_P$ transfer function when compared to the process time constant of 186s. The process instability clearly shows that both $t_{s,2\%}$ and ζ values were too aggressive when the dead time was included. Instead of choosing better constant values through inspection, it was decided to use the well-established Ciancone tuning rules [**8**] for disturbance rejection which take into account process dead time.

8.7.2 Ciancone tuning rules PI design

As explained in Section 4.1, the Ciancone tuning rules describe the relationship between the process dynamics and the controller gain (K_c), process gain (K_{pr}) and integral time (T_I). The relationships shown by Figure 4-2 can be rewritten mathematically by defining relational factors K_1 and K_2 and the formulating:

$$K_c = \mathrm{K}_1 / K_{pr} \qquad \textbf{Eq. 8-6}$$

$$T_I = \left(\theta + \tau_{pr}\right) \cdot K_2 \qquad \textbf{Eq. 8-7}$$

The process dynamics were represented by finding the dimensionless dead time fraction of each loop. T:

Loop 1 $$\frac{\theta}{\theta + \tau} = \frac{141}{141 + 186} = 0.43 \ \therefore K_1 = 0.8 \ and \ K_2 = 0.65$$

Loop 2 $$\frac{\theta}{\theta + \tau} = \frac{46}{46 + 149} = 0.23 \ \therefore K_1 = 2 \ and \ K_2 = 0.5$$

The above relational factor can now be used in Eq. 8-6 and Eq. 8-7 to find K_P and K_I for each loop:

Table 8-7: Ciancone PI controller parameters

	K_p	K_i
Loop 1	28.17	3.976
Loop 2	2.19	0.67

The controller parameters shown in Table 8-7 above are a lot more conservative for loop 1, while being somewhat more aggressive for loop 2. To ensure stability, and as T_{E1} may show slower dynamics, loop 2 was detuned by reducing the parameters by 50%. The controller was again implemented in Simulink and given a set point changes:

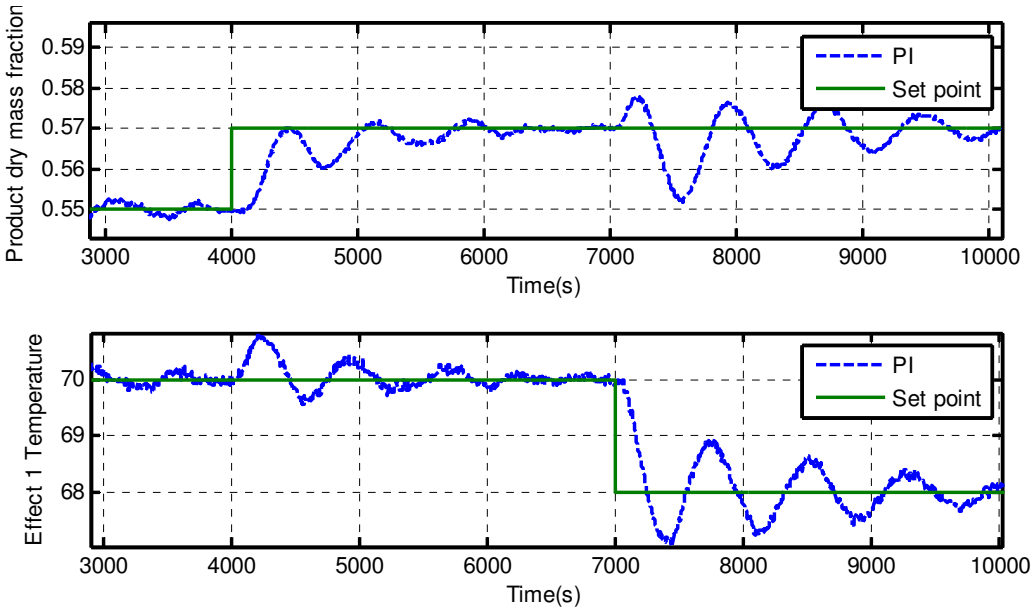

Figure 8-10: PI controller set point tracking when using Ciancone tuning rules

Figure 8-10 shows that the PI controller is stable, but with large oscillations seen after the T_{E1} step at 7 000s. The oscillations imply that the T_{E1} control parameters are still too aggressive. Product dry mass control on the other hand seems a bit too conservative as W_P shows no overshoot. Therefore loop 1 control constants were increased by 10% while loop 2 parameters were reduced to 10% of the original values shown in Table 8-7. The set point tracking with the new parameters are shown below:

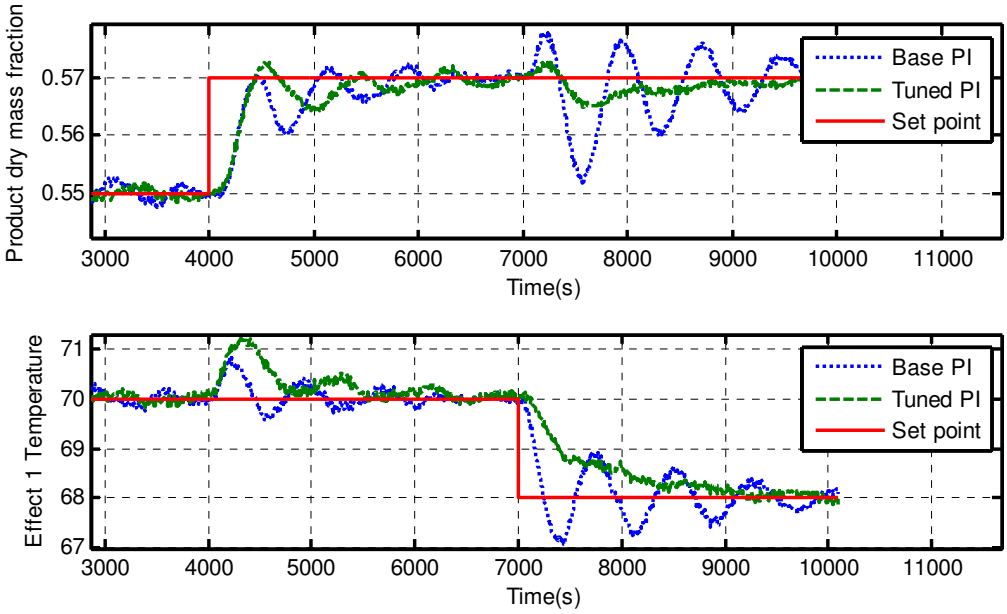

Figure 8-11: Fine-tuned and base PI controller set point tracking when using Ciancone tuning rules

Figure 8-11 above shows that the fine-tuned PI controller exhibits stable operation, while the desired small overshoot in W_P response and smooth T_{E1} response were also achieved. The W_P integral action was slow during a T_{E1} step, yet quick when T_{E1} was kept constant. Increasing loop 1 K_I introduced larger overshoot and greater oscillations. It was therefore decided to keep the adjusted constants of the fine-tuned PI controller in Figure 8-11, which will hereafter be referred to simply as the PI controller

8.7.3 Disturbance rejection and set point following

The most important function of the controller is to keep the control variables at desirable levels while rejecting disturbances adequately. To quantify the performance of the PI controller various input disturbances as well as set point changes were introduced.

The base case PI controller was tested and compared against the optimal state space and fuzzy designs of the subsequent sections. Refer to Section 8.11.2 for the corresponding results. If the comparison reveals that the PI controller may outperform either state space or fuzzy designs additional tuning methods could be investigated, e.g. using the manipulated variable response to distinguish between proportional and integral effects or comparing Ziegler-Nichols to the Ciancone tuning results.

8.8 Optimal state space controller design

The first advanced form of control implemented was the linear quadratic regulator (LQR). A LQR allows one to easily add disturbance dynamics into the system (as extra states) as well as to specifically tailor the solution to respond in various ways to certain states.

As explained in section 0, the LQR uses a cost function (J) that quantifies control effort and state deviation together with weighting matrices $\mathbf{Q}_{1\text{-}2}$ as shown by Eq. 8-8, repeated below as Eq. 8-8:

$$J = \frac{1}{2}\sum_{k=0}^{N}[\alpha_c \,.\, \mathbf{x}^{\mathrm{T}}\mathbf{Q_1}\mathbf{x} + \mathbf{u}^{\mathrm{T}}\mathbf{Q_2}\mathbf{u}] \qquad \textbf{Eq. 8-8}$$

In terms of LQR tuning the selection of $\mathbf{Q_1}$ and $\mathbf{Q_2}$ is the most important step. It specifies both how aggressively each manipulated variable should be used as well as how closely to follow each control variable set point. Furthermore, it should be noted that the optimisation routine only takes into account the relative sizes both between the **Q** matrices and not the absolute values of the weighting. By adding a factor α_c, one can manipulate the relative weighting of the states versus the inputs without changing each individual element.

8.8.1 State space representation

Before optimisation could be employed to minimize *J*, by searching for an optimal gain matrix (**K**), the system of linear transfer functions, shown in Table 8-5, had to be represented in discrete state space form. This was done by writing an m-script (shown in Appendix A) to convert the identified models into continuous state space and then using the Matlab ***c2d*** function to convert the matrices into discrete form. The resulting continuous are shown in Appendix A, with the Simulink setup shown below:

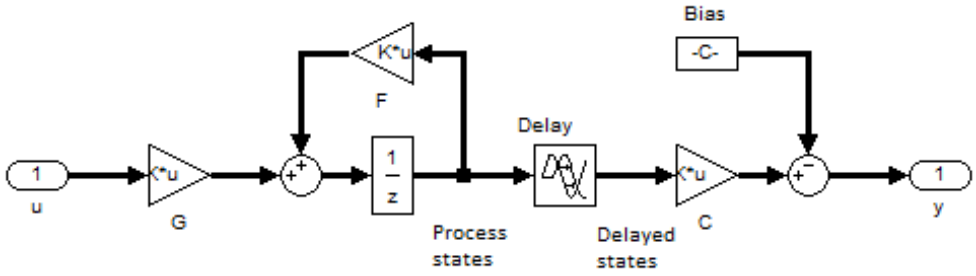

Figure 8-12: Discrete state space model

Traditionally, each state would represent an internal function of the system. In the evaporator system one would ideally want the temperature of each effect to be a state. In this way the states all have tangible meaning which allows using direct process knowledge for tuning and selecting maximum deviations. Currently, the states were identified using input steps; as such, each state is a representation of the particular input variable's influence on a specific output variable. The advantage of this method is that all the states are easily separable which allows us to penalise the effect of P_S on W_P without a heavy cost also given to its effect on T_{E1}.

8.8.2 Kalman estimator

In addition to the state space model, a Kalman estimator was used to update the states by comparing the linear model outputs to that of the semi-empirical model. The Kalman filter application has many parallels to optimal state feedback control with the design of the estimator gain accomplished by minimizing a cost function similar to Eq. 8-8. The estimator cost function (J_E), shown below in Eq. 8-9, is comprised of a terms representing the model states (**x**) and sensor readings ($\mathbf{y_s}$), with weighting matrices $\mathbf{R_w}$ and $\mathbf{R_v}$ scaling the relative size of each element. Furthermore a factor α_E was added to specify the degree to which the estimator divides trust between the linear model and sensor readings.

$$J_E = \frac{1}{2}\sum_{k=0}^{N}[\alpha_E \cdot \mathbf{x}^{\mathrm{T}}\mathbf{R_w}\mathbf{x} + \mathbf{y_s^{\mathrm{T}}}\mathbf{R_v}\mathbf{y_s}] \qquad \text{Eq. 8-9}$$

Instead of updating the delayed states shown in Figure 8-12, it was decided to update the pre-delay states. This allowed the estimator action to be quicker and to have improved stability; the resulting Kalman estimator is shown below, with the optimal gain **L** included:

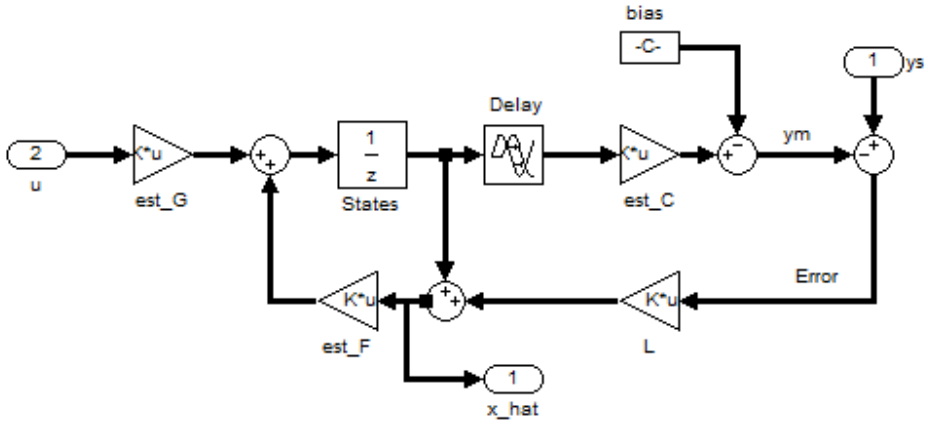

Figure 8-13: Discrete Kalman estimator

8.8.3 Weighting matrices

Again, as with optimal control, the selection of the weight matrices offers the largest obstacle to designing a good estimator. One approach relies on quantifying the relative noise in each signal by determining the covariance of the inputs and outputs respectively. By inspecting historical data, the following **R** matrices were calculated:

$$\mathbf{R}_v = \begin{bmatrix} 1.3e^{-5} & 2.4e^{-4} \\ 2.4e^{-4} & 1.9e^{-2} \end{bmatrix} \qquad \mathbf{R}_w = \begin{bmatrix} 3.17e^{-5} & 3.78e^{-4} & 2.92e^{-8} & 2.43e^{-4} & 1.45e^{-3} \\ 3.78e^{-4} & 2.50e^{-1} & 2.58e^{-6} & 1.90e^{-2} & 3.37e^{-2} \\ 2.92e^{-8} & 2.58e^{-6} & 2.51e^{-9} & 9.72e^{-6} & 1.57e^{-6} \\ 2.43e^{-4} & 1.90e^{-2} & 9.72e^{-6} & 2.50e^{-1} & 1.62e^{-2} \\ 1.45e^{-3} & 3.37e^{-2} & 1.57e^{-6} & 1.62e^{-2} & 2.49e^{-1} \end{bmatrix}$$

Various α_E factors were tested for stability and general error reduction by setting up multiple simulations and comparing the estimator output to that of the semi-empirical model. It was found that the Kalman estimator provided significant error reduction, while maintaining stability, at an α_E factor of 14. Therefore, the estimator was made more sensitive to the measured outputs. Increasing α_E any further introduced oscillations into the predicted outputs.

By implementing the above matrices and weights into the Matlab function DLQE, which also takes inputs in the form of the state space matrices **F** and **G**, the optimal gain was found (**L**). To test whether the Kalman estimator improves model accuracy, training set 9_2 was used while comparing the semi-empirical, linear and Kalman outputs during control:

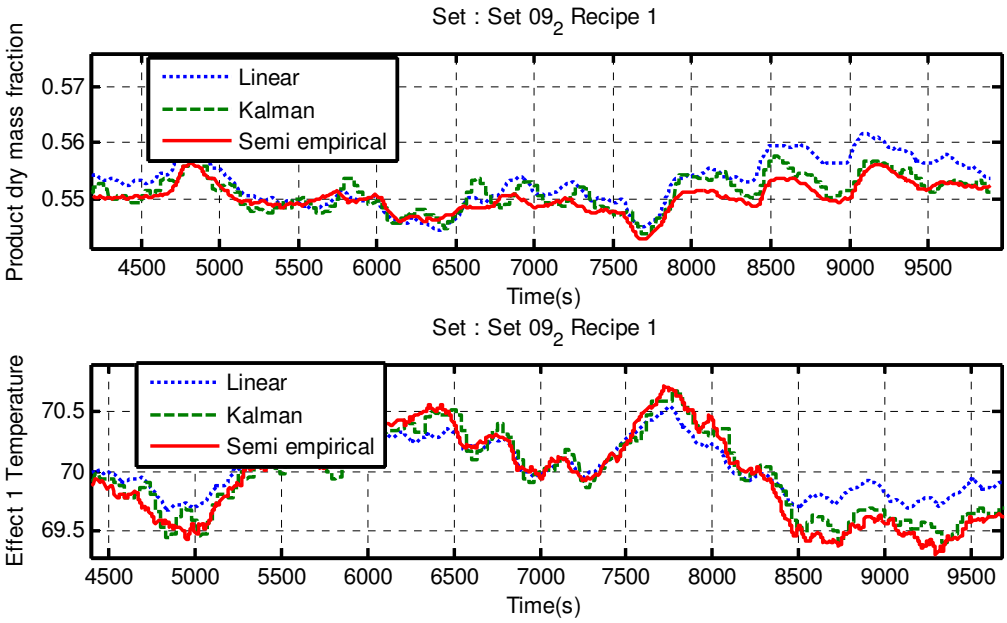

Figure 8-14: Comparison of linear model and Kalman filter predictions against the semi-empirical model

The Kalman estimator clearly improves the linear model performance without introducing instability. Note that both process and sensor noise were included with only the disturbance inputs taken from historical data. Therefore the above figure depicts the circumstances the Kalman estimator is likely to face during normal operation.

8.8.4 Addition of integral states

As with PI control, integral terms ensure zero off set steady state following of the set point. Adding integral action to the LQR solution is relatively simple and done by augmenting the state space representation with an integral state for each controlled variable. Each integral state is only dependent on its previous value and the new error between the control variable and set point.

The general state space representation (Eq. 4-12) is augmented with integral states, **v**(k), and the reference input, **r**, as shown below:

$$\begin{bmatrix} x(k+1) \\ v(k+1) \end{bmatrix} = \begin{bmatrix} F & 0 \\ cF & 1 \end{bmatrix} \begin{bmatrix} x(k) \\ v(k) \end{bmatrix} + \begin{bmatrix} g \\ cg \end{bmatrix} u(k) - \begin{bmatrix} 0 \\ -1 \end{bmatrix} r \qquad \textbf{Eq. 8-10}$$

The mathematics behind implementing integral states was explained in section 4.2.2 and resulted in a discrete state space system with 12 states (10 from the transfer functions and an integral for each of the output variables).

8.8.5 Initial weighting selections and controller structure

As a first estimation, the diagonals of the weighting matrices, $\mathbf{Q_1}$ and $\mathbf{Q_2}$, were chosen as the inverse of the maximum deviation of each state or the maximum acceptable deviation of each input variable. All elements not on the diagonals were set to 0, simplifying future tuning. Using the maximum deviation

also has the advantage of scaling each state and variable to similar magnitudes which in turn eases fine tuning of the controller. The factor α_c was initially chosen as 1 to give equal importance to the scaled states and inputs. The elements on the diagonal of each matrix are shown below:

Table 8-8: Diagonal elements of the weighting matrices Q_1 and Q_2

		W_F	T_F	F_1	P_S	$T_{E2}(+)$	$T_{E2}(-)$	*Integral*
$\mathbf{Q_1}$	W_P	0.1	0.1	0.2	0.3	0.5	0.5	0.1
	T_{E1}	-	0.8	0.8	0.8	1		3
$\mathbf{Q_2}$	*Inputs*	1	1	1	2	1.2	-	-

The $\mathbf{Q_2}$ values for each measured disturbance (i.e. W_F, F_1 and P_S) were set to one as control may only be performed with the manipulated variables. As with the Kalman estimator, Matlab was used to find the optimal gain (**K**) by calling the ***DLQR*** function with the augmented states and weighting matrices as inputs. The optimal gain was split up into two matrices; the first 10 columns used for feedback ($\mathbf{K_x}$) and the last two used for integral ($\mathbf{K_i}$) action as showed by the complete Simulink control structure below:

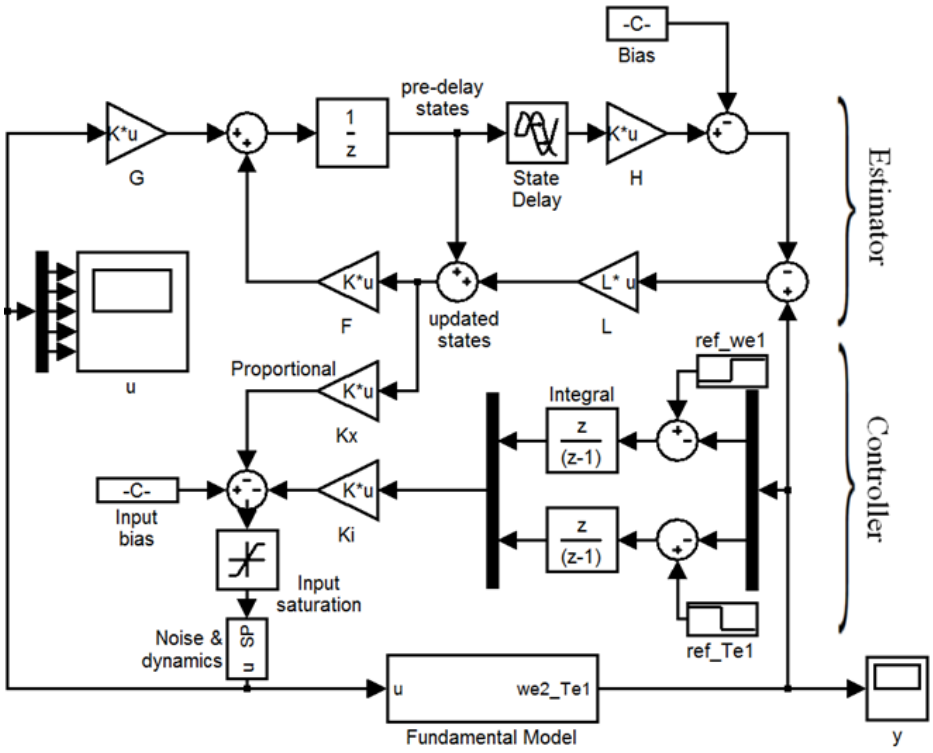

Figure 8-15: Simulink controller setup

Note the input bias and saturation blocks added. The input bias ensures the controller starts off in the correct region for each variable and was calculated using the initial states and normal input variable values:

$$Input_{bias} = (Normal\ manipulated\ variable\ values) - (initial\ states) \cdot \mathbf{K}_x \quad \text{Eq. 8-11}$$

The saturation block limits the available range for control and was found by inspecting historical data. The limits are shown below for each manipulated variable:

Table 8-9: Saturation limits for manipulated variables

Variable	Lower limit	Upper limit	Units
P_S	3	10	bar
T_{E2}	50	70	°C

Furthermore, a noise and dynamics block is added in front of the simulation model and estimator to include actuator working and process noise. Feed dry mass, temperature and flow rate disturbances are also added within this block. Lastly, the controller structure already shows the use of delayed states and an estimator. The effect of each of these decisions will be investigated.

8.8.6 Tuning and simulations

The first simulations were performed without the estimator connected (i.e. **L** set to zero) and without using the pre-delayed states. Both omissions were done to minimise the possible sources of instability. Thereafter the pre-delayed states were used and finally the estimator included. The resulting controllers will be referred to as LQR_1, LQR_2 and LQR_3 respectively. The same set point changes used for the tuning of the PI controller were introduced to tune the LQR solutions as shown in Figure 8-16:

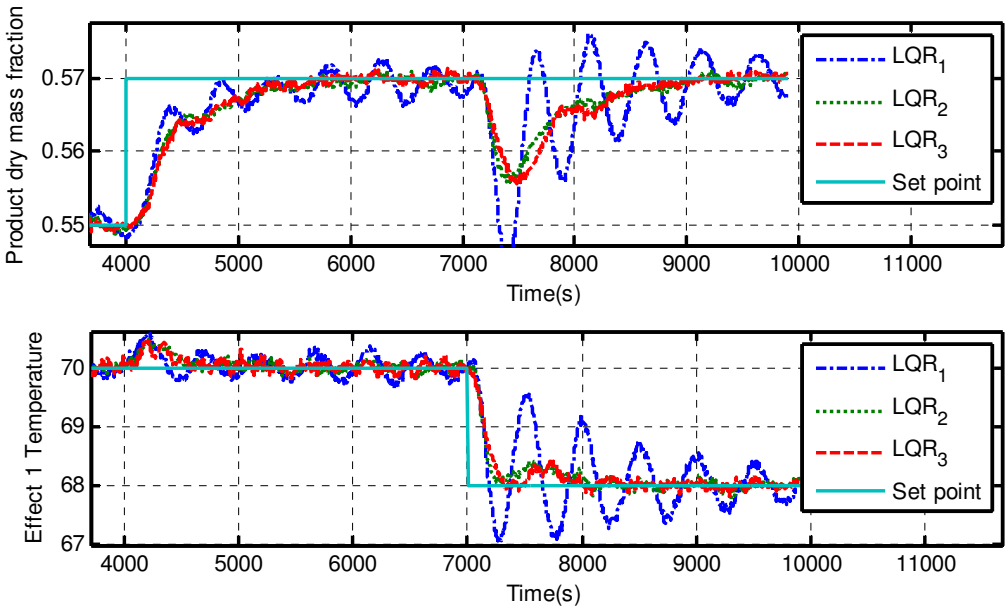

Figure 8-16: Set point tracking of various LQR structures

The delayed state LQR_1 proved to show the most aggressive controller action, resulting in large oscillations. The over-use of manipulated variables arose from the delay block. Each input first had to propagate through the states and the delay block before any rectifying action could be seen by the

controller. Note though that the rise and settling times of LQR_1 are not quicker than that of either LQR_2 or LQR_3. It can be seen that the increased manipulated usage seen from LQR_1 does not provide any benefit.

Introducing the use of the pre-delay states greatly improved the controller action by completely removing the oscillations seen with LQR_1. LQR_2 could observe the effect of changing manipulated variables far quicker than LQR_1 and could therefore act correctly on the errors.

It is interesting to also note that the estimator provides almost no benefit to control at this early stage as both LQR_2 and LQR_3 give similar responses.

From Figure 8-16 one can also see that the integral action on T_{E1} is too strong as the controller quickly follows the T_{E1} set point causing large deviations in W_P. In reality, W_P should be controlled more tightly and not have the sluggish set point tracking seen in the figure above. Additionally, inspection of the manipulated variables showed numerous small changes to P_S (as seen in Figure 8-17 below). The steam may be altered frequently, as it is governed by fast actuator dynamics, yet it was assessed that the current action should be reduced by relying slightly less on P_S than shown in Table 8-8.

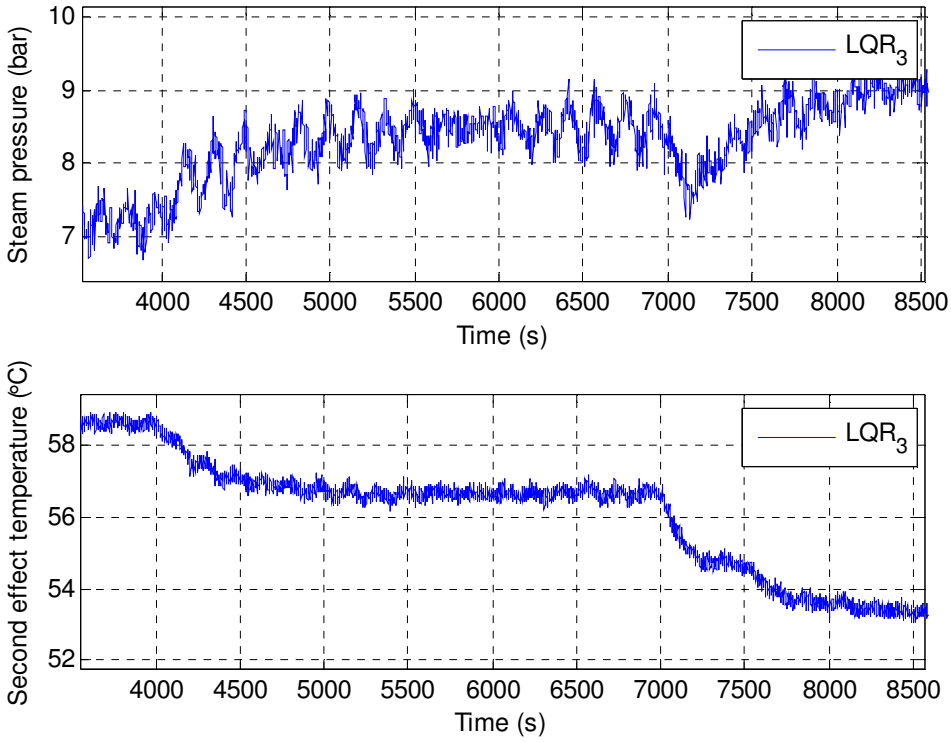

Figure 8-17: LQR_3 use of manipulated variables

Adjustments for LQR_3 were made to both $\mathbf{Q_2}$ to decrease the relative use of P_S. The integral states were also updated to tighten control on W_P and loosen T_{E2} control. Thereafter the effect of α_c was investigated by running multiple simulations at varying values while keeping all other parameters constant. The resulting set point tracking is shown below:

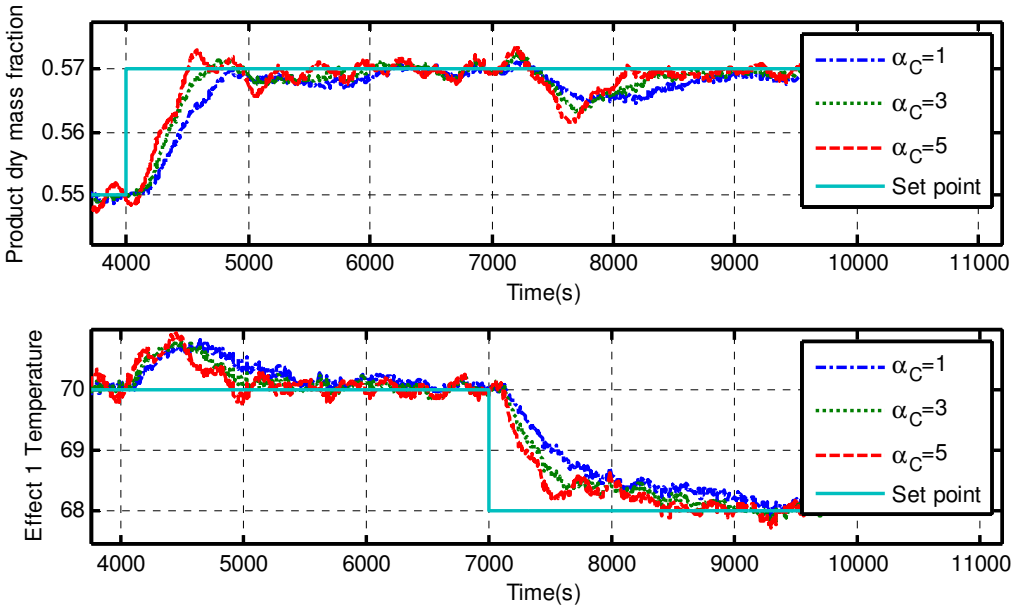

Figure 8-18: Tuned LQR$_3$ with different α_c factors

From Figure 8-18 above, it can be seen that W_P now responds optimally to a set point change (small amount of overshoot with relative quick settling time) for α_c values between 1 and 3. Values below 1 result in an overdamped reaction, i.e. no overshoot. T_{E2} also responds in a similar overdamped manner for all tested values of α_c. A small level of overshoot is allowed for W_P and as such the choice of final tuning lies between the higher α_c values. The rise time gain for $\alpha_c = 3$ is not substantial enough to justify the intensified oscillation seen before final settling occurs compared to the oscillation free $\alpha_c = 1$ curve. Therefore the final set point tuning for the LQR solution sets $\alpha_c = 1$ and the diagonal weighting matrices as:

Table 8-10: Diagonal elements of the weighting matrices Q_1 and Q_2

		W_F	T_F	F_1	P_S	T_{E2}(+)	T_{E2}(-)	Integral
Q_1	W_P	0.1	0.1	0.2	0.3	0.5	0.5	0.09
	T_{E1}	-	0.8	0.8	0.8	1		9
Q_2	*Inputs*	1	1	1	0.8	1.2	-	-

8.8.7 Disturbance rejection tuning

In addition to the set point tuning done in the previous section, one can also increase the response of the optimal controller for certain disturbances without affecting the overall control drastically. This separation is allowed as the linear model includes separate states for a single disturbance to each output, i.e. $F_1 \rightarrow W_P$ and $F_1 \rightarrow T_{E1}$. By splitting $\mathbf{K_x}$ into separate columns for each state, the specific feedback gain for a disturbance-output pair can be enhanced or reduced. Three additional tuning factors are considered (multiplied with each of the respective disturbance states), namely:

α_{WF} : Feed dry mass to product dry mass disturbance factor
α_{TH} : Feed temperature to product dry mass disturbance factor
α_{F1} : Feed flow rate to product dry mass disturbance factor

Note that F_1 is included as a disturbance seeing as no control is performed by the LQR on F_1. None of the T_{E1} disturbance states were increased as temperature control objectives allow for more variance.

To test the effect of changing each of these parameters, the step disturbances shown in Table 8-11 below were introduced:

Table 8-11: Disturbance steps

Variable	Time (s)	Initial value	Final value	Units
W_F	3000	0.35	0.36	Dry mass fraction
T_H	5000	105	108	°C
F_1	7000	9950	11 150	kg/hr

Process and sensor noise additions were not removed to ensure that the LQR tuning would not cause an unstable response under normal conditions. The resulting response of the LQR controller to disturbance inputs (with α_D equal to each disturbance α) is shown below in Figure 8-19:

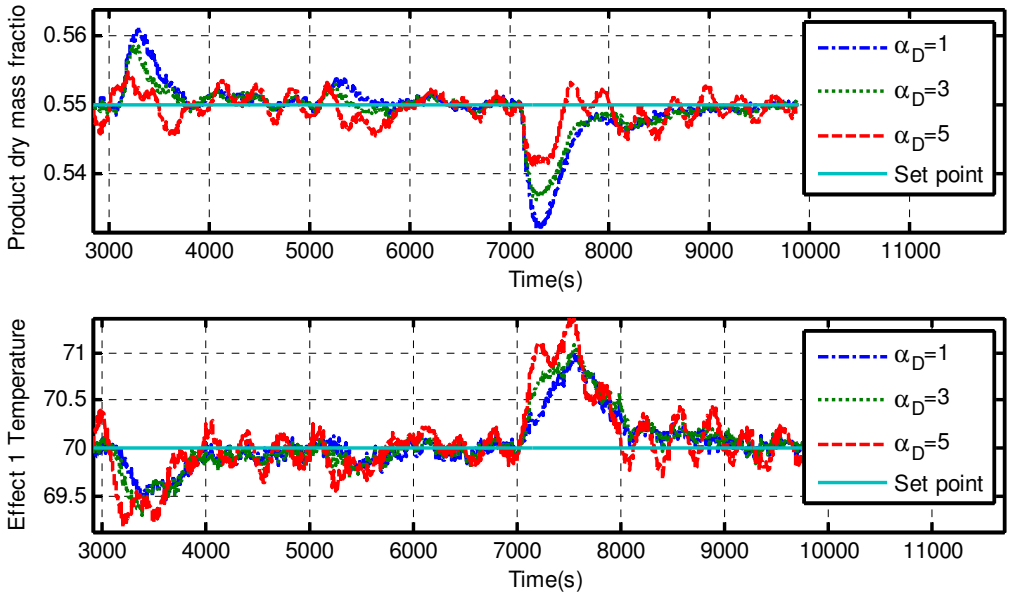

Figure 8-19: LQR$_3$ disturbance rejection tuning

Figure 8-19 shows that the process response to disturbances can be altered significantly by changing the disturbance rejection factors. For a W_F disturbance, a α_{WF} value of between 3 and 5 limits the maximum W_P deviation to below 0.01, while T_{E1} deviation is kept below 1°C. At α_{WF}=5 the controller action is strong enough to force the W_P deviation into the opposite direction, while at a value of 3 the deviation is still completely above the set point. Yet at α_{WF} = 5 oscillation is observed for W_P, indicating a too

aggressive controller. Therefore a value in between should ensure the response stays as close as possible to the set point, while reducing the observed oscillations.

Similar action is seen for T_H, yet at $\alpha_{TH} = 3$ the response is already very close to the set point with only a small deviation seen in T_{E1}. Lastly the F_1 disturbance provided the largest deviation, albeit with a fairly large input step. Again it can be seen that at higher factors ($\alpha_{F1} = 5$) the deviation is pulled into the opposite direction. The corresponding T_{E1} deviation is, however, greater than 1°C, therefore an in-between value of 4 was chosen. The final choice of factors is shown below in Table 8-12:

Table 8-12: Final disturbance rejection factor choice

$\alpha_{WF} =$	4	$\alpha_{TH} =$	3	$\alpha_{F1} =$	4

The disturbance rejection factors proved successful because of the use of the pre-delay states as shown in Figure 8-15. By using these states the effect of each disturbance could be detected before an error was seen in the output variables. Another option would have been to increase the controller action on W_P by specifying tighter control of the integral state – this approach could, however, lead to instability as normal process noise would also present in the same way as disturbance influences.

To better quantify the advantage of using the pre-delay and disturbance tuning factors, the tuned LQR_3 solution is compared to that of a tuned LQR_1 solution:

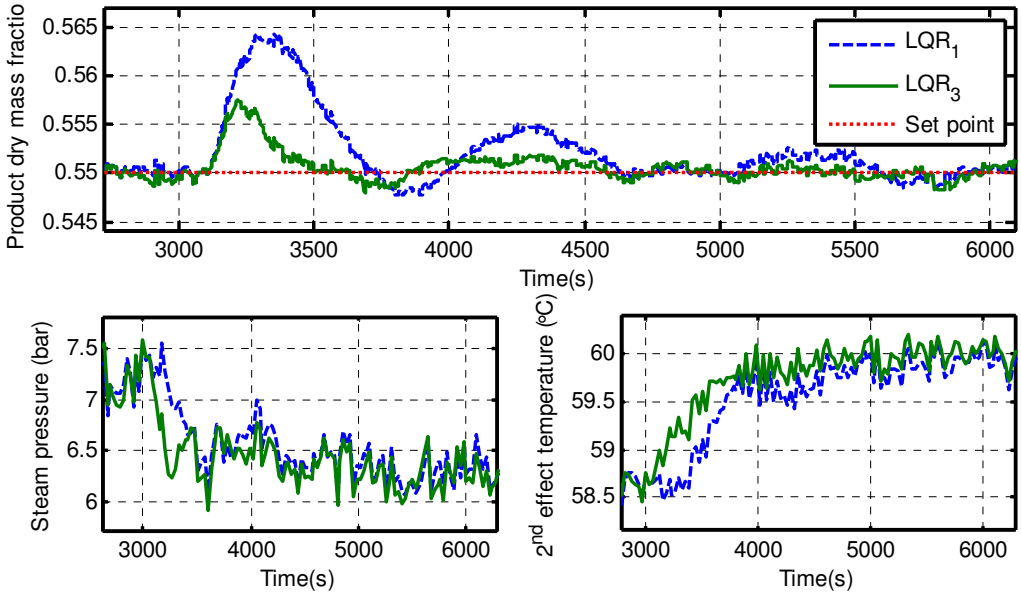

Figure 8-20: LQR_1 and LQR_3 feed dry mass disturbance rejection comparison

The difference in the controller response to a W_F step is clear: by using pre-delay states, LQR_3 starts changing both manipulated variables as soon as the disturbance occurs, while LQR_1 has a delay because the disturbance first needs to propagate through the FFE and be picked up in the output variable. Similar comparisons can be made for each of the other disturbances.

8.9 Fuzzy control

In contrast to the previous techniques investigated, fuzzy logic control does not require any known process model by focusing heavily on process knowledge. This makes fuzzy logic ideal for rapid controller development as well as helping the operators understand the mechanism of the controller. Section 4.3 shortly discussed various forms of the fuzzy controller. The first fuzzy controller investigated will be the fuzzy PI controller.

The PI fuzzy controller reacts to the change in error, ΔE, quickly and continuously to the error, E. The calculation of the two terms is shown below in Eq. 8-12 and Eq. 8-13:

$$E = Setpoint - output \quad \text{Eq. 8-12}$$

$$\Delta E = Error(k+1) - Error(k) \quad \text{Eq. 8-13}$$

As mentioned above, the fuzzy controller requires two inputs, namely the error and change in error. Furthermore, the fuzzy controller may have more than one output, yet for simplicity each control loop will be treated as an MISO (multiple-input single-output) unit.

8.9.1 Defining variable membership functions and relative ranges

As shown in Figure 4-4, each fuzzy variable is split into various membership functions (MF). Initially five MFs will be chosen for each variable, i.e. big negative (BN), small negative (SN), zero (Z), small positive (SP) and big positive (BP). Triangular MFs were chosen, with possible inclusion of other forms if the observed control action is not smooth. The resulting general representation of the MFs for a given variable is shown below in Figure 8-21:

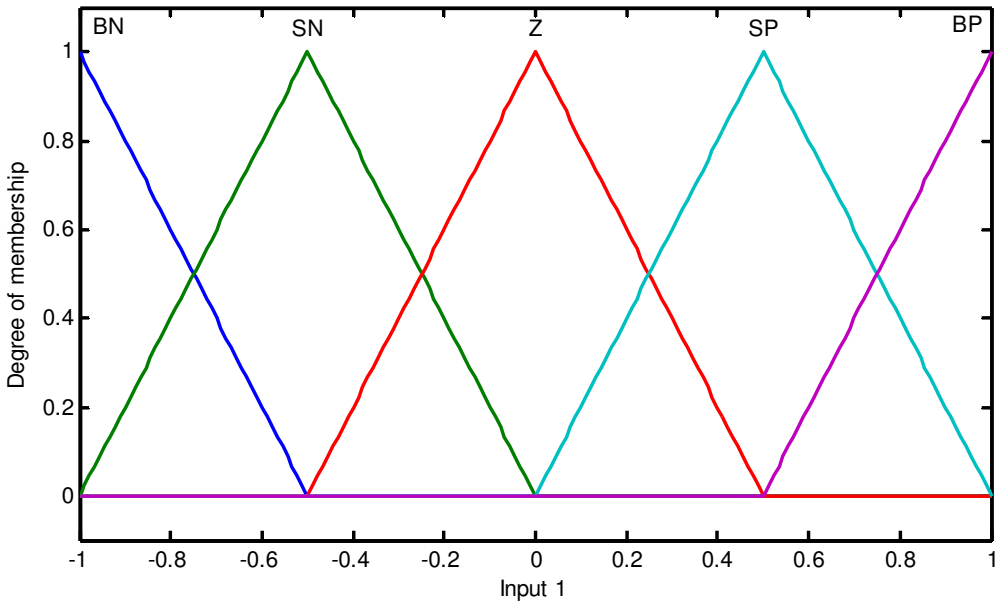

Figure 8-21: Selected general triangular membership functions for a fuzzy variable

In addition to the type and number of MFs, one also needs to define the individual ranges of each function. In keeping with the generic fuzzy formulation, a script was written to dynamically create the individual MF ranges by specifying an overall variable range (FR). The relative range calculation is shown below:

Table 8-13: Membership function relative range in relation to overall variable range (FR)

Membership function	Lower	Upper
Big Negative (BN)	-1.5 x FR	-0.5 x FR
Small Negative (SN)	-1.0 x FR	0 x FR
Zero (Z)	-0.5 x FR	+0.5 x FR
Small Positive (SP)	0 x FR	+1.0 x FR
Big Positive (BP)	+0.5 x FR	+1.5 x FR

By defining the MF ranges using the above specifications the tuning of the fuzzy controller is simplified to choosing the overall range of each variable as well as the control rules.

8.9.2 Fuzzy PI rule specification

Once the MFs have been selected, one needs to specify the fuzzy rules that govern the control action. These rules take the IF-THEN form explained in Section 4.3. Instead of defining each rule separately, an Excel table was used to generate numeric representations of the rule which could then be fed into Matlab. Note that the fuzzy rules are created in velocity form, i.e. the output term is the desired change in the output variable and not the desired absolute value.

Product dry mass loop

The control loops of Section 8.4 were again investigated. Loop 1, the product dry mass loop, is strongly coupled to steam pressure, P_S. An increase in steam will cause increased evaporation and therefore increased product dry mass fraction. The opposite is also true in that a steam decrease will decrease the product dry mass fraction. Therefore a positive error (W_P below the set point) needs to be countered by increasing the steam pressure thereby forcing W_P back to the set point. Note that again the opposite will also be true, namely that if a negative error is observed the controller needs to decrease P_S to force W_P lower (and closer to the set point).

Secondly, if the change in error is positive, in addition to the error being positive, the controller action will need to be stronger to first reverse the momentum of the system and then decrease the total error. The same is true for if ΔE and E are both negative. In the case where ΔE is positive and E is negative (or vice versa) the error is already being decreased and the controller action may therefore be reduced to limit overshoot. Lastly, if ΔE is zero, the controller should act as described in the above paragraph.

Note that for the Excel representation, and input into Matlab, the MF names were converted into numeric values, i.e. 1 for BN, 2 for SN, 3 for Z, 4 for SP and 5 for BP. The rule surface created using the above logic is shown in Table 8-14 below:

Table 8-14: Product dry mass control surface

$P_S \rightarrow W_P$			Input 1 : Error (E)				
			BN	SN	Z	SP	BP
			1	2	3	4	5
Input 2 : Change in error (ΔE)	BN	1	1	1	2	3	4
	SN	2	1	2	3	3	5
	Z	3	1	2	3	4	5
	SP	4	1	3	3	4	5
	BP	5	3	3	4	5	5

Again note the interesting application of fuzzy logic used at small positive error values while the change in error is small or big negative. In these circumstances, the absolute error is decreasing – as such the controller action may be kept constant. Setting up the rules to reflect this process knowledge should decrease overshoot dramatically without influencing the speed of response for large errors.

First effect temperature

The second control loop, $T_{E2} \rightarrow T_{E1}$, has the same relative input-output variable interaction as seen in control loop 1. Increasing the manipulated variable (in this case T_{E2}) causes an increase in the control variable (T_{E1}). Therefore the control surface was initially chosen to be identical to that seen in Table 8-14. The rules of both fuzzy controllers can also be represented by a surface plot as shown below in Figure 8-22 (note that the variable ranges are not yet specified and that the controller output is shown only as "Output 1"):

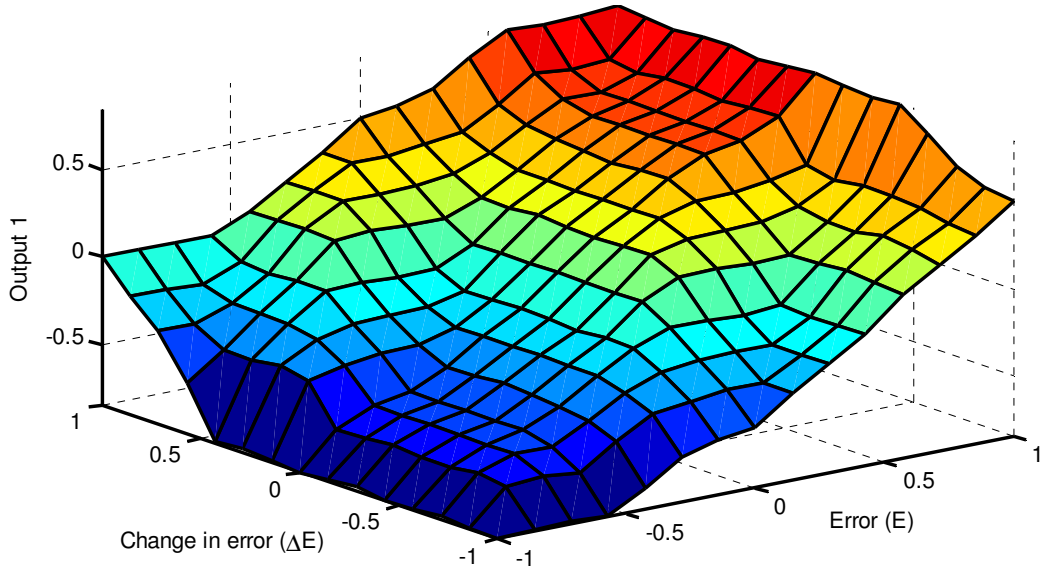

Figure 8-22: Fuzzy control surface for loop 1 and loop 2

8.9.3 Fuzzy PI control structure and overall variable range selection

It should be noted that at this stage the control loops, variables, rules and MF have already been defined. As such, the fuzzy controller is virtually complete without the need of any absolute measurement or parameter from the process. The current fuzzy controller structure is shown below:

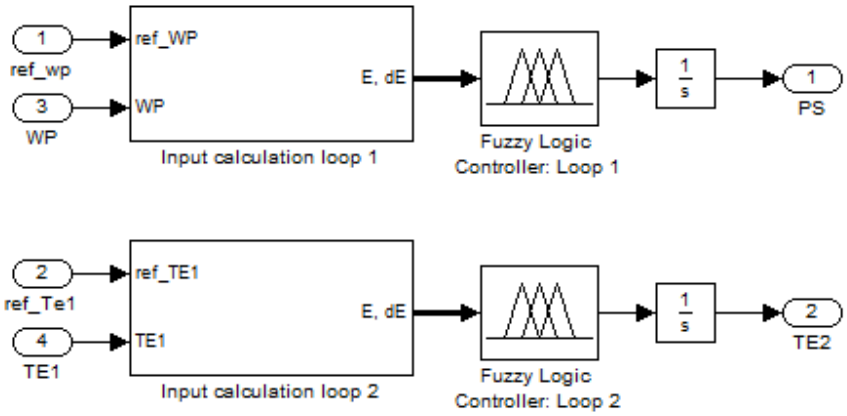

Figure 8-23: Fuzzy PI controller Simulink structure

All that is still required is to select the variable ranges. As mentioned earlier, the overall variable ranges define both the inputs that the fuzzy controller can successfully describe as well as the size of the resulting control action. If an input falls outside of the specified range, the fuzzy controller will treat it as still being in the closest MF. Under these circumstances, the controller should still function, but will not be able to successfully distinguish absolute input variable sizes or adjust the response appropriately.

With adequate process knowledge, estimates can be made of the expected ranges for each input and output variable as shown in below:

Table 8-15: Range estimate for fuzzy variables

	Loop 1 : W_P		**Loop 2 : T_{E1}**	
	Fuzzy range	Unit	Fuzzy range	Unit
E	0.05	fraction	3	°C
ΔE	0.01	fraction/10s	0.5	°C/10s
P_S	0.23	bar/minute	-	-
T_{E1}	-	-	0.3	°C/minute

Note that the normal operating range for P_S is 3 to 10 bar, while the normal T_{E2} operating range is between 50°C and 68°C (Section 8.4.3). With this in mind, it can be seen that the initial fuzzy change range for P_S is far bigger in relation to its normal operating range than chosen for T_{E2} (7% and 1%). Therefore it will take 30 minutes to cover the whole P_S range, while a full 60 minutes is required to change T_{E2} from the minimum to maximum allowable value. These time frames are desirable as the FFE temperatures need to be kept as constant as possible while the supply steam may be used extensively.

8.9.4 Fuzzy PI rule adjustment and range fine tuning

The initial ranges were selected in the section above with the rules specified earlier in the chapter. The fuzzy controller was created by relying on process knowledge instead of performing experiments on the process. Yet the simulation model will be very helpful in tuning the fuzzy controller.

The fuzzy rules and ranges were implemented in Matlab using the Fuzzy Logic Toolbox as well as the previously mentioned script (Appendix A) to calculate dynamic ranges. The resulting controller was first subjected to the same set point changes used for PI and LQR tuning:

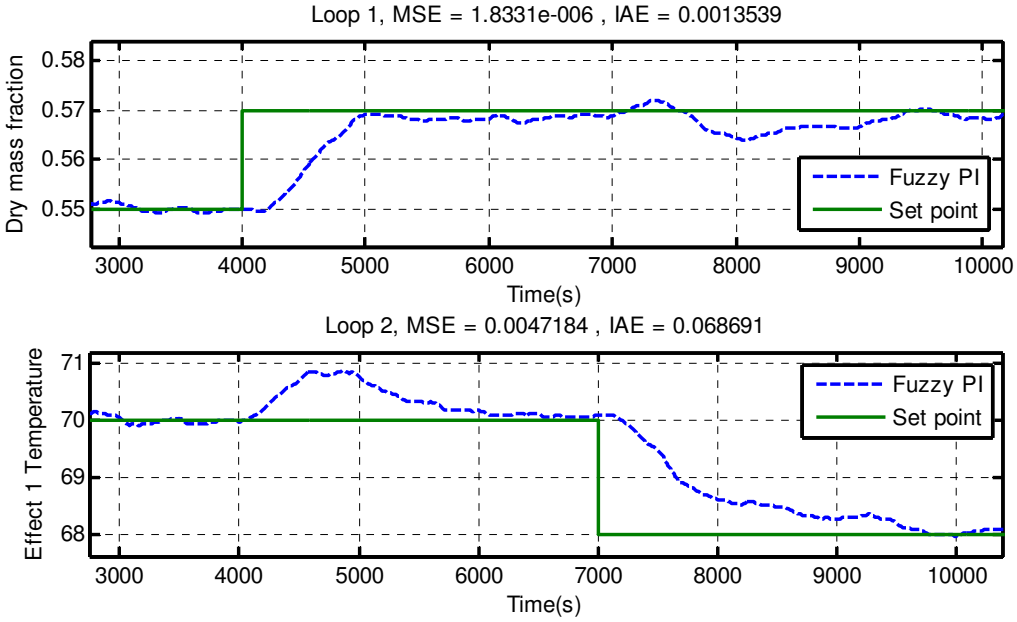

Figure 8-24: Fuzzy PI set point tracking

From Figure 8-24 it can be seen that the FPI controller achieves zero offset tracking for both output variables. The rise time for W_P is fairly slow at a 1 000s, while the T_{E2} rise time was comparable to the PI controller (2 700s versus 2 800s). The initial controller performance is, however, promising and shows that the knowledge based design was successful.

Note also the long time required by the FPI to reject the disturbance in W_P created by a T_{E1} set point change. This clearly shows that the controller was not aggressive enough. The lack of any overshoot in both output variables also points to a detuned controller.

To fine-tune the controller response and improve response times, the size of both the error and change in error was recorded for each output variable. If the observed ranges are found to be too wide it would mean that the controller never entered into the larger input MFs and as such the output response would be too small.

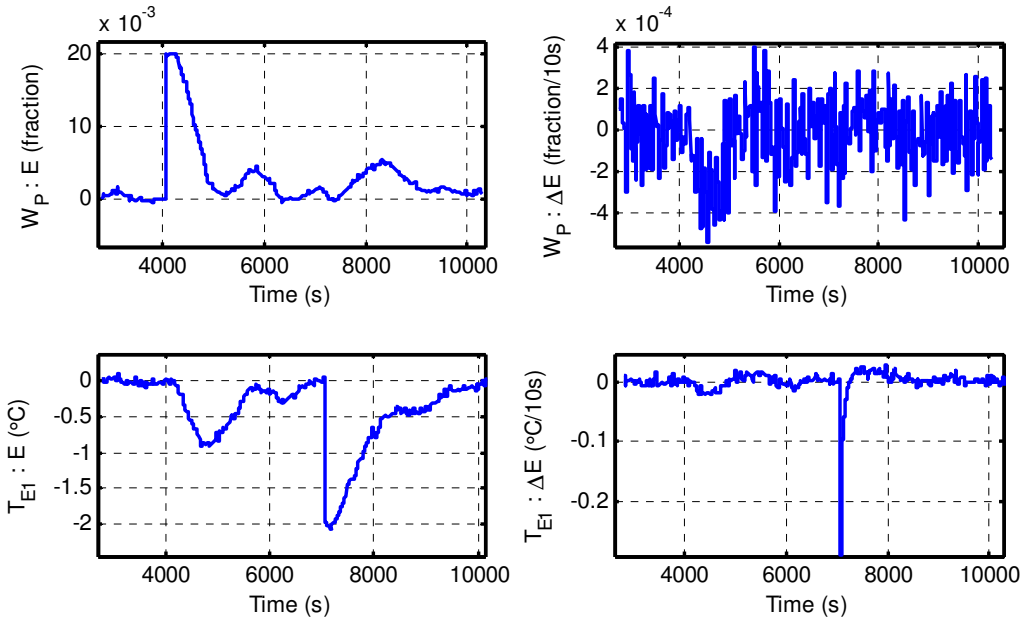

Figure 8-25: FPI error and change in error trends for output variables

From Figure 8-25 it is clear that some of the input variable ranges chosen in Table 8-15 were incorrect. For example, the product error never exceeds a dry mass fraction of 0.02, even with a set point change included in the simulation, yet the initial range was chosen at 0.05. Furthermore, the noise on ΔE for W_P hides the overall trend. One only wants the FPI controller to act on the medium time frame trends, i.e. not try to counter inherent sensor noise. A first order filter with a time constant of 30s was included, with the resulting ΔE shown below:

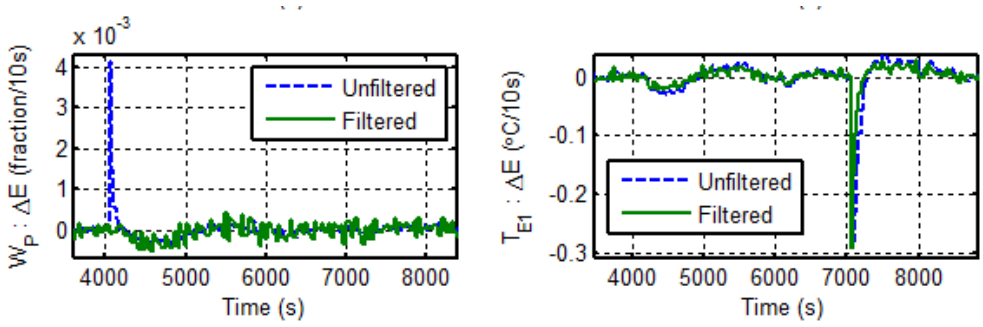

Figure 8-26: Comparison between filtered and unfiltered ΔE

Note that the controller sample time of 30s hid the spike seen in W_P ΔE at 4 000s, as the set point change occurred between two controller sampling instants. By selecting the filter time constant equal to the sampling time one ensures that large spikes will be picked up by the controller. The additional delay should not have a negative impact on the control action as it only effects the ΔE FPI action.

The fuzzy variable ranges of the initial FPI controller (FPI_1) were tuned resulting in FPI_2. The tuning increased the available output range for T_{E2}, while slightly reducing the P_S output range. The input error ranges were both narrowed, which also increased the controller action as the outermost MFs were now also used. Finally, the rules shown in Table 8-14 were also updated to have a narrower band of zero action, i.e. both small positive and small negative MFs for ΔE were no longer assumed to cancel out the opposite small error resulting in a final FPI_3 controller. All three versions of the FPI controller are compared below:

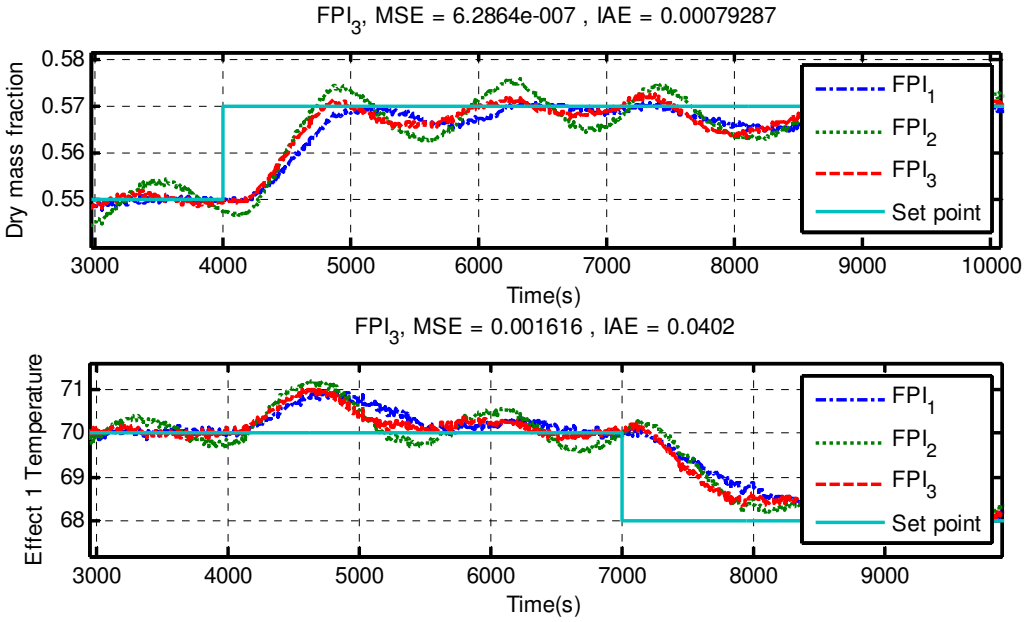

Figure 8-27: Fuzzy PI controller tuning

Note that FPI_2 showed more aggressive action than FPI_1, which resulted in a shorter rise time, but also in pronounced oscillation of W_P. The fuzzy rules were therefore adjusted, as mentioned earlier, to remove the oscillations by continuing to update the controller output at small E values even where ΔE shows that E is already being reduced. Consequently, FPI_3 retained the shorter rise time of FPI_2 without the oscillations. The final fuzzy variable ranges are shown below:

Table 8-16: Tuned range selection for fuzzy variables

	Loop 1 : W_P		Loop 2 : T_{E1}	
	Fuzzy range	Unit	Fuzzy range	Unit
E	0.035	fraction	2.5	°C
ΔE	0.004	fraction/10s	0.4	°C/10s
P_S	0.18	bar/minute	-	-
T_{E1}	-	-	0.36	°C/minute

The final rule surfaces for both loop 1 and loop 2 are also shown below in Figure 8-28. Note the smaller zero action range:

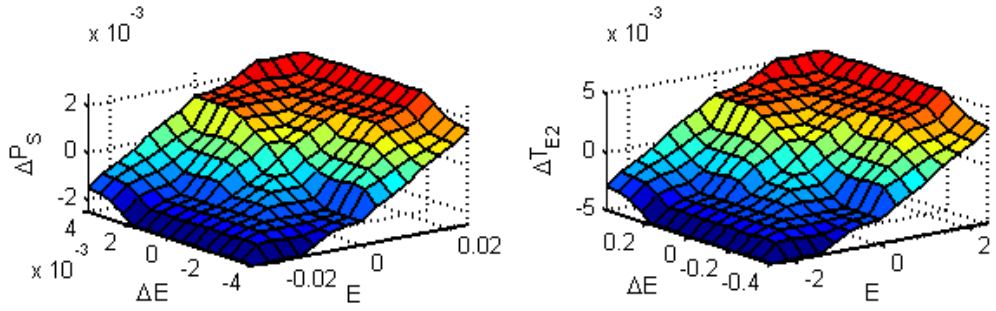

Figure 8-28: FPI3 rule surfaces for Loop 1 (left) and Loop 2 (right)

8.9.5 Disturbance rejection rules and tuning

The initial fuzzy controller showed adequate set point tracking performance with very little required tuning. The controller requirements are, however, two fold, with disturbance rejection being equally important as the process will normally be kept at constant set points. The disturbance rejection capabilities of FPI_3 were investigated by introducing the same W_F, T_H and F_1 steps as described for both PI and LQR control:

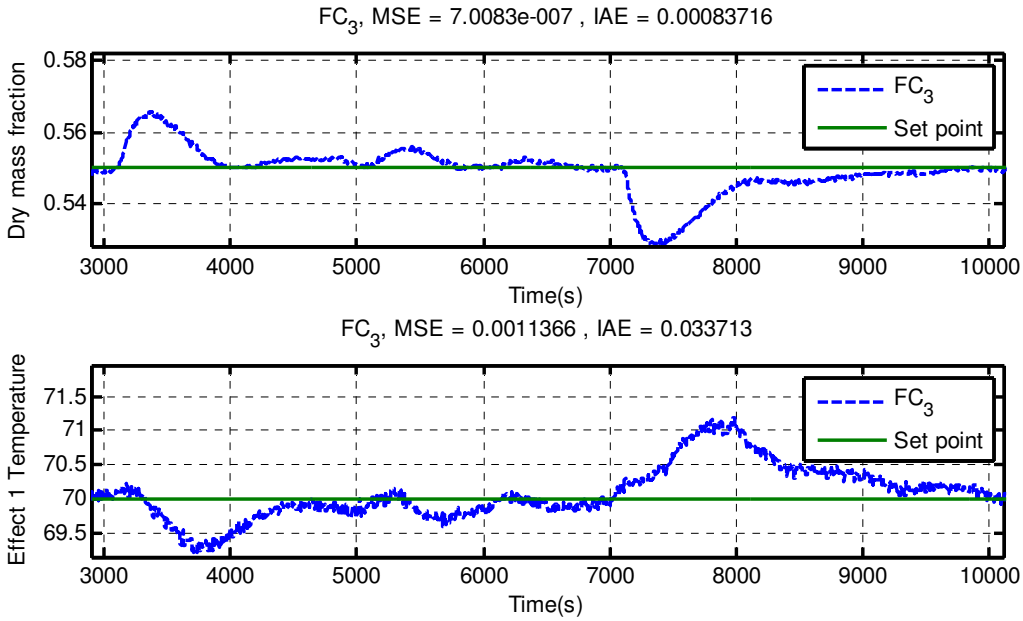

Figure 8-29: FC_3 disturbance rejection

From Figure 8-29 above, it is clear that FC3 did not provide adequate disturbance rejection as the WF step at 3 000s exceeded the maximum W_P deviation (±0.01 dry mass fraction) limit. Furthermore the F_1

step at 5 000s also exceeded a dry mass fraction increase in W_P of more than 0.01. The current fuzzy controller was already tuned aggressively (as shown by Figure 8-27) and as such one can conclude that additional tuning will not greatly improve disturbance rejection without causing excessive oscillations.

8.9.6 Predictive fuzzy control structure

The same time delay difficulties faced during the design of the LQR controller apply when designing fuzzy control as well. For quick disturbance rejection, the controller needs to start corrective action before the error is seen in the output, i.e. predict the error as soon as a disturbance input variable starts to deviate significantly. As seen in Figure 8-29, the initial fuzzy controller did not use any prediction and as such the rejection was slow and inadequate.

LQR control negated the process delay by using states from a linear model before the delay was calculated; thereby acting on any modelled disturbance as soon as it occurred. The same model predictive element is possible with fuzzy control, but would require the identification of a model - thereby removing the simple development followed for the initial design. Even though the state space model is available, this section will assume it is not and investigate another approach which again relies on process knowledge and is much less involved than model identification.

Fuzzy prediction rules

Instead of identifying a complete model, a fuzzy rule was created for each of the major known disturbances, i.e. W_F and F_1. The rules relate the absolute value and rate of change of the disturbance variable to a fixed addition to the manipulated variable. Therefore two complimentary predictive rules, shown below, were added to the initial fuzzy controller to form a predictive fuzzy controller (PFC):

Predictive rule 1 : IF W_F increases drastically, decrease P_S to negate the resulting W_P deviation (the reverse case requiring a P_S increase)

Predictive rule 2 : IF F_1 increases drastically, increase P_S to negate the resulting W_P deviation (the reverse case requiring a P_S decrease)

As with the rules of the FC, the PFC rules require fuzzy variable ranges to be defined for each input and output variable included. The respective variables are W_F, ΔW_F, F_1 and ΔF_1. The fuzzy ranges were estimated and fine-tuned to produce the values seen in Table 8-17:

Table 8-17: Fuzzy variable ranges for predictive fuzzy controller

	W_F prediction			**F_1 prediction**	
Variable	Fuzzy range	Unit	Variable	Fuzzy range	Unit
W_F	0.03	fraction	F_1	1250	kg/h
ΔW_F	0.001	fraction/10s	ΔF_1	830	(kg/h)/10s
P_S	2.5	bar	P_S	1	bar

It is important to note that the predictive rules are not in velocity form, i.e. the output is an absolute value instead of the desired change in output variable used by the previous rules. In this way, the predictive rules give the manipulated variable a bias instead of dynamics. Additionally, this bias is added

instantaneously to the manipulated variable set point when a disturbance is introduced, thereby giving the desired quick response missing from the FC.

Combining the base rule logic of Table 8-17 with the above selected limits, the rule surfaces shown in Figure 8-30 were constructed. Note that the surface was created by again extrapolating the base logic into 25 smaller rules:

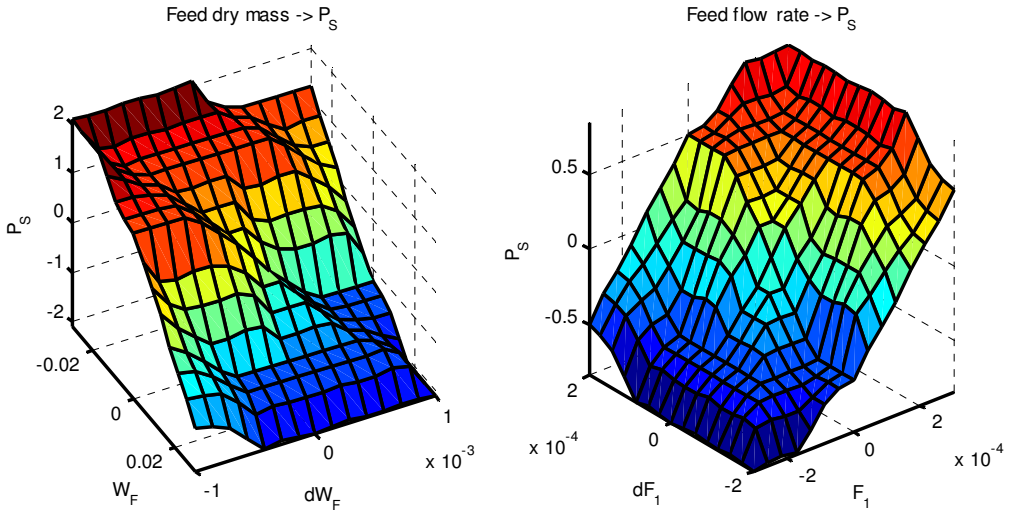

Figure 8-30: Fuzzy predictive rules

Both rules were developed only for the W_P control loop as T_{E1} allows more variation and already showed good response under the initial FC.

8.9.7 Fuzzy predictive controller disturbance rejection

The FPC only differs from the FC in predictive rules; during set point changes these predictive rules stay constant as the error does not form part of the rule input. As such, only the disturbance rejection will differ from the FC. The disturbances defined in Table 8-11 were again introduced into the system and the controller response observed:

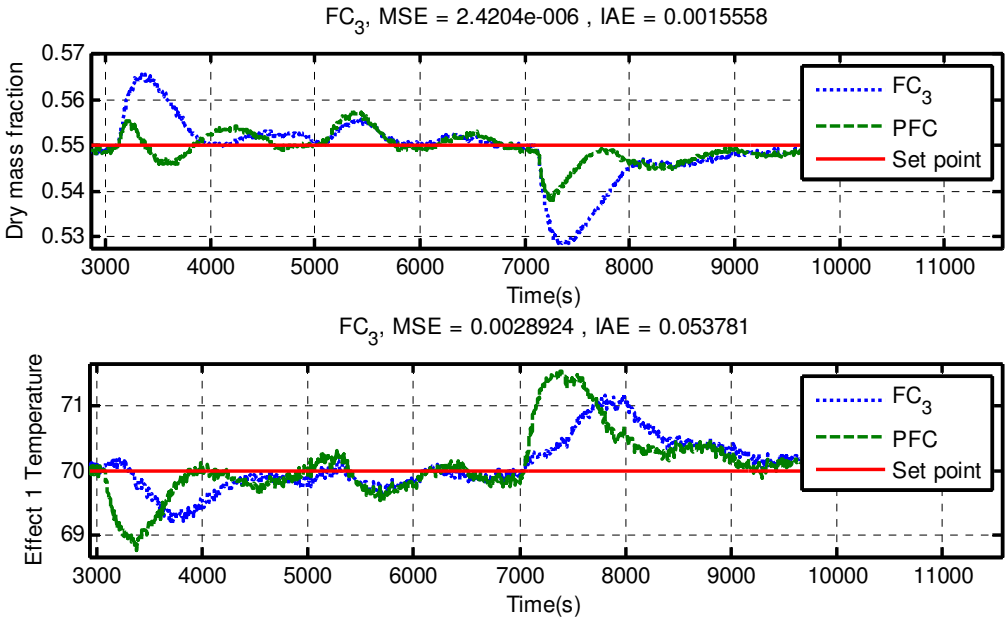

Figure 8-31: Predictive and initial fuzzy control disturbance rejection

From Figure 8-31 it is easy to see the drastic improvement in the W_P disturbance rejection of the PFC compared to that of the initial FC. Note that the maximum deviation for a W_F disturbance is below a dry mass fraction change of 0.005, far better than the 0.014 of the normal FC. Furthermore, the large F_1 disturbance was contained to a maximum deviation in dry mass fraction of around 0.01, again a significant improvement over the FC. Also note the process reaction is virtually identical for the middle T_H disturbance as no predictive rule was created for this circumstance. The deviation is again far below the maximum allowed while the disturbance step was quite large (+3°C).

8.10 Fuzzy feed flow rate optimiser

Currently, the local FFE plant allows operators to change the manipulated variables, P_S and T_{E2}. The operators also try to maximise F_1 as well as adhere to product quality restrictions. The control solutions designed in the chapter all attempt to follow output variable set points, while rejecting disturbances by predicting process deviations. The designed controllers can therefore all take over the manipulated variable changes, but none have been designed to maximise production rate. Consequently, it is very possible that the FFE will always run at below its maximum capacity.

There are various ways to try and optimise the local FFE, yet all may be reduced down to maximising the feed flow rate for any given process state. The FFE maximum evaporative capacity is restricted by the energy available from P_S and the rate at which the condenser can remove energy from the system.

Logically, if the process operates close to its maximum capacity one also expects the manipulated variables to be close to their respective maximums. From the historical data, and control simulations (Section 8.12), it can be seen that P_S is the manipulated variable that reaches saturation most often. It was decided to assume the condenser action will not reach saturation and maximise the use of P_S, which will then imply maximum use of F_1 and an optimised process. If simulations show that the condenser action saturates this assumption would be invalid and an optimiser that accounts for condenser action will also be required.

Fuzzy membership functions and variable ranges

The same approach to fuzzy variable ranges will be employed as was used in Section 8.9.1, namely in specifying an overall range that will then be split up into 5 smaller membership functions (MFs). The optimiser will only consider one input variable, P_S, with the aim to keep P_S as close as possible to its maximum, i.e. about 9bar (90% of the 10bar maximum). The rule surface was created with a dummy variable so that the same generating scripts could be used.

The optimiser takes the form of a fuzzy proportional controller, referred to as the fuzzy feed optimiser (FFO), which is severely detuned to not interfere with any of the control solutions of this chapter. If one makes the optimiser too aggressive the other controllers will always act quickly on F_1 changes. Therefore it was decided that the FFO output, change of F_1 per second, would be limited to 0.575 (kg/h)/s (which is about a 2070kg/h set point change that the optimiser can make per hour). With these limits and chosen variables the following rule surface was defined:

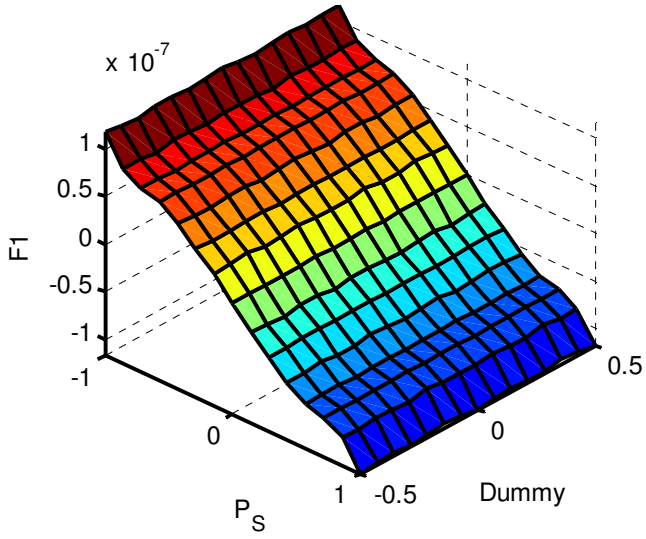

Figure 8-32: Fuzzy optimiser rule surface

Note that the rule surface effectively ensures that if the steam pressure is not at 9bar, F_1 will be changed until the pressure reaches 9bar. Secondly the slow output action may not be enough to ensure that the FFO does not interfere with the other controllers. Therefore it was decided to place a long time constant (800s) linear filter on the P_S fuzzy input variable. This will ensure that no noise or sudden P_S changes will affect the FFO.

Fuzzy feed optimiser simulation

To test the FFO, a simulation was run where all the disturbance variables were kept constant and all the controllers active. Once the FFE reached steady state a feed dry mass fraction increase of 0.01, at 13 000s, was introduced:

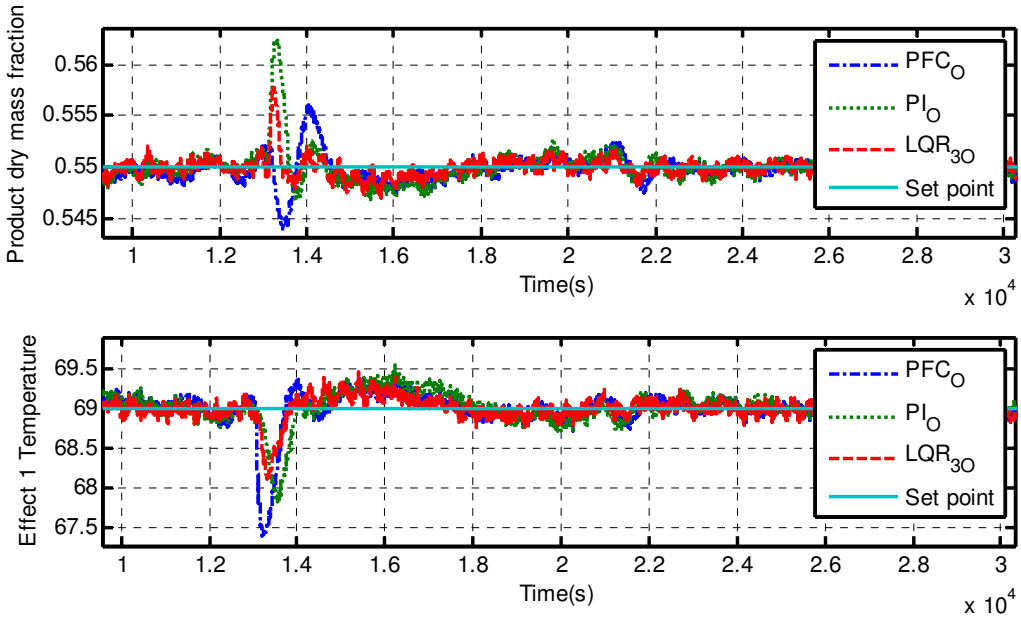

Figure 8-33: Feed disturbance rejection with fuzzy feed optimiser enabled

Note that on Figure 8-33 all the controllers are denoted with an added "O" to signify that the FFO was enabled. Figure 8-33 shows that the FFO does not cause a great difference in controller action when compared to the previous sections without the optimiser. The real validation of the optimiser was the use F_1 and P_S input variables shown below:

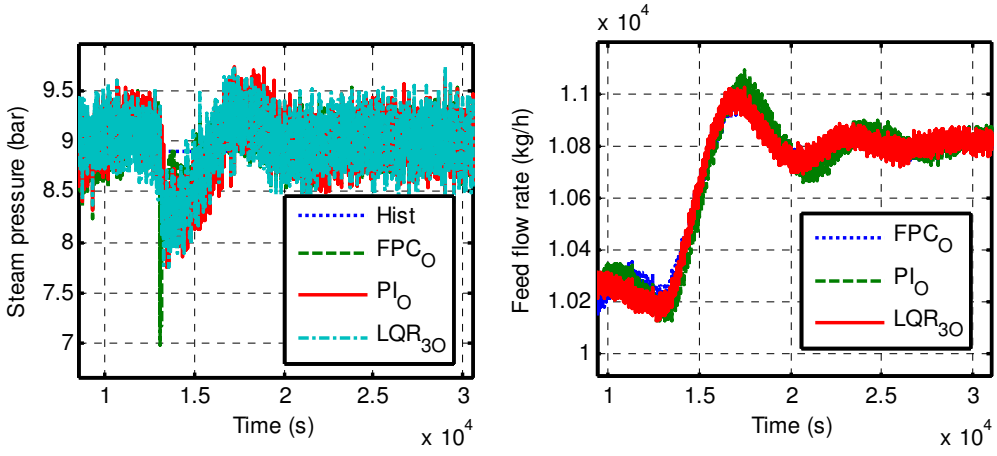

Figure 8-34: Steam pressure and feed flow rate under fuzzy feed flow optimisation

At 13 000s, when the W_F step disturbance was introduced, the controllers automatically lowered P_S to immediately prevent the product dry mass of going too far of specification. All the controllers managed to almost completely reject the W_F disturbance and return to the set points within ±2 000s. At the same time the FFO acted on the decreased P_S and shifted F_1 up as there was now spare evaporative capacity (because of the higher feed dry mass fraction). The FFO required 4 500s to increase F_1 (with an even longer settling time), more than double the amount of time the controllers took to reject the disturbance. Therefore the FFO was slow enough not to interfere greatly with the other controllers.

Additional qualities of the fuzzy feed optimiser

Although the FFO was designed to maximise F_1, it serves other purposes as well. If the evaporator reaches maximum capacity, P_S will increase past 9bar which will cause the FFO to reduce F_1, which will in turn ease the load on the evaporator and allow proper set point tracking. Therefore, the FFO not only maximises F_1, it also ensures the evaporator will be able to achieve the output set points under various circumstances. This functionality is shown by comparing a constant F_1 set point to that of the FFO for a W_F set point change (that overloads the evaporator at the chosen constant F_1 flow rate):

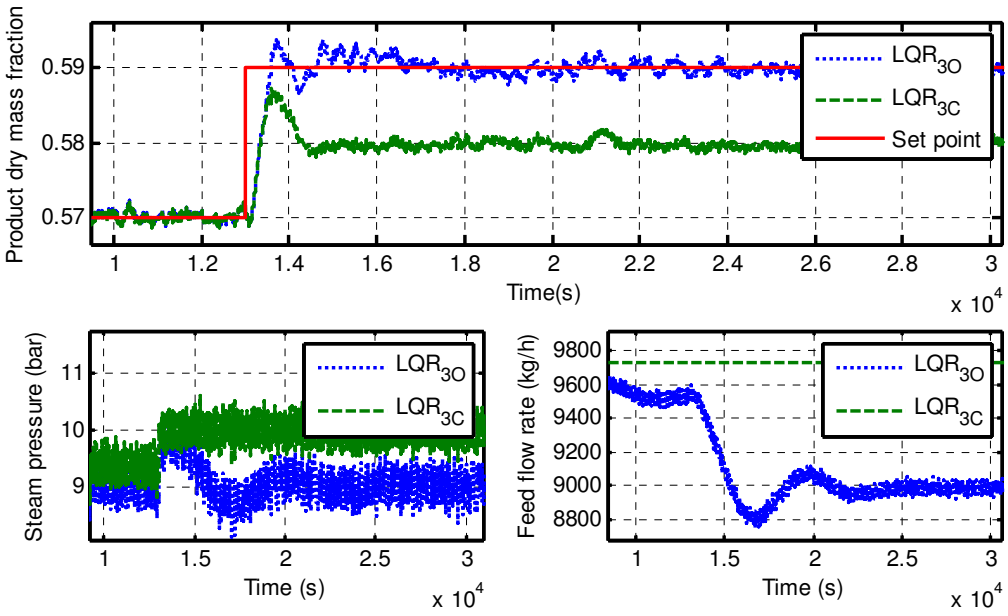

Figure 8-35: Fuzzy optimiser evaporator capacity management

From Figure 8-35 it can clearly be seen that a set point change that would have caused steam saturation, when an incorrect constant F_1 was chosen, can be performed without saturation using the FFO. By using the FFO the controllers can be run on various recipes without the operators needing to specify new feed flow rates.

8.11 Controller comparison

Once all of the controllers developed in this chapter were finalised and tuned, a meaningful comparison could be made. The comparison will focus on the final versions of each controller, i.e. base case PI, state space LQR and the predictive fuzzy controller (FPC). Performance will be evaluated for three major circumstances, i.e. set point tracking, disturbance rejection and overall error when subjected to historical disturbance inputs.

It should also be emphasized that all the controllers were subjected to the same process and measurement noise while also using the same average sampling technique. This was done to ensure that the true performance of the controllers could be judged while all other circumstances were kept constant.

8.11.1 Set point tracking

The FFE will always operate under certain given set points which will be chosen to give optimal product quality and throughput. These set points may, however, change under different process conditions or for different raw materials. Therefore any controller needs to follow a given set point with zero offset and transition from one set point to another smoothly.

The controllers were compared by introducing set point changes similar to those used for tuning, as shown by Figure 8-36 below:

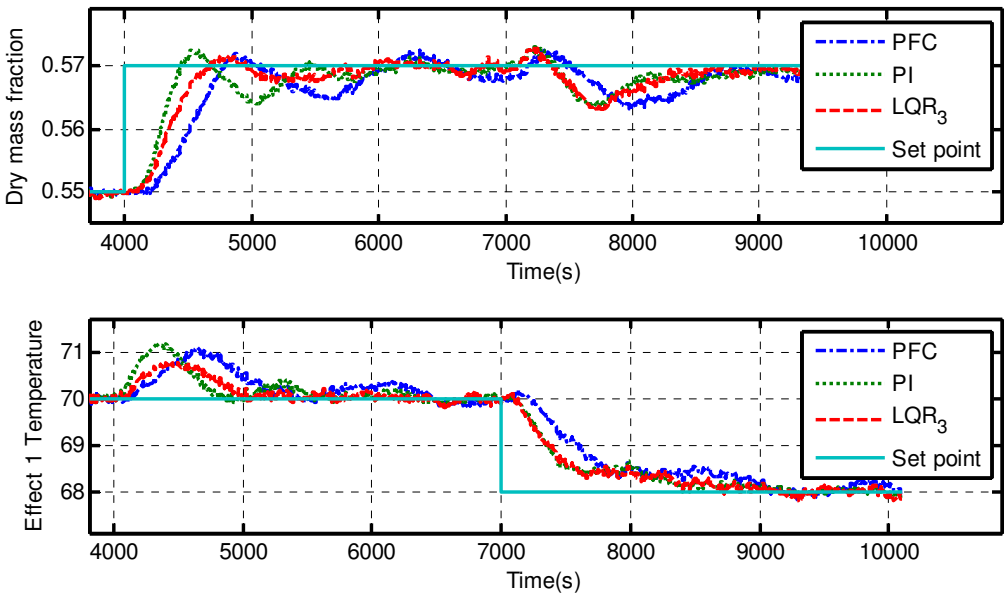

Figure 8-36: Set point tracking controller comparison

For the product dry mass control loop, the simplest controller, i.e. PI, showed the quickest rise time (±450s), but also showed the largest oscillations, and a settling time between that of LQR_3 and PFC. The PFC showed the slowest rise time with the longest settling time (±2 000s). The disturbance introduced in

T_{E1} for a W_P set point step was best rejected by the LQR controller, with both the PI and PFC controllers showing significantly larger maximum deviations. Again it was seen that PFC took the longest time to reach zero offset.

The first effect temperature control loop was also shown in Figure 8-36. As with the W_P loop, the PFC showed the longest settling and rise times. Interestingly, the PI and LQR controllers showed a virtually identical response in both T_{E1} and W_P for a T_{E1} set point change.

All the controllers showed some overshoot for a W_P set point change while showing a clearly overdamped slower response for T_{E1} set point changes. The performance of each controller was also measured by calculating the IAE and MSE values, as well as recording maximum deviation during a set point change of the other loop. All the performance metrics are shown in Table 8-18 below:

Table 8-18: Controller set point tracking numerical performance comparison

Loop 1: Product dry mass (W_P)						
	MSE	IAE	Max dev	Unit	Rise time	Settling time
PFC	7.70E-09	2.16E+01	7.00E-03	Fraction dry mass	810s	2000s
PI	4.40E-09	1.56E+01	5.90E-03	Fraction dry mass	440s	1400s
LQR_3	5.11E-09	1.51E+01	6.00E-03	Fraction dry mass	620s	800s
Loop 2: First effect temperature (T_{E1})						
	MSE	IAE	Max dev	Unit	Rise time	Settling time
PFC	3.83E-01	2.73E+03	1.00	°C	2100s	3000s
PI	2.61E-01	2.03E+03	1.30	°C	2100s	2100s
LQR_3	2.28E-01	1.86E+03	0.70	°C	2100s	2100s

Table 8-18 reiterates what was seen in Figure 8-36, namely that the PFC consistently displayed the largest errors (both MSE and IAE) due to having the slowest rise and settling times. PI and LQR_3 control show similar results for both MSE and IAE values; the only difference seen in the maximum T_{E1} deviation during a W_P set point change.

The settling times for T_{E1} are extremely long, i.e. 2 100s to 3 000s. However, a final observation must be made on these values as only part of the true response is represented. Even though the times are long both LQR and PI controllers reach 75% of the final value within 600s with FPC reaching the same mark at 800s. The response after this point is mainly driven by integral action on the various controllers – which were designed to be slow allowing tighter control on WP. In conclusion, the long settling times are acceptable as the controlled variable, T_{E1}, quickly reacts to decrease the error substantially.

8.11.2 Disturbance rejection

The second function of the controllers is to adequately reject various disturbances acting on the process. It is expected that the process will optimally be run at constant fixed set points; as such disturbance rejection is of paramount importance. There are three measured disturbances, i.e. feed dry mass, feed temperature and feed flow rate; of these it is expected that the feed flow rate may change constantly,

either from operator's inputs or a feed optimiser. Large feed W_F disturbances are also possible when switching from one milk source to another, while T_H disturbances are limited to major process upsets.

By using the above process knowledge, all three measured input disturbances were introduced with the controller performance shown below in Figure 8-37:

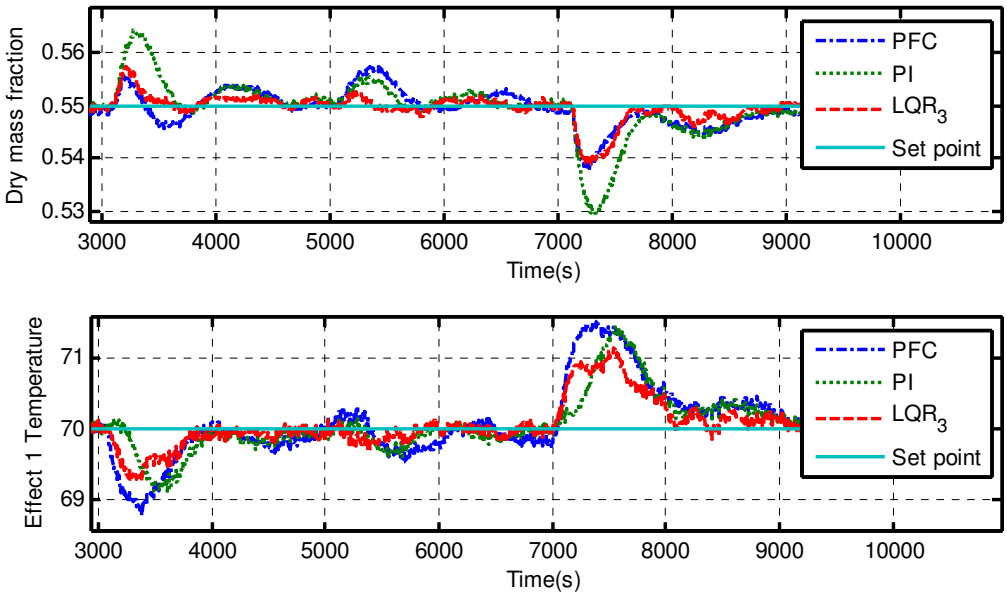

Figure 8-37: Disturbance rejection controller comparison. W_F step at 3 000s, T_H step at 5 000s and F_1 step at 7 000s

From the above figure it can clearly be seen that the LQR controller shows the strongest disturbance rejection for both W_P and T_{E1}. For a W_F step disturbance (at 3 000s) both the PFC and LQR controller were able to limit the maximum deviation of W_P below the specified 0.01 fractional increase limit. The PFC showed slightly lower maximum deviation, but included some overshoot in W_P and a significantly increased maximum deviation in T_{E1}. The PI controller exceeded the maximum deviation by 40% and also introduced a larger deviation in T_{E1} than seen under LQR control.

For the T_H disturbance, at 5 000s, all the controllers restrict the W_P deviation below the limit. The LQR however outperformed the other methods, which was expected as it was the only controller designed for a T_H disturbance as well. The input disturbance step was however fairly large and all three controllers performed well.

Finally the F_1 disturbance at 7 000s again showed similar results for PFC and LQR control. The only difference being a slightly increased deviation in T_{E1} under PFC. Both of these controllers kept the max deviation around a fractional decrease of 0.01, which is very good as the F_1 deviation was fairly large. The PI controller again showed the largest deviations.

The numerical performance factors shown in Table 8-18 were again calculated for the disturbance rejection simulation and are shown below in Table 8-19 (note that the units for all W_P values are dry mass fractions and °C for any T_{E1} related value):

Table 8-19: Controller disturbance rejection numerical performance comparison

	Feed dry mass disturbance					
	PFC		***PI***		***LQR$_3$***	
	W_P	T_{E1}	W_P	T_{E1}	W_P	T_{E1}
MSE	7.86E-11	2.29E-01	3.21E-09	1.22E-01	1.15E-10	7.71E-02
IAE	4.02E+00	6.65E+02	6.43E+00	4.93E+02	2.62E+00	3.80E+02
Max deviation	5.00E-03	1.20E+00	1.40E-01	8.00E-01	7.00E-03	7.00E-01
	Feed temperature disturbance					
	PFC		***PI***		***LQR$_3$***	
	W_P	T_{E1}	W_P	T_{E1}	W_P	T_{E1}
MSE	3.72E-10	4.26E-02	8.73E-11	2.48E-02	2.95E-12	1.13E-02
IAE	3.55E+00	2.56E+02	2.73E+00	1.79E+02	1.23E+00	1.26E+02
Max deviation	7.00E-03	4.00E-01	3.00E-03	3.00E-01	5.00E-03	2.00E-01
	Feed flow rate disturbance					
	PFC		***PI***		***LQR$_3$***	
	W_P	T_{E1}	W_P	T_{E1}	W_P	T_{E1}
MSE	9.68E-10	4.50E-01	1.11E-08	2.77E-01	9.00E-10	1.96E-01

Table 8-19 reiterates what was seen in Figure 8-37. Namely, that the PFC and LQR solutions performed the best over the range of disturbances and that both adequately control the process.

Additionally, the feed dry mass disturbance also shows the difference in information given by MSE and IAE calculations. Comparing the PFC and LQR MSE values it is found that the PFC does marginally better, yet on the IAE values the LQR shows better performance. This apparent discrepancy is a result of the LQR controller showing a greater maximum deviation, but also settling quicker than the PFC. Therefore the PFC always keeps W_P closer to the set point, minimising MSE, but the error persists longer, resulting in a larger IAE value than seen for LQR.

Manipulated variable use

The controlled variable response has been thoroughly analysed and compared between the different controllers. Another important factor is the controller manipulated variable use. Ideally one wants the manipulated variables to change smoothly so as not to strain the valves and actuators too much. This conservation always needs to be weighed against the tightness of control desired. The more active the control the heavier the use will be of the manipulated variables.

The two manipulated variables used in all the controllers were: P_S for product dry mass and T_{E2} for the first effect temperature control. Both these variables were monitored during the set point and disturbance rejection tests of the previous section. Firstly the P_S and T_{E2} used for set point tracking are shown in below:

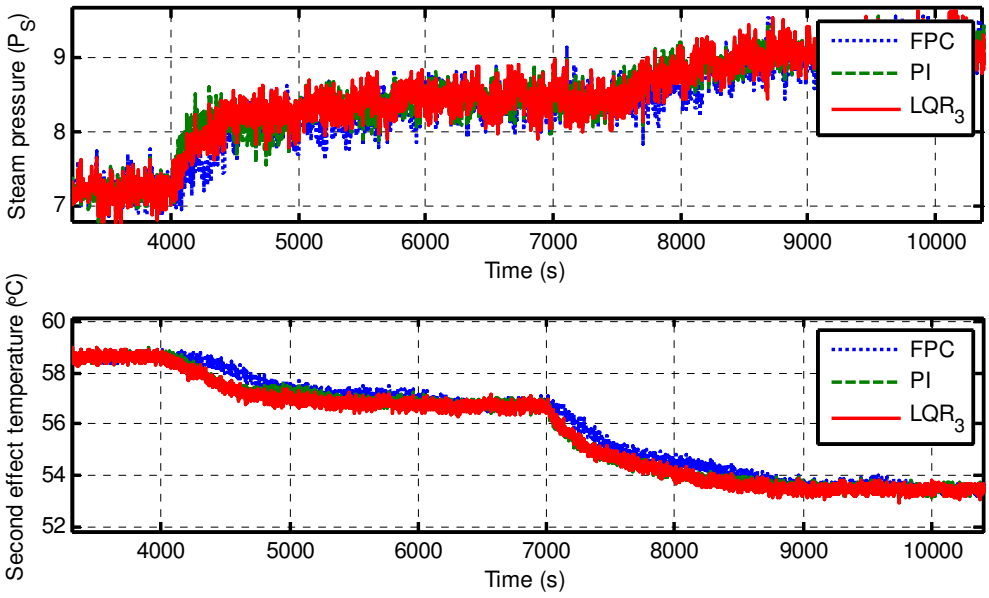

Figure 8-38: Manipulated variable use: set point tracking with noise

Note that it is difficult to distinguish the difference between the manipulated variable use of the controllers, because of noise added. To ease the comparison the figure was redrawn without noise:

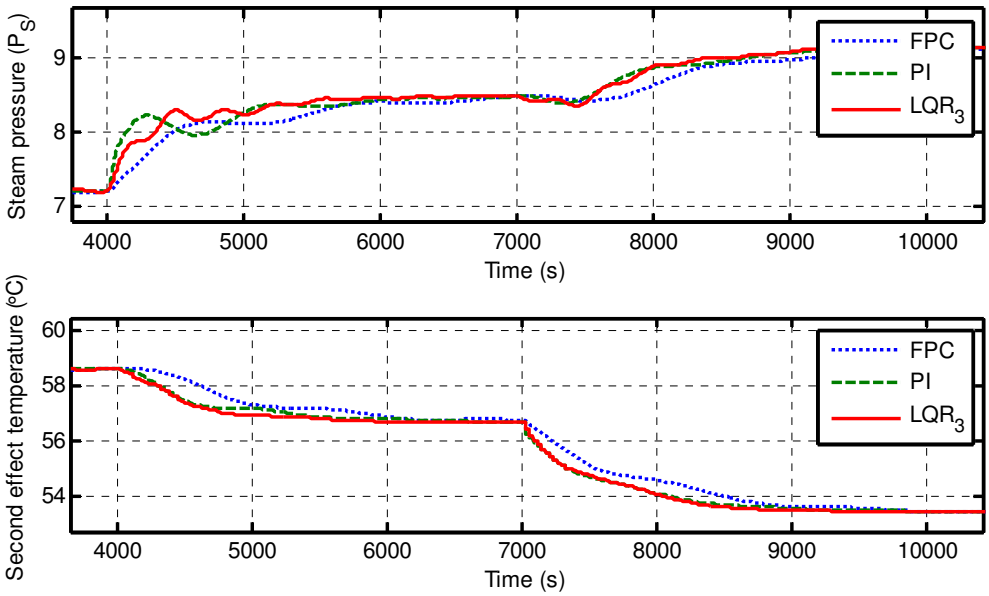

Figure 8-39: Manipulated variable use: set point tracking without noise

It is interesting to refer back to Figure 8-36 where the controller set point tracking was compared. At the time it was remarked that the PFC showed the slowest response while PI and LQR control were virtually identical, Figure 8-39 explains these observations well. From the figure above it is clear that for steam pressure the PI controller has the quickest action while LQR shows the most oscillation and PFC has the slowest, smoothest variable use. For T_{E2} both the PI and LQR controllers show virtually identical use, with PFC again showing slower action. This explains the quick action of PI during set point following as well as the quick settling LQR response and the slower PFC tracking.

The manipulated variable use for disturbance rejection tests are shown below in Figure 8-40, note that the W_F step disturbance was introduced at 3 000s, a T_H disturbance at 5 000s and finally a F_1 disturbance at 7 000s (as described in Table 8-11):

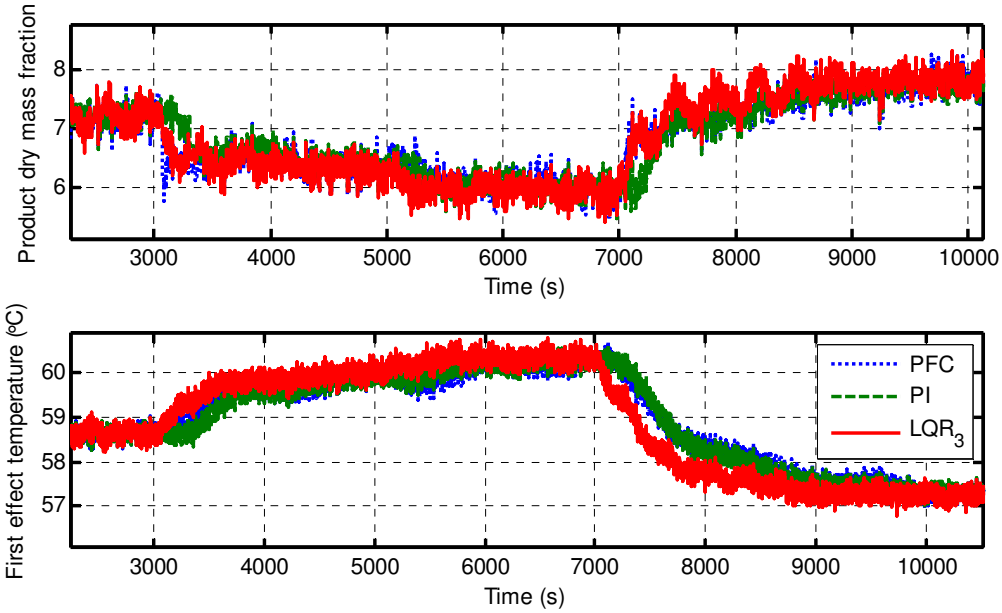

Figure 8-40: Manipulated variable use disturbance rejection without noise

From Figure 8-40 above a clearer distinction can be made of variable use between the controllers. The figure re-affirms that the LQR controller has very strong oscillatory P_S action, while the PI controller now shows the most subtle P_S use. In contrast to the set point tracking example the PFC now shows the quickest P_S action. This is because the predictive rules only act on input disturbances as described earlier and do not influence the controller during normal operation. Furthermore, the P_S use of the PFC might be quick, but is very stable when compared to LQR_3 P_S use – again because the predictive fuzzy rules do not act after the initial disturbance cancelling adjustment. In conclusion, the LQR_3 solution needed to be tuned aggressively to match the performance of the PFC, which in turn introduced the visible P_S oscillations. As these oscillations have a period of ±350s they are acceptable, but are cause for concern.

In conclusion, although the LQR controller shows comparable, if not better, results than the PFC when one looks at the controlled variable, one must remember the additional stress placed on the steam actuator.

8.12 Controllers compared to operator control

The hypothesis formed in Section 1.5 stated that a controller can be designed that performs better than the current operator control. This section aims to show that the controllers designed in this chapter prove the hypothesis.

8.12.1 Simulation bias

As seen in Chapter 6 the fundamental model was shown to adequately describe the local FFE operation. It was, however, noted that certain influences, not included in the model, introduced a near constant bias to the prediction of W_P and T_{E1} as shown for recipe 1 in Figure 6-22 and redrawn as Figure 8-41 below:

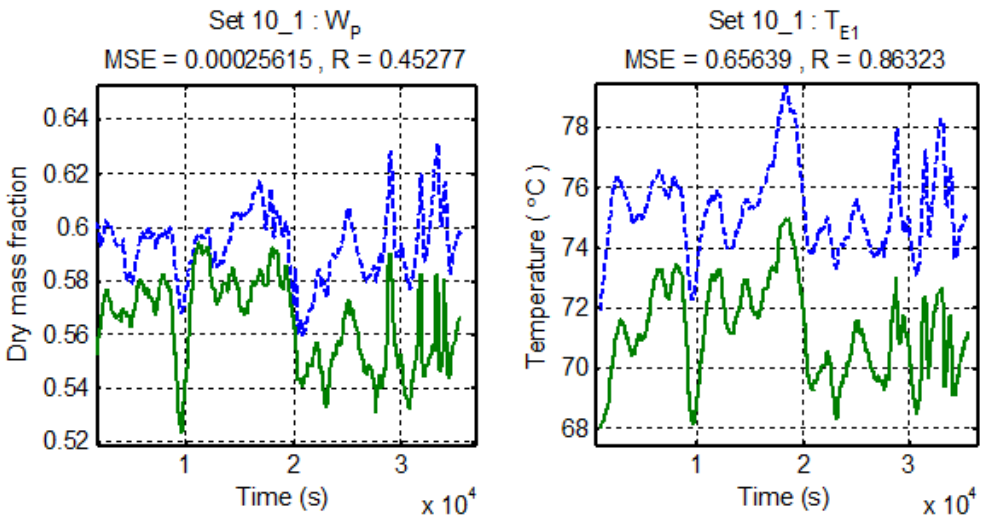

Figure 8-41: Constant bias between simulation and historic data for recipe 1

Although the controllers may be able to overcome the bias, it would require substantial changes in manipulated variable levels. These changes will most likely push both P_S and T_{E1} out of normal operating conditions. Therefore the assumption is made that the bias was caused by vitamin and oils additions specific to each recipe used. This allows one to find and remove a constant bias per recipe. As such the controller is allowed to rectify only process deviations and not overcome unrealistic errors that will not be seen in practice. Note on Figure 8-41 that the process reacts identically to external stimuli, except for the bias. This implies that the process has linear gains over normal operating regions and removing the bias should not influence system dynamics.

The biases were calculated for each recipe by taking the average of the difference between the model output and the historical data values, with the result shown below:

Table 8-20: Recipe output variable biases

	W_P	Unit	T_{E1}	Unit
Recipe 1	-0.01	Fraction dry mass	-3.64	°C
Recipe 2	-1.48	Fraction dry mass	0.57	°C
Recipe 6	0.08	Fraction dry mass	7.5	°C
Recipe 9	-0.06	Fraction dry mass	4.36	°C

8.12.2 Control of validation data sets: recipe 1

Two methods of comparison will be used. Firstly F_1 will be treated as a disturbance variable to simulate the situation where production rates are controlled by operators. Secondly F_1 will be fixed at 90% of the maximum flow seen in historical data, i.e. 11 200 kg/h which was 400 kg/h more than the average feed flow rate over all the recipes. The set points were chosen as 0.55 product dry mass fraction and a first effect temperature of 68°C.

Operator comparison: historical data set 10_1

The disturbance variables, including feed flow, were read from historical data set 10_1. Note that sensor noise was still added although process noise was neglected to ensure only the historical variance acts on the system. The constant set point tracking is shown below:

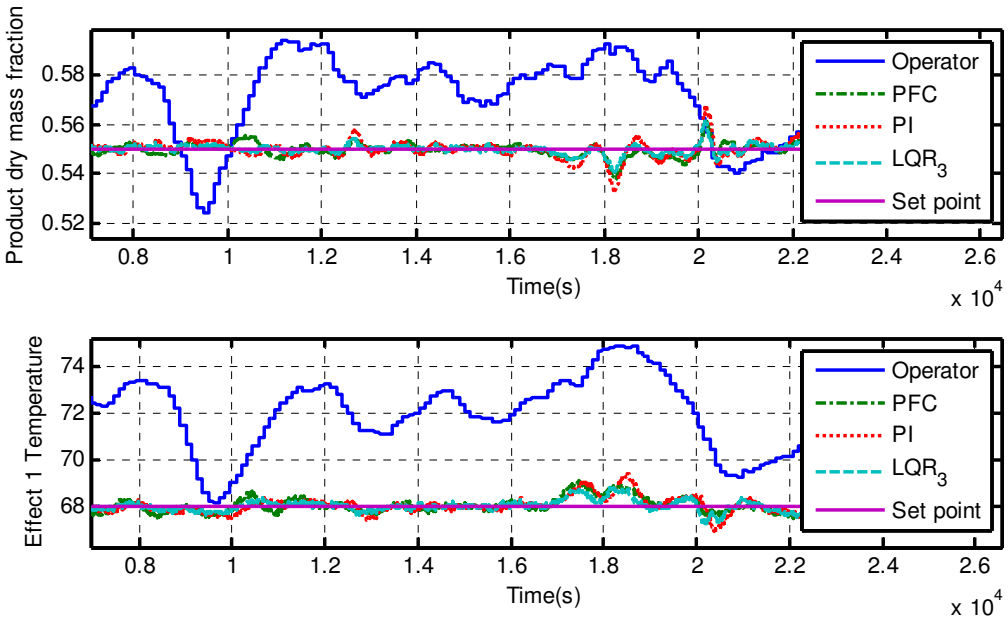

Figure 8-42: Comparison of designed controllers and operator control, Recipe 1 validation set 10_1

Note the drastic reduction of variance in both W_P and T_{E1} for all forms of designed control when compared to operator control. In addition to the visual comparison, the performance factors for each controller were also calculated as shown in Table 8-21 below:

Table 8-21: Overall controller comparison using historic disturbances from set 10_1

Control type	MSE		IAE		Standard deviation		Max deviation	
	W_P	T_{E1}	W_P	T_{E1}	W_P	T_{E1}	W_P	T_{E1}
Operator	1.7E-07	2.62	365	34068	0.017	1.62	0.04	3.40
PFC	2.2E-10	0.08	44	5185	0.002	0.28	0.01	1.10
PI	8.4E-10	0.10	48	5178	0.003	0.31	0.02	1.40
LQR_3	9.9E-11	0.05	27	3652	0.002	0.21	0.01	0.80

Note that the MSE, IAE and max deviation values for operator control were calculated by assuming that the set point for each control variable lay at the average value of the output for that data set. While this may not be the case, it should still give a ball park figure for operator control. It should also be noted that the calculated standard deviation value is directly comparable to other control methods if one assumes that the operators maintained a constant set point.

With these assumptions taken into account, Table 8-21 again emphasizes what was seen in Figure 8-42. Namely, that the operator control is far worse than the next worst performing controller (PI), with standard deviations 500% higher. The same great difference is seen in max deviations, with operator control again exceeding the values of all the designed controllers.

As T_{E2} was not treated as a manipulated variable, it was decided to compare LQR_3 T_{E2} use against the condenser pressure (P_C) of the historical data. Even though this comparison will not give information to the levels of the manipulated variables, it may still give insight to the difference in controller strategy:

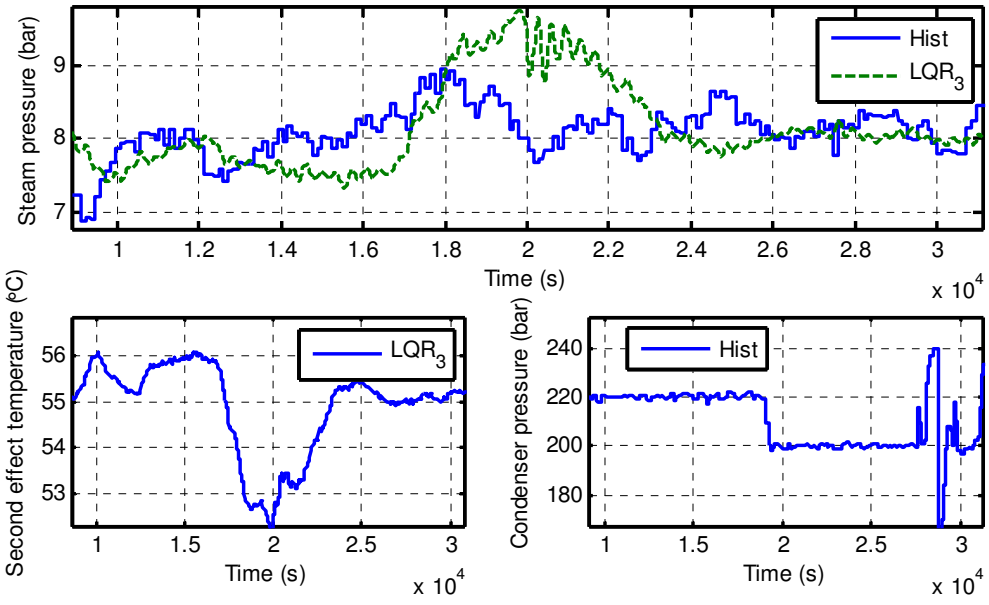

Figure 8-43: Comparison of manipulated variable use between operator and LQR_3 control for set 10_1

The most apparent difference seen in Figure 8-43 is that the current operator was very conservative with respect to condenser action. Whereas the LQR_3 controller made various T_{E2} adjustments (which imply a P_C change) the operators kept P_C almost completely constant.

It is very interesting to observe that P_C was dropped by the operators at ±18 000s, which corresponds to the LQR3 T_{E2} drop at ±17 000s. Therefore the operators took the same remedying action, only much later. This leads one to suspect that the operator control was hampered by speed at which rectifying decisions were made as well as highlight the predictive capabilities of LQR_3.

Operator comparison: historical data set 12_1

A second validation set for recipe 1 data, set 12_1, was also investigated with the results shown below in Figure 8-44:

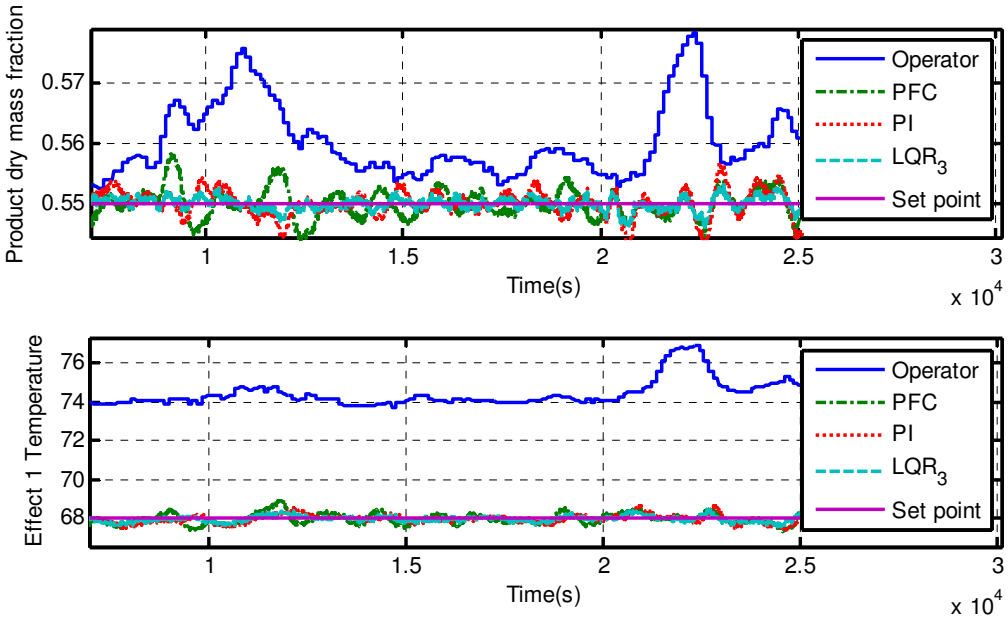

Figure 8-44: Comparison of designed controllers and operator control, Recipe 1 validation set 12_1

Figure 8-44 highlights an interesting scenario. The product dry mass fractions of operator control is fairly close to that of the designed controllers, while the first effect temperatures differ greatly. This implies that the operators are running the process at conditions away from the optimal, i.e. over or under utilisation of manipulated variables. The calculated performance factors are shown below in Table 8-22:

Table 8-22: Overall controller comparison using historic disturbances from set 12_1

Control type	MSE		IAE		Standard deviation		Max deviation	
	W_P	T_{E1}	W_P	T_{E1}	W_P	T_{E1}	W_P	T_{E1}
Operator	3.9E-09	0.37	99	10602	0.005	0.61	0.02	2.47
PFC	9.0E-11	0.07	44	5562	0.002	0.27	0.01	0.98
PI	6.3E-11	0.05	40	4328	0.002	0.21	0.01	0.65
LQR_3	3.6E-12	0.02	20	3064	0.001	0.15	0.00	0.48

LQR_3 again provided the best performance variables, with the lowest IAE, MSE, standard deviation and max deviation values. For set 12_1 PI control however outperformed PFC in all the calculated performance criteria.

To investigate why the PFC performed the worst, as well as to determine why the operator control showed high T_{E1} values, both the condenser and steam pressures were compared in Figure 8-45 below:

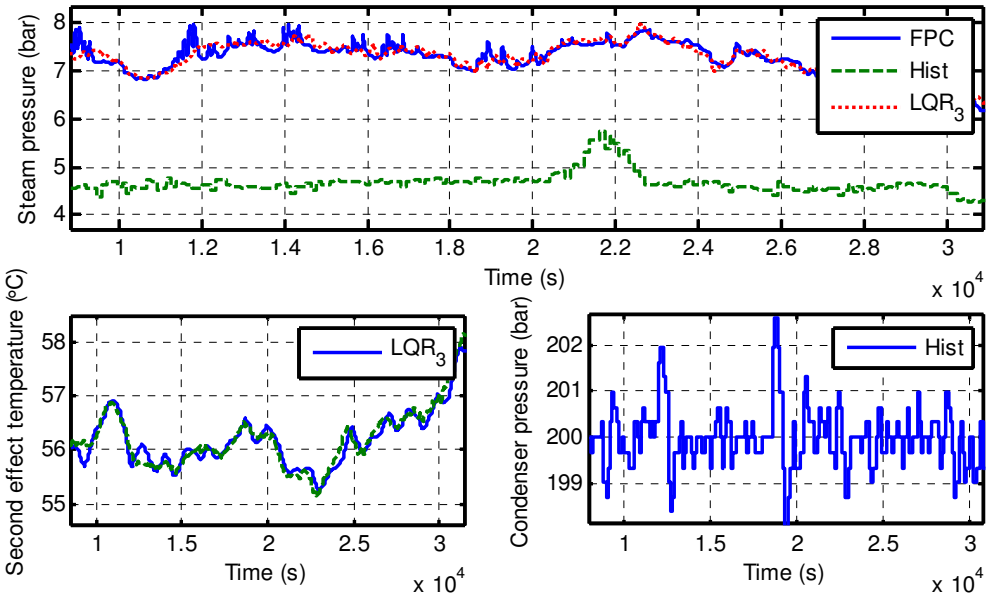

Figure 8-45: Comparison of manipulated variable use between operator and LQR_3 control for set 12_1

Firstly, from Figure 8-45 it is clear that the operators used very low steam pressure while keeping P_C constant. All the variance in P_C may be accounted for by normal process and sensor noise. Furthermore, compared to Figure 8-43, one can safely deduce that no control was performed on P_C. If the operators were to raise P_S and lower P_C it would also be possible to maintain W_P at ±0.55 dry mass fraction while restricting T_{E1} to below 70°C.

Secondly, Figure 8-45 shows that the PFC manipulated variable use is extremely close to that of LQR_3 even though the performance factors varied significantly. The one difference is seen as small spikes on P_S for PFC. Closer inspection revealed that these spikes are as a result of the predictive fuzzy rules. This is also seen by comparing P_S to T_{E2} on Figure 8-45 – no spikes are observed for T_{E2} as T_{E2} had no predictive rules influencing it. Even though the PFC already filters the inputs, future versions may have to also filter predictive outputs to remove the spikes seen.

8.12.3 Control of validation data sets: recipe 2

The same procedure that was followed for recipe 1 comparisons, was again employed for recipe 2. With the inspection of the historical data done in Section 3.2, the dry mass set point of W_P for recipe 2 was determined to be a dry mass fraction of 0.50.

The biases, of Section 8.12.1, were added to the other recipes to ensure that the controller made the correct use of manipulated variables. For recipe 2, the historical product dry mass fraction was over 2, which implied that each 1kg of concentrated milk contained 2kg solids – clearly impossible. Therefore, as mentioned earlier, the recipe 2 W_P was treated as a sensor anomaly and the W_P bias subtracted from the historical data (instead of being added to the model outputs). The T_{E1} bias did, however, fall well within reason, at 0.57°C, and was added to the model output as before.

Operator comparison: historical data set 03_1

The only validation set used for recipe 2 was set 03_1. The results of both W_P and T_{E1} set point tracking are shown below:

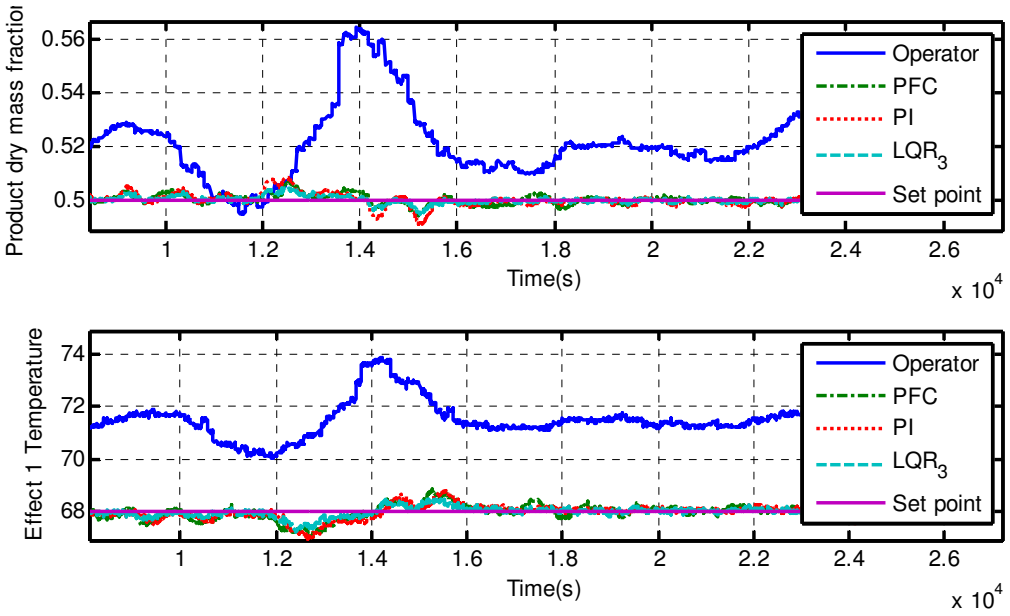

Figure 8-46: Comparison between designed controllers and operator control, Recipe 1 validation set 03_1

From Figure 8-46, one can again observe the drastically decreased deviation seen in both W_P and T_{E1} for all the designed controllers. Operator control showed a large W_P increase at ±13 000s which none of the designed controllers emulated. The designed controllers all performed relatively well, with no clear distinction made between the three methods, except for PI control which showed slightly greater deviations during the time period from 12 000s to 16 00s for both W_P and T_{E1}.

The numerical performance parameters are shown below in Table 8-23 below to offer a more in-depth comparison of the designed controllers:

Table 8-23: Overall controller comparison using historic disturbances from set 03_1

	MSE		IAE		Standard deviation		Max deviation	
	W_P	T_{E1}	W_P	T_{E1}	W_P	T_{E1}	W_P	T_{E1}
Operator	1.10E-07	0.33	215	9195	0.012	0.58	0.04	2.31
PFC	3.60E-11	0.06	30	4371	0.002	0.25	0.01	0.99
PI	1.60E-10	0.06	36	4142	0.002	0.24	0.01	1.03
LQR_3	1.40E-11	0.03	22	2912	0.001	0.17	0.01	0.79

The decreased standard deviation of both control variables from operator to designed controllers is dramatic once again. A decrease of 600% was seen for W_P standard deviation, while T_{E1} saw a decrease of 232% when compared to the worst performing designed controller, i.e. FPC. Although it showed higher standard deviations than PI or LQR_3 controllers, PI control showed the largest W_P maximum deviation as well as MSE and IAE values. This reflects the poor PI performance seen in Figure 8-46. To investigate the controller deviations seen between 12 000s and 16 000s on Figure 8-46 the manipulated variables were compared:

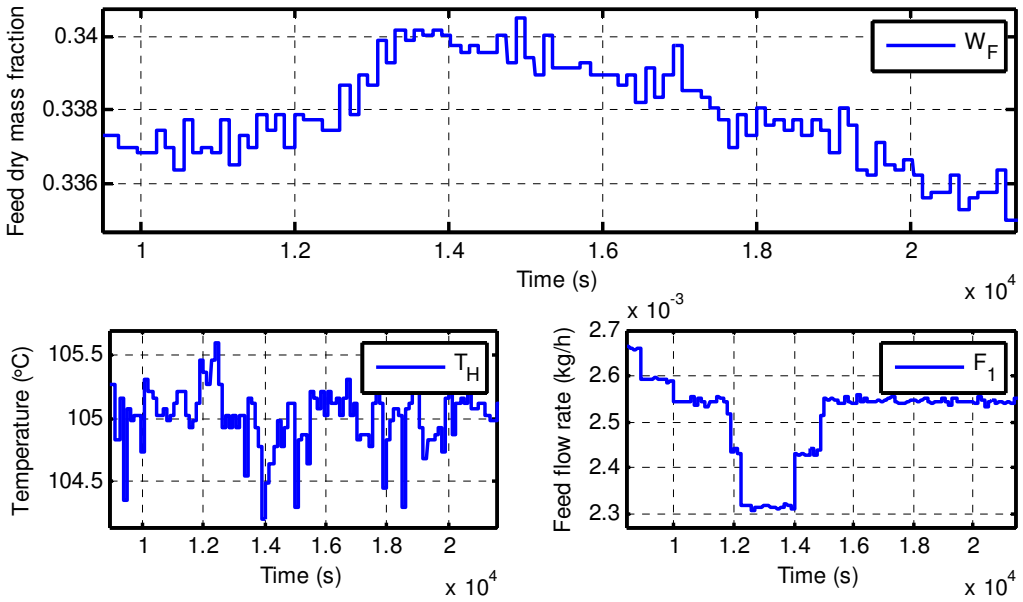

Figure 8-47: Disturbance inputs for historical set 03_1

Figure 8-47 proves very interesting, especially when comparing F_1 and W_F. The operator reduced F_1 at ±12 200s, while a W_F increase was seen at 12 500s. Both of these variables will cause W_P to increase, which led to the large increase seen in Figure 8-46. The ideal action would have been to decrease P_S and increase F_1, thereby immediately reducing the energy available for evaporation while also increasing the required amount of water to be evaporated. These actions would then negate W_F increase. The designed controller manipulated variable use is shown below:

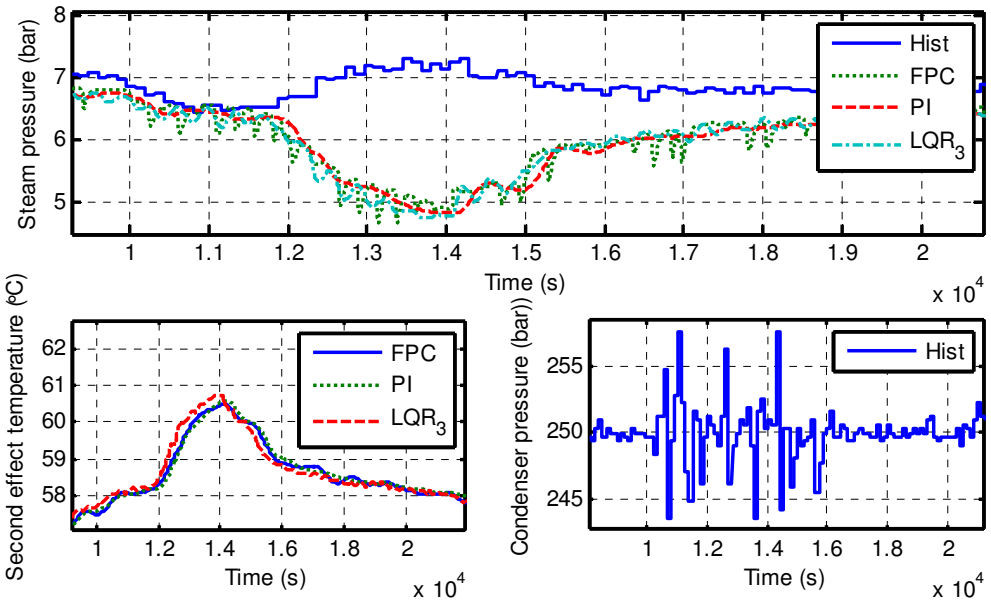

Figure 8-48: Comparison of manipulated variable use between operator and LQR$_3$ control for historical set 03_1

Note from Figure 8-48 that all of the designed controllers performed the reduction of P_S while the operators in reality increased P_S. Also note that the designed controllers increased T_{E2} to cause an increase in T_{E1}, which would negate the T_{E1} drop from decreased PS.

8.12.4 Control of validation data sets: recipe 6

Recipe also had a low W_P set point, determined in 3.2, i.e. a product dry mass fraction of 0.51. As the sensors showed no large offset, as seen for recipe 2, the bias was again added to the model output.

Operator comparison: historical data set 05_1

The only validation set used for recipe 6 was set 05_1. The results of both W_P and T_{E1} set point tracking are shown below in Figure 8-49:

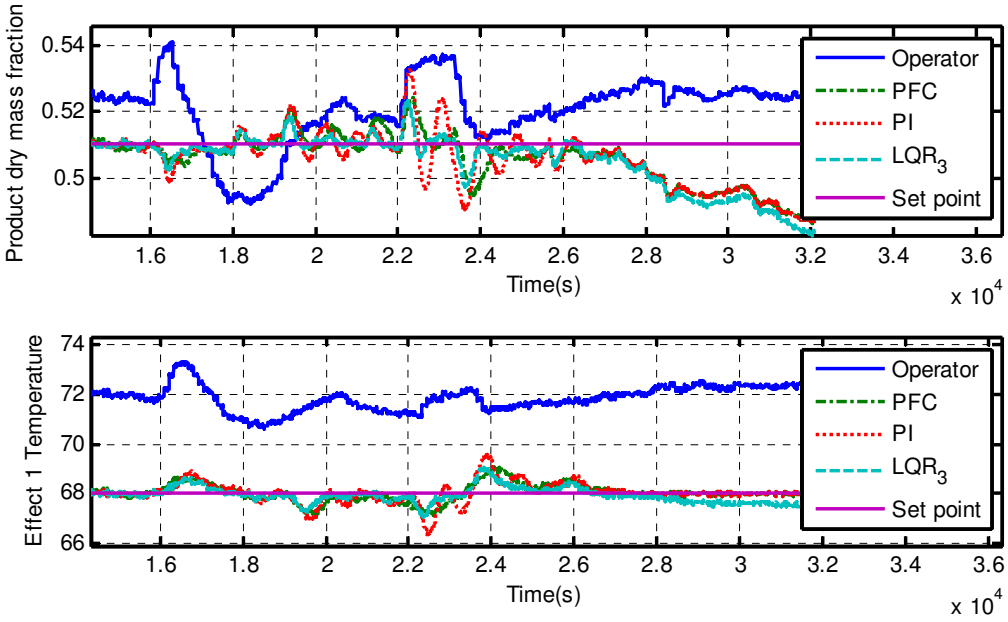

Figure 8-49: Comparison between designed controllers and operator control, Recipe 1 validation set 05_1

As seen above, the designed controllers perform well up until 26 000s, with the only exception being some oscillations seen in PI control around 23 000s. As 26 000s the designed controllers start hitting P_S saturation limits (at 10bar) and as such the W_P control quickly deteriorates. T_{E1} is still kept fairly close to its set point as T_{E2} was still not at saturation limits.

There are two solutions to ensure that the controller does not reach saturation. One option is to increase T_{E1}, the increased temperature allows for greater evaporation. Alternatively one can limit the feed flow rate (F_1) allowing the evaporator to maintain the same temperature and meeting the required product dry mass fraction, yet reducing the production rate. As temperatures at or above 70°C cause excessive fouling, which will reduce the available time of the evaporator, it was decided to rather decrease the flow rate to a conservative 10 000kg/h while also increasing the T_{E1} set point to 69°C:

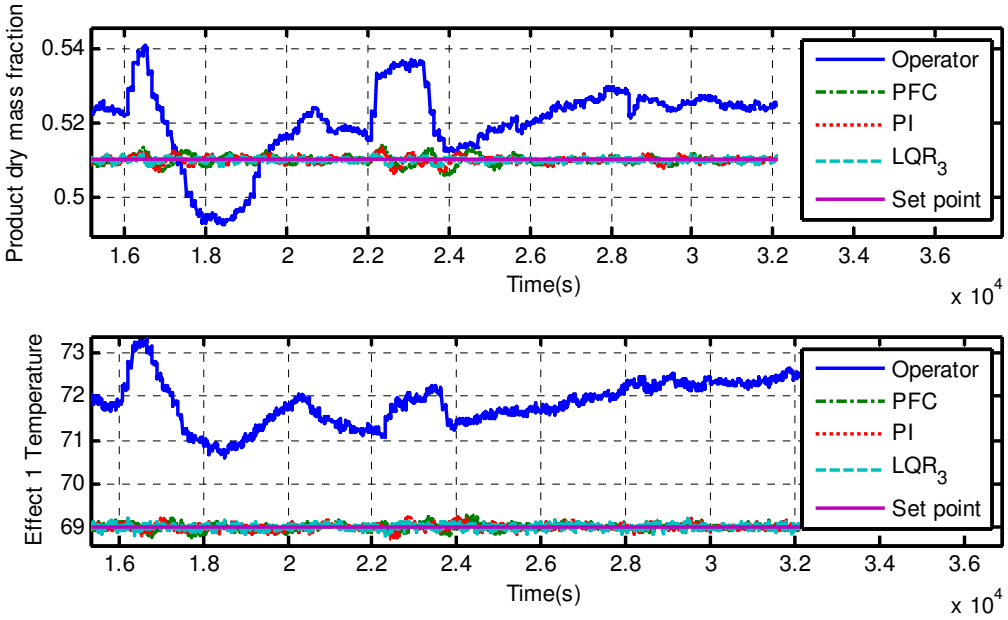

Figure 8-50: Comparison between designed controllers and operator control, validation set 05_1, manual feed flow

From Figure 8-50, it is clear that lowering F_1 allowed the controller to maintain both W_P and T_{E1} at the respective desired set points without P_S saturation. Note also that T_{E1} never rises above 70°C and that the deviation is seen at 22 000s is a lot less pronounced, which implies that the deviation was exaggerated because of operator changes.

The lower F_1 flow rate of 10 000kg/h is a significant decrease, but ensuring the FFE does not foul will increase process run time and minimise costly cleaning cycles. Additionally this validation set proves that operator selection of feed flow rate is inadequate, further justifying the development of the feed flow optimiser (Section 8.10) which will be evaluated in Section 8.13.

Table 8-24: Overall controller comparison using historic disturbances from set 05_1

	MSE		IAE		STD		Max deviation	
	W_P	T_{E1}	W_P	T_{E1}	W_P	T_{E1}	W_P	T_{E1}
Operator	3.50E-08	0.295	214	11340	0.011	0.54	0.027	1.43
PFC	5.40E-12	0.005	19	1354	0.001	0.07	0.005	0.27
PI	2.60E-12	0.005	17	1348	0.001	0.07	0.004	0.27
LQR3	3.00E-13	0.004	11	1181	0.001	0.06	0.002	0.23

Table 8-24 above shows that LQR_3 control consistently outperformed both PFC and PI control, which showed almost identical performance to each other. Furthermore, the standard deviations seen are a lot smaller than for previous recipes, which again implies that excessive operator F_1 changes are hampering the designed controllers.

Lastly the manipulated variable use was also investigated:

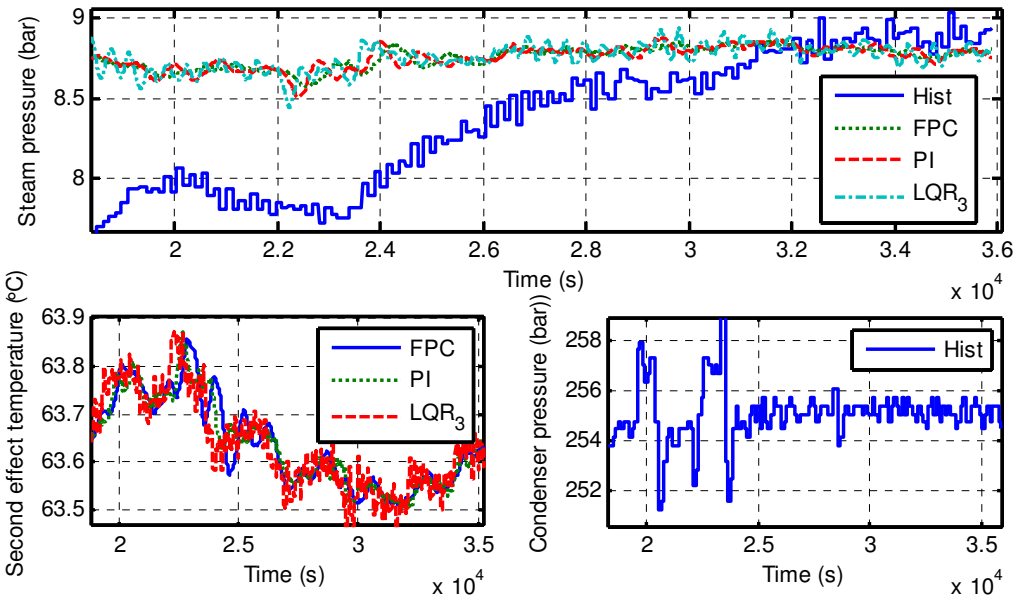

Figure 8-51: Comparison of manipulated variable use between operator and LQR_3 control for set 05_1

Figure 8-51 above, shows that with a constant feed flow rate it is possible to keep all process variables relatively constant. P_S is also far away from saturation, implying that there is unused evaporative capacity and the conservative 10 000kg/h feed flow can be increased.

8.12.5 Control of validation data sets: recipe 9

Recipe also had the highest W_P set point, determined in 3.2, i.e. a product dry mass fraction of 0.62. The modelling bias calculated was fairly large and therefore included in the simulation.

Operator comparison: historical set 06_1

As with recipe 6, the validation data set disturbances resulted in controller saturation. Instead of the limiting F_1 approach followed earlier, it was decided to increase T_{E1} until stable operation was observed:

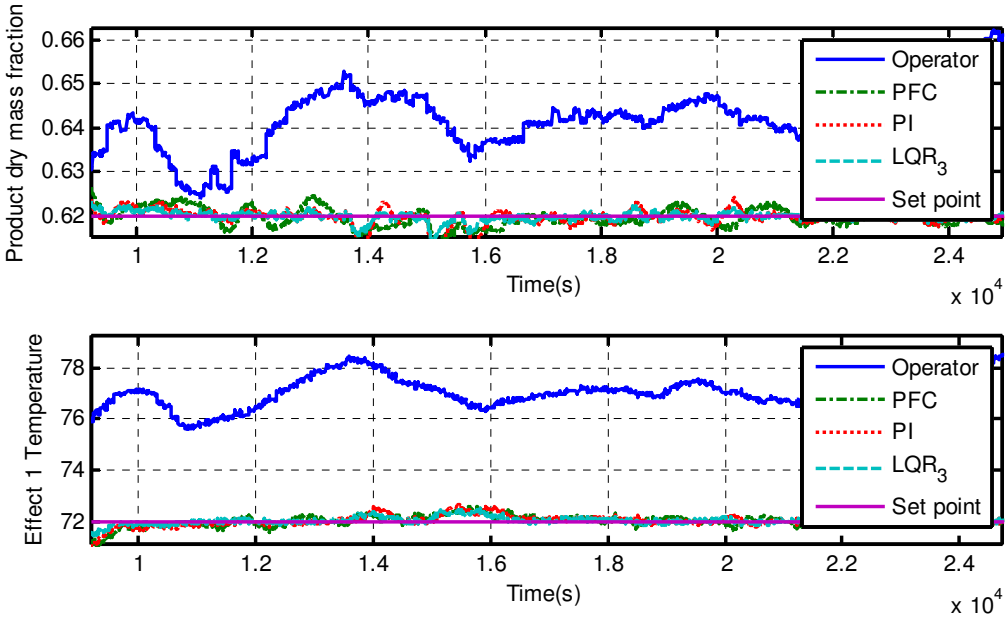

Figure 8-52: Comparison between designed controllers and operator control, Recipe 1 validation set 06_1

Increasing T_{E1}, to 72°C which is still lower than the historical values, also resulted in stable control action while achieving the W_P set point. The designed controllers still show better performance than operator control. The calculated parameters are shown in Table 8-25 below:

Table 8-25: Overall controller comparison using historic disturbances from set 06_1

	MSE		IAE		Standard deviation		Max deviation	
	W_P	T_{E1}	W_P	T_{E1}	W_P	T_{E1}	W_P	T_{E1}
Operator	6.30E-08	0.731	185	14341	0.01	0.85	0.042	4.26
PFC	1.70E-10	0.04	44	3552	0.002	0.2	0.011	0.97
PI	1.70E-10	0.037	32	3082	0.002	0.19	0.012	0.96
LQR_3	2.10E-11	0.018	20	2268	0.001	0.13	0.007	0.69

For recipe 9 PI control again outperformed FPC, with LQR_3 control continuing to show the best overall performance.

To circumvent the saturation problems without adjusting the T_{E1} setup, thereby minimising fouling, the controllers will only be run through all the validation data sets once the fuzzy feed optimiser has been tested and implemented in Section 8.13.

8.13 Fuzzy feed optimiser comparison

The previous section confirmed that feed flow plays an important role in FFE control. If F_1 is changed too dramatically, large control variable deviations are observed, while incorrect F_1 flow rates cause controller saturation. The fuzzy optimiser developed in Section 8.10 evaluates both W_F and P_S to determine the optimum feed flow rate. This optimum is defined as the feed flow rate that results in stable, yet high, use of P_S within the saturation limits.

To ease optimiser comparison, only LQR_3 control will be used. One instance of the controller will have the optimiser enabled (LQR_{3O}), the other will use a constant F_1 set point (LQR_{3C}) and finally the last operator F_1 historical values (LQR_3). From the previous section it can be concluded that the controllers all perform similarly and therefore if the fuzzy optimiser is sufficient for LQR_3, it will be sufficient for the other methods as well.

8.13.1 Optimiser comparison for historical data set 05_1 (recipe 6)

This historical set disturbances caused controller saturation as described in Section 8.12.4. The controller comparison is shown below in Figure 8-53:

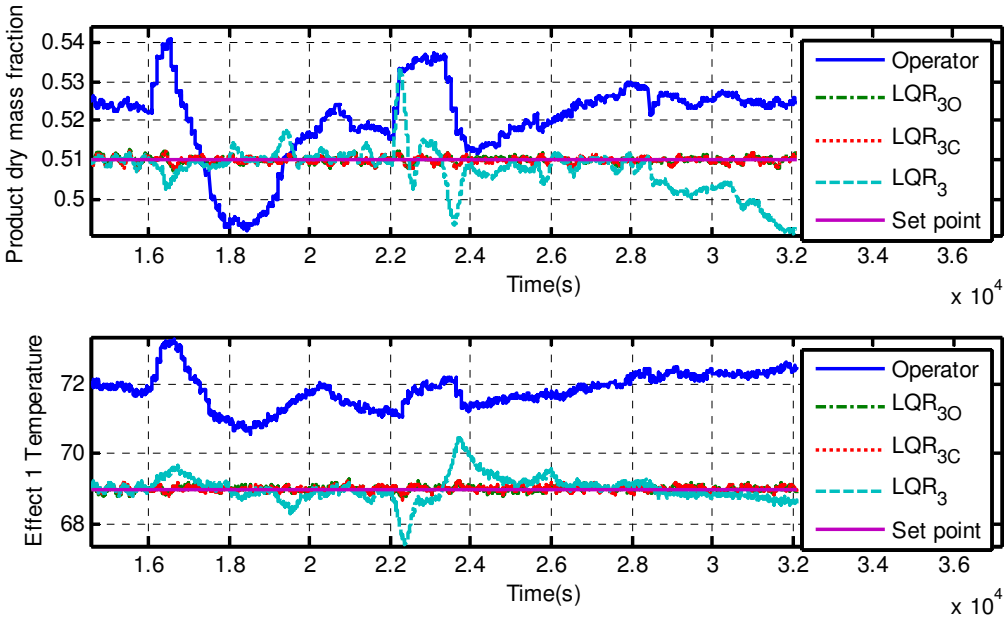

Figure 8-53: Fuzzy feed optimiser LQR controller comparison on historical set 05_1

As seen previously, the LQR_3 controller subjected to operator F_1 control hit saturation limits and could not follow the set points past 26 000s for W_P and 30 000s for T_{E1}. Additionally under these conditions the LQR controller showed the largest deviations and greatest error. Although it cannot easily be distinguished on Figure 8-53, LQR_{3O} and LQR_{3C} performed identically, with LQR_{3O} showing a slightly increased F_1:

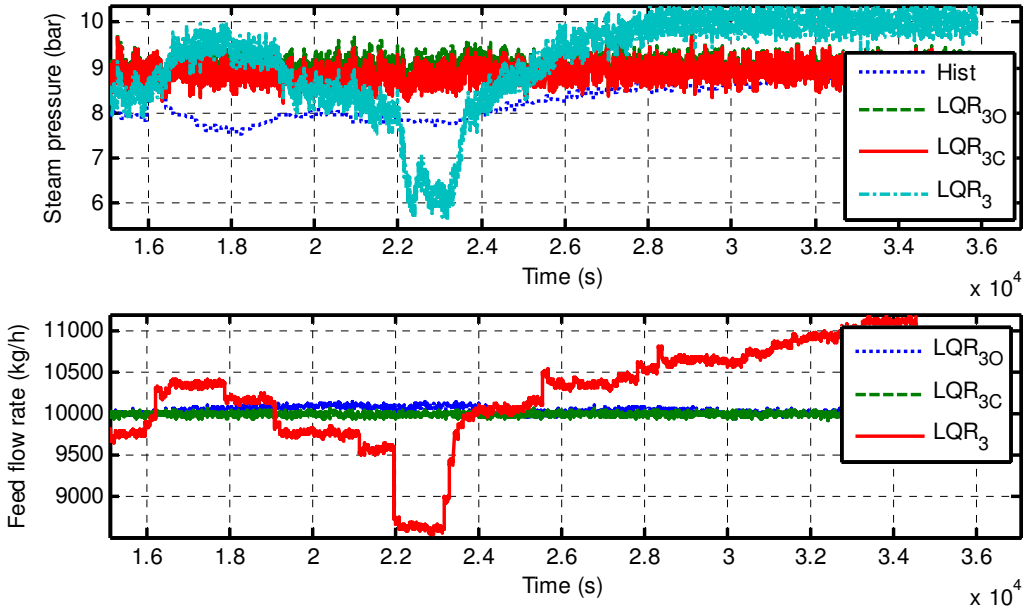

Figure 8-54: Optimiser feed flow rate and steam use comparison, historical set 05_1

On Figure 8-54 it is seen that LQR_3 control reaches the upper saturation point for P_S fairly often while P_S for LQR_{3O} is on average 0.2bar higher than LQR_{3C}. Furthermore the optimiser kept F_1 very constant and 50kg/h higher than the chosen constant flow rate. The feed consumption and evaporation rate for the time period shown on Figure 8-54 was calculated with the results shown below:

Table 8-26: Evaporation and feed flow comparison with feed optimiser, historical set 05_1

Type of F_1 control	Average FFE evaporation variables					
	Evaporated flow		Feed flow		Steam pressure	
Historic values	3 567	(kg/h)	10 126	(kg/h)	8.19	(bar)
Optimiser (LQR_{3O})	3 665	(kg/h)	10 054	(kg/h)	9.01	(bar)
Constant (LQR_{3C})	3 522	(kg/h)	10 000	(kg/h)	8.89	(bar)
Operator (LQR_3)	3 567	(kg/h)	10 126	(kg/h)	8.99	(bar)

From Table 8-26 above, it is seen that under operator feed flow management no advantage was gained in terms of average evaporated flow when using LQR control (yet some improvement seen on W_P set point tracking as shown in Figure 8-53). The constant F_1 flow rate allowed the controller to follow the control variables set point, although at the cost of 45kg/h reduction in evaporation rate. Finally under the fuzzy optimiser the LQR solution could provide a 98kg/h evaporation rate increase while still following given set points. It should be noted that the average F_1 flow rate did decrease by 72kg/h, but that P_S averaged 0.82bar higher (compared to operator management), which points to a more effective use of steam especially compared to LQR_3.

8.13.2 Optimiser comparison for historical data set 06_1 (recipe 9)

LQR_{3O} did provide a substantial benefit to LQR_{3C}, as seen in the previous section. It is, however, possible for the argument to be made that with proper constant F_1 selection the same improvements may be seen. The advantage of the optimiser is that it can dynamically find this optimum F_1 flow rate when process conditions change; refer back to the W_F disturbance in Section 8.10. This means that even though the final F_1 flow rate might be similar, the optimiser can reach this without the operators needing to constantly estimate the correct flow rate.

To show this dynamic optimisation the second historical set that introduced controller saturation is investigated, i.e. set 06_1. In contrast to Section 8.12.5 the T_{E1} set point will not be adjusted, but a constant feed flow rate of 10 000kg/h and optimiser feed flow rate used:

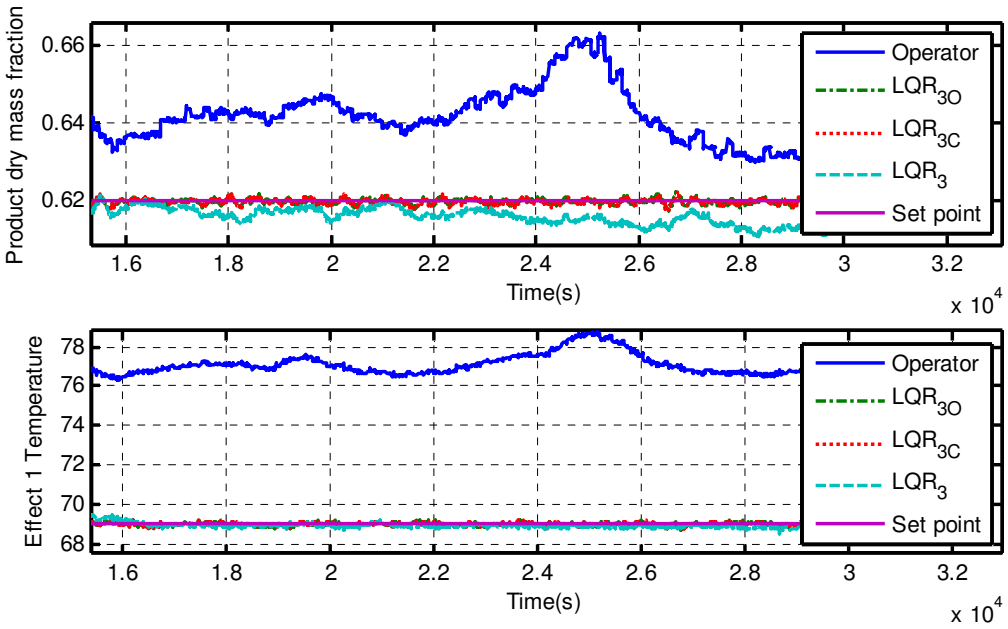

Figure 8-55: Fuzzy feed optimiser LQR controller comparison on historical set 05_1

The effect of P_S saturation for LQR_3 is clear from Figure 8-55 above with the controller unable to reach the desired W_P set point. In essence the FFE controller was over-constrained by specifying both a low T_{E1} and high W_P set point while also requiring a high feed flow rate. The optimiser again successfully removed this over burdening of the controller by ensuring the FFE always operates close to maximum capacity (P_S of ± 9bar). To judge whether the optimiser provided better performance than the constant selected F_1 flow rate the evaporation rates were again calculated:

Table 8-27: Evaporation and feed flow comparison with feed optimiser, historical set 05_1

Type of F_1 control	Average FFE evaporation variables					
	Evaporated flow		Feed flow		Steam pressure	
Historic values	5 163	(kg/h)	11 501	(kg/h)	9.23	(bar)
Optimiser (LQR_{3O})	5 042	(kg/h)	10 807	(kg/h)	9.01	(bar)
Constant (LQR_{3C})	4 490	(kg/h)	10 000	(kg/h)	7.50	(bar)
Operator (LQR_3)	5 163	(kg/h)	11 501	(kg/h)	10.00	(bar)

Table 8-27 again shows that LQR_3 control caused P_S saturation (at 10bar), while the optimiser kept P_S close to the maximum (at 9bar) and the constant F_1 flow rate underutilised P_S (at 7.5bar). Even though the evaporation rate and feed flow rate was significantly lower than for operator control, LQR_{3O} did manage to follow the desired set points and outperform LQR_{3C} by a large margin.

Therefore it can be concluded that the fuzzy feed optimiser is a good alternative to keeping the feed rate constant or increasing the T_{E1} set point. The optimiser allows the controller to minimise fouling by adhering to T_{E1} set point while maximising FFE throughput.

8.13.3 Optimiser feed flow advantage

The final comparison for the fuzzy optimiser investigated the advantage delivered in terms of throughput for data sets where the manipulated variables were not saturated due to process restrictions or operator feed flows. The comparison was done with recipe 1 historical data set 10_1.

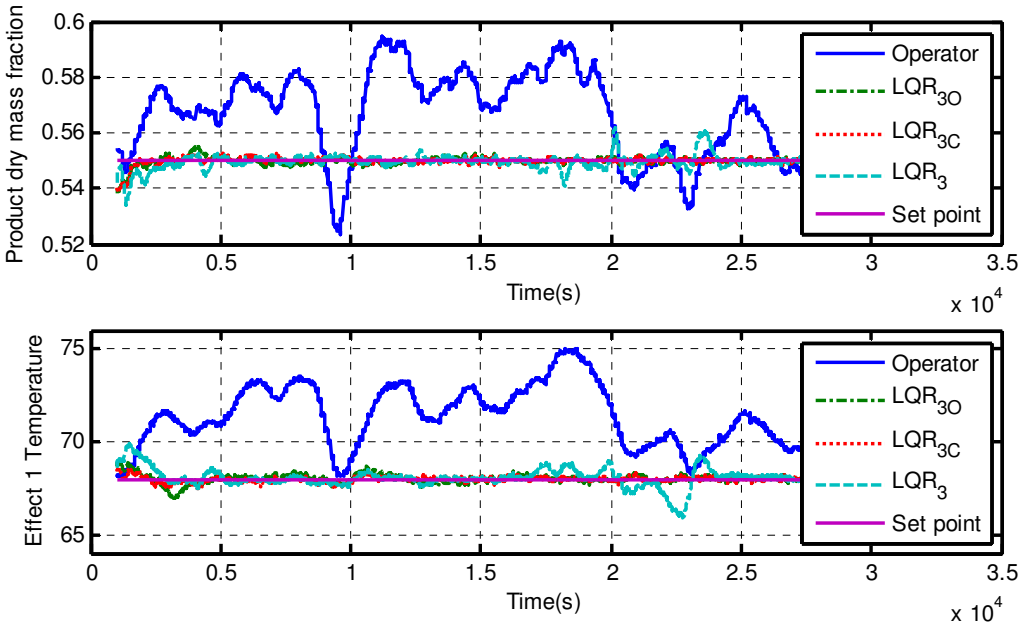

Figure 8-56: Fuzzy feed flow optimiser compared to other operator and constant feed flows

From Figure 8-56, it can be seen that both the constant and fuzzy feed optimiser LQR controllers perform well with identical zero offset following and negligible output variable deviations. The achieved feed flows for each method is compared below (note that the same constant feed flow rate used previously was again employed):

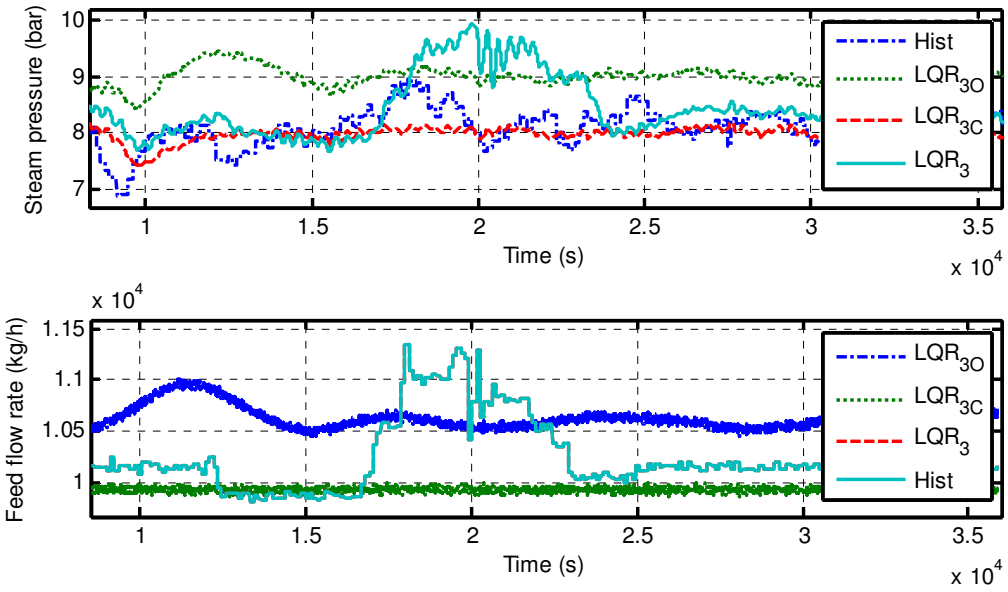

Figure 8-57: Optimiser feed flow rate and steam use comparison, historical set 10_1

Note that the steam pressure noise was omitted when drawing Figure 8-57 to ease comparison. Figure 8-57 clearly shows that, while both LQR_{3C} and LQR_{3O} performed identically in terms of set point tracking, there was a large difference in the amount of feed processed. The average evaporation rates as well as feed flow rates are shown below in Table 8-28 :

Table 8-28: Evaporation and feed flow comparison with feed optimiser, historical set 10_1

Type of F_1 control	**Average FFE evaporation variables**					
	Evaporated flow		Feed flow		Steam pressure	
Historic values	3 682	(kg/h)	10 252	(kg/h)	8.15	(bar)
Optimiser (LQR_{3O})	3 978	(kg/h)	10 634	(kg/h)	9.02	(bar)
Constant (LQR_{3C})	3 568	(kg/h)	9 936	(kg/h)	7.98	(bar)
Operator (LQR_3)	3 682	(kg/h)	10 252	(kg/h)	8.45	(bar)

By using the fuzzy feed optimiser, feed flow was increased by 382kg/h over that of the operator, while the evaporation rate increased by 296kg/h. The other significant improvement of the fuzzy feed optimiser was the ability of the controller to still follow the set points with precision, thereby reducing fouling and increasing the production rate.

8.13.4 Aggregated validation set controller results

When comparing the controllers in Section 8.12, a lot of manipulated variable saturation was observed. As the overall controller performance on validation data would have been severely hampered by this saturation, the fuzzy feed optimiser was used to prevent saturation. This allows one to only compare the controller performance without the time consuming feed flow rate or T_{E1} set point selection process.

Table 8-29: Comparison of controller performance on validation data using fuzzy feed optimiser

	MSE		IAE		Standard deviation		Max deviation	
	W_P	T_{E1}	W_P	T_{E1}	W_P	T_{E1}	W_P	T_{E1}
Operator	9.6E-08	0.876	197	14690	0.010	0.75	0.036	2.31
PFC_O	1.6E-11	0.019	31	2639	0.002	0.14	0.005	0.53
PI_O	1.1E-11	0.012	25	2142	0.001	0.11	0.005	0.41
LQR_{3O}	1.7E-12	0.009	17	1823	0.001	0.09	0.003	0.35

All the validation sets except historical data set 10_1 performed without error. For historical data set 10_1 the predictive fuzzy controller condenser function was saturated. As such this data set results were left out the final comparison. As this was only a single case of saturation it will be treated as an outlier not indicative of the respective controllers.

From Table 8-29 one can see that, as throughout Section 8.12, the PI_O controller outperformed the PFC_O. In reality each and every performance metric was worse for PFC_O, except the maximum deviation of W_P which was the same as the PI_O controller. Furthermore, it should be noted that the LQR_{3O} again performed the best, with the lowest error and deviation values. For both control variables the LQR_{3O} controller reduced the standard deviation by an order of magnitude, the same being true for max deviation, MSE and IAE values.

8.14 Controller conclusions

The controller selection, development and comparison formed the core of the current work and as such the controller conclusions will be made as part of the overall conclusions presented in the following chapter.

Chapter 9 - Conclusions

The hypothesis of Chapter 1 was three fold, and stated that a controller could be developed that improved on operator control, increased production rate and maintained product quality and safety specifications. These three elements will be treated as the key measures of success for the designed controllers.

As it was not possible to gain access to the actual local FFE plant, a model needed to be created to simulate the process adequately. Without this model the controllers could possibly still be designed, especially fuzzy control which does not require any process model, yet a multitude of assumptions would need to be made. Additionally, there would be no way of testing and comparing the controllers which would leave the hypothesis mute. Therefore, even though the model was not included in the hypothesis, it is as integral to testing the hypothesis as the controller designs are.

9.1 Semi-empirical modelling conclusions

The semi-empirical model development methodology was inherently iterative. At first many assumptions were made to produce the simplest possible model, which was gradually improved upon until the model represented the structure of the local FFE as well as the data. Each iteration of the model will be concluded in this section.

9.1.1 First approximation model

The simplest model created assumed that both TVR and condenser actions were constant, no flashing occurred and the homogeniser was treated as an extra pass. Although these assumptions were very restrictive, the approximation model acted as a proof of concept, with the model responding according to process logic when the assumptions were included in the reasoning. The correlation of both W_P and T_{E1} were very low at -0.14 and -0.002.

9.1.2 First revision model

The first revision model added dynamic formulation of both the TVR and condenser actions. In addition flashing and variable milk density were added. The correlation to historical data increased dramatically with W_P and T_{E1} values rising to 0.788 and 0.809 respectively. This revision model validated the proof of concept that the approximation model showed.

9.1.3 Second revision model

Before any tuning could be performed, the internal model structure had to be altered to reflect the local FFE. This included modelling the homogeniser as a recycle and adding inventory tanks to both evaporators. The correlation of W_P and T_{E1} improved slightly to 0.80 and 0.81 respectively. The increase indicated that although the new structure is more realistic, the earlier assumptions were valid.

9.1.4 Tuned semi-empirical model

The second revision model may possibly already represent the local FFE well enough. Yet certain parameter influences were not understood, i.e. heat transfer coefficients, recycle ratio and thermal inertia. It was found that both heat transfer coefficients and the recycle ratio influenced model bias, with the final values chosen at 325 W/m^2.°C and 1 800 W/m^2.°C for effect 1 and effect 2 heat transfer

coefficients. A recycle ratio of 0.1 (fluid fraction fed back from first effect product to feed) was chosen as well as a thermal mass for both effects of 2x106 J/°C.

The tuned semi-empirical model showed very high correlation values of 0.84 and 0.83 for W_P and T_{E1} respectively. Although other data sets were also used for training, data set 09_2 provided a lot of process deviation and proved suitable as central training set.

9.1.5 Semi-empirical model on different data sets

Once the training and tuning was complete, the tuned semi-empirical model was run on all of the training and validation data sets. The results were surprising, as recipe 1 training data sets showed low correlation of 0.32 and 0.62 for W_P and T_{E1} correlation. Inspection showed that two of the data sets showed very low correlation values, yet that the model still represented most of the process dynamics well. This also casts doubt on the use of correlation for comparison. Recipe 2, recipe 6 and recipe 9 all showed high W_P and T_{E1} correlations with the lowest W_P correlation at 0.69 and the lowest T_{E1} correlation at 0.6. This proved that the model was indeed applicable to different data sets and further strengthened the notion of outlier sets for recipe 1.

Validation data saw a rise in W_P and T_{E1} correlation for recipe 1 data, to 0.38 and 0.75 respectively. Recipe 6 showed correlations of 0.74 and 0.79 for W_P and T_{E1}, while recipe 2 reported values of 0.27 and 0.63, with recipe 9 showing correlations of 0.45 and 0.79. Graphical representation of the validation data sets also showed good correlation between the model and historical data.

The semi-empirical model proved very effective at predicting both W_P and T_{E1} trends for both training and validation data sets and was therefore judged to be suitable for control simulations.

9.2 Data based modelling conclusions

As stated previously, the data based models served a dual purpose. Firstly, to establish a meaningful standard to measure the semi-empirical model against and secondly, offering a simulation alternative to semi-empirical modelling. The conclusion of the data based models will focus on transfer function and autoregressive with exogenous inputs (ARX) models.

9.2.1 Transfer function compared to ARX modelling

Data based modelling offered fast development speeds and did not require as much process knowledge. These features make data based models ideal for situations like the current study, where a large data set is received without a lot of process knowledge attached.

The ARX model quickly gave relatively good W_P prediction, but struggled to match the transfer function T_{E1} predictions. The transfer function modelling required the setting of variable limits and clean data selection to show anything but spurious results. Of the two methods, the transfer function model gave the most consistent results.

9.2.2 Data based models compared to the semi-empirical model

The transfer function model compared well with the semi-empirical model, except for lower T_{E1} prediction correlation to historical data. The discrepancy might be because of the two staged condenser

action which is assumed to only be a single stage by the transfer function model. The ARX model showed very low T_{E1} correlation and was therefore not suitable for the local FFE modelling.

9.3 Controller conclusions

Firstly the control loops, sampling time and developed linear model sections are concluded. Thereafter each controller is evaluated against the major aspects of the hypothesis, namely if the controller offered a substantial improvement over operator based control, while also adhering to product quality and safety standards. The fuzzy feed optimiser is also concluded and measured against the "increased production rate" clause in the hypothesis. Lastly the control solutions as a whole will be evaluated against the hypothesis.

9.3.1 Control loops

The two main control variables are the final product concentration (W_P) and the first effect temperature (T_{E1}), with corresponding manipulated variables being motive steam pressure (P_S) and the cooling water flow to the condenser (F_{CW}). The interaction between F_{CW} and T_{E2} is very quick and as such the choice was made to use T_{E2} as manipulated variable (implementing a PI controller for $T_{E2} \rightarrow F_{CW}$). This will allow for easier implementation on the real plant as only the T_{E2} controller will need to be redeveloped – a relatively simple task if steps can be performed to identify the condenser process.

9.3.2 Sampling time and filtering

A sampling time of 10s was chosen with a corresponding control period of 30s selected. This allowed the sampled data to be averaged over three sampling periods to ensure most of the sensor noise could be filtered out.

9.3.3 Linear process model

A linear process model was identified by applying step tests to the semi-empirical model and then fitting first order transfer functions to the output variable responses. The model was found to adequately represent the semi-empirical model, although some minor non-linearities were present. By successfully identifying the model, it was proven that, if the correct step tests were performed on the actual plant, transfer function models could be developed from real process data.

9.3.4 PI control

The first controller developed was a base case PI controller to act as benchmark for the other controllers. Tuning via time specification failed to yield a stable controller, most likely due to the large process dead times. The Ciancone tuning rules proved to find tuning parameters that resulted in stable controller action and had the added benefit of being designed specifically for disturbance rejection.

The PI controller showed zero offset control variable set point following and stable dynamic response. Some oscillations were observed for W_P set point tracking, while T_{E1} set point tracking showed a clearly overdamped response with no oscillations.

After further simulation and testing, it was found that the PI controller could not adequately reject a feed dry mass fraction disturbance. A W_P deviation greater than the 0.01 fractional increase of the feed was observed. Various authors have established the inadequacy of the PI controller for a dairy FFE

system [**6**] [**5**] [**2**]. Therefore similar PI controller inadequacy of this study confirmed that the local FFE can be directly compared to other authors' work.

Although the PI controller could not satisfy the defined disturbance rejection performance requirements it should be noted it offered a substantial improvement over the operator control. Standard deviation reductions were observed of 500%, for both W_P and T_{E1} control on recipe 1 historical data.

9.3.5 Linear quadratic regulator

The identified linear model was used to create a Kalman filter which used the process variable covariance as weighting matrices. The Kalman filter provided stable estimation which reduced the error between the linear and the semi-empirical models.

The LQR was designed using the square inverse of the maximum deviation of each state, or input variable, as weighting matrices. The states from the linear model were at first delayed and then used for feedback control, which resulted in the LQR_1 controller which showed pronounced oscillation. The oscillations were again the result of the process dead times. In addition to the LQR_1, a second and third LQR solution was created. LQR_2 used the pre-delay states while LQR_3 also included the Kalman filter. Both LQR_2 and LQR_3 provided stable control and efficient set point tracking with a small amount of overshoot and short W_P settling time (1 400s).

Disturbance rejection simulations showed the advantage that LQR_2 and LQR_3 gained from using pre-delay states. As soon as a disturbance was introduced, the controller started with rectifying actions reducing the maximum deviations drastically compared to PI control. The LQR solution proportional control action was increased for each of the disturbance states to ensure the controller could meet the disturbance rejection criteria.

The maximum deviation of W_P for a W_F disturbance was a 0.007 fractional increase, well below the 0.014 of the PI controller. This meant that LQR_3 control marginally outperformed the cascade controller proposed by Bakker which suppressed W_P deviation to 0.0075. Performance on the other disturbances also improved drastically - with a +3°C T_H step completely rejected while a large 1 200kg/h F_1 step caused a 0.01 fractional decrease in W_P.

The final LQR solution showed a dramatic improvement in performance when compared to operator control. Reductions in standard deviations of 1 300% and 670% were seen for W_P and T_{E1} control respectively when compared to operator control. The same trend was observed for IAE improvements, while MSE values saw even larger margins. In terms of providing a better alternative for FFE control than the operator based control, LQR solution definitely supports the hypothesis.

9.3.6 Fuzzy control

It is interesting to note that the fuzzy controller was almost entirely designed without any process data. The membership functions were designed as relative values to an absolute fuzzy variable range and could therefore be defined before the process data was investigated. Process knowledge gained while developing the semi-empirical model was used to specify the relevant rules. Only after the complete structure of the controller was completely designed was the semi-empirical model run, the input

variables investigated and ranges selected. A small amount of fine-tuning was done on the output ranges, which resulted in a controller that gave comparable results to the PI controller without the need of identified parameters or process models.

It was found, however, that this initial fuzzy controller could not meet the disturbance rejection criteria, although it could perform set point tracking relatively well. Fuzzy predictive rules were formulated to predict process behaviour on key disturbances. These predictions were then used to give an absolute addition or subtraction to P_S value, based on the disturbance absolute value. The linear model was not used in order to fully test whether a fuzzy controller developed only using process knowledge could provide comparable performance to other control methods.

The resulting predictive fuzzy controller (PFC) managed to suppress the W_P deviation to a fractional increase of 0.005 when subjected to the W_F disturbance. This meant that it outperformed both LQR and PI controllers. A large T_{E1} deviation, +1.2°C, was seen during this rejection – about twice that seen in the LQR and one and a half times that of the PI controller.

For feed flow rate disturbance steps the PFC outperformed PI control, but not the LQR controller. No predictive rule was created for T_H disturbances and as such the PFC performed the worst out of all three the controller with maximum deviations of 0.007 fractional increase and 0.4°C seen for W_P and T_{E1} respectively. Yet these deviations are still very small, with the T_H disturbance being very large at +3°C.

The PFC showed less of an improvement over operator control than the LQR controller, but still performed remarkably well. W_P and T_{E1} standard deviation was decreased by 710% and 470% respectively. These improvements were similar for maximum deviations and the IAE, but much larger for MSE improvement indicating very close set point following. Therefore, in terms of improving on operator control, the PFC also confirms the hypothesis.

9.3.7 Fuzzy feed optimiser

The hypothesis of Chapter 1 also stated that the improved controllers would be able to provide increased production rates while adhering to product safety and quality standards. None of the designed controllers changed the feed flow rate and as such could not support the hypothesis fully as the production rates were kept the same as that of the operators.

Yet the controllers already adhered to the product quality standards by reducing both the IAE and standard deviation of the output variables drastically. This meant that T_{E1} could be kept under 70°C, thereby virtually eliminating the major source of fouling. By ensuring tight W_P set point tracking, the viscosity of the concentrated product can be kept at desired levels, further reducing fouling and ensuring downstream quality (which relies heavily on constant pre-determined viscosities).

A fuzzy feed optimiser (FFO) was developed to keep the FFE close to maximum capacity. Optimisation was based on maximising the feed flow rate for any given process state. This was done by monitoring P_S, i.e. if P_S was low the process had spare evaporative capacity, while a high P_S meant that the process was over burdened. An optimum P_S of 9bar (90% of the maximum) was chosen to ensure the evaporator was running at 90% of its maximum capacity, allowing some room for the controllers to reject disturbance.

Additionally the FFO was detuned and made use of long filtered inputs to ensure it did not affect the other controllers. On average the FFO was found to raise the feed flow rate by 4.8%, with the lowest comparison to operator data being 91% of the operator flow rate. Here it must be remembered that the FFO still allowed the controllers to reach the required set points, while operator control almost constantly exceeded the first effect temperature limit.

9.4 Hypothesis and objectives

The data based models showed a lot of promise, but failed to predict T_{E1} well enough to be considered for control simulations. The semi-empirical model was, however, validated by its representation of historical data, but also by comparison to the data based models. It was found to accurately portray the local FFE under various conditions. The parameter estimation and tuning was therefore found to be adequate with the final tuned model selected for controller simulations and hypothesis testing.

All the controllers showed remarkable improvements over the operator control. Standard deviation, the MSE, the IAE and the maximum deviations observed all showed decreases of 500% upwards compared to operator control. This set point following improvement came while maintaining the feed flow rate at an average of 4.8% higher than the operators and preventing the evaporator temperatures from exceeding 70°C. Both PFC and LQR controllers outperformed literature controllers and proved to successfully reject all the major input disturbances. Therefore the hypothesis was proved.

Chapter 10 - Recommendations

The recommendations are split into two sections, namely modelling and controller recommendations.

10.1 Modelling recommendations

Plant access

If plant access could be obtained, step tests may be performed and the data based models better identified. This would decrease the modelling development time significantly and allow for even more in-depth controller studies.

Operator knowledge

All three models were created without input from operators working on the local FFE. If one could incorporate their knowledge, experience and concerns, the models could be tuned to deliver even better correlations and predictions.

In-depth heat transfer coefficient and falling film modelling

A lot of simplifying assumptions were made in order to develop the models. In the latest literature, FFE modelling focus has shifted away from overall system modelling towards explaining the complex vapour liquid interactions [**33**] inside the effects as well as investigation of the falling film properties [**34**]. Yet Bojnourd, et al. [**30**] successfully developed and validated a fundamental model similar to that of Quaak [**3**]. Lastly a general FFE model has been developed [**22**], which is claimed to be applicable to various liquors – from the paper industry to that of the dairy industry.

If one could incorporate the specific falling film dynamics, complex fluid interactions and dynamic heat transfer coefficients, it may be possible to create a very accurate FFE model.

Fault detection

The semi-empirical model offers an opportunity to introduce errors throughout the plants. Different fault detection algorithms may then be developed and tested using the generated process data. This would allow quick fault detection development as well as testing on a model proven to represent a real world process.

10.2 Controller recommendations

Decoupled PI control with feed forward action

The PI controller performed well when compared to the more advanced control techniques. Even though it was found to be insufficient, some promise was observed. Two of the major problems were disturbance rejection and introducing an error to a control variable if a step in another control variable is desired.

As a linear model seems to be fairly accurate for the FFE in terms of control purposes, a PI controller with feed forward action can be developed. This controller would work similarly to the PFC and may provide adequate disturbance rejection. If the control loops are decoupled it may also be possible to affect a set point change in one controlled variable without such a large effect on the other.

Operator knowledge

As with the modelling, operator knowledge could be used extensively for control solutions. As example all the historical data set points were estimated from averages and the effect of different recipe can be seen, but not unequivocally explained. If an experienced operator could be involved with the controller simulations it would negate a lot of the data problems and uncertainties faced.

Inclusion of other process units

In future studies the other FFE units, i.e. direct steam injector, pasteuriser, homogeniser, etc, could also be included to increase the accuracy of the model. Furthermore, a supervisory controller may then be developed which can monitor and update the various unit set points to ensure optimal stable operation.

Fault detection use for control

If the fault detection algorithm is developed, it could be used to define a process state or disturbance condition. The controller may then be tuned to react differently under certain process condition which could lead to a highly optimised diverse control solution.

References

[1] J Winchester, "Model based analysis of the operation and control of falling film evaporators," Massay University, Christchurch, PhD Thesis 2000.

[2] S Paramalingam, "Modelling, optimisation and control of a falling-film evaporator," Massay University, Christchurch, PhD Thesis 2004.

[3] P Quaak and J.B.M Gerritsen, "Modelling dynamic behaviour of multiple-effect falling-film evaporators," in *Computer applications in chemical engineering*, Amsterdam, 1990.

[4] N.T Russel, H.H.C Bakker, and R.I Chaplin, "A comparison of dynamic models for an evaporation process," *IChemE*, vol. 78, no. Part A, 2000.

[5] J Winchester and C Marsh, "Dynamics and control of falling film evaporators with mechanical vapour recompression," in *Proceedings of the American Control Conference*, California, 1999.

[6] H.H.C Bakker, C Marsh, S Paramalingam, and H Chen, "Cascade controller design for concentration control in a falling-film evaporator," *Food control*, no. 17, pp. 325-330, 2004.

[7] C.A Ramırez, M Patel, and K Blok, "From fluid milk to milk powder: Energy use and energy efficiency in the European dairy industry," *Energy*, no. 31, 2006.

[8] T.E Marlin, *Process control: designing processes and control systems for dynamic performance 2nd Edition*. New York: McGraw-Hill, 2000.

[9] D O'Callahan and P Cunninham, "Modern process control techniques in the production of dried milk products – a review," *Lait*, vol. 85, pp. 335-342, 2005.

[10] P.F. Fox and P.L.H McSweeney, *Dairy chemistry and biochemistry*, 1st ed. Dordrecht, Netherlands: Kluwer Academic Publishers Group, 1998.

[11] L.K Creamer, L.E Pearce, J.P Hill, and M.J. Boland, "Journal of agricultural and food chemistry," vol. 50, no. 25, pp. 7187-7193, 2002.

[12] M.C. Georgiadis and S. Macchietto, "Dynamic modelling and simulation of plate heat exchangers under milk fouling," no. 55, pp. 1605-1619, 2000.

[13] B Bansai and X.D Chen, "A critical review of milk fouling in heat exchangers," *Comprehensive Reviews in Food Science and Food Safety*, vol. 5, no. 2, pp. 27-33, 2006.

[14] M Henningssona, K Östergrena, R Sundbergc, and P Dejmeka, "Sensor fusion as a tool to monitor dynamic dairy processes," *Journal of food engineering*, vol. 76, pp. 154-162, 2005.

[15] M Gopal, *Digital control and state variable methods*, 2nd ed. Singapore: McGraw-Hill, 2003.

[16] D O'Callaghan and P Cunningham, "Modern process control techniques in the production of dried milk products - a review," *Lait*, no. 85, pp. 335-342, 2005.

[17] G.F Franklin, J.D ce HallPowel, and A Emami-Naeini, *Feedback control of dynamic systems*, 5th ed. New Jersey: Pearson Prenti, 2009.

[18] B Kosko, *Neural networks and fuzzy systems*. New Jersey, United States of America: Prentice-Hall Inc., 1992.

[19] R.S Ranganathan, H.A Malki, and G Chen, "Fuzzy predictive PI control for processes with large time delays," *Expert systems*, vol. 19, no. 1, February 2002.

[20] S Sajidman and H.B Kuntze, "Integration of fuzzy control and model based concepts for disturbed industrial plants with large dead-times," *Fuzz-IEEE*, 1997.

[21] C.L Chen and M.J Jong, "Fuzzy predictive control for the time-delay system," in *Second IEEE International Conference on Control*, 1993, pp. 236-240.

[22] M Foley, "The Application of Fuzzy Logic in Determining Linguistic Rules and Associative Membership Functions for the Control of a Manufacturing Process," Dublin Institute of Technology, Dublin, M.Eng Thesis 2011.

[23] P Cunnigham, P Canty, T O'Mohanny, B O'Connor, and D O'Callaghan, "System identification of a falling film evaporator in the dairy industry," in *International Control Conference*, Glasgow, 2006.

[24] Z Stefanov and K.a Hoo, "A distributed-parameter model of black liquor falling film evaporators. Part I. Modeling of a single plate," *Ind. Eng. Chem*, no. 42, pp. 1925-1937, 2003.

[25] P Quaak, van Wijck, and J van Haren, "Comparison of process identification and physical modelling for falling film evaporators," vol. 5, no. 2, 1994.

[26] N.T Russel and H.H.C Bakker, "Modular modelling of an evaporator for long-range prediction," *Artificial Intellignece in Engeneering*, vol. II, pp. 347-355, January 1997.

[27] M Gopal, *Control Systems, Principles and Design 2nd Edition*. Boston: McGrawHill, 2002.

[28] G Stephanopoulos, *Chemical Process Control: An Introduction to Theory and Practise*. London: Prentace Hall International Editions, 1984.

[29] R Sinnott and G Towler, *Chemical engineering design.*: Butterworth-Heinemann, 2009, vol. 5th Edition.

[30] F.M Bojnourd, M.A Fanaei, and H Zohreie, "Dynamic simulation of multi-effect falling-film evaporator: Milk powder production plant," in *The 6th International Chemical Engineering Congress & Exhibtion*, Kish Island, 2009.

[31] P.E Minton, *Handbook of evaporation technology*. New jersy: Noyes Publications, 1986.

[32] K.M Kam, P Saha, M Tadé, and G.P Rangaiah, "Models of an Industrial Evaporator System for Education and research in Process control," *Dev. Chem Eng Mineral Process*, no. 10, pp. 105-127, 2002.

[33] N.P.K Bushnell, "The Study of Liquid/Vapour Interaction Inside a Falling Film Evaporator in the Dairy Industry," University of Canterbury, Christchurch, PhD Thesis 2008.

[34] K.L Ang, "Investigation of rheological properties of concentrated milk," Christchurch, New Zealand, M.Eng Thesis 2011.

[35] T.E Marlin, *Process Control: Designing processes and control systems for dynamic performance*, 2nd ed. Boston: McGraw-Hill, 2000.

Appendix A: Matlab scripts and results

ARX model time

Product dry mass as y(t):

A(q)y(t) = B(q)u(t) + e(t

A(q) = 1 - 1.304 q^-1 + 0.3895 q^-2 - 0.1029 q^-3 + 0.002541 q^-4 + 0.09262 q^-5

B1(q) = 0.1328 q^-1 - 0.09077 q^-2

B2(q) = 0.0008931 q^-1 + 0.0005939 q^-2

B3(q) = -30.3 q^-1 + 23.53 q^-2

B4(q) = 0.008327 q^-1 - 0.005054 q^-2

B5(q) = -8.443e-005 q^-1 + 8.56e-005 q^-2

First effect temperature as y(t)

A(q)y(t) = B(q)u(t) + e(t)

A(q) = 1 - 1.309 q^-1 + 0.1251 q^-2 + 0.2786 q^-3 - 0.008931 q^-4

+ 0.02056 q^-5 - 0.1392 q^-6 + 0.08667 q^-7 - 0.03066 q^-8+ 0.2165 q^-9 - 0.1892 q^-10

B1(q) = 0.454 q^-1 + 6.218 q^-2 + 3.729 q^-3 - 2.215 q^-4 - 7.98 q^-5

- 0.3762 q^-6 + 5.474 q^-7 + 0.8481 q^-8 - 8.856 q^-9+ 4.836 q^-10

B2(q) = 0.05746 q^-1 + 0.04889 q^-2 + 0.07898 q^-3 + 0.002433 q^-4

- 0.07486 q^-5 + 0.01033 q^-6 + 0.02949 q^-7 - 0.01466 q^-80.03663 q^-9 + 0.0253 q^-10

B3(q) = 87.83 q^-1 - 167 q^-2 - 380 q^-3 + 56.12 q^-4 + 442.9 q^-5

- 937.4 q^-6 + 494.6 q^-7 + 463.8 q^-8 - 193.4 q^-9+ 12.92 q^-10

B4(q) = 0.1203 q^-1 + 0.02766 q^-2 - 0.07578 q^-3 - 0.0363 q^-4 - 0.02124 q^-5 + 0.01233 q^-6 - 0.01811 q^-7 + 0.01098 q^-8+ 0.002544 q^-9 + 0.03558 q^-10

B5(q) = 0.008445 q^-1 - 0.004721 q^-2 - 0.01025 q^-3 + 0.007648 q^-4 + 0.009088 q^-5 - 0.01226 q^-6 + 0.0108 q^-7 + 0.002373 q^-8+ 0.0001327 q^-9 - 0.005651 q^-10

Linear state space model

The Matlab script used to convert transfer functions to continuous state space models is shown below:

```
function [A,B,C,D]=get_MIMO(K,tau,u,y)
%u => states with corresponding u's
%y => states for y, every state can only be used once
n=length(K);

A=zeros(n);
B=zeros(n,max(u));
C=zeros(max(y),n);
D=zeros(max(y),max(u));

for i=1:n
    A(i,i)=-1/tau(i);
    B(i,u(i))=K(i)/tau(i);
    C(y(i),i)=1;
end

end
```

Identified linear process model from semi-empirical model:

$$A = \begin{bmatrix} -0.01024 & 0 & 0 & 0 & 0 & 0 & 0 & 0 & 0 & 0 \\ 0 & -0.00673 & 0 & 0 & 0 & 0 & 0 & 0 & 0 & 0 \\ 0 & 0 & -0.01254 & 0 & 0 & 0 & 0 & 0 & 0 & 0 \\ 0 & 0 & 0 & -0.00535 & 0 & 0 & 0 & 0 & 0 & 0 \\ 0 & 0 & 0 & 0 & -0.01614 & 0 & 0 & 0 & 0 & 0 \\ 0 & 0 & 0 & 0 & 0 & -0.00464 & 0 & 0 & 0 & 0 \\ 0 & 0 & 0 & 0 & 0 & 0 & -0.01101 & 0 & 0 & 0 \\ 0 & 0 & 0 & 0 & 0 & 0 & 0 & -0.00497 & 0 & 0 \\ 0 & 0 & 0 & 0 & 0 & 0 & 0 & 0 & -0.00918 & 0 \\ 0 & 0 & 0 & 0 & 0 & 0 & 0 & 0 & 0 & -0.0067 \end{bmatrix}$$

$$B = \begin{bmatrix} 0.015084 & 0 & 0 & 0 & 0 \\ 0 & 1.50E\text{-}05 & 0 & 0 & 0 \\ 0 & 0 & -1.18792 & 0 & 0 \\ 0 & 0 & 0 & 0.000152 & 0 \\ 0 & 0 & 0 & 0 & -5.42E\text{-}05 \\ 0 & 0 & 0 & 0 & 4.51E\text{-}05 \\ 0 & 0.000676 & 0 & 0 & 0 \\ 0 & 0 & 4.579641 & 0 & 0 \\ 0 & 0 & 0 & 0.012567 & 0 \\ 0 & 0 & 0 & 0 & 0.006104 \end{bmatrix}$$

$$C = \begin{bmatrix} 1 & 1 & 1 & 1 & 1 & 1 & 0 & 0 & 0 & 0 \\ 0 & 0 & 0 & 0 & 0 & 0 & 1 & 1 & 1 & 1 \end{bmatrix}$$

$$D = \begin{bmatrix} 0 & 0 & 0 & 0 & 0 \\ 0 & 0 & 0 & 0 & 0 \end{bmatrix}$$

Fuzzy variable range create

```
function a=getFuzz(in1,in2,or1,ruleList,nvar)
%load Plant.mat;aSP=getFuzz(0.7e-5,0.05);
a=newfis('FPIC');
range=[in1 in2 or1];                %Input range
ivar={'input','input','output'};    %var types
inout=[1 2 1];                      %corresponding #
%nvar={'E','dE','Ps'};               %var names
mfN={'BN','SN','Z','SP','BP'};      %MF description
re=[-1.5 -1 -0.5;                   %MF ranges
    -1 -0.5 0
    -0.5 0 0.5
    0 0.5 1
    0.5 1 1.5
    ];
for j=1:3
    a=addvar(a,ivar{j},nvar{j},[-range(j) range(j)]);
    for i=1:5
        a=addmf(a,ivar{j},inout(j),mfN{i},'trimf',range(j).*re(i,:));
    end
end
a=addrule(a,ruleList);
end
```

Appendix B: Modelling on validation data sets

All the final models were compared on the validation data sets (note that the means were removed as one is only interested in the dynamic response):

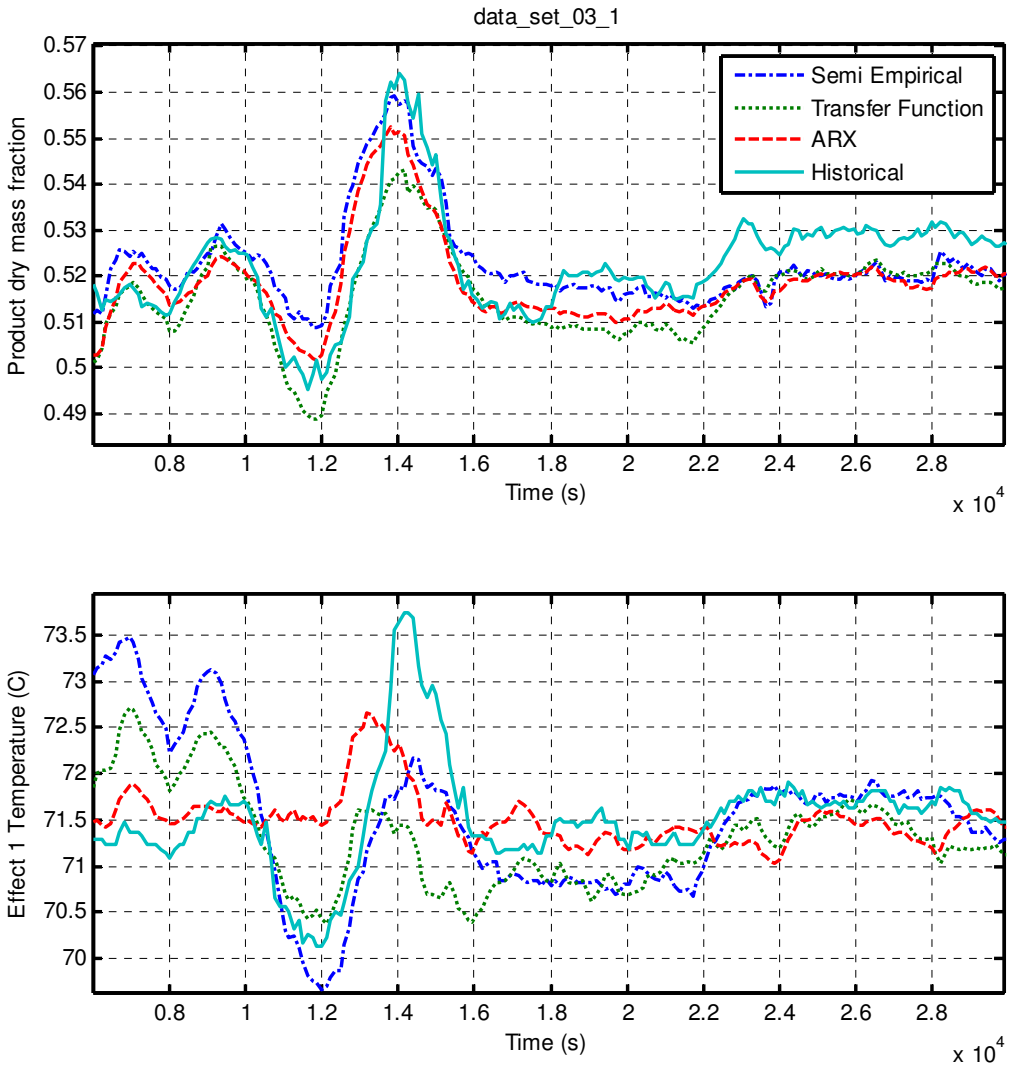

Figure B-1: All models compared on historical data set 03_1

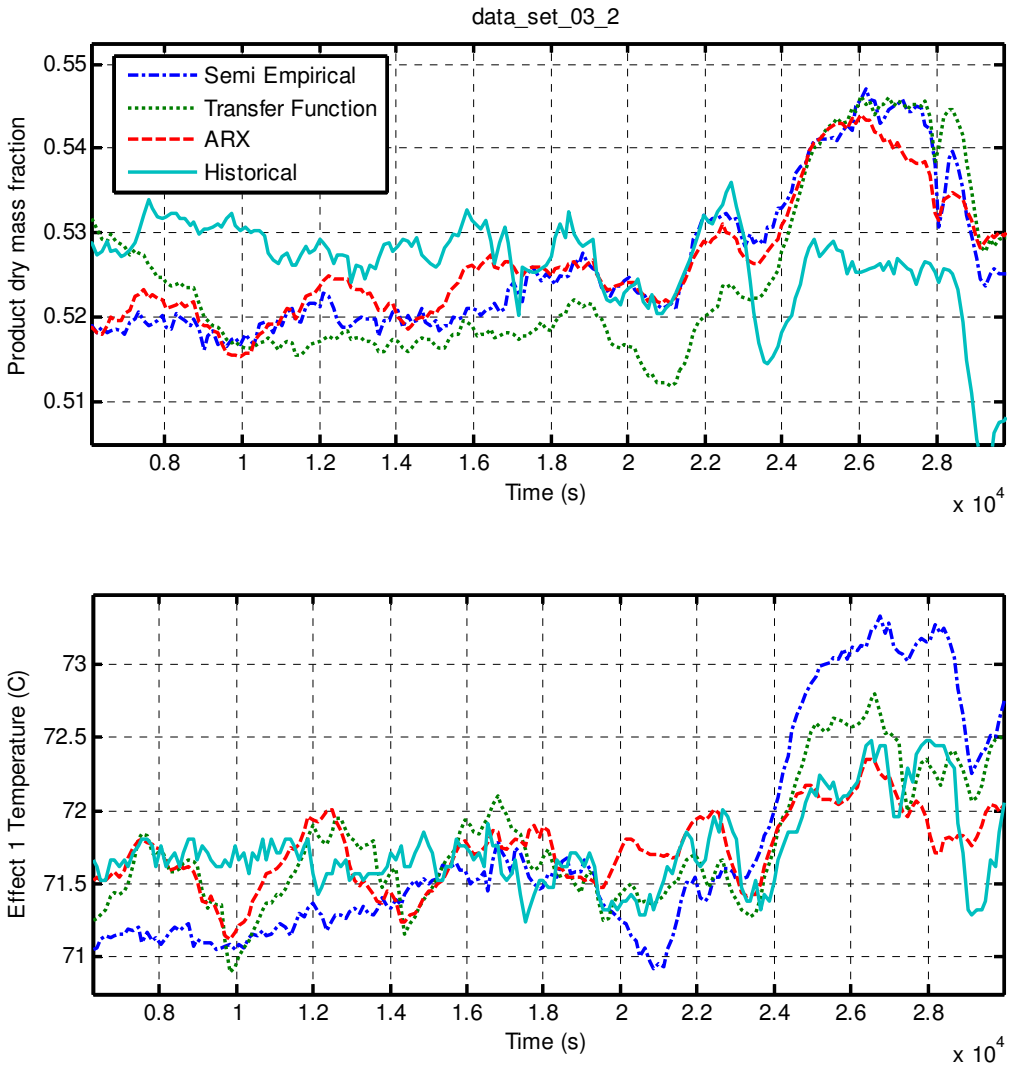

Figure B-2: All models compared on historical data set 03_2

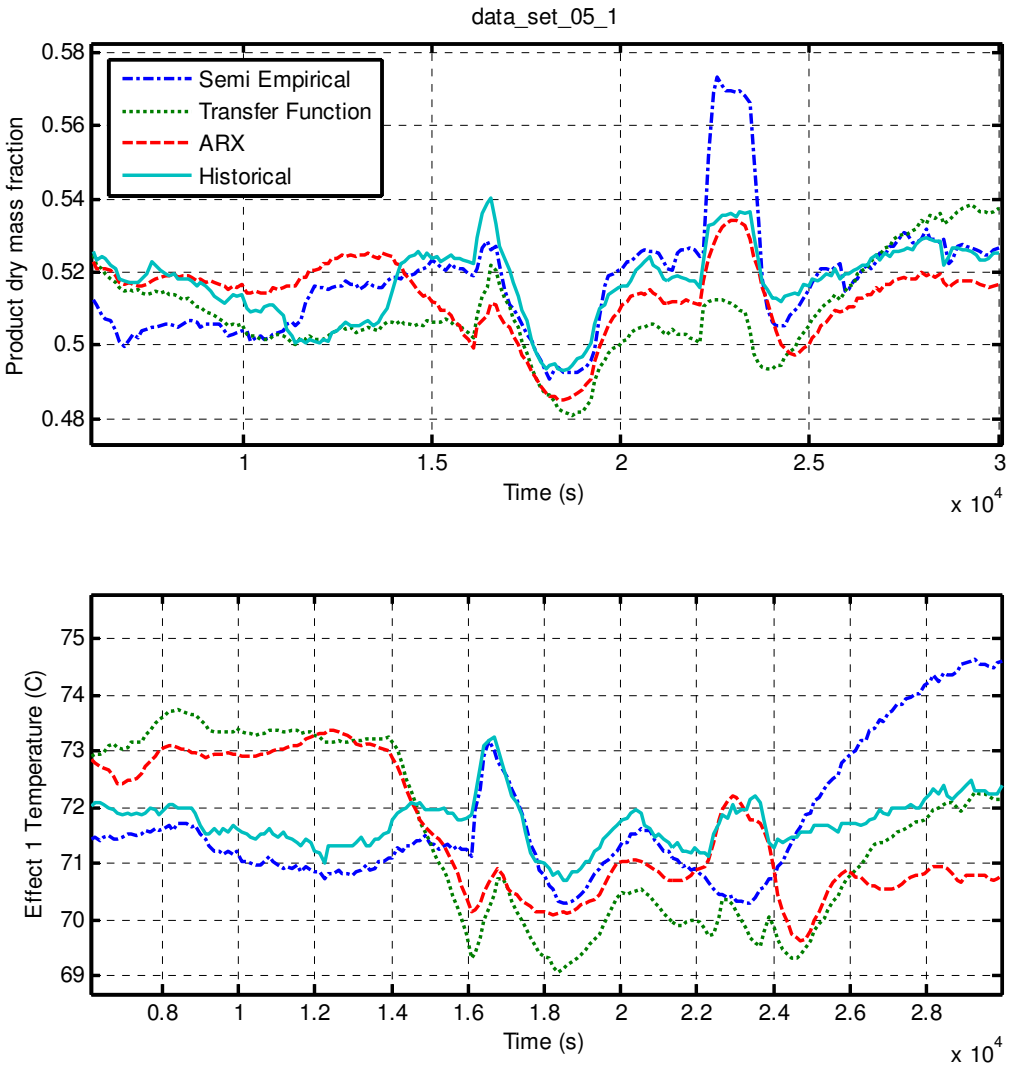

Figure B-3: : All models compared on historical data set 05_1

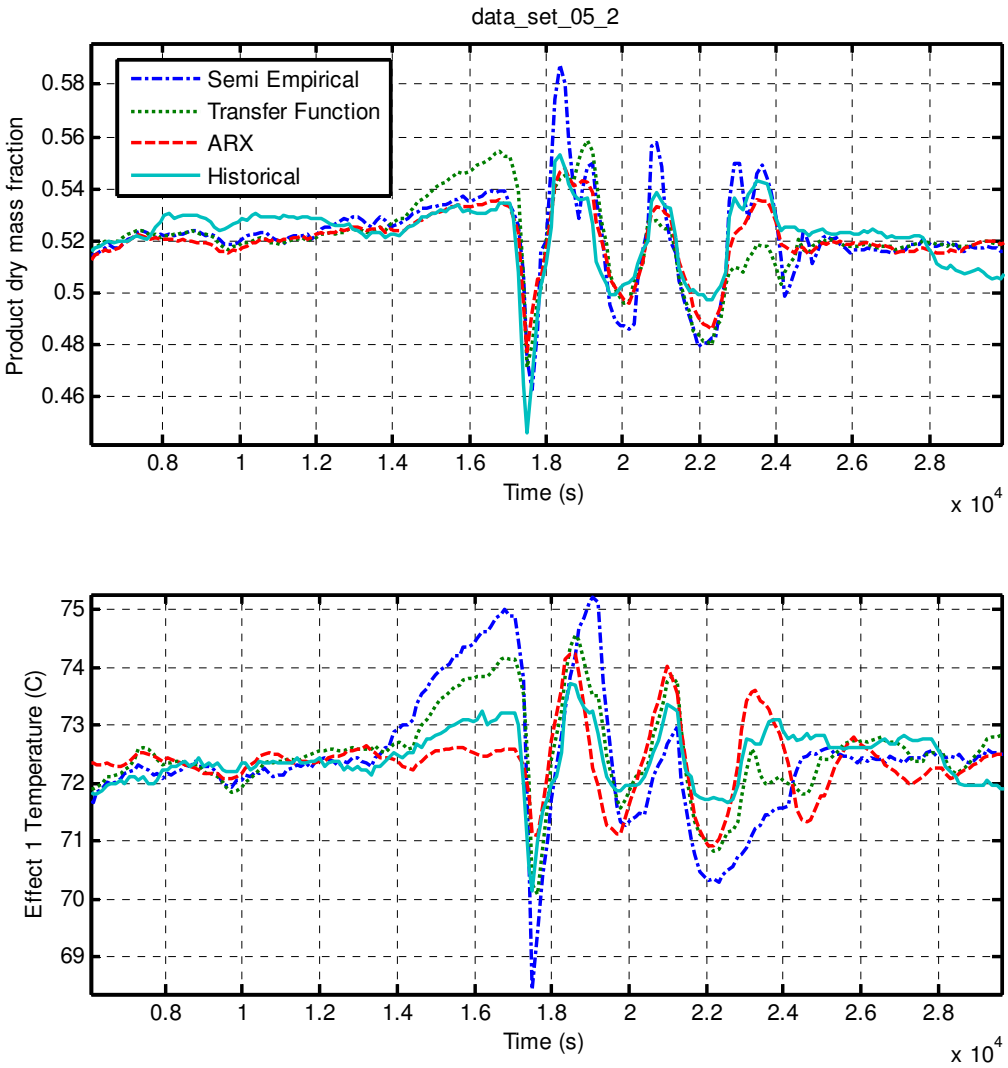

Figure B-4: All models compared on historical data set 05_2

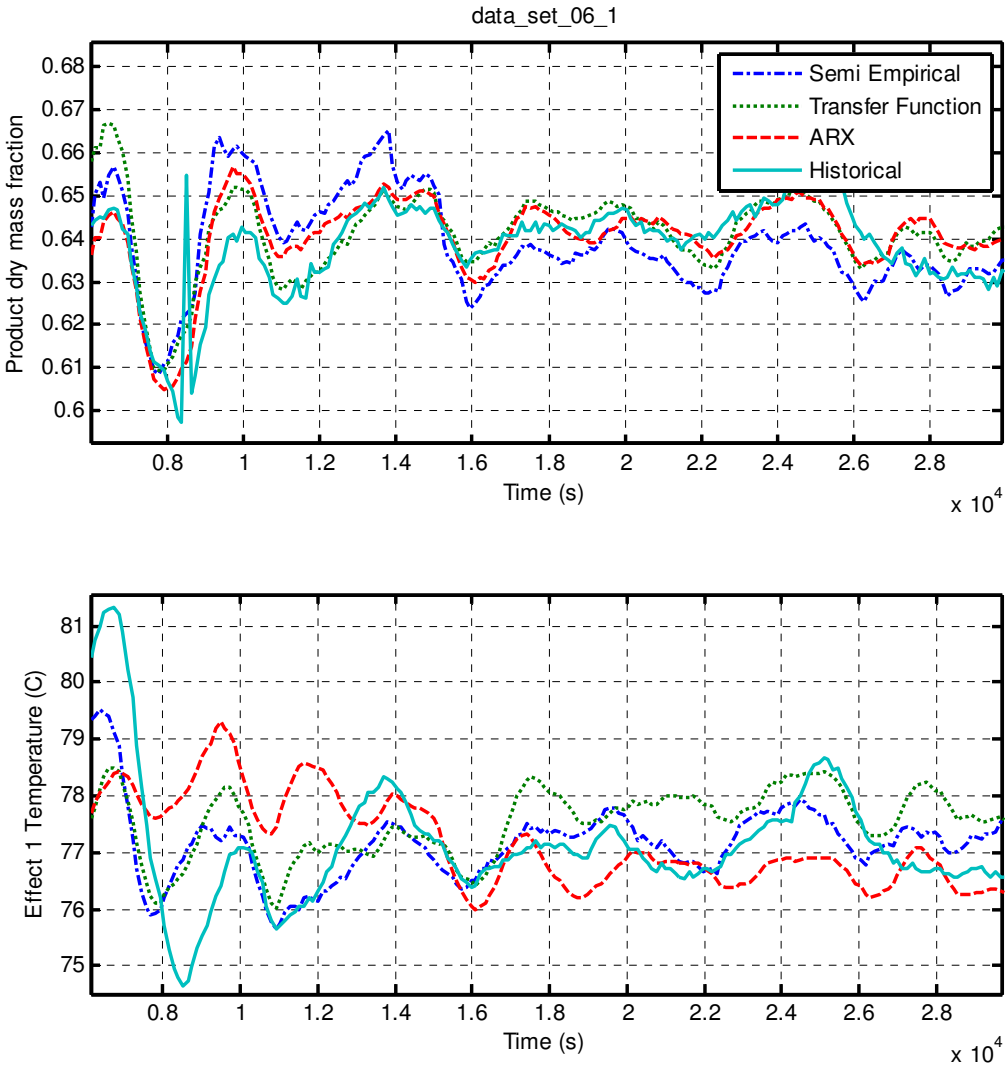

Figure B-5: All models compared on historical data set 06_1

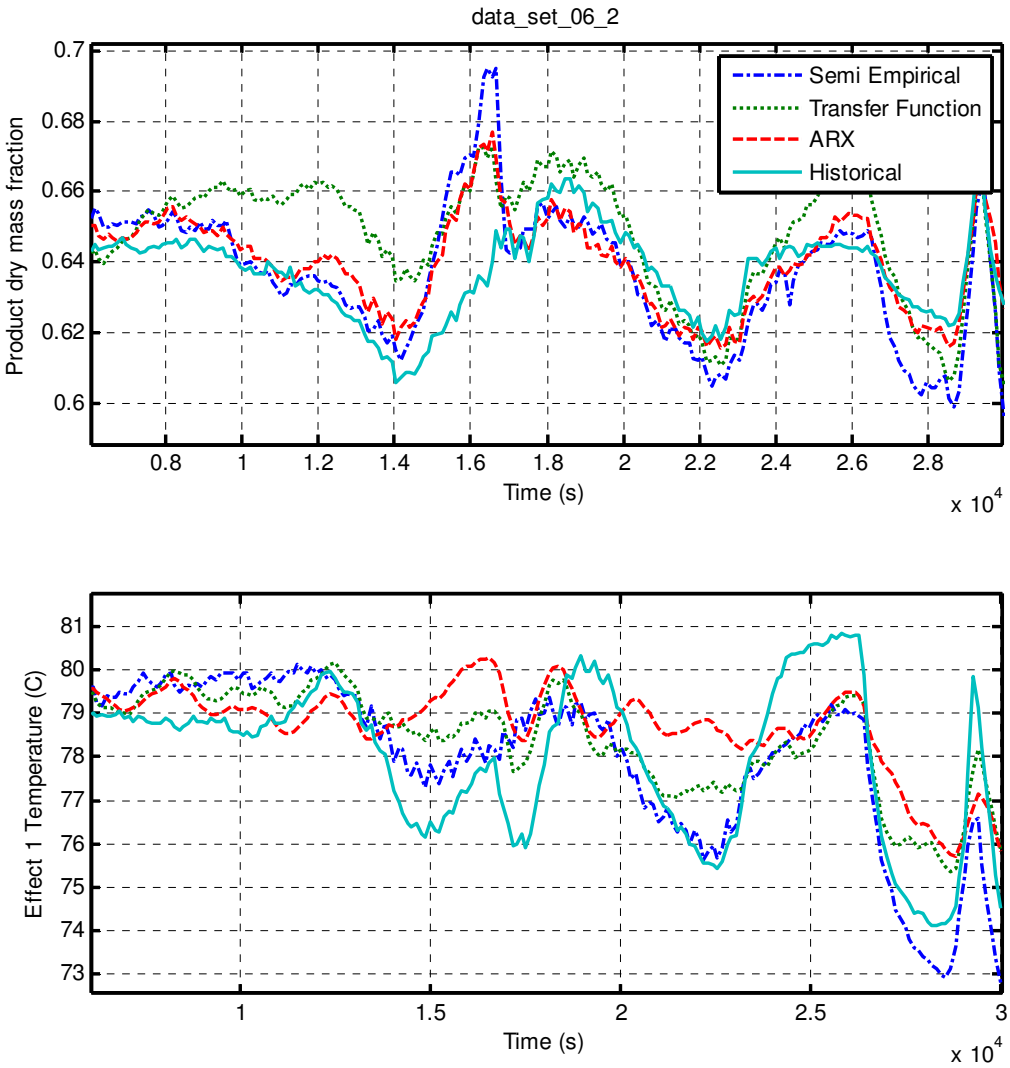

Figure B-6: All models compared on historical data set 06_2

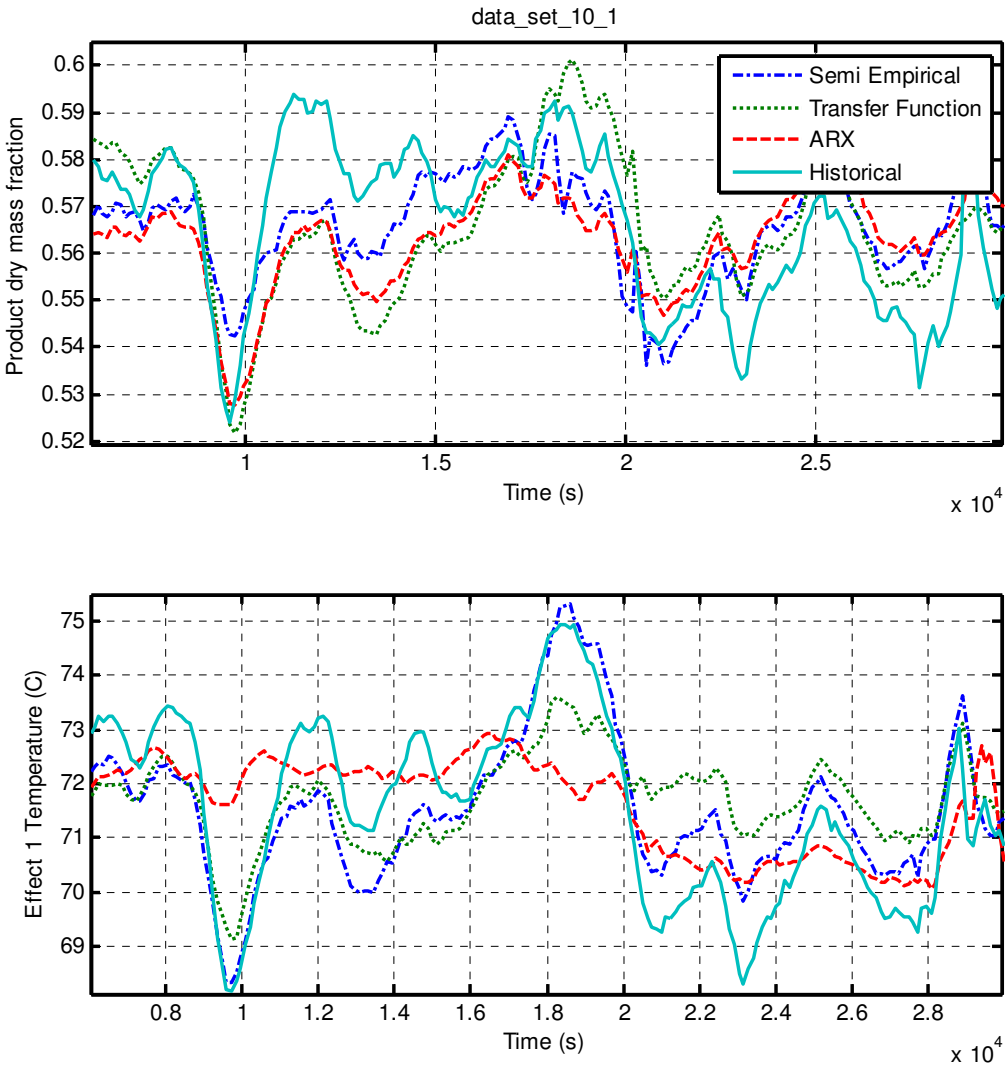

Figure B-7: All models compared on historical data set 10_1

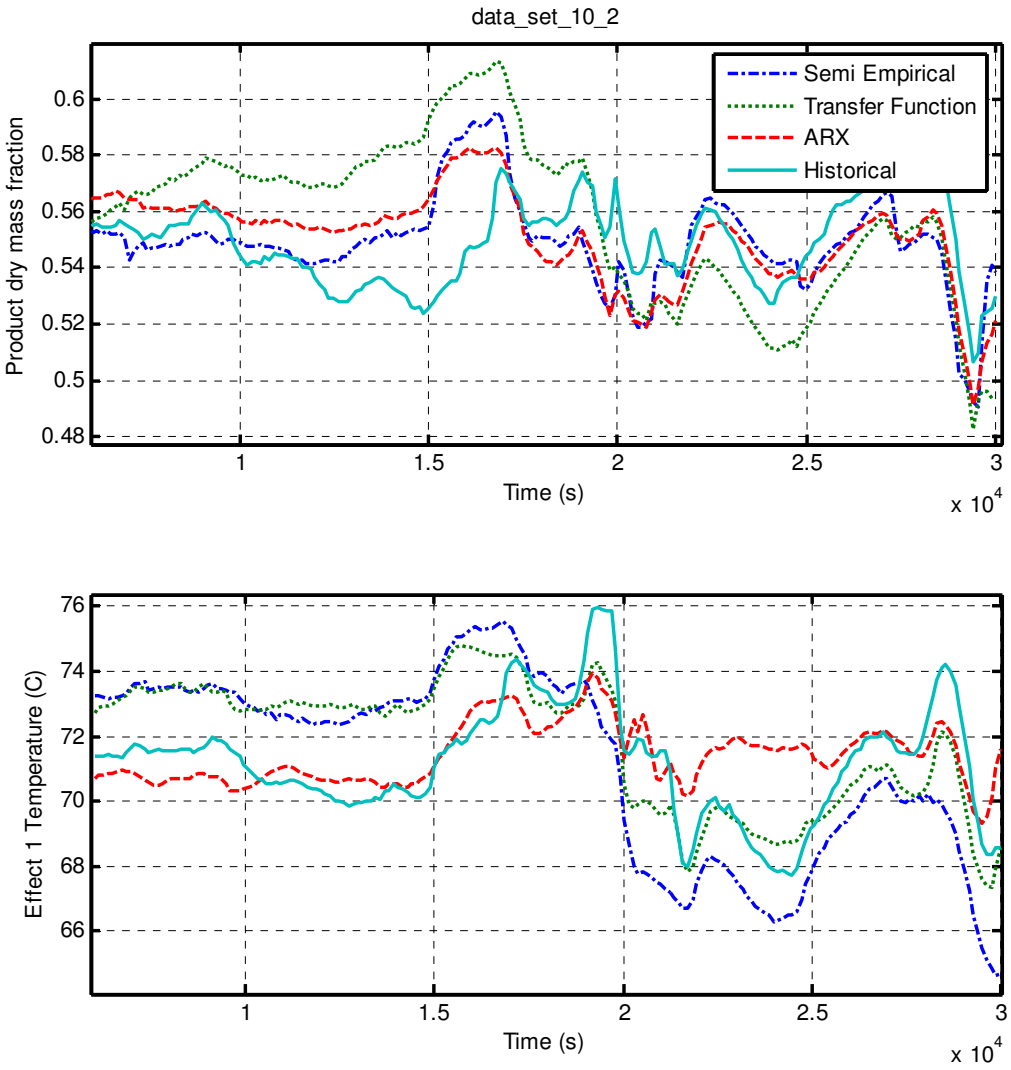

Figure B-8: All models compared on historical data set 10_2

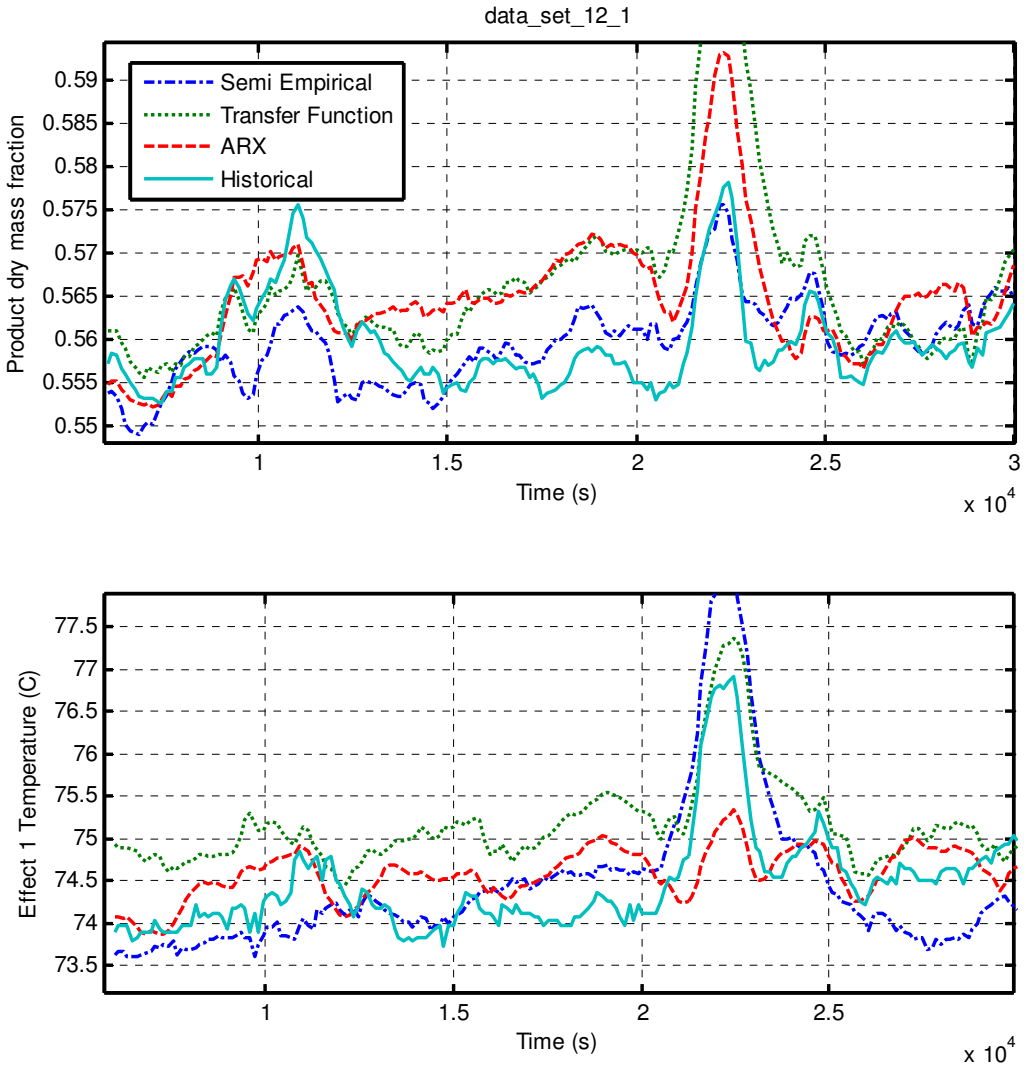

Figure B-9: All models compared on historical data set 12_1

Appendix C: Controller simulations

All the validation data recipes are shown below with the fuzzy feed optimiser enabled and constant set point.

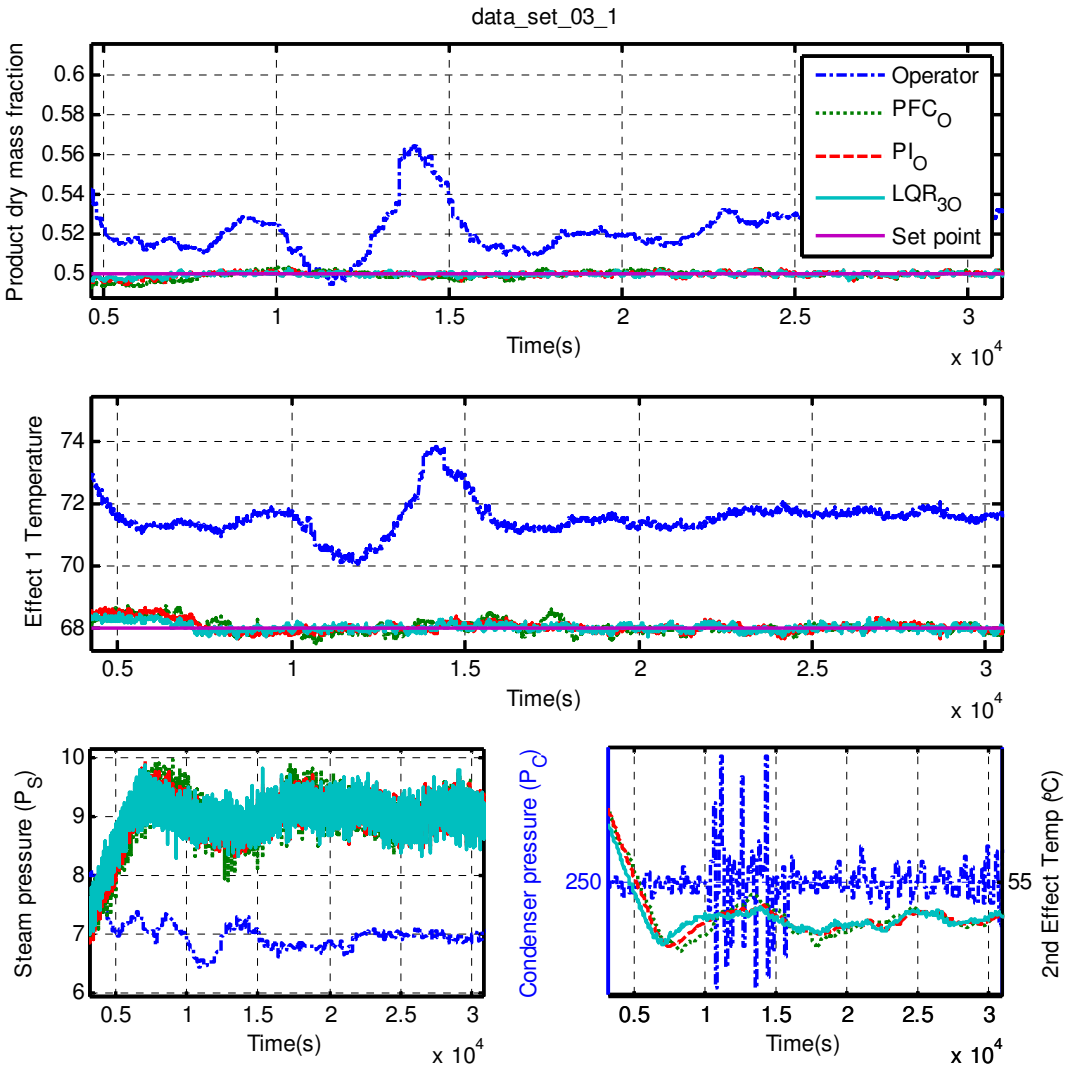

Figure C-1: All controllers including optimiser on historical data set 03_1

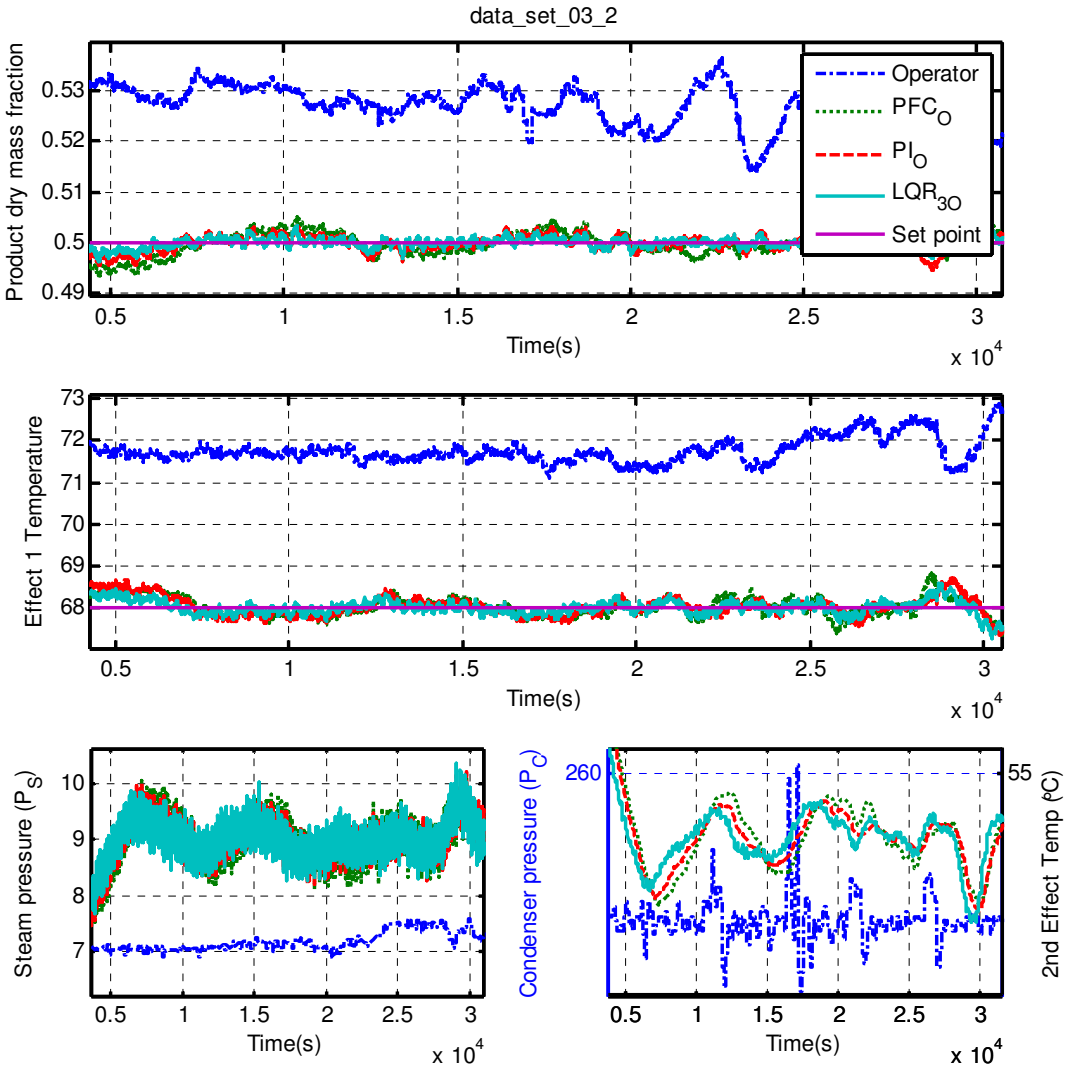

Figure C-2: All controllers including optimiser on historical data set 03_2

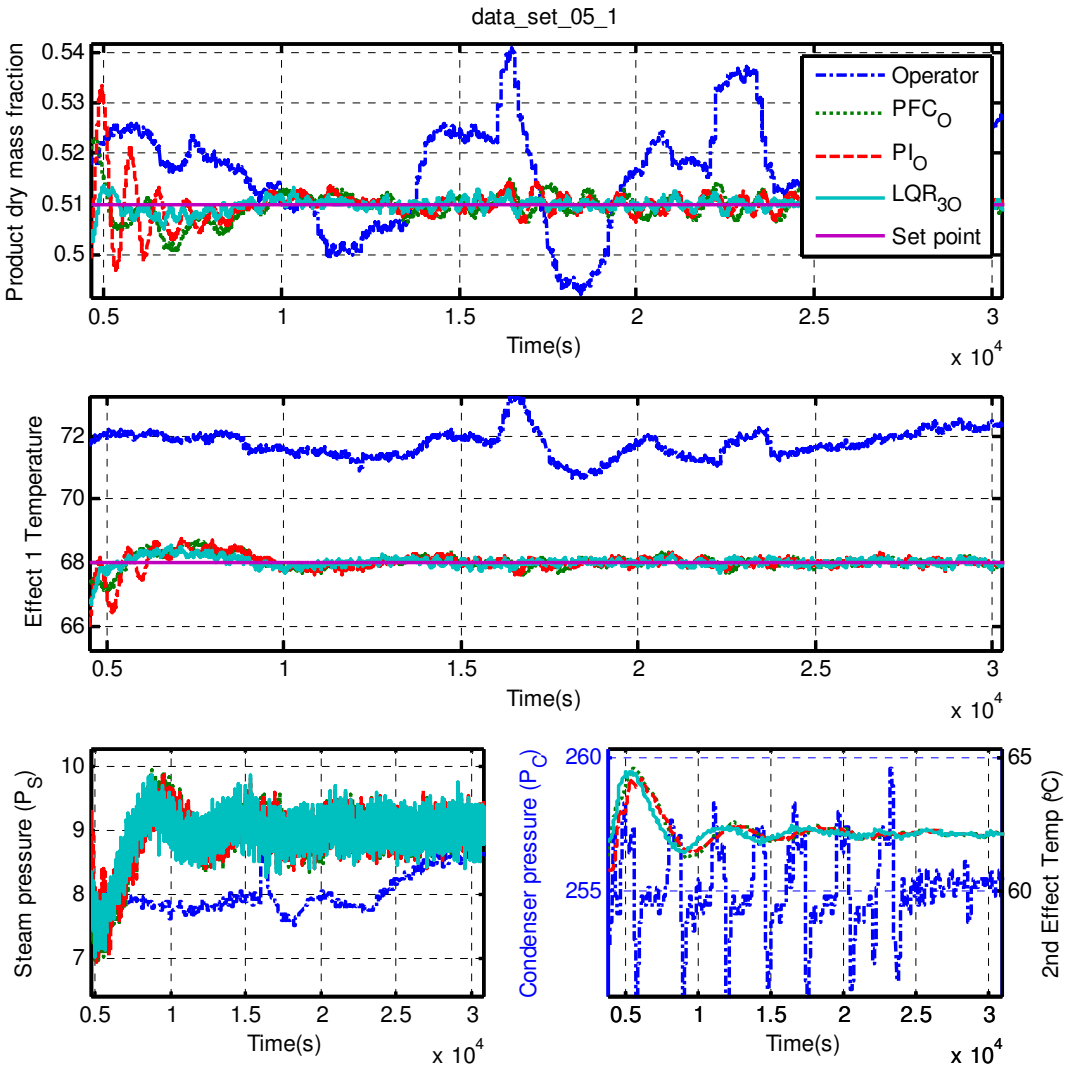

Figure C-3: All controllers including optimiser on historical data set 05_1

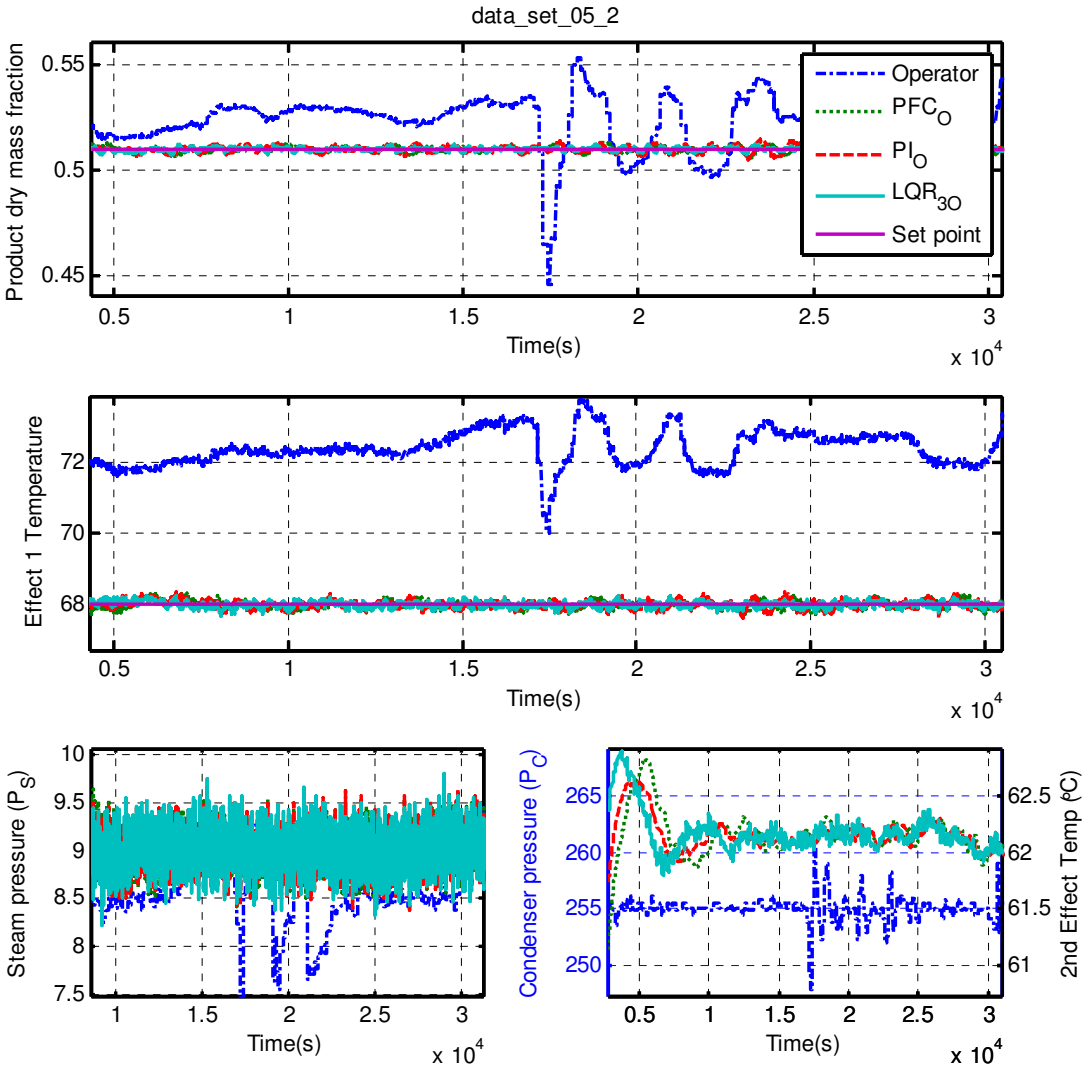

Figure C-4: All controllers including optimiser on historical data set 05_2

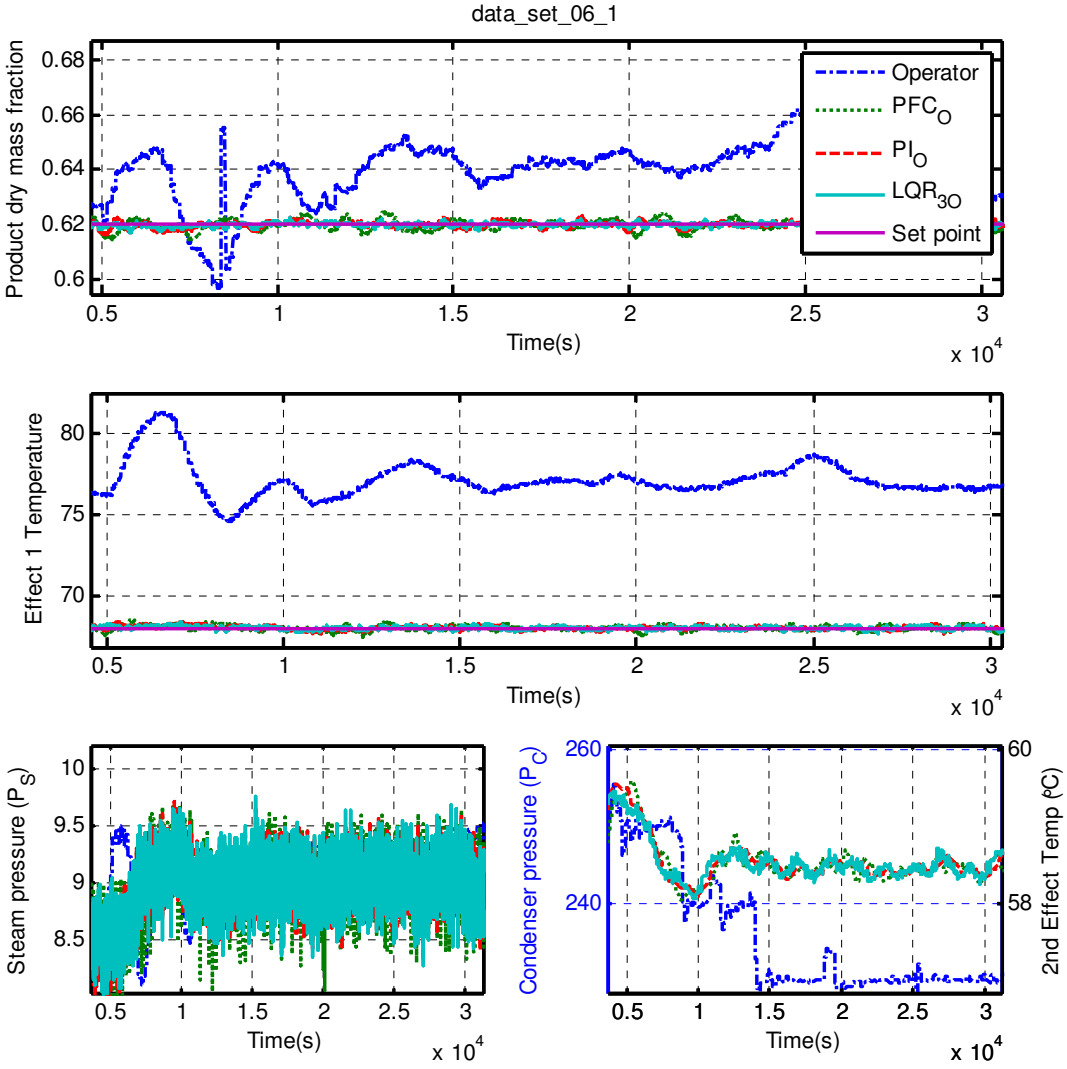

Figure C-5: All controllers including optimiser on historical data set 06_1

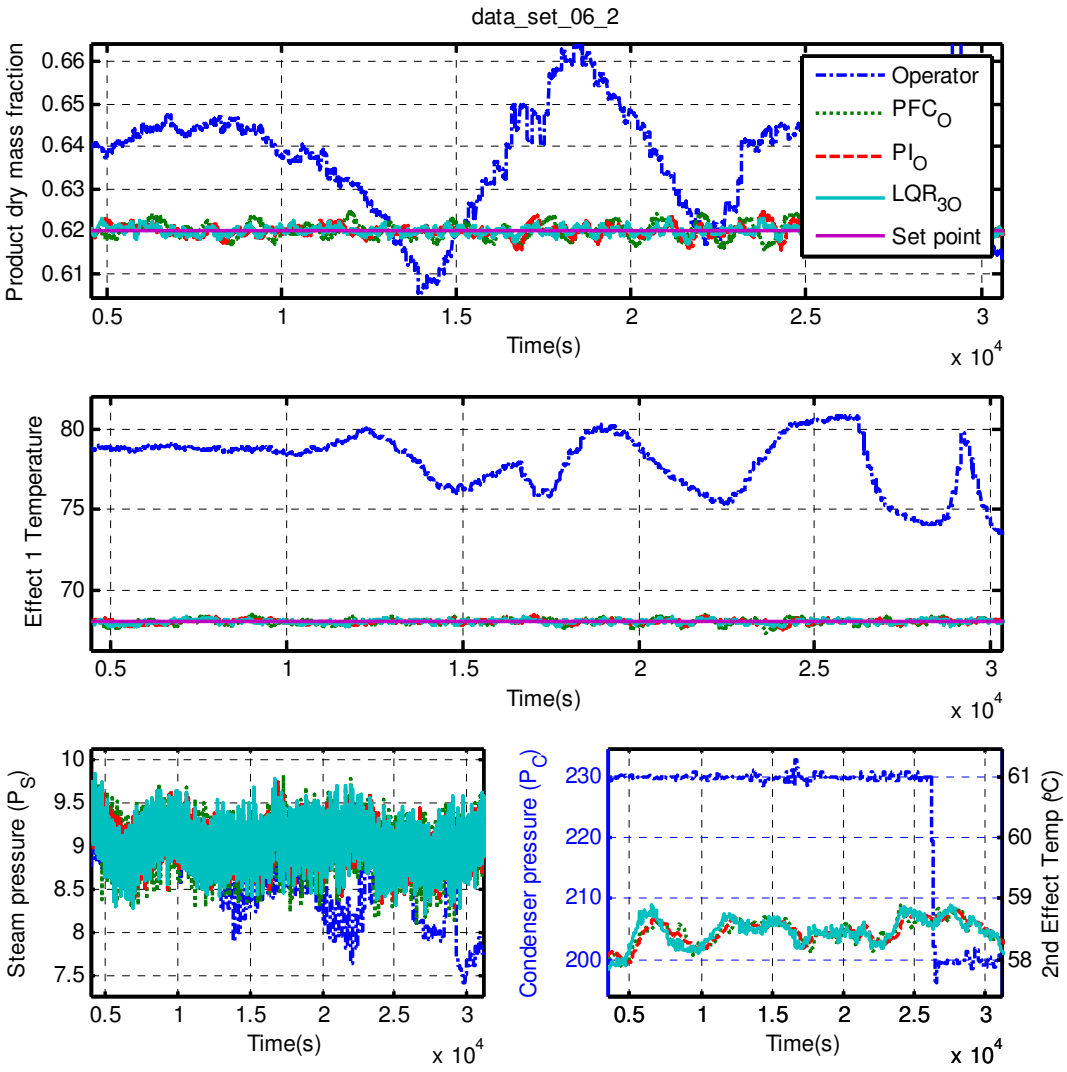

Figure C-6: All controllers including optimiser on historical data set 06_2

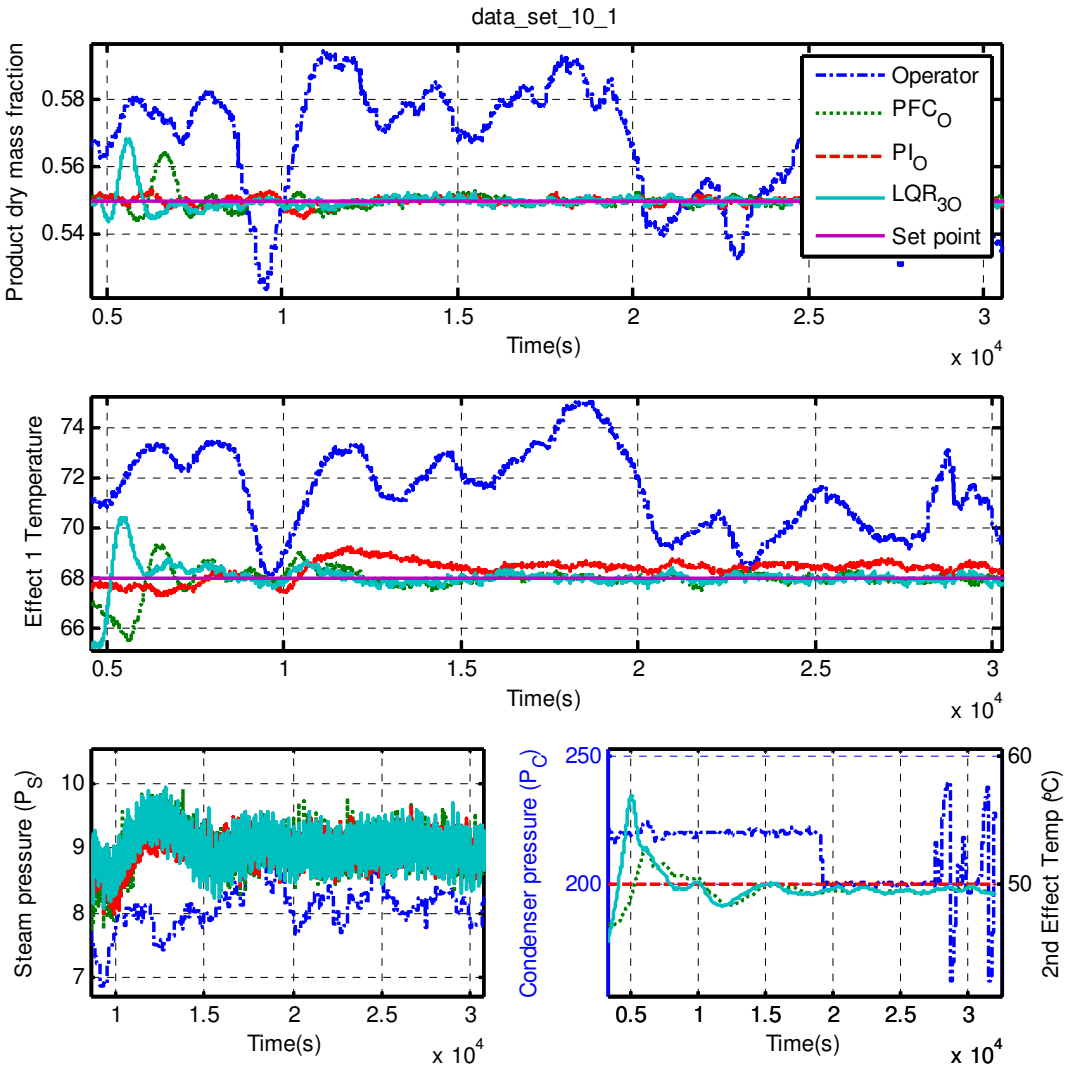

Figure C-7: All controllers including optimiser on historical data set 10_1

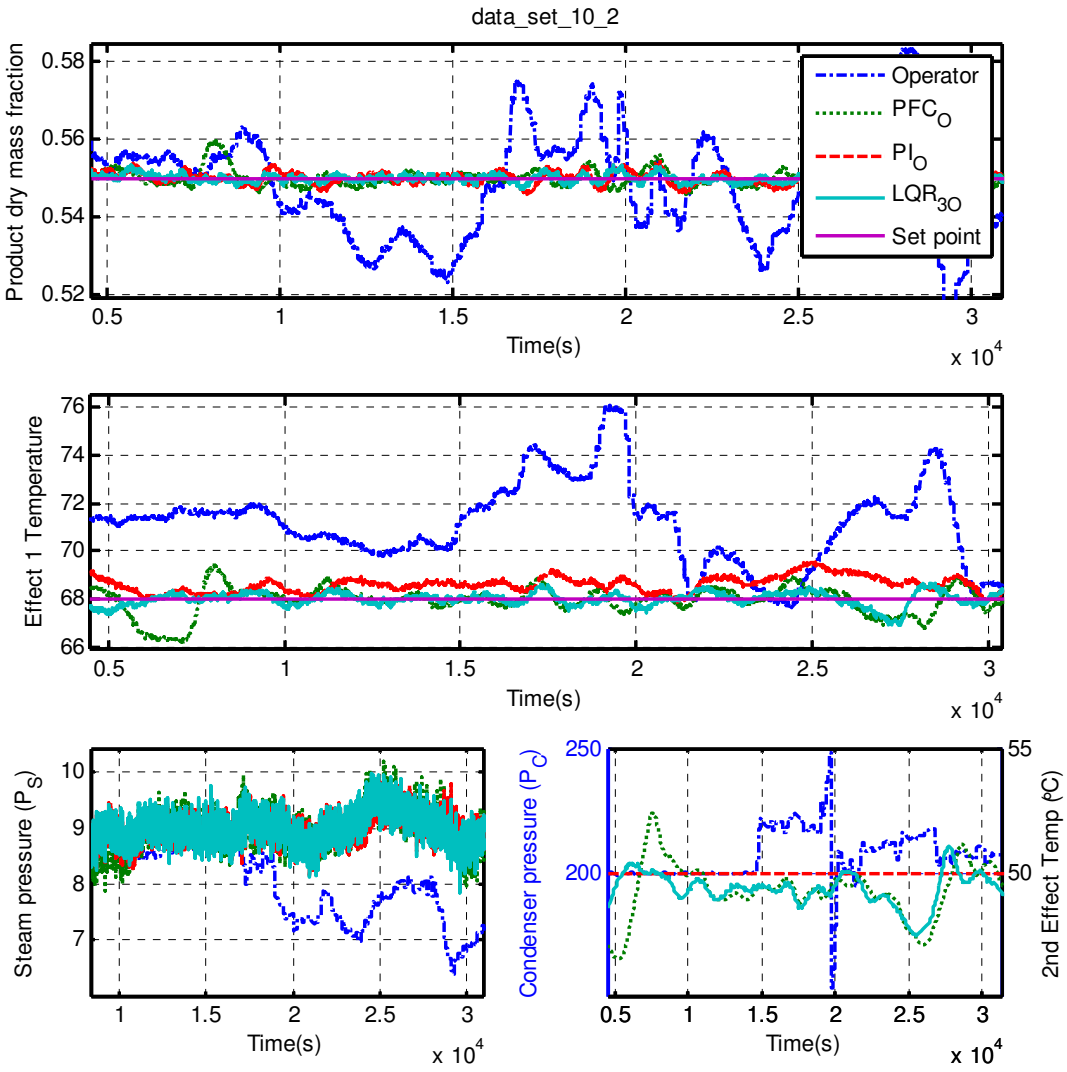

Figure C-8: All controllers including optimiser on historical data set 10_2

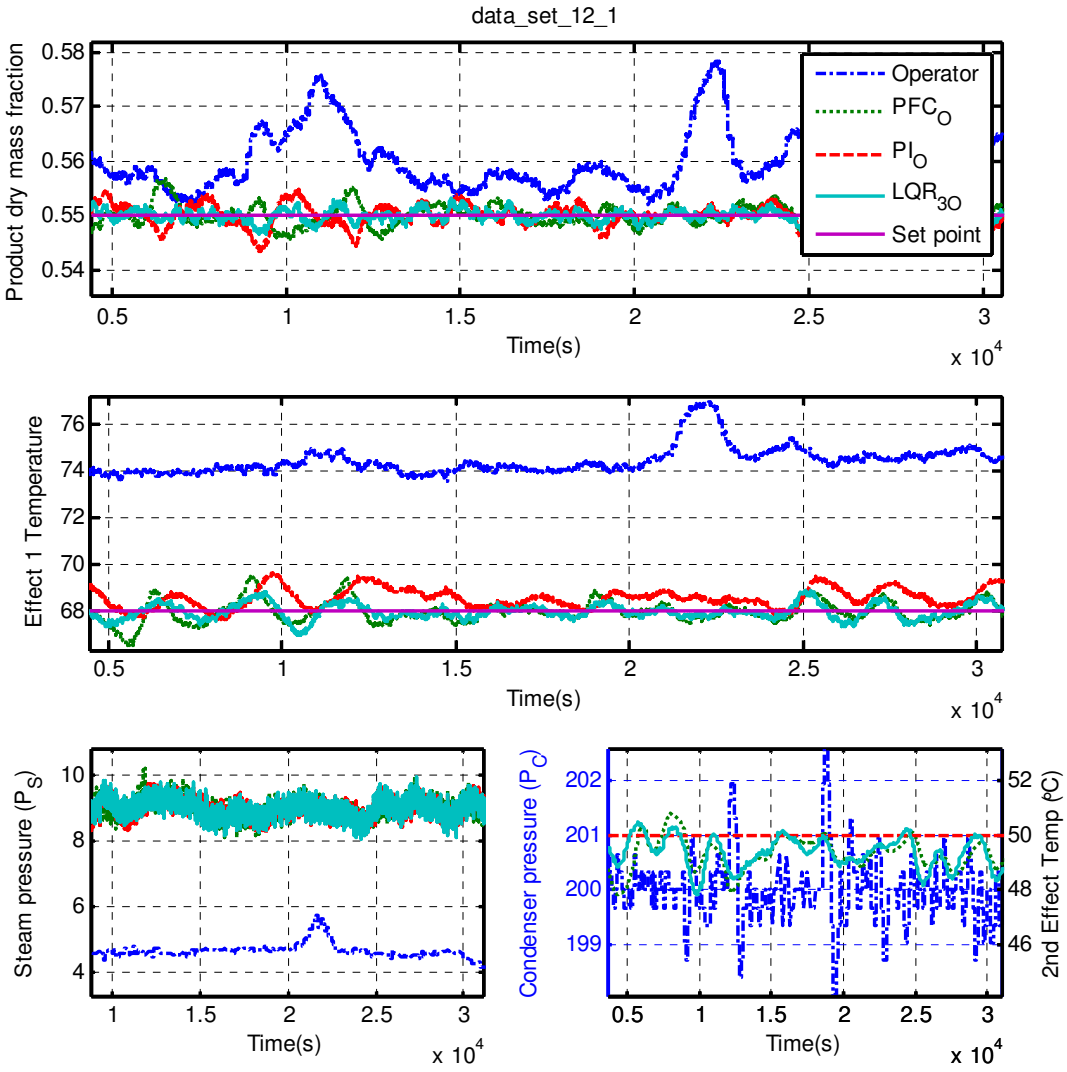

Figure C-9: All controllers including optimiser on historical data set 12_1